

POLY(VINYL ALCOHOL) NANOCOMPOSITE HYDROGELS FOR
INTERVERTEBRAL DISC PROSTHESES

(Spine title: PVA Nanocomposite Hydrogels for IVD Prostheses)

(Thesis format: Monograph)

by

Elaine Y. L. Wong

Biomedical Engineering Graduate Program

A thesis submitted in partial fulfillment
of the requirements for the degree of
Doctor of Philosophy

The School of Graduate and Postdoctoral Studies
The University of Western Ontario
London, Ontario, Canada

© Elaine Y. L. Wong 2012

THE UNIVERSITY OF WESTERN ONTARIO
School of Graduate and Postdoctoral Studies

CERTIFICATE OF EXAMINATION

Supervisor

Dr. Wankei Wan

Supervisory Committee

Dr. John de Bruyn

Dr. John Medley

Dr. Amin Rizkalla

Examiners

Dr. Brian Amsden

Dr. Don Hewson

Dr. Jeffrey Hutter

Dr. James Johnson

The thesis by

Elaine Y. L. Wong

entitled:

**Poly(Vinyl Alcohol) Nanocomposite Hydrogels for Intervertebral Disc
Prostheses**

is accepted in partial fulfillment of the
requirements for the degree of
Doctor of Philosophy

Date _____

Chair of the Thesis Examination Board

ABSTRACT

Spinal fusion is currently the gold standard for surgical intervention of intervertebral disc (IVD) diseases leading to neck and back pain failing conservative treatments. However, fusion removes motion between the vertebrae and can result in adjacent level degeneration. Total disc replacement (TDR) is an emerging treatment alternative that preserves motion, but materials found in clinically available devices bear little resemblance to the properties of the native IVD. Poly(vinyl alcohol) (PVA) hydrogels are biocompatible, have mechanical behaviour similar to natural tissues, and properties that can be tuned by varying polymer concentration and physical crosslinking through freeze-thaw cycling. Furthermore, their properties can be modified with the addition of nanofillers. In the present study, PVA hydrogels and its nanocomposites containing Laponite and bacterial cellulose (BC) were investigated in compression and crossing-paths wear for potential application in cervical TDR. While increases in PVA concentration increased stiffness and decreased time-dependent response in neat PVA hydrogels, viscous response increased with nanofiller addition. BC addition also increased stiffness of the hydrogels without large changes in water content. To measure wear in the hydrogels, a technique using three-dimensional ultrasound imaging was developed. Wear volume and depth decreased with decreasing water content, while fatigue wear was eliminated with the addition of nanofillers in crossing-paths wear. Finally, a two-component PVA hydrogel demonstrated that compression properties could be tailored by mimicking the natural IVD structure. These results indicated that various parameters could be used to optimize the properties of PVA and PVA-nanocomposite hydrogels for applications in cervical TDR.

Keywords: hydrogel, poly(vinyl alcohol), Laponite, bacterial cellulose, nanocomposites, mechanical properties, strain rate dependence, crossing-paths wear, three-dimensional ultrasound imaging, intervertebral disc

ACKNOWLEDGEMENTS

First of all, I would like to sincerely thank my supervisor, Dr. Wankei Wan, for his inspiration in the field of biomaterials and medical devices. I am grateful for his all his ideas, helpful advice, guidance, encouragement and support that culminated with the completion of this thesis. I am also thankful for the direction my advisory committee has given to my project, especially Dr. John Medley for his helpful insight in wear testing and for the loan of the wear tester.

The following people have contributed their expertise and assistance to the work in this thesis: Dr. Jim Lacefield for the use of the ultrasound equipment at Robarts and his knowledge in ultrasound imaging and analysis, the staff at the Biotron for their advice and training on sample preparation and SEM, Clayton Cook from the University Machine Services for help with designing various parts and moulds, Michael Roach from 3M for advice on adhesives and providing us with a sample, Dr. Leonardo Millon for instruction and advice on PVA and mechanical testing, Darcy Small and Dr. Kenneth Wong for the TEM images, Dr. Donna Padavan for help on SEM, Dr. Karen Kennedy for assistance in the preparation and testing of the IVD prototype, undergraduate students Rachel Brown and Ghaleb Sater for their work in the laboratory, Andrew Norman, Jordan DeMello and Xinsheng Li for providing the bacterial cellulose, and Dr. Jian Liu for performing EDX on the cellulose samples. Thank you also to other colleagues in my lab and BME for their friendship through the years.

I am truly blessed to have enjoyed valuable friendships outside of the lab: friends from the King's community for keeping me rooted and for the wonderful gifts of music and fellowship; and my relatives and friends, especially Anabela, Amanda, Calvin, Karen, Sarah, Wailan, and my EngSci family, who have touched my life and stuck with me through thick and thin. I am humbled by your presence in my life.

I wish to honour my parents, to whom this thesis is dedicated, for supporting me from the moment I hurriedly entered the world. All of this would not have been possible

without their love, care and sacrifices to provide me with the opportunities they did not have. Finally, to my brilliant husband, I would like to acknowledge and thank him for his unwavering patience and for lending his competency in computer graphics. There are no words worthy to express my gratitude for his love and unfaltering faith in me.

Dedicated to my parents

TABLE OF CONTENTS

CERTIFICATE OF EXAMINATION	ii
ABSTRACT	iii
ACKNOWLEDGEMENTS	iv
TABLE OF CONTENTS	vii
LIST OF TABLES	xii
LIST OF FIGURES	xiv
LIST OF APPENDICES	xx
LIST OF ABBREVIATIONS	xxi
LIST OF SYMBOLS	xxiii
CHAPTER 1 INTRODUCTION	1
1.1 Background and Motivation	1
1.2 Objectives	3
CHAPTER 2 LITERATURE REVIEW	4
2.1 Prevalence of Neck and Back Pain	4
2.2 Intervertebral Discs	5
2.2.1 Intervertebral Disc Anatomy	6
2.2.2 Degenerative Disc Disease	9
2.2.3 Intervertebral Disc Mechanics	9
2.2.3.1 Compressive Stress-Strain Behaviour and Strain Rate Dependence	10
2.2.3.2 Stress Relaxation and Creep	12
2.2.3.3 Mechanical Properties of IVD Components	13
2.2.3.4 Summary	15
2.2.4 Current and Emerging Treatments	15
2.3 Cervical Artificial Discs	17
2.3.1 BRYAN Disc	19
2.4 PVA Hydrogels	21
2.4.1 Physically Crosslinked PVA	21
2.4.2 Characterization of PVA Hydrogel Structure	23

2.4.3 Mechanical Properties	25
2.4.3.1 Unconfined Compression	25
2.4.3.2 Stress Relaxation, Creep and Dynamic Mechanical Properties	27
2.4.4 Effects of aging and salt on PVA hydrogels	29
2.4.5 Biocompatibility	31
2.5 Nanofillers and Nanocomposites	32
2.5.1 Laponite	33
2.5.2 Bacterial Cellulose	35
2.5.3 PVA Hydrogel-Based Nanocomposites	36
2.6 Hydrogel-based Artificial IVD	39
2.7 Wear Testing	40
2.7.1 Lubricant	41
2.7.2 Wear and Friction of Hydrogels	42
2.7.3 Characterization of Wear	43
2.7.4 Crossing-Paths Wear	45
2.8 High Frequency 3D Ultrasound Imaging	46
2.9 Motivation for Thesis	47
CHAPTER 3 MATERIALS AND METHODS	48
3.1 Materials	48
3.2 Preparation of PVA and PVA-Nanocomposite Hydrogels	49
3.2.1 Preparation of PVA Solutions	49
3.2.2 Preparation of PVA-Laponite Solutions	50
3.2.3 Preparation of PVA-BC Solutions	50
3.2.4 Pouring Solutions in to Moulds	52
3.2.5 Freeze-Thaw Cycling	52
3.2.6 Aging in Water and Solutions	52
3.3 Structure Studies	53
3.3.1 Scanning Electron Microscopy	53
3.3.1.1 Critical Point Drying	53
3.3.1.2 Scanning Electron Microscopy	54
3.3.2 Differential Scanning Calorimetry	54
3.4 Mechanical Testing	55
3.4.1 Unconfined Compression	55
3.4.2 Stress Relaxation	56
3.4.3 Creep	57
3.4.3.1 Creep Modelling	57

3.4.4 Cyclic Compression Testing _____	59
3.5 Crossing-Path Wear _____	60
3.5.1 Three-Dimensional Ultrasound for Characterization of Wear _____	63
3.5.2 Scanning Electron Microscopy _____	64
3.6 Two-Component Hydrogel IVD Structure _____	64
3.6.1 Mould Design _____	65
3.6.2 Two-Component Hydrogel Disc _____	65
3.6.3 Compression Testing of Two-Component Hydrogel Disc _____	66
3.7 Statistics _____	66
CHAPTER 4 COMPRESSION PROPERTIES OF PVA AND PVA-NANOCOMPOSITE HYDROGELS _____	67
4.1 Composition and Structure of Hydrogels _____	68
4.1.1 Laponite _____	69
4.1.2 Bacterial Cellulose _____	69
4.1.3 Water Content of Solutions and Hydrogels _____	70
4.1.4 Porous Structure of Hydrogels _____	71
4.1.5 Aging of Hydrogels in Water and PBS _____	73
4.1.5.1 Decrease in Mass and Volume _____	74
4.1.6 Crystallinity of Hydrogels _____	76
4.2 Unconfined Compression of Hydrogels _____	77
4.2.1 PVA Concentration _____	78
4.2.2 Nanofiller Addition _____	79
4.2.3 Effect of Aging in Water and PBS _____	81
4.2.4 Strain Rate Dependence _____	84
4.3 Stress Relaxation and Creep _____	87
4.3.1 Stress Relaxation _____	87
4.3.2 Creep _____	89
4.4 Cyclic Compression Testing _____	95
4.5 Discussion _____	95
4.5.1 Structure of PVA and PVA-NC Hydrogels _____	95
4.5.2 Compression Properties _____	100
4.5.3 Strain Rate Dependence _____	105
4.5.4 Stress Relaxation and Creep _____	106
4.5.5 Cyclic Compression Testing _____	109
4.5.6 Comparison to the Natural IVD and Application to IVD Device Design _____	110
4.5.7 Proposed PVA Hydrogel IVD Design _____	115

4.6 Concluding Remarks _____	119
CHAPTER 5 TRIBOLOGY TESTING OF PVA AND PVA-NANOCOMPOSITE HYDROGELS	120
5.1 Crossing-Paths Wear Testing _____	120
5.2 Volume and Depth of Wear Track _____	121
5.3 Wear Track Surfaces and Substructure _____	123
5.3.1 Surface of Unworn Areas _____	126
5.3.2 Wear Track Surfaces _____	126
5.3.2.1 PVA Hydrogels _____	128
5.3.2.2 PVA-NC Hydrogels _____	129
5.3.3 Subsurface Structure _____	131
5.4 Discussion _____	133
5.5 Concluding Remarks _____	147
CHAPTER 6 DESIGN OF A MULTI-COMPONENT PVA HYDROGEL-BASED CERVICAL IVD PROSTHESIS	149
6.1 IVD Prototype Composition _____	149
6.2 Unconfined Compression _____	151
6.2.1 Strain Rate Dependence _____	151
6.3 Stress Relaxation and Creep _____	155
6.4 Discussion _____	157
6.4.1 Prototype Design and Performance _____	157
6.4.2 Parameters for Optimization of Properties _____	166
6.4.3 Implementation of a Hydrogel-Based IVD Device _____	169
6.5 Concluding Remarks _____	171
CHAPTER 7 CONCLUSIONS AND FUTURE WORK	173
7.1 Conclusions _____	173
7.2 Future Work _____	175
BIBLIOGRAPHY	178
APPENDIX A PBS PREPARATION	201
APPENDIX B ENERGY-DISPERSIVE X-RAY SPECTROSCOPY OF PHOSPHORYLATED-BACTERIAL CELLULOSE	204
APPENDIX C PROCEDURE FOR FITTING OF UNCONFINED COMPRESSION DATA	207

APPENDIX D SAMPLE HOLDER FOR CROSSING-PATHS WEAR TESTER	210
APPENDIX E MATLAB PROGRAM EXTRACTING ULTRASOUND IMAGES	212
APPENDIX F COPYRIGHT PERMISSIONS	214
CURRICULUM VITAE	222

LIST OF TABLES

Table 2.1: Amount of water, collagen, proteoglycans and cells in each component in the intervertebral disc structure. Collagen and proteoglycans are reported as percentages of the dry weight. _____	8
Table 2.2: Compressive force acting on cervical discs in various neck positions as calculated and presented by Cripton et al. [50] based on pressures measured inside the discs [52, 53] using Nachemson's relationship [54] and disc dimensions from Pooni et al. [36]._____	10
Table 2.3: Orientation and location dependence of tensile moduli of human lumbar annulus fibrosus from non-degenerated intervertebral discs. Data from Elliott and Setton [67] with additional data from Guerin and Elliott [68] for the outer circumferential AF. _____	14
Table 2.4: Compressive moduli from unconfined compression of freeze-thaw PVA hydrogels in the literature. _____	27
Table 3.1: PVA and PVA-NC solution compositions. _____	49
Table 3.2: Composition of the 25% alpha calf serum (ACS) lubricant for crossing-path wear testing. _____	61
Table 4.1: Water contents of unfilled PVA and 10% PVA-NC solutions and hydrogels (n=5) after 6 FTC. _____	71
Table 4.2: Tangent and secant moduli of fresh PVA hydrogels at 0.25 and 0.45 strain tested at a strain rate of 100%/s. _____	79
Table 4.3: Tangent and secant moduli of fresh Laponite-filled 10% PVA-NC hydrogels at 0.25 and 0.45 strain tested at a strain rate of 100%/s. _____	80
Table 4.4: Tangent and secant moduli of fresh BC and pBC-filled 10% PVA-NC hydrogels at 0.25 and 0.45 strain tested at a strain rate of 100%/s. _____	81
Table 4.5: Change in tangent and secant modulus at 0.45 strain after one week of aging in water and PBS for unfilled PVA hydrogels tested at 100%/s. _____	101
Table 4.6: Change in tangent and secant modulus at 0.45 strain after one week of aging in water and PBS for 10% PVA-NC hydrogels tested at 100%/s (- indicates no statistical change)._____	103

Table 4.7: Parameters of elastic and viscous components from fitting of the three-parameter-solid model to creep data from unfilled PVA and 10% PVA NC hydrogels after aging in PBS, and of human lumbar IVD and PVA hydrogels from literature. _____	114
Table 5.1: Comparison of hydrogel wear depth and volume measurements from the literature and current study. _____	137
Table 6.1: Statistical differences in load at 0.25 strain found between strain rates for the two-component and single component PVA hydrogels ($p < 0.05$). _____	153
Table 6.2: Slopes from linear fits of percent change in load from 1%/s at 0.25 strain to logarithm of strain rate of two-component and single component PVA hydrogels, and canine IVD. (R^2 values of the fits are shown in parentheses.) _____	154

LIST OF FIGURES

Figure 2.1: Human vertebral column (Gray, 1918) [32] (a). IVDs are found between vertebrae in the cervical, thoracic and lumbar regions with the exception of C1 and C2. Anatomy of a cervical vertebra depicting nerve impingement due to herniated NP and joint degeneration (b); reproduced with permission from [33], Copyright Massachusetts Medical Society. _____	5
Figure 2.2: Structure of the intervertebral disc, consisting of the annulus fibrosus, nucleus pulposus and endplate, and attached to the vertebral body. Adapted from [35]. _____	6
Figure 2.3: Shape of cervical, thoracic and lumbar IVD. Redrawn from Pooni et al. [36]. _____	7
Figure 2.4: Stress-strain data of oxtail IVDs displaying low modulus toe regions and loading rate dependence [57]. Reprinted with permission from Race A, Broom ND, Robertson P. Effect of loading rate and hydration on the mechanical properties of the disc. Spine. 2000;25(6): 662–669. _____	11
Figure 2.5: Artificial cervical disc replacements: Prestige ST (A), Bryan (B), Prodisc-C (C) [77]. Reprinted with permission from Anderson PA, Rouleau JP. Intervertebral disc arthroplasty. Spine. 2004;29(23):2779–86. _____	18
Figure 2.6: Schematic of PVA hydrogel structure produced by freeze-thaw cycling as determined by SANS. Cycle 0 represents the PVA solution before thermal cycling. Reprinted with permission from [105]. Copyright 2007 American Chemical Society. _____	24
Figure 3.1: Stainless steel platens in a temperature-controlled bath used in compression testing of hydrogel cylinders. _____	55
Figure 3.2: Spring (E_i) and dashpot (η_i) models for viscoelastic creep; the “three-parameter-solid” model (a), Burger’s model (b) and Bausch model (c). _____	58
Figure 3.3: Front view (left) and top view (right) of a retrofitted wear pod set up for crossing-paths wear testing. _____	60
Figure 3.4: Pin for crossing-paths wear testing consisting of a sapphire sphere counter surface glued with epoxy to an acrylic post. _____	61
Figure 3.5: Aluminum backing glued to the underside of a hydrogel sample with rubber toughened cyanoacrylate to prevent wear on the bottom surface. _____	62

Figure 3.6: Set-up for 3D ultrasound imaging of the hydrogel samples after crossing-paths wear testing. The linear motor translated the ultrasound probe to acquire successive B-mode image planes for 3D images. _____	64
Figure 3.7: Schematic of the two-component hydrogel disc, 7 mm in thickness, consisting of an outer annulus component of 20 mm outer diameter and an inner nucleus component of 8 mm diameter. (All measurements in the diagram are in millimetres.) _____	65
Figure 4.1: TEM of spin-coated 10% PVA solution with 1% Laponite showing dispersion of discrete discs, and agglomerated stacks (indicated by arrows). _____	69
Figure 4.2: TEM of bacterial cellulose (a) and phosphorylated bacterial cellulose (b) prepared from dispersions in water. _____	70
Figure 4.3: SEM of fractured cross-sections of critical point dried unfilled 10% PVA (a), 15% PVA (b), and 20% PVA hydrogels (c). _____	72
Figure 4.4: SEM of 0.75% (a) and 1% (b) Laponite-filled 10% PVA NC hydrogel fractured cross-sections. _____	72
Figure 4.5: SEM of fractured cross-sections of 0.48% BC (a), 0.25% pBC (b), and 0.4% pBC (c) in 10% PVA. _____	73
Figure 4.6: Profile of decreasing mass (a) and volume (b) of hydrogels over 7 days of aging in water and PBS (0.48% BC-10% PVA-NC hydrogels shown). Mass and volume are expressed as fractions of their initial values. _____	74
Figure 4.7: Mass (a) and volume (b) after 7 days of aging in water and PBS for unfilled PVA and 10% PVA-NC hydrogels, expressed as fractions of their initial values. All samples experienced decreases in mass and volume. _____	75
Figure 4.8: Crystallinity determined by DSC in dried PVA in unfilled PVA and 10% PVA-NC hydrogels. _____	76
Figure 4.9: Effect of PVA concentration on stress-strain curves from unconfined compression of fresh unfilled PVA hydrogels, tested in 37 °C water at a strain rate of 100%/s. _____	78
Figure 4.10: Effect of Laponite addition on the stress-strain curves of fresh 10% PVA hydrogels, tested in 37 °C water at a strain rate of 100%/s. _____	79
Figure 4.11: The effect of BC and pBC addition on fresh 10% PVA hydrogels, tested in 37 °C water at a strain rate of 100%/s. The stress-strain curves of 10% and 20% PVA highlights the difference in shape from those of BC- and pBC-filled hydrogels. _____	80

Figure 4.12: Tangent (a) and secant (b) moduli of unfilled PVA hydrogels at 0.45 strain, tested at a strain rate of 100%/s fresh, and after one week of aging in water and PBS. _____	82
Figure 4.13: Tangent (a) and secant (b) moduli of 10% PVA-NC hydrogels at 0.45 strain, tested at a strain rate of 100%/s fresh, and after one week of aging in water and PBS. _____	83
Figure 4.14: Stress-strain curves of 1% Laponite-10% PVA hydrogels, tested after one week of aging in PBS at strain rates of 1, 10 and 100%/s, demonstrating strain rate dependent behaviour. _____	84
Figure 4.15: Linear relationship between change in stress from 1%/s and logarithm of strain rate. The slope was used to quantify the degree of strain rate dependence. Fits for 1% Laponite-10% PVA hydrogels, tested fresh, and after aging for 7 days in water and PBS, are shown. _____	85
Figure 4.16: Degree of strain rate dependence at 0.45 strain for unfilled PVA (a) and 10% PVA-NC (b) hydrogels. Linear fits have R^2 of at least 0.8225. ^o No statistical difference in stress at 0.45 strain between strain rates of 1%/s and 10%/s. ^x No statistical difference in stress at 0.45 strain between strain rates of 10%/s and 100%/s. _____	86
Figure 4.17: Stress relaxation at 0.25 strain of unfilled PVA hydrogels in PBS. Increased PVA concentration resulted in decreased stress relaxation. _____	88
Figure 4.18: Stress relaxation at 0.25 strain of Laponite-containing 10% PVA-NC hydrogels in PBS in comparison to 10% PVA. Addition of Laponite resulted in increased stress relaxation. _____	88
Figure 4.19: Stress relaxation at 0.25 strain of BC and pBC-containing 10% PVA-NC hydrogels in PBS compared to 10% PVA. Addition of BC and pBC resulted in increased stress relaxation. _____	89
Figure 4.20: Stress remaining after one hour of stress relaxation at 0.25 strain in unfilled PVA (a) and 10% PVA-NC hydrogels (b) tested fresh in water, and after 7 days of aging in PBS. _____	90
Figure 4.21: Creep data of a 10% PVA sample tested fresh in 37 °C water at a constant stress of 0.05 MPa, and fitted with the three-parameter-solid, and the four-parameter Burger's and Bausch viscoelastic models. _____	91
Figure 4.22: Creep curves of unfilled PVA hydrogels in 37 °C PBS at a stress of 0.05 MPa for one hour. Increased PVA concentration results in reduction of the initial strain and creep. _____	92

Figure 4.23: Creep of Laponite-filled hydrogels compared to 10% PVA in 37 °C PBS at a stress of 0.05 MPa for one hour. Addition of Laponite resulted in increased creep. _____	92
Figure 4.24: Creep of BC and pBC-filled hydrogels compared to 10% PVA in 37 °C PBS at a stress of 0.05 MPa for one hour. Addition of BC and pBC resulted in increased creep. _____	93
Figure 4.25: Percent increase in strain after creep testing at 0.05 MPa stress for one hour. The increase of PVA concentration (a) decreased creep, while the addition of nanofillers into 10% PVA (b) increased the amount of creep in the hydrogels. _____	94
Figure 4.26: $\tan \delta$ for unfilled PVA (a) and 10% PVA-NC (b) hydrogels aged and tested in PBS. Viscous damping increased as strain frequency was increased, and with increases in polymer concentration and nanofiller addition. _____	96
Figure 4.27: Linear relationship of stress to water content in unfilled PVA and 10% PVA-NC hydrogels, fresh and after aging in water and PBS (strain: 0.45, strain rate: 100%/s). Hydrogels filled with the high aspect ratio BC and pBC were stiffer than unfilled and Laponite-filled hydrogels relative to its water content. _____	104
Figure 5.1: Schematic of crossing-paths wear testing on PVA and PVA-NC hydrogel surfaces. The 9.525 mm diameter spherical sapphire counter surface pin was translated linearly over a length of 8.5 mm and rotated over 28° for each stroke under a normal load of 5 N. Each sample was tested at a frequency of 1 Hz for 500 000 cycles. _____	121
Figure 5.2: B-mode plane from 3D US showing the flat surface of 10% PVA hydrogel before testing (a), outlining of the indent on the top surface of the hydrogel to determine area using the polygon function in ImageJ (b), and a schematic of indent outlining (c). _____	122
Figure 5.3: B-mode images from 3D US of hydrogels showing the cross-sections of wear tracks in 10% PVA (a), 20% PVA (b), and nanocomposites of 10% PVA with 1% Laponite (c), 0.48% BC (d) and 0.4% pBC (e). _____	122
Figure 5.4: Volume of the indent created after crossing-paths wear testing on unfilled PVA hydrogels (a) and 10% PVA-NC hydrogels (b), measured using ImageJ on 3D US image planes. Wear testing was performed under a normal load of 5 N with a linear reciprocating stroke length of 8.5 mm and 28° pin rotation at 1 Hz for 500 000 cycles. The spherical sapphire counter surface was 9.525 mm in diameter. _____	124
Figure 5.5: Maximum depth of wear tracks after crossing-paths wear testing on unfilled PVA hydrogels (a) and 10% PVA-NC hydrogels (b), measured	

- from 3D US image planes using ImageJ. Wear testing was performed under a normal load of 5 N with a linear reciprocating stroke length of 8.5 mm and 28° pin rotation at 1 Hz for 500 000 cycles. The spherical sapphire counter surface was 9.525 mm in diameter. _____ 125
- Figure 5.6: Schematic showing the unworn portion of the hydrogel, and middle and ends of the wear track (a), and a photograph of a hydrogel sample immediately after wear testing (b). The wear track was slightly yellow in colour from the ACS lubricant and the ends of the wear track were more indented than in the middle. _____ 126
- Figure 5.7: SEM of critical point dried unworn sections of hydrogel samples after crossing-paths wear testing: 10% PVA (a), 20% PVA (b), and 10% PVA-NC filled with 1% Laponite (c), 0.48% BC (d), 0.25% pBC (e) and 0.4% pBC (f). Debris on the hydrogel surfaces was likely material worn away from wear testing. _____ 127
- Figure 5.8: SEM of the middle (left column) and end (right column) portions of the wear track surfaces of critical point dried the 10% PVA hydrogel (a, b) and 20% PVA hydrogel (c, d). Arrows indicate the direction of linear reciprocation. _____ 128
- Figure 5.9: SEM of the middle (left column) and end (right column) portions of the wear track surfaces of critical point dried 10% PVA-NC hydrogels filled with 1% Laponite (a, b), 0.48% BC (c, d), 0.25% pBC (e, f) and 0.4% pBC (g, h). Arrows indicate the direction of linear reciprocation. _____ 130
- Figure 5.10: SEM images of liquid nitrogen freeze-fractured, critical point dried hydrogel cross-sections under the wear track of unfilled 10% PVA (a) and 20% PVA (b), and 10% PVA-NC containing 1% Laponite (c), 0.48% BC (d), 0.25% pBC (e) and 0.4% pBC (f). Pores under the wear tracks were collapsed and deformed in 10% PVA and 10% PVA-0.25% pBC. _____ 132
- Figure 5.11: Wear volume versus secant modulus (1%/s strain rate) for unfilled PVA hydrogels and 10% PVA-NC hydrogels in PBS. Wear volume decreased with increased PVA concentration as 10% PVA-based hydrogels had significantly greater wear volumes compared to 15% and 20% PVA hydrogels. _____ 134
- Figure 5.12: Examples of deviations from flatness at the surface of hydrogels in B-mode 3D US planes away from the wear track: 10% PVA showing a slightly irregular surface (a), 0.75% Laponite in 10% PVA with convexity at the surface (b), and 0.4% pBC in 10% PVA with concavity at the surface (c). _____ 136
- Figure 6.1: Photograph of the two-component PVA hydrogel prototype with concentric 20% PVA annulus and 10% PVA nucleus components. The dotted circle delineates the interface between the two components. _____ 150

Figure 6.2: Data from unconfined compression of the 20%/10% PVA two-component hydrogel (Sample 1) at strain rates between 0.001%/s and 100%/s (a), and the data from 0.001%/s fitted with the 5-parameter exponential growth model (b). The model was not able to fit the toe region between 0 to 0.02 strain. _____	152
Figure 6.3: Average loading curves from unconfined compression of the 20%/10% PVA two-component hydrogel, tested at strain rates from 0.001%/s to 100%/s. _____	153
Figure 6.4: Linear relationship between change in load at 0.25 strain from 1%/s and logarithm of strain rate for the 20%/10% PVA two-component hydrogel prototype. _____	154
Figure 6.5: Stress relaxation at 0.25 strain of the 20%/10% PVA two-component hydrogel prototype after 1 h was decreased compared to 10% and 20% PVA. _____	155
Figure 6.6: The four-parameter viscoelastic models and the double exponential model provided better fits than the three-parameter-solid viscoelastic model for Sample 1 of the 20%/10% PVA two-component hydrogel prototype (a). The average creep curves for the two-component hydrogel prototype under an axial load of 40 N, and for 20% and 10% PVA under an applied stress of 0.05 MPa (b). _____	156
Figure 6.7: Experimental load-strain curves of the 20%/10% PVA two-component hydrogel prototype compared to predictions from the Voigt model (a), and 20% PVA of the same cross-sectional area as the two-component prototype (b). The two-component hydrogel was capable of supporting higher loads than predicted in both instances. _____	161

LIST OF APPENDICES

Appendix A	PBS Preparation _____	201
Appendix B	Energy-Dispersive X-Ray Spectroscopy of Phosphorylated- Bacterial Cellulose _____	204
Appendix C	Procedure for Fitting of Unconfined Compression Data _____	207
Appendix D	Sample Holder for Crossing-Paths Wear Tester _____	210
Appendix E	MATLAB Program for Extraction of Ultrasound Images _____	212
Appendix F	Copyright Permissions _____	214

LIST OF ABBREVIATIONS

3D	Three-dimensional
ACS	Alpha-calf serum
AF	Annulus fibrosus
ANOVA	Analysis of variance
B-mode	Brightness-mode
BC	Bacterial cellulose
BSA	Bovine serum albumin
CLSM	Confocal laser scanning microscopy
CNT	Carbon nanotubes
CoCr	Colbalt chromium alloy
COF	Coefficient of friction
DMSO	Dimethyl sulfoxide
DSC	Differential scanning calorimetry
F-T	Freeze-thaw
FDA	United States Food and Drug Administration
FOV	Field of view
FTC	Freeze-thaw cycle
FTIR	Fourier transform infrared spectroscopy
HA	Hyaluronic acid
HAp	Hydroxyapatite
HO	Heterotropic ossification
IVD	Intervertebral disc
Lap	Laponite
Mc	Million cycles
MMT	Montmorillonite
NC	Nanocomposite
NMR	Nuclear magnetic resonance spectroscopy
NP	Nucleus pulposus
NSAID	Non-steroidal anti-inflammatory drug
PAAc	Poly(acrylic acid)
pBC	Phosphorylated bacterial cellulose
PBS	Phosphate buffered saline
PEG	Poly(ethylene glycol)
PEO	Poly(ethylene oxide)
PET	Poly(ethylene terephthalate)
PG	Proteoglycan
PEEK	Polyetheretherketone
pHEMA	Poly(2-hydroxyethyl methacrylate)
PMMA	Poly(methyl methacrylate)

PVA	Poly(vinyl alcohol)
PVP	Poly(vinyl pyrrolidone)
SANS	Small angle neutron scattering
SAXS	Small angle x-ray scattering
SEM	Scanning electron microscopy
TDR	Total disc replacement
TEM	Transmission electron microscopy
UHMWPE	Ultrahigh molecular weight polyethylene
US	Ultrasound imaging
UV-Vis	Ultraviolet-visible spectrophotometry
XRD	X-ray diffraction

LIST OF SYMBOLS

A	Cross-sectional area, mm ²
E_i	Spring constant of spring element i in viscoelastic models
E_{secant}	Secant modulus, MPa
$E_{tangent}$	Tangent modulus, MPa
F	Load, N
f	Percentage of dry mass in hydrogels, %
h	Height, mm
m	Mass, g
M_n	Number average molecular weight, g/mol
r	Radius, mm
R_a	Average roughness, nm or μm
t	Time, seconds or hours
V	Volume, mm ³
W	Dry weight of hydrogels, %
X	Crystallinity, %
δ	Phase shift angle, rad
ΔH_m	Heat of melting, J/g
ε	Strain
η_i	Viscosity of dashpot element i in viscoelastic models
σ	Stress, MPa

Chapter 1

INTRODUCTION

1.1 BACKGROUND AND MOTIVATION

Neck and back pain affects many adults [1], leading to work absenteeism [2], disability claims [3, 4] and decreased quality of life [5]. Diseases of the intervertebral discs (IVD) are among the causes of neck and back pain [6, 7], which are becoming increasingly important in an aging population. IVDs maintain the space between vertebrae, allow for motion in the spine, distribute and transfer load to the vertebrae, and provide shock absorption [8]. IVDs are highly hydrated, and have low cell numbers and little to no vascularity [6]. Therefore, if they are injured or diseased, they have limited abilities to heal and regain function. The focus of this thesis is in developing a material for cervical IVD replacement.

Degenerative changes of the IVD include disc prolapse, endplate damage and loss of disc height [6]. Spinal fusion remains the gold standard for surgical treatment, but segmental motion is removed [7]. An emerging treatment alternative is artificial disc replacement, which preserves segmental motion at the affected level. However, clinically available devices are comprised of materials that bear little resemblance in mechanical properties to the native tissue. These treatments may lead to degeneration of the adjacent discs or failure of the implant, requiring further intervention [9].

Poly(vinyl alcohol) (PVA) is a biocompatible hydrophilic polymer that can be physically crosslinked to form a hydrogel, without potentially toxic chemical crosslinkers that could leach out if left unreacted [10]. PVA hydrogels can be formed to mimic the water content and mechanical properties of biological tissues [11, 12]. Many works, in-

cluding those from our group, have demonstrated the use of low temperature thermal cycling to produce PVA hydrogels for cardiovascular [11-16], orthopedic [17-25] and drug delivery applications [26, 27]. Parameters such as polymer concentration [23], number of freeze-thaw cycles [11, 23] and filler addition [13, 24, 28, 29] allow for highly tunable properties in PVA-based hydrogels.

Nanocomposites (NC) are a class of materials in which at least one of the components possess a dimension in the nanometer range. Nanofillers have a very high surface area to volume ratio due to their small dimensions. Since properties of a composite depend on the properties of its components and their interfaces, only a small amount of nanofiller is required to significantly modify the properties of a matrix material [30]. Two different nanofillers were added to PVA hydrogels in this thesis to investigate the effect of filler aspect ratio on hydrogel properties: Laponite, a low aspect ratio, synthetic inorganic clay; and bacterial cellulose, a high aspect ratio nanofibre derived from *Acetobacter xylinum* fermentation.

This work investigated the effects of PVA concentration and nanofiller addition on the compression and wear properties of hydrogels relevant to cervical IVD applications. Furthermore, a PVA hydrogel structure comprised of components of different PVA concentrations was produced to demonstrate that a coherent multi-component structure could be fabricated for a potential IVD replacement.

1.2 OBJECTIVES

The main objective of this thesis was to determine the effects of composition on PVA and PVA-NC hydrogels with the goal of designing materials for potential applications in cervical IVD replacements.

The specific objectives were:

1. To determine the effects of increasing PVA concentration, and adding Lapo-nite and bacterial cellulose on the compression properties of PVA hydrogels (Chapter 4)
2. To characterize the effects of crossing-paths wear as a function of PVA con-centration and nanofiller addition, which included the development of a wear measurement technique using high frequency three-dimensional ultrasound imaging to quantify wear in soft materials such as PVA hydrogels (Chapter 5)
3. To design a coherent, multi-component PVA-based hydrogel device based on the native IVD structure (Chapter 6)

Chapter 2

LITERATURE REVIEW

This chapter will examine the background and motivation behind the proposed treatment of severe cervical intervertebral disc disease by surgical replacement with a PVA hydrogel-based IVD prosthesis. In order to develop a set of design criteria for the hydrogel material to be used in an artificial IVD, the properties of natural IVDs and cervical total disc replacements (TDR) approved by the US FDA are reviewed. Literature on PVA hydrogels and nanocomposites, as well as on potential nanofillers – particularly Laponite and bacterial cellulose – and consideration of the use of these materials in orthopedic devices are surveyed. This was done to demonstrate the suitability of PVA hydrogels for IVD applications and to gain insight into how the materials could be combined and tailored to achieve the desired properties for implementation in an IVD replacement device. Furthermore, since articulating surfaces are found in all clinically available cervical TDRs, possible designs for a PVA hydrogel-based device could also incorporate articulation in which wear must be minimized. Therefore, methods and results of characterizing wear of hydrogels, and the usage of three-dimensional ultrasound to image PVA hydrogels are presented.

2.1 PREVALENCE OF NECK AND BACK PAIN

Neck and back pain, which affects 70–85% of adults at some point in their lives [1, 5, 7], is the second most common cause of disability in the United States [1] and impacts quality of life [5]. A 2002 US national survey found that within a three month period, 4% of adults had experienced neck pain, 17% had low back pain, and 9% had both

[1]. Annual prevalence of neck pain in workers ranged from 11.0% in the United Kingdom to 47.8% in Québec, Canada [3], and limits work activities of up to 14.1% of workers [2]. Work absenteeism accounted for up to 11.3% of all insurance claims with the Ontario Workplace Safety & Insurance Board [3]. Risk factors for neck and back pain include age, gender, ethnicity, health factors, activity levels, work conditions and socioeconomic status [1, 3, 31].

2.2 INTERVERTEBRAL DISCS

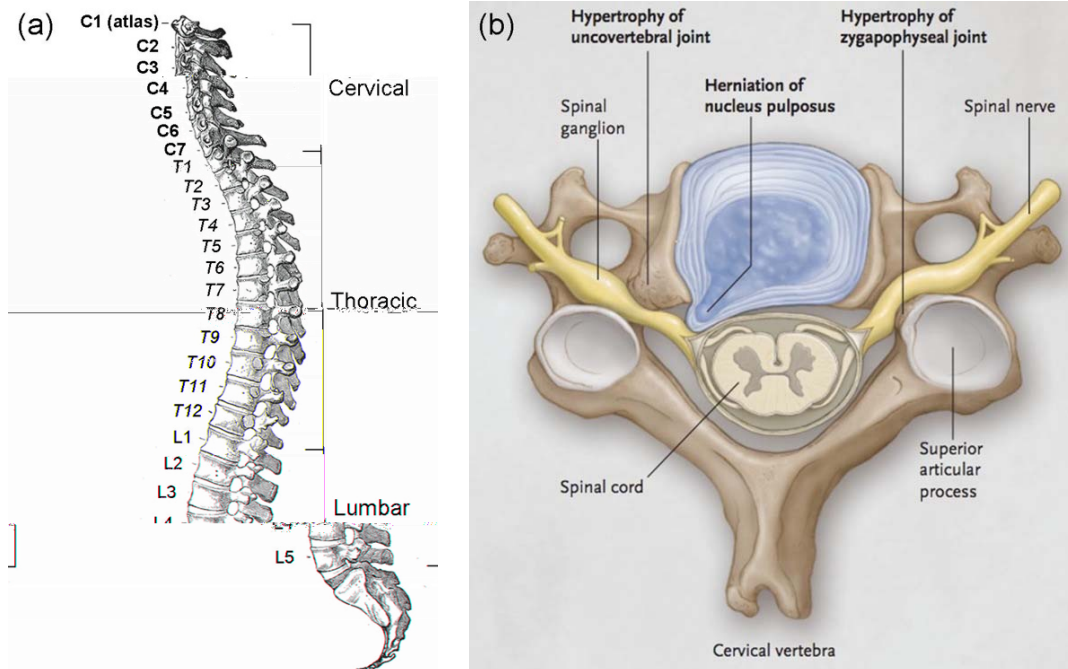


Figure 2.1: Human vertebral column (Gray, 1918) [32] (a). IVDs are found between vertebrae in the cervical, thoracic and lumbar regions with the exception of C1 and C2. Anatomy of a cervical vertebra depicting nerve impingement due to herniated NP and joint degeneration (b); reproduced with permission from [33], Copyright Massachusetts Medical Society.

IVDs are found between vertebrae in three regions of the vertebral column – cervical, thoracic and lumbar (Figure 2.1), except for between C1 and C2 in the cervical region. Along with the facet joints posterior to the disc, which limit the degree of mobility and protect the disc from shear stresses, IVDs allow for motion and articulations in the

spine [34]. IVD functions include maintaining disc space, allowing for flexion, extension, rotation and lateral bending between vertebral segments, transferring load to the vertebral bodies and absorbing shock [8]. This review focuses on axial compression properties and cervical IVDs, where data is available. However, lumbar discs have been more commonly studied in the literature.

2.2.1 Intervertebral Disc Anatomy

IVDs are cartilaginous in nature and consist of the nucleus pulposus (NP), annulus fibrosus (AF) and endplates (Figure 2.2). They are composed of varying quantities of water, proteoglycans (PG), collagen and cells.

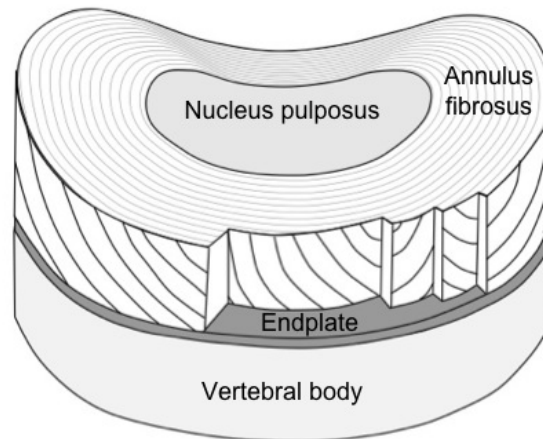


Figure 2.2: Structure of the intervertebral disc, consisting of the annulus fibrosus, nucleus pulposus and endplate, and attached to the vertebral body. Adapted from [35].

IVDs differ in shape between regions in the vertebral column (Figure 2.3). In the cervical spine, cross-sectional areas of human cervical IVD range from 200 mm^2 at C2–3 to 400 mm^2 at C6–7 [36]. Panjabi reported that the width and depth of cervical discs to be 16.0–23.5 mm and 12.0–18.0 mm, respectively. Cervical disc height is approximately 7 mm [37], but varies from 4.5 to 6.5 mm in cadaveric specimens [38].

Pooni et al. found that the NP cross-sectional area in a cervical disc was approximately 100 to 200 mm^2 [36], though this is unlikely to be constant through the thickness

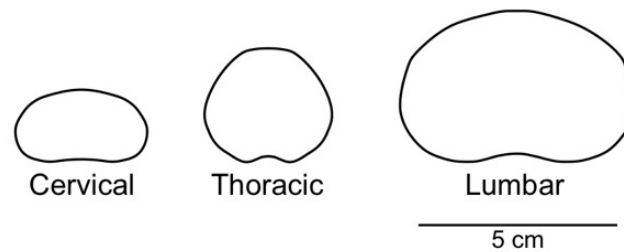


Figure 2.3: Shape of cervical, thoracic and lumbar IVD. Redrawn from Pooni et al. [36].

of the disc. Within a healthy disc, the NP has a swelling pressure of 0.1–0.2 MPa in a recumbent position and up to 1–3 MPa when standing or lifting [35], and supports load through hydrostatic pressure. Its dry weight is made up of proteoglycans (PGs) held in a collagen type II network. The major component of PGs is aggrecan, composed of glucosaminoglycans (GAGs) such as keratin sulphate and chondroitin sulphate [6, 37]. Chondroitin sulphate possesses both sulphate and carboxylic acid groups, which enhances its water binding ability [37]. These fixed negative charges provide the osmotic potential that allows the tissue to swell, maintain pressure during loading and re-swell after load removal.

The AF resembles fibrocartilage, and has highly organized layers of type I collagen, the structure of which depends on the location of the disc [35, 37]. The AF experiences tensile loads from the pressurized NP when an IVD is loaded axially, but can also withstand direct loading due to bending, rotation and translation.

The endplates are calcified adjacent to the bone and hyaline in nature towards the disc [35]. Their average thickness is approximately 0.6 mm and thinnest at the centre [39]. Endplates allow for nutrients, proteins, waste, and water diffusion and transport into and out of the disc through marrow contact channels [40] and capillaries [41]. Fluid flow occurs primarily through the endplates into vertebral bodies. Since the IVD supports loads through hydrostatic pressure arising from the NP, and there is approximately 20% volumetric reduction each day due to water loss that is recovered with rest [42], transport of fluid through the endplates is important to the performance of the disc. The

resistance to flow is directional in isolated endplates; flow out of the disc is an order of magnitude higher than into the disc, such that load bearing could be achieved through the increase of hydrostatic pressure, and allows for rehydration of the disc during rest [40]. Resistance increased for outward flow is a result of poroelastic compressive strain and loss of fluid. The endplate is also selective to size and charge, impeding movement of large proteins and enzymes, as well as negatively charged ions such as sulphates and chlorides [43].

The proportion of extracellular matrix and cellular components in the IVD differs and is related to its function. The relative proportions of water, collagen, PGs and cells in the NP, AF and endplates are summarized in Table 2.1.

Table 2.1: Amount of water, collagen, proteoglycans and cells in each component in the intervertebral disc structure. Collagen and proteoglycans are reported as percentages of the dry weight.

Component	Nucleus pulposus [35, 37]	Annulus fibrosus [35]	Endplates [39, 44, 45]
Water	70–90%	70–78%	54.1–57.5, 60.4%
Collagen	20%	60–70%	65.6–66.4%
Proteoglycans	30–50%	10%	15.1–19.6%
Cell density	4×10^6 cells/cm ³	9×10^6 cells/cm ³	250–325 cells/mm ² (observed optically)

With aging, water content decreases to approximately 70% in both the NP and AF [37], the demarcation between the two becomes less apparent and disc height decreases [35]. In the NP, collagen content increases along with a decrease in the amount and molecular weight of PG aggregates [6] as it becomes more solid than fluid-like [35]. A loss in pressurization in the disc may result in the inward bulging of the AF and load in compression rather than tension [35]. Defects, such as cracks and fissures, and degeneration of the AF layers develop, which can further compromise the integrity of the disc and can lead to disc prolapse [6]. Exposed nucleus material, previously protected in an avascular environment, may elicit an inflammatory response following prolapse [34]. The endplates may become more loaded at the peripheries from the AF, which can lead to fracture [35], allow the NP to bulge into vertebral bodies at high loads [6], or become separated from the vertebral body [43]. Endplates may also become less porous, inhibiting

the transport of fluid, nutrient and waste and leading to chemical and mechanical changes in the disc [34].

2.2.2 Degenerative Disc Disease

Back pain that is severe and chronic is often suspected to be discogenic [46], originating from the degenerated IVD [47], which may be due to disc prolapse, radial fissures in the annulus and internal disc disruption [6]. A compromised IVD structure may lead to innervation towards the nucleus and endplates, compression of surrounding tissue, and abnormal stress distribution across the damaged disc during loading [6, 7]. Degeneration may be caused by aging-related loss of disc hydration, injurious loading, and decrease in nutrient supply and waste removal that affect cell synthesis or result in cell death [7, 35]. In low oxygen conditions, anaerobic cell activity leads to accumulation of lactic acid, inhibiting cell activity [6]. Cells are also sensitive to cyclic loading; an optimum range of loading regimes allows for normal cell function, and maintenance and repair of the extracellular matrix [48]. Mechanically accelerated disc degeneration could occur with immobilization, since loads that are too low reduce cell synthesis, or high rates, magnitudes or frequency of loading that result in disc damage [48, 49]. Disc degeneration could be caused by genetics, aging, nutritional deficit or loading history. It is precipitated by injury or fatigue failure, mediated by abnormal cellular response, and characterized by structural failure of the disc [6]. Degenerative disc disease describes a painful, degenerated disc and typically affects the cervical and lumbar regions of the spine.

2.2.3 Intervertebral Disc Mechanics

Cripton et al. [50] calculated the compressive forces acting on cervical IVDs based on pressures measured inside the discs in various neck positions (Table 2.2). Discs possess an inherent hydrostatic pressure due to confinement of the NP by the AF, and due to forces from ligaments in the spine [51].

Table 2.2: Compressive force acting on cervical discs in various neck positions as calculated and presented by Cripton et al. [50] based on pressures measured inside the discs [52, 53] using Nachemson’s relationship [54] and disc dimensions from Pooni et al. [36].

Neck position	Disc pressure (kPa)	Compressive force (N)
Reclining	310	53
Upright	449	75
Flexion (anterior bending)	590	100
Extension (posterior bending)	910	155

Moduli and maximum stress of IVDs increased from the cervical to lumbar region in a canine model [55]. Moroney et al. [56] tested adult human cervical disc segments and found that stiffness in compression was 492 ± 472 N/mm. The large uncertainty may be due to the various stages of degeneration in the discs, but the age, gender and medical history of the discs were not available to the authors. Degeneration tended to decrease compressive stiffness and increase shear stiffness. Variation in compressive strength of IVDs from 2.8 to 13.0 kN was attributed to adaptive remodeling by Adams and Roughley [6].

2.2.3.1 Compressive Stress-Strain Behaviour and Strain Rate Dependence

The stress-strain curves of IVDs loaded in compression are non-linear, described as having an initial toe region, up to 0.05–0.12 strain [55, 57], of low modulus before reaching the higher modulus linear region (Figure 2.4). This may arise from the straightening of the collagen crimp in the AF when it is loaded in tension, resulting in lateral bulging and the two regions on the stress-strain curve [55]. Physiological strain of the IVD in compression is up to approximately 15% [58].

Strain rate dependence in IVDs was demonstrated by Cassidy et al. [55] using a canine model. Testing at strain rates from 1.67×10^{-5} to 1.67 s^{-1} , moduli in the linear portion of thoracic and lumbar IVD stress-strain curves were 50–130 MPa and maximum stresses were 6.5–19 MPa, and both increased linearly with the logarithm of strain rate. Linear dependence of stress and moduli on the log of strain rate were also demonstrated

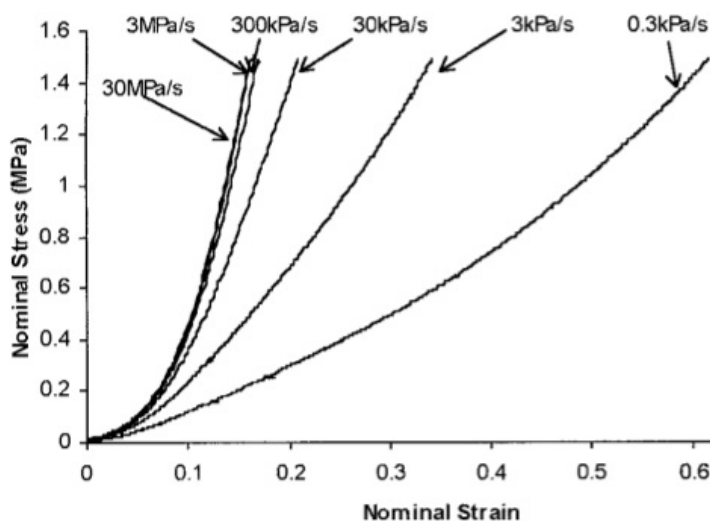


Figure 2.4: Stress-strain data of oxtail IVDs displaying low modulus toe regions and loading rate dependence [57]. Reprinted with permission from Race A, Broom ND, Robertson P. Effect of loading rate and hydration on the mechanical properties of the disc. *Spine*. 2000;25(6): 662–669.

in cartilage [59, 60]. Excised bovine caudal IVDs in compression also showed dependence of final strain and stiffness on loading rates over six orders of magnitude from 0.3 kPa/s to 30 MPa/s [57]. Stiffness of human lumbar IVDs also increased linearly with the log of displacement frequency by 45% from 0.001 to 1 Hz in dynamic compression, while phase angle decreased by 36% [61]. Both fluid flow and viscoelastic effects from the solid matrix were implicated in the frequency dependence of stiffness and phase angle.

Fluid flow depended on the frequency of loading [62]. There was increased transport of water and ions in the centre of the nucleus due to high levels of pressurization at higher loading frequencies (0.1 and 1 Hz) whereas flow was greater at the periphery of the annulus at 0.01 Hz. These results are consistent with the initial bulging of the disc during rapid loading, and subsequent loss and redistribution of fluid, which occurs with slower rates of loading. Depending on the rate of loading, pressurization of fluid serves to enhance the load bearing properties of the disc, while fluid loss contributes to the dissipation of energy. The effect of hydration on compression modulus was also investigated by Race et al. [57]. Controlled fluid loss was induced through creep. While

modulus increased after 30 minutes of creep, the disc became more compliant after two hours of induced fluid loss that resulted in a loss of disc height. This provides evidence that while the initial load bearing mechanism is through fluid pressurization, loss of fluid over time results in the transfer of load to the solid matrix.

2.2.3.2 Stress Relaxation and Creep

Stress relaxation of canine IVDs, tested at 100% humidity, at 0.05 and 0.15 strain resulted in less than 10% of the initial stress remaining after 30 minutes, and 5.1% and 15.1% volume reduction, respectively, due to water loss [55]. However, the discs were tested at 100% humidity rather than immersed in a buffer, which may have affected the rate of water loss as the presence of ions could have an effect on osmotic pressure. The mechanism for stress relaxation was postulated by the authors to be due to the transport of water from the disc through the endplates into the vertebral bodies.

Burns et al. [63] performed creep testing on human thoracic and lumbar spine segments. Equilibrium deformation was not always attained after 8 hours of loading, and permanent deformation occurred. Lumbar discs experienced more creep than ones from the thoracic region, which may have been due to greater disc heights in lumbar discs. The Kelvin model of creep was found to be insufficient for fitting the creep data. Although a four-parameter model, consisting of two parallel Kelvin units, was found to be a better fit for the initial part of the creep curve, the three-parameter-solid model, which consists of a Kelvin unit in series with a spring, was found to be sufficient by the authors.

In human thoracic and lumbar spine segments [64], the greatest deviation of the three-parameter-solid model fit from creep data was in initial part of the curve. The initial strain was approximately 0.1 and increased by 20% after 30 minutes under the estimated body weight. Creep tests were performed in a sealed bag with the vertebral posterior elements and ligaments intact. It was also noted that testing was done immediately after thawing, from an unloaded state, but loading and activities during the day would

decrease disc height and increase stiffness. Therefore, these testing conditions may have underestimated the stiffness and creep resistance of the IVDs.

Degeneration resulted in lowered time-dependent viscoelastic response, leading to an increase in initial strain upon loading followed by lowered creep deformation over time [64, 65]. Swelling pressure in the disc decreased from 1–2 MPa in the normal disc to 0.03 MPa in a degenerate disc, and compression stiffness decreased from 1.0 MPa to 0.4 MPa [35]. These would contribute to the detriment of load bearing and viscoelastic properties. The decrease in swelling pressure is a consequence of a decrease in GAGs, which provide fixed negative charges to maintain an osmotic potential [62, 66].

2.2.3.3 Mechanical Properties of IVD Components

Mechanical properties of the AF, NP and endplates have also been studied. The AF is highly anisotropic and mechanical properties are dependent on location due to orientation and spatial distribution of collagen fibres (Table 2.3). The highest stiffness is in the circumferential direction and in the anterior outer portion of the disc [67, 68]. However, there was no difference in the linear region modulus between the outer and inner portion in the axial direction [67]. The moduli from the toe region of the stress-strain curves, which result from uncrimping of collagen fibres, were not significantly different between locations and orientations.

Collagen fibres in the AF lamellae would orientate towards the direction of loading with tensile strain, decreasing the angle between adjacent lamellae [68]. The change in orientation, along with collagen uncrimping, contributes to the difference between toe and linear region moduli. The tensile toe modulus of outer AF tissue from human lumbar discs in the circumferential direction increased with degeneration to 5.68 MPa, correlating with decreased hydration and possible increase in tissue density [68, 69]. Orientation did not affect the modulus of AF under confined compression. Confined compressive aggregate modulus varied from 0.56 to 1.1 MPa in human lumbar AF, with no significant difference between healthy and degenerated tissue [69]. With degeneration, decrease in

Table 2.3: Orientation and location dependence of tensile moduli of human lumbar annulus fibrosus from non-degenerated intervertebral discs. Data from Elliott and Setton [67] with additional data from Guerin and Elliott [68] for the outer circumferential AF.

Direction	Region of stress-strain curve	Tensile modulus (MPa)	
		Outer	Inner
Circumferential	Toe	2.52 – 2.53	1.70 ± 1.21
	Linear	17.45 – 29.35	5.60 ± 4.67
Axial	Toe	0.27 ± 0.28	0.34 ± 0.21
	Linear	0.82 ± 0.71	0.96 ± 1.17
Radial	Toe	0.19 ± 0.04	–
	Linear	0.45 ± 0.25	–

swelling and non-linearity of the equilibrium stress-strain curve suggest that the AF load bearing mechanism shifted from fluid pressurization to direct loading on the solid matrix.

The NP was characterized as a weak gel, with storage modulus always greater than the viscous loss modulus in rheological studies [8], and stiffness is much lower than that of the AF [70]. The isotropic solid modulus of the NP was calculated from the aggregate [71] and shear moduli [70] to be 0.14 MPa [72]. Dynamic shear stress was found to be frequency dependent, and energy dissipation decreased for degenerated discs due to increased solid-like behaviour [70]. Under unconfined compression between non-porous stainless steel plates, the equilibrium toe and linear moduli of human NP tissue were 3.25 ± 1.56 kPa and 5.39 ± 2.56 kPa, respectively, and relaxation at increments of 0.05 strain was approximately 66% after 5 minutes [73]. The NP supports load mainly by swelling and pressurization within the AF and between the endplates [74], and contributes to load distribution and energy dissipation [70].

Using indentation testing, the stiffness and strength of vertebral endplates were found to be greatest at the posterior and lateral positions and lowest in the centre [75]. Stiffness was between 80 and 175 N/mm, and failure occurred between 60 and 180 N. However, since these tests were performed with the endplate still anchored onto the vertebral bone, the spatially varying endplate thickness and the subsurface bone density may have influenced the results. In confined compression against a porous filter, the aggregate modulus of baboon endplates was found to be 0.44 ± 0.24 MPa [44]. Fluid pressurization was instantaneous with the application of load and decreased with time as load was

transferred to the solid matrix at equilibrium. The authors postulated that fluid pressurization within the endplates is responsible for distributing stress across the endplate, allowing for efficient load transfer from the disc to vertebral bodies.

2.2.3.4 Summary

The AF, NP and endplates in an IVD possess unique material, structural and mechanical properties that are related to the function of each component within the disc. Although the mechanical properties of individual components contribute to disc function, the mechanical properties of the intact IVD are also a function of hydration and the rate at which fluid and ions move in and out. Inherent viscoelasticity of the tissue components, fluid pressurization and transport all likely contribute to time dependent properties in the disc [61]. Hydration, osmotic potential and fluid pressurization of the IVD are important determinants in energy dissipation, load bearing and load distribution in the spine. The NP provides hydrostatic pressure to sustain and distribute load, while increases in disc pressure translate to circumferential tensile loads in the AF. The endplates serve to regulate pressurization through the transport of fluid and ions, as well as maintain nutritional and waste removal requirements to preserve cell population and function in the disc. Loss in hydration decreases disc height and reduces the mobility of the joint. Degenerated discs are characterized by pain, structural deficiencies, decreased swelling pressure and loss of function. Depending on the severity of degeneration, treatment options are available for alleviating clinical symptoms and restoring function.

2.2.4 Current and Emerging Treatments

Discogenic neck pain may require surgical intervention if conservative treatments, such as rest, anti-inflammatory medication, traction and physical therapy [76], are not successful in relieving pain and restoring mobility. Spinal fusion is the current gold standard for surgical treatment, in which bone growth is stimulated to join two adjacent vertebral bodies following removal of the affected disc. It may be performed with an auto-

graft, associated with decreased fusion time but also an increased risk of donor site morbidity, or an interbody cage, which can result in a solid fusion, maintain height and better positioning, but subsidence is a potential complication [76]. While successful in providing stability and removing the cause of pain, fusion also eliminates segmental motion, altering biomechanics and possibly leading to adjacent segment disease [34, 77]. 92% of patients who have received fusion either due to trauma or degenerative changes developed adjacent segment degeneration five years after surgery, pointing to a biomechanical cause rather than inherent degeneration [77].

Other surgical procedures include removal of herniated disc material, without restoring nucleus volume [34], and decompression of the nerves or spinal cord by increasing the spinal canal space. In the cervical spine, fusion was more often performed (87% of initial surgeries) and had a lower rate of reoperation (4.9%) than non-fusion surgical procedures (10%) [78]. Non-fusion procedures are possibly providing symptomatic relief but further treatment would be required as the disease progresses.

NP replacements have been investigated for surgical treatment of degenerative IVD. By intervening before irreparable damage is incurred in the AF, NP replacements could provide proper loading on the annulus to encourage healing. They should be able to transport nutrients to the AF to maintain and promote proper function of the annulus cell population since the AF has minimal vascularity [34]. However, NP replacements cannot be used when the annulus or endplates are compromised. They are also more easily dislodged at the point of insertion [77]. Materials investigated for NP replacements include preformed or partially dehydrated synthetic hydrogels, and injectable elastomers and in situ curable polymers, such as silicone, polyurethane and protein-based hydrogels [79, 80]. In addition, a mechanical articulating lumbar NP replacement constructed from polyetheretherketone (PEEK) is currently being evaluated in clinical studies in the US [81].

Regenerative medicine strategies are being researched to reverse disc regeneration, repair damaged tissue and fabricate a living replacement of the complex IVD struc-

ture. Reviews have been published on the mechanical requirements of tissue engineered discs and disc components [82], mechanobiology and response of cells to mechanical stresses [83], cell types and postnatal development [7], and the use of growth factors in disc regeneration [84]. Using a 3D-printing technique, a structure resembling the IVD was fabricated using degradable polyurethane, resulting in a concave up J-shaped unconfined compressive stress-strain curve that reached a stress of 50 kPa at 0.5 strain [85]. However, the scaffold would not be mechanically sufficient as an IVD replacement on its own.

As an alternative to fusion, artificial total disc replacements (TDR) have been developed to preserve motion following removal of an affected disc.

2.3 CERVICAL ARTIFICIAL DISCS

The goal of artificial disc devices is to restore disc height and allow for segmental motion at the affected level, thereby avoiding immobilization following surgery, donor site complications, degeneration of adjacent discs, and allowing for faster return to normal activities [77]. Approved artificial cervical disc devices include the Bryan disc (Medtronic), Prestige (Medtronic) and Prodisc-C (Synthes) (Figure 2.5). A review by Bartels et al. presents known artificial discs and available data on their range of motion and wear [86].

In a study of a workers' compensation group [87], there was a greater risk of non-unions with fusion, and more returned to work at 6 weeks after TDR than fusion. Furthermore, those with the Bryan disc returned to work sooner than those with the Prestige. Clinical outcomes of TDR, measured by pain, generally do not differ from fusion or have only minor improvements [76, 88]. However, TDR is associated with longer operative and recovery times [76, 88], as well as increased costs over fusion with an interbody cage [76]. The main advantage of TDR over fusion is the preservation of motion, the quality of which is related to implant design [89].



Figure 2.5: Artificial cervical disc replacements: Prestige ST (A), Bryan (B), Prodisc-C (C) [77]. Reprinted with permission from Anderson PA, Rouleau JP. Intervertebral disc arthroplasty. *Spine*. 2004;29(23):2779–86.

The FDA approved version of the Prestige disc, Prestige ST, has a stainless steel-on-stainless steel articulation and is secured with screws. The latest iteration, Prestige LP, is fabricated with titanium alloy, rendering it compatible with magnetic resonance imaging, and is hardened with titanium carbide at the articulating surfaces for improved wear resistance. In addition, it uses rails and roughened plasma sprayed surfaces rather than screws for fixation [77, 86, 90]. Prodisc-C has a cobalt chromium alloy articulating against an ultrahigh molecular weight polyethylene (UHMWPE) insert, in a ball and socket configuration [77]. Attachment to the vertebral bone is achieved using a keel and plasma sprayed titanium surface to encourage bone ingrowth [90]. The Prestige ST had a volumetric wear rate of 0.18 mm^3 per million cycles (Mc), which was 0.19% of the total implant mass after 20 Mc [91]. Mass loss of UHMWPE in Prodisc-C due to wear was at a rate of 0.88 mg/Mc and the mean wear particle size was $0.37 \text{ }\mu\text{m}$ [86]. UHMWPE wear particles are implicated in host response and aseptic loosening of artificial joints [92], but loosening and displacement of artificial discs could have serious consequences due to their location. While the Prestige and Prodisc-C designs are reminiscent of artificial hip and knee joints, the Bryan disc design is closer to that of the natural IVD and therefore it is reviewed in further detail.

2.3.1 BRYAN Disc

The Bryan disc [77, 90, 93, 94] consists of a bioconvex, hyperelastic polyurethane core sandwiched between concave titanium shells and sealed with a stiffer polyurethane sheath, which prevents tissue ingrowth into the disc. Fixation is through bone ingrowth into sintered titanium, which is osteoconductive. Saline is injected into the core during implantation and provides lubrication. This design allows for axial compliance, shock absorption and unconstrained motion similar to the native IVD [95], which are not possible with the high modulus materials and design of the Prestige and Prodisc-C.

Since articulating surfaces are sealed, wear particles from the polyurethane core should remain in the Bryan disc, shielding wear debris from potential host response. In simulator testing, wear debris was contained within the disc [91]. Polymeric wear debris was found outside of the disc in some of the animals in primate and caprine models, but no inflammation or phagocytosis of wear particles was found [93]. The wear debris could have come from the damaged sheath or migrated from the core. Also, polyurethane was not found in distant sites, unlike with polyethylene, poly(methyl methacrylate) and metal wear particles. Clinical and radiological evaluations of patients with Bryan disc arthroplasties at one or two levels revealed no obvious signs of implant wear, loosening or osteolysis after eight years [95]. However, some intracellular debris and chronic inflammation was found in the periprosthetic tissue of retrieved Bryan discs, while no metallic wear debris, acute inflammation or other adverse host response were found [91].

Wear of Bryan discs in simulator studies has been characterized. One study [93] was conducted in bovine calf serum with an axial load of 130 N for 10 Mc combining flexion-extension and axial rotation, where one million cycles represents approximately one year of use. The wear rate was 1.2 mg/Mc, or volumetric wear rate of 0.96 mm³/Mc. The particles were globular in shape, with an average diameter of 3.9 μm, much larger than the UHMWPE wear particles from Prodisc-C and on the higher end of the particle size range eliciting the greatest host response. After 10 Mc of bending followed by 10 Mc of axial rotation at a load of 150 N, a height loss of 0.75 ± 0.48% and volumetric

wear rate of $0.57 \text{ mm}^3/\text{Mc}$ resulted, and no metal wear debris was detected [91]. The discrepancy in wear rate could be due to the use of different loading profiles.

Artificial discs may be susceptible to heterotopic ossification (HO) [96], when bone growth occurs in soft tissues or outside of the skeletal structure [97]. In TDR, it has been attributed to bracing after surgery, incomplete coverage of endplates by the implanted disc [94], and milling of bone and muscle damage during the insertion process [96], and may be prevented with nonsteroidal anti-inflammatory drugs (NSAIDs) [98]. HO incidence of up to 66.2% has been reported in Prodisc-C [99]. While some studies did not find incidences of HO in the Bryan disc after 24 [88] and 12–43 months [100], it was found in 13–18% of patients with single level arthroplasty after 12–43 months in other studies [76, 101]. HO occurred in 47.6% of patients eight years after one and two level TDR with the Bryan disc, and all but one (83.3%) developed HO in the inferior disc after bi-level arthroplasty [95]. Fusion of the prostheses occurred in six cases (22%), three of which were from the bi-level group. Since there is lower range of motion in the inferior level, the risk of HO and device fusion increases. However, decreased range of motion due to HO and implant fusion had no effect on clinical outcome, as there was no increase in pain or limitations to activity. Furthermore, adjacent level degeneration was found radiographically only in patients who had pre-existing degeneration prior to TDR.

Three patients were given fusion after disc arthroplasty for adjacent level disease in [88]. Since fusion effectively developed in most patients with bi-level Bryan disc arthroplasty, the value of performing a subsequent TDR for adjacent level degeneration would have to be considered. On the other hand, Sekhon et al. suggested that cervical arthroplasty with the Bryan disc may be performed after previous cervical fusion unless hypermobility is present or the facet joints were previously resected [100].

The Bryan disc offers a design closer to that of the natural IVD, has more favourable polymer wear characteristics and incidences of HO than Prodisc-C, and presents no metal wear debris, which is generated by the Prestige disc. Subsidence of implants into vertebral bodies is a possible risk in lumbar disc arthroplasty [77], but it has not been dis-

cussed with cervical TDR and may be prevented with a properly sized implant [98]. Despite favourable published clinical outcomes regarding cervical TDR, there was no significant difference in pain between arthroplasty and fusion procedures 6 months to 2 years after surgery [102]. The potential complications and cost of performing cervical TDR with currently available devices may also outweigh the clinical benefits when compared to fusion, but the procedure shows promise as an alternative in the surgical treatment of discogenic neck pain and in preventing fusion-related adjacent level degeneration.

2.4 PVA HYDROGELS

PVA is a hydrophilic polymer that can be dissolved in an aqueous solution and crosslinked to form hydrogels with high water content. Physical crosslinking eliminates the need for chemical crosslinkers that can be potentially toxic if left unreacted. Thermal cycling by repeated freezing and thawing is one approach to physical crosslinking, allowing for control over crosslinking through freezing and thawing rates, and the number of freeze-thaw cycles. Stress-strain curves of PVA hydrogels produced in this manner are similar in shape to natural tissues and these hydrogels have been investigated for use in implantable medical devices for a range of applications.

2.4.1 Physically Crosslinked PVA

PVA is able to crystallize through hydrogen bonding and weaker van der Waals forces [10]. Dissolved in an aqueous solution, PVA can be physically crosslinked to form hydrogels in a phase separation process, resulting in polymer-rich regions, in which crystallites are formed, and polymer-poor regions [103-105]. Methods to induce physical crosslinking in PVA include freeze-thaw (F-T) cycling and the addition of poly(ethylene glycol) (PEG) into PVA solutions [106-108].

The structure and properties of F-T PVA hydrogels are dependent on the PVA solution and processing factors. Molecular weight may affect the size and number of crystallites [10, 109], and increased polymer concentration results in an overall increase in the proportion of the polymer-rich region and decrease in porosity [110]. Freezing rates affect the formation of ice crystals [111], while thawing rates have been found to affect gel formation and mechanical properties [11, 12, 112, 113], and hydrogels do not form at thawing rates above 10 °C/min [112]. However, controlled F-T cycling is not performed in some studies, which relied on freezing in a freezer held at constant temperature and thawing at room temperature, and could affect the structure of the hydrogel as freezing and thawing rates are not controlled [114-116]. As the number of freeze-thaw cycles (FTC) increases, the number and size of crosslinking crystalline domains increase, leading to a densification of the polymer-rich region, hydrogel stability [104, 105, 109, 117] and shrinkage [12], with a corresponding improvement in mechanical properties [13, 24, 103, 105, 114]. There is a maximum number of FTCs beyond which results in no significant difference in mechanical properties [12, 13, 103, 116]. The addition of salts and electrolytes impacts the gelation, swelling and mechanical properties of PVA hydrogels [27, 118-120]. Anisotropic tensile properties have also been introduced to PVA by stretching after one FTC before additional cycling, leading a higher modulus and an elongated structure in the direction of stretching [14]. PVA hydrogels fabricated through F-T cycling are stable in water up to 70 °C, at which point crystalline domains melt out [113].

Addition of poly(vinyl pyrrolidone) (PVP) to further stabilize freeze-thaw PVA hydrogels has been employed. Thomas et al. found that 1% addition of PVP resulted in the lowest amount of polymer loss, and did not influence Young's modulus of the hydrogels [121]. However, Ma et al. found that tensile and compressive moduli were maximized at PVP addition of 1 wt%, and negative effects were only apparent with additions greater than 4 wt% [122]. PVA-PVP blends have been investigated for use as nucleus pulposus and cartilage replacements [22, 116, 121-124].

PEG could be added during PVA dissolution to induce phase separation when the solution temperature is lowered to room temperature. The molecular weight of PEG affected the properties of the gel [108], but this method does not offer the ability to tune properties through additional processing parameters during gelation. Repeated dehydration and rehydration [108], and high temperature annealing [106] of these hydrogels after washing out the PEG were used to improve their creep resistance.

2.4.2 Characterization of PVA Hydrogel Structure

The study of PVA hydrogel structure has been undertaken using various analytical methods. Differential scanning calorimetry (DSC) has been used to determine the degree of crystallinity of PVA. PVA melting occurs between 190 and 235 °C, and the heat of melting (ΔH_m) of 100% crystalline PVA is 138.6 J/g [125]. Hydrated PVA hydrogels have a significantly lower melting point due to the presence of a solvent [104, 126, 127]. DSC has been performed at a rate of 5–10 °C/min up to 250 °C with nitrogen purging [109, 128] for dried hydrogels. Hassan and Peppas [109] found that crystallinity ranged approximately from 30 to 60% in dried PVA hydrogels. Crystallinity increases with number of FTCs, resulting from the formation of secondary crystalline domains and the growth of primary crystallites by up to 50% [104].

Fourier transform infrared spectroscopy [10, 125], nuclear magnetic resonance spectroscopy [104, 129] and x-ray diffraction (XRD) [117, 128] have also been used to determine crystallinity in PVA. Using XRD, Ricciardi et al. [117] found that crystallite size in as-formed 11 wt% PVA-D₂O hydrogels increased from 2.8 nm to 3.9 nm and dried hydrogels had a crystallinity of 44–50%. Crystallite size was determined to be 3–8 nm by small angle x-ray scattering (SAXS) [104] and approximately 3 nm by small angle neutron scattering (SANS) [105, 130]. SANS also showed that crystallites were separated by 19–25 nm of amorphous polymer in the polymer rich region (Figure 2.6) [105], while cryogenic transmission electron microscopy (cryo-TEM) showed a separation of 30 nm [104].

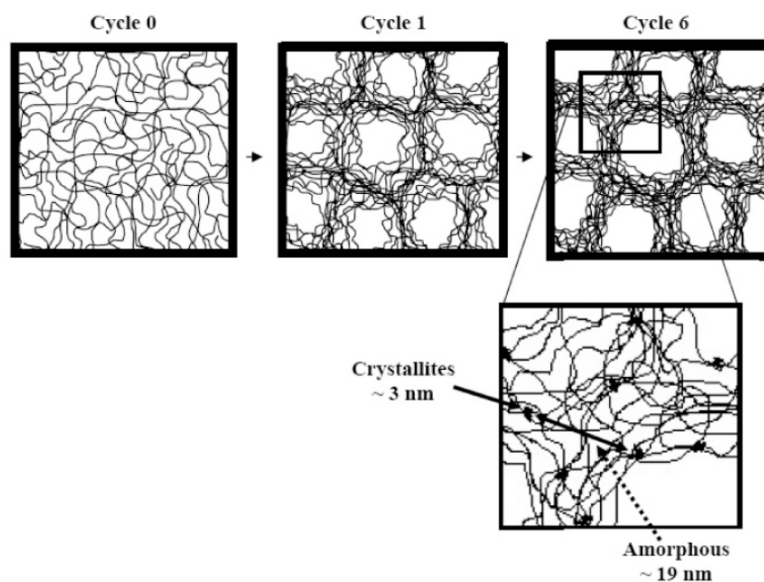


Figure 2.6: Schematic of PVA hydrogel structure produced by freeze-thaw cycling as determined by SANS. Cycle 0 represents the PVA solution before thermal cycling. Reprinted with permission from [105]. Copyright 2007 American Chemical Society.

Imaging techniques have been used to study the structure of physically crosslinked PVA hydrogels. 5-(4,6-dichlorotriazinyl)aminofluorescein (5-DTAF) labeling of PVA enabled examination of the hydrogels in a hydrated state using confocal laser scanning microscopy (CLSM) with fluorescence [106, 131]. Optical microscopy of PVA hydrogel slices showed that separation of polymer rich and polymer poor regions became more evident with increased PVA concentration and number of FTCs, with pore sizes of up to 50 μm [116], which increased with water content [19, 103]. The use of scanning electron microscopy (SEM) to examine hydrogel structure requires the removal of water due to the high vacuum environment in the microscope, but attempts should be made to maintain the pore structure [103, 132, 133]. Environmental SEM was also used to observe hydrogel structure in the hydrated state [123]. Our group has prepared PVA hydrogel cross-sections for SEM by ethanol dehydration, followed by CO_2 critical point drying then freeze-fracturing in liquid nitrogen [16, 24].

Nakaoki and Yamashita [134] used DSC and Raman spectroscopy to characterize three states of water in the hydrogels: free water that freezes near 0 $^\circ\text{C}$, freezable bound water, for which the endothermic peak is shifted to lower temperatures, and non-freezable

water that is tightly bound to PVA molecules. With increasing PVA concentration, the amount of free water and freezable bound water decreased, while the proportion of non-freezable water increased with an increasing number of $-OH$ groups. This agrees with the model that pores are mostly filled with water while amorphous PVA molecules are swollen with water and held together by crystalline domains [117]. Pores in PVA hydrogels were found to be interconnected [115]. With increased F-T cycling, water mobility and diffusion coefficient decreased [114, 115].

2.4.3 Mechanical Properties

Impact load testing showed that PVA with water content as low as 20% can provide better load damping and shock absorption than UHMWPE, transmitting a lower peak stress upon impact loading [18]. The non-linear concave-up or J-shape stress-strain curves of freeze-thaw PVA hydrogels resemble those of natural tissue in contrast to other synthetic polymers such as UHMWPE [11]. Viscoelastic mechanical behaviour has also been studied through stress relaxation, creep and dynamic mechanical testing. The focus of this section will be on compression properties.

2.4.3.1 Unconfined Compression

In unconfined compression, cylindrical hydrogel samples are typically tested between non-porous platens and allowed to expand laterally while compressed. Investigating the use of Salubria biomaterial for focal cartilage replacement, Stammen et al. [19] tested PVA hydrogels containing 20% and 25% PVA made with 0.9% saline. Samples were equilibrated in water at 37 °C before testing, then compressed to 0.65 strain at strain rates of 100 and 1000%/min, but the authors did not specify if testing was done in air or fluid. Strain rate dependence was apparent at high strains but not at low strains, likely from increasing pressurization with strain. Tangent compressive moduli increased from approximately 2 MPa at 0.3 strain to 20 MPa at 0.65 strain in both hydrogels. Extensibility decreased with increased PVA concentration; the failure stress and strain were 2.1

MPa at 0.6–0.62 strain for the 20% PVA hydrogel and 1.4 MPa at 0.45–0.47 strain for the 25% PVA hydrogel. Strain rate dependence was not found in shear, in which sample volume is conserved, leading to the hypothesis that fluid flow contributed to the compressive stress-strain behaviour and strain rate dependence.

Millon et al. [24] tested 10% PVA hydrogels made using 1, 3 and 6 cycles of controlled F-T cycling for cartilage replacement or other orthopedic applications. Unconfined compression was performed at 1, 10 and 100%/s to 0.45 strain in water at 37 °C. Strain rate dependence was also apparent only at high strains in 6 FTC hydrogels, and a statistical difference in stress at 0.45 strain was only found between strain rates of 1 and 100%/s, which was 0.13–0.16 MPa. Wang and Campbell [23] produced 3–40 wt% PVA hydrogels using the same F-T conditions as Millon et al. Cylindrical sample dimensions were approximated to lumbar intervertebral disc dimensions, which are approximately 4 cm in diameter and 1 cm in height [135]. Unconfined compression was performed at 3 mm/min to approximately 0.25 strain. Tangent moduli was lowest in 3 FTC-3% PVA and highest for 6 FTC-40% PVA, increasing with both number of FTC and PVA concentration.

Joshi et al. found that tangent compressive moduli of 6 FTC PVA hydrogels containing 84% water and 1–5% PVP did not vary with PVP concentration [58]. Compressive moduli were also determined after fatigue cyclic loading to 0.15 strain for up to 10 million cycles at 5 Hz. Tangent modulus decreased by 24% at 0.15 strain, but no change was found at 0.2 and 0.25 strain. Permanent deformation of the hydrogels resulted in a 5% increase in diameter and 17% decrease in height. In Holloway et al., PVA hydrogels containing 1 wt% PVP and 10 to 35 wt% total polymer were compressed at a rate of 100%/min to 0.15 strain in phosphate buffered saline (PBS) at 37 °C [116]. Compressive modulus in the linear portion of the stress-strain curve, between 0.01 and 0.05 strain, did not increase beyond 5 FTCs, and increased with polymer concentration.

Compressive moduli from the above studies are listed in Table 2.4. There are discrepancies in describing compressive moduli due to the non-linearity of stress-strain curves and strain rate dependence of PVA hydrogels. Tangent moduli vary to a large degree depending on the strain at which they were calculated, and strain rate may have an effect on the apparent stiffness. Using only one portion of the stress-strain curve would not provide a complete representation of hydrogel behaviour. Also, hydrogel composition, F-T cycling parameters, and testing conditions such as temperature and immersion in fluid all influence the compressive behaviour of PVA hydrogels.

Table 2.4: Compressive moduli from unconfined compression of freeze-thaw PVA hydrogels in the literature.

Study	PVA [%]	Solvent	Additive	FTC	Test environment	Strain rate	Modulus [MPa] (strain)
Stammen 2001 [19]	20, 25	0.9% saline	—	Unknown	Water, 37 °C, equilibrated prior to testing	100, 1000%/min	Tangent: 2.08–3.02 (0.3), 16.51–19.06 (0.6)
Millon 2009 [24]	10	Water	—	1, 3, 6	Water, 37 °C	100%/s	Tangent: 0.039–1.18 (0.45)
Wang 2009 [23]	3–40	Water	—	1, 3, 6	Water, 37 °C	3 mm/min	Tangent: 0.001–1.303 (0.05), 0.001–2.117 (0.20)
Joshi 2006 [58]	11–15	Water	1–5% PVP	6	PBS, 37 °C	100%/min	Tangent: 0.23 (0.15), 0.4 (0.25)
Holloway 2011 [116]	10–35	Water	1% PVP	6	PBS, 37 °C	100%/min	Linear: 0.070–0.801 (0.01–0.05)

2.4.3.2 Stress Relaxation, Creep and Dynamic Mechanical Properties

Viscoelastic properties such as stress relaxation, creep and viscous damping may be desirable in a biomaterial for IVD applications, since these properties are found in the natural IVD. PVA hydrogels also display viscoelastic behaviour. In stress relaxation tests, 25% PVA hydrogels decreased to 45% of the initial stress after 24 hours at 0.2 compressive strain [19], while 10% PVA also relaxed to approximately 45% of the initial stress after 1 hour at 0.45 strain [24]. Wang and Campbell [23] performed stress relaxation for only 30 seconds at 0.25 strain, and the degree of relaxation attained was less than 20% for all compositions. Their study found that rate of stress relaxation increased with

the stiffness of the material, increasing with both polymer concentration and number of FTCs. The degree of stress relaxation was found to decrease with increasing polymer concentration in PVA hydrogels by Kobayashi [136]. However, the degrees of stress relaxation in PVA hydrogels are much lower than in the natural IVD, which decreases to less than 10% of the initial stress after only 30 minutes [55]. Compressive stress relaxation data was successfully fitted to a double exponential decay function by both Millon et al. [24] and Wang and Campbell [23], as was previously done for tensile stress relaxation [11, 13].

Stauffer and Peppas [114] examined creep in 15 wt% PVA with 2–5 FTCs by applying stress for 15 s. However, only final strain was plotted against applied stress, and creep curves were not shown. Final strains of 2 FTC hydrogels were 0.10 to 0.18, increasing linearly with applied stress up to 3.5 MPa, while over the range of applied stress, 5 FTC hydrogels had approximately the same final strain of 0.085. Wang and Campbell [23] applied a compressive stress of approximately 0.2 MPa for 30 s in their creep tests. The increase in strain during creep was found to be highest in hydrogels with low polymer concentrations. For 15–40 wt% PVA hydrogels with 6 FTCs, the increase in strain ranged from 1.8 to 2.5%, but neither the initial nor final strain was specified. Creep data in this study was fitted with the three-parameter-solid model used in IVD creep.

PVA hydrogels were simulated by a poro-viscoelastic model consisting of the three-parameter-solid model for the solid phase and a fluid phase that can be exuded during creep [137]. Creep strains of 0.1–0.2 were obtained experimentally for hydrogels containing 40–60% PVA after 8 hours at 0.5 MPa stress, and both initial and final strains decreased with increasing PVA concentration. The poro-viscoelastic model successfully modelled creep behaviour in these hydrogels. The solid polymer phase and flow of the fluid phase both likely contributed to viscoelastic properties.

Dynamic properties of PVA hydrogels have been investigated in shear. The storage modulus tended to increase with increasing frequency of loading, but this effect appeared to be small for frequencies up to 10 Hz [29, 138], and decreased with increasing

cyclic strains, which may have been due to polymer deformation that was not immediately recovered between loading cycles [119]. $\tan \delta$ decreased with increased loading frequency, indicating more elastic behaviour with faster loading [29]. PVA hydrogels can be characterized as highly elastic with $\tan \delta$ values on the order of 0.01, compared to at least 0.1 in rubber, since the large proportion of water in hydrogels results in low internal friction [139]. By increasing PVA concentration from 15% to 20% in hydrogels containing 3% HA, shear storage modulus increased while loss modulus remained similar, thus decreasing $\tan \delta$ [29]. This indicates an increase in elastic behaviour with higher polymer content.

In general, mechanical properties are dependent on the structure of PVA hydrogels, as stiffness increases with polymer concentration and F-T cycling. Viscoelastic properties correlate with polymer concentration and modulus of the hydrogels. Under compression, the role of water flow and permeability also appear to be important in load bearing, strain rate dependence, stress relaxation and creep in PVA hydrogels.

2.4.4 Effects of aging and salt on PVA hydrogels

Willcox et al. [104] investigated the aging of 1–12 FTC 19 wt% PVA hydrogels, produced using controlled F-T cycling, for up to one year. Aging in water had a similar effect as additional F-T cycling, as crystallinity also increased. Mass decreased by 8% for 1 FTC and 5% for 12 FTCs due to weeping of water that pooled on the surface of the hydrogels. Hassan and Peppas also determined that polymer dissolution decreased with increasing number of FTCs, and that dissolved polymer was not from the crystalline region [109]. PVA hydrogels initially swelled as soluble PVA was replaced by water in the polymer-poor regions and smaller crystallites dissolved leading to an initial decrease in crystallinity [109, 112]. Shrinkage of the hydrogels occurred with aging, reaching equilibrium swelling over time. Modelling of crystallite dissolution showed that smaller crystallites with lamellar thickness of less than 185 Å dissolved within 10 minutes, while those greater than 215 Å remained stable and provided stability for the hydrogel [140].

However, the model did not account for the increase in crystallinity over time. Longer polymer chains were more likely to have entanglements that inhibit crystalline formation during F-T cycling, leading to a larger degree of rearrangement over time with higher molecular weight [109].

After 1000 hours of water flow through a packed column of PVA hydrogel beads, the modulus of the beads increased by approximately 25–35% [112]. PVA/PVP hydrogels that were fabricated, stored and tested in PBS also increased in compressive moduli after 56 days of aging, which was attributed to equilibration of the hydrogels [58]. However, the amount by which modulus increased was not specified.

In biomedical applications, implanted biomaterials would be in an environment with salts and other solutes. PVA hydrogels may be made with solutions such as saline or PBS to approximate the *in vivo* environment. However, the addition of salts has consequences on the formation and properties of PVA hydrogels. The addition of salts to PVA during dissolution decreases the freezing point of aqueous PVA solutions, which is to be expected due to the freezing point depression of water. While Gordon reported the freezing point of PVA solutions in water to be $-18.7\text{ }^{\circ}\text{C}$ [141], solutions of PVA, theophylline and 11% NaCl did not freeze until $-30\text{ }^{\circ}\text{C}$ [118]. Salts disrupt inter- and intramolecular hydrogen bonding in PVA and, above a certain concentration, also between PVA and water [142]. When prepared with low concentrations of NaCl (0.0125–0.0625 M) rather than with distilled water, 2.5% PVA hydrogels gelled by liquid nitrogen freezing and room temperature thawing decreased in crystallinity and became weaker [27].

Osmotic pressure effects have to be taken into account due to the high water content of hydrogels if they were prepared with a solution non-isotonic with their environment. Volume change and swelling kinetics in response to changes in concentration in the external solution may be due to a combination of mobile ion diffusion, internal frictional forces within the polymer network and between polymer and water, and the elastic response of the polymer network [143]. 11% PVA hydrogels decreased in mass in 1–3 M NaCl solutions due to water loss [144]. Deswelling increased with the concentration of

the solution, resulting in 10–45% decrease in mass after 2600 minutes that was not completely reversible when placed back into water. Since dissolved ions in salt solutions can move freely into the PVA hydrogel structure, osmotic pressure decreases over time, but this may not be the case *in vivo* due to the presence of macromolecules. Spiller et al. [123] dissolved PEG with molecular weight of 20,000 g/mol into PBS to attain an osmotic pressure of 0.95 atm, which was found to be a good *in vitro* model compared to *ex vivo* implantation into defects excised from cartilage in bovine femoral condyles. 10 wt% PVA/PVP hydrogels deswelled by approximately 23% and 65% after soaking for up to 4 weeks in PBS and PEG solution, respectively. Pores decreased in size and connectivity in PEG solution while porosity remained high in PBS alone. Compressive moduli increased by 50% in PBS and by 300% in PEG solution after four weeks. With increasing PVA concentration, deswelling decreased in PEG solutions [116]. After 24 days, swelling ratios were approximately 0.8 and 1 for 10% and 20% PVA hydrogels in PBS, and 0.4 and 0.65 in PEG solution, respectively. Being able to predict or mitigate dimensional changes of hydrogels *in vivo* is important because shrinkage may cause migration of hydrogel implants and unexpected change in mechanical properties.

2.4.5 Biocompatibility

Although PVA hydrogels are not cytotoxic, they are not adhesive to cells or tissue due to their hydrophilicity [10, 16, 145]. Surface modification or functionalization, as well as composites with cell attractive substances, have been used to increase cell affinity and proliferation on PVA hydrogel substrates to support tissue regeneration [16]. These strategies may be explored for fixation of a PVA hydrogel IVD replacement device to the vertebral bone.

Host response to PVA implants in animal models has ranged from limited inflammatory reaction [17] to loose fibrous tissue [146] and fibrosis [22]. Inflammation was elicited only in the subchondral vertebral bone where PVA wear particles from a NP replacement were found, and not in the surrounding disc space where there was no wear

particles [146]. Particles of UHMWPE (50–300 μm), however, caused intense inflammation in rat knee joints while only mild reactions were found with PVA particles after two months [18].

PVA was implanted into rabbits as a meniscal replacement and no obvious signs of breakage or wear were observed up to two years [21]. PVA hydrogel mitigated the progression of osteoarthritis compared to knees treated with meniscectomy and there was only a slight increase in implant stiffness from the initial state. The use of PVA hydrogels for resurfacing of cartilage was investigated in a canine knee model, in which a gap between the hydrogel implant and surrounding cartilage was observed [18, 147]. There was a high rate of extrusion (20–33%) of a PVA hydrogel NP replacement that was implanted in baboon lumbar discs because of osmotic pressure-related shrinkage within the disc, and the implant was also slightly flattened [146]. These studies highlighted the implications of osmotic effects on shrinkage of hydrogels that affected their performance *in vivo*. Due to the proximity of IVD implants to the spinal cord, implant migration and host response could have serious consequences.

2.5 NANOFILLERS AND NANOCOMPOSITES

Nanofillers are defined by materials having at least one dimension less than 100 nm, and may be of various aspect ratios ranging from fibres to plates to spheres [148]. They have large surface area to mass ratios due to their small size, leading to high filler connectivity and small interparticle separation when dispersed in a matrix compared to larger fillers [149]. Improvements on properties may be dependent on their size, shape, aspect ratio, modulus, dispersion, alignment and interaction with the matrix in a nanocomposite (NC) [150].

The interaction between nanofillers and the matrix becomes increasingly important due to the high surface area of the fillers [148]. In a polymer matrix, strong interactions result in adsorption of polymer chains onto filler surfaces, possibly leading to de-

creased chain mobility and altered crystallinity. Even at low nanofiller additions, the interface may comprise a large proportion of the NC, resulting in properties changes not achievable in composites containing larger reinforcements at the same filler content. More stable and discrete nanofiller dispersion also results from strong interfaces. Conversely, a poor interface would have negative effects on the mechanical properties. Larger nanofillers [149] and those with higher aspect ratios [151] usually confer greater increases in stiffness.

The addition of clays, most commonly montmorillonite (MMT), to hydrophilic polymers has been investigated. MMT is a naturally occurring smectic aluminosilicate that has hydrophilic surfaces. Increasing amounts of MMT decreased crystallinity and melting temperature, and increased storage modulus [152, 153]. MMT was well dispersed and limits the mobility of amorphous PVA while crystalline PVA chains were folded parallel to the clay surface [152].

PVA was able to hydrogen bond to nano-silica particle surfaces to initiate nucleation upon annealing [154]. Crystallinity was found to increase to a maximum at 0.5 wt% silica addition. At the same filler mass, silica of 22 nm gave the highest increase in crystallinity, since smaller sizes resulted in insufficient space between particles for crystal growth, whereas larger ones resulted in a smaller number of nucleation sites. It appears the effect of nanofiller addition on crystallinity, and presumably mechanical properties, may not be easily predicted and depends on factors such as size, aspect ratio, filler concentration and filler surface properties.

2.5.1 Laponite

Laponite is a synthetic smectic silicate clay with the chemical formula $\text{Na}^{+}_{0.7}[\text{Si}_8\text{Mg}_{5.5}\text{Li}_{0.3}\text{O}_{20}(\text{OH})_4]^{0.7-}$ [155]. It is disc-shaped with a diameter of approximately 30 nm and a height of 1 nm. The clay faces are negatively charged and sodium counter-ions balance the charges between clay discs, while the edges are positively charged. In solution, sodium ions dissociate from the clay disc surfaces to form disper-

sions due to electrostatic repulsion [156], while electrostatic attraction can result in edge-to-face structures [155, 157, 158]. In solutions above a certain concentration or ionic strength, Laponite flocculates due to screening of electrostatic repulsion forces, allowing attractive van der Waals forces to dominate [157]. Oxygen and hydroxyl groups on Laponite help with the adsorption of hydrophilic polymers onto its surface [159].

Polymer solutions of Laponite and polyethylene oxide (PEO) in water have been investigated extensively. Depending on Laponite and PEO concentrations, these solutions can form reversible gels as PEO chains adsorb onto multiple Laponite surfaces, which act as crosslinks [160, 161]. Viscosity increases with the addition of Laponite to PEO solutions due to structural changes of the adsorbed polymer and bridging of Laponite particles [162], forming clusters or aggregates [163]. However, at high polymer and low Laponite concentrations, clay surfaces are saturated and thus the amount of bridging is likely to be minimal [162]. While solution viscosity was increased, the increase in relaxation time was lower in high concentration PEO solutions with small degrees of Laponite addition.

In a polyurethane with a polar hard segment and a hydrophilic soft segment [164], Laponite particles in the hard segments were primarily exfoliated, while ones in the soft segment regions were intercalated or flocculated. Crystallinity in the hard segments decreased with Laponite addition, but tensile toughness and extensibility decreased because of hindrance to molecular alignment in the soft segment with strain. Additional tuning of NC properties may be possible by designing the filler dispersion within the specific matrix. By preferentially incorporating Laponite into the hard segments, the filler was able to hydrogen bond and reinforce the hard crystalline domains, increasing stiffness without sacrificing extensibility of the polyurethane since the soft segments were not affected [164, 165]. Laponite was suitable in this case due to their small size and could be located exclusively in the hard segments.

The only example of PVA-Laponite NCs in the literature was in the form of annealed membranes [159]. The PVA was rendered partially hydrophobic by grafting of *N*-

tertiary butyl acrylamide at 2 mol% before Laponite addition. Both melting temperature and crystallinity decreased with Laponite addition, indicating the formation of less stable crystallites. Dynamic mechanical testing showed that storage modulus and $\tan \delta$, which is typically associated with the proportion of amorphous polymer, decreases with Laponite addition. Since crystallinity decreased with Laponite, it was attributed to a stiffer amorphous phase in which Laponite impeded chain movement. NC membranes had a smaller swelling ratio than unfilled membranes because Laponite functioned as crosslinkers, preventing swelling when placed in water. However, as temperature increased, swelling increased in NC membrane while decreasing in the unfilled membranes due to the hydrophilic nature of Laponite.

2.5.2 Bacterial Cellulose

Bacterial cellulose (BC) can be produced by *Acetobacter xylinum* in either shaken or static culture [166]. The glucose units in cellulose are bound through β -1,4 linkages, and hydrophilicity is imparted by the three $-OH$ groups on each glucose unit [167]; BC suspensions can possess up to 99% water [166]. BC has a degree of polymerization of 4000–10 000 and fibre lengths ranging from 100 nm to several microns [168]. BC produced in our laboratory had a fibre diameter of 35–90 nm, 60% crystallinity, and modulus, determined by atomic force microscopy, of 78 ± 17 GPa [169]. Crystal modulus of BC found by theoretical modelling and experimental measurements are in the range of 100–160 GPa [167], but moduli of fibres would depend on the crystallinity and alignment of crystalline domains, which are hypothesized to be parallel to the fibre axis [169].

Reinforcement efficiency of a filler is affected by its aspect ratio and dispersion. As aspect ratio increases, there could be a tendency for fibres to become entangled, but the concentration threshold for filler connectivity decreases [166]. BC has been investigated as a filler in the form of whiskers, fibres and as a component in double network hydrogels [166-168]. Matrix modulus is theoretically maximized at whisker fraction of 1 %

w/v with width of 10–20 nm and aspect ratio of 100, when filler connectivity occurs [170]. Further increase in both filler content and aspect ratio leads to no further enhancements, and negative effects on modulus as aggregation occurs at high filler content [166, 168]. Crystallinity of polycaprolactone and starch matrices increased with the addition of BC [166].

There are concerns of poor compatibility and moisture on NC properties with the addition of BC into hydrophobic matrices [166]. Surface modification of BC may be done to increase compatibility with the matrix. Researchers have also taken advantage of surface reactions to produce a template for growth of calcium phosphate in simulated body fluid [171, 172]. BC was graft-polymerized with acrylic acid to provide nucleation sites for calcium phosphate growth [171]. Another group phosphorylated the primary alcohol group of the glucose unit using phosphoric acid (H_3PO_4) prior to incubation in $CaCl_2$, forming nucleation sites for hydroxyapatite growth in simulated body fluid [172]. Surface reactions could be used to modify BC to have the desired surface characteristics for use in a NC.

2.5.3 PVA Hydrogel-Based Nanocomposites

In PVA hydrogel-sulphonated polyester beads, addition of up to 1 wt% MMT, a plate-like nanoclay, served as nucleation sites for crystallization and increased crystallinity, but steric hinderance decreased crystallinity above 5 wt% MMT [128]. The compressive tangent modulus at 0.3 strain increased by 20% and 90% with 0.1% and 1% MMT addition, respectively, in 6 FTC-10% PVA hydrogels [173]. Graphene oxide, which has the form of hydrophilic nanosheets, was added at up to 1.0 wt% to F-T PVA hydrogels [174]. Water content was slightly higher in these NCs compared to pure PVA hydrogels due to the hydrophilic nature of graphene oxide. The carboxylic acid and hydroxyl groups on graphene oxide may hydrogen bond with PVA, forming crosslinks and decreasing swelling at higher filler content. Compressive stress at 20% strain increased by 40% with 0.8 wt% filler addition.

The addition of nano-hydroxypaptite (nano-HAp) to PVA solutions before F-T cycling has been investigated for artificial cartilage applications. TEM showed HAp particles formed agglomerates with sizes greater 100 nm, and their addition caused crystallinity in the hydrogels to decrease due to disruption of hydrogen bonds in PVA [175]. Tensile strength increased with increasing addition of needle-like nano-HAp, while modulus improvement was greatest at 1.5 wt% [28]. SEM after vacuum drying showed a transition from round pores in unfilled PVA hydrogels to a dense fibrillated structure with the addition of nano-HAp. In rheological tests, storage and loss moduli increased with increased HAp to a maximum of 6 wt% [29]. Crosslinks formed by hydrogen bonding of fillers to PVA were hypothesized to strengthen the network. However, agglomeration of nanofillers tended to occur at high filler content, resulting in a decrease in reinforcement effectiveness [25, 29].

Bacterial cellulose-PVA NC hydrogels were investigated for cornea replacements [176]. Membranes of BC were soaked in PVA solution, followed by F-T cycling then dehydration and rehydration. The resulting BC content was very high, ranging from 12–27 wt%. Crystallinity of PVA decreased with increasing BC, which the authors attributed to the hydrogen bonding between BC and PVA disrupting hydrogen bonding in PVA. However, since the amount of PVA decreased with increasing BC, the decrease in crystallinity may be due to lower PVA concentrations. Young's modulus increased by 48–126 times and tensile strength by 22–125%, while strain at the yield point decreased by 60–80%.

Millon et al. investigated BC-PVA hydrogels in both tension and compression for cardiovascular and orthopedic applications [13, 24]. BC addition changed the shape of the tensile stress-strain curves, with modulus increasing sharply at 0.4 strain, compared to flatter curves from pure PVA hydrogels [13]. The addition of 0.61 wt% BC resulted in tensile tangent moduli 2 and 5 times that of unfilled 10 wt% PVA at 0.3 and 0.6 strain, respectively. By increasing PVA concentration from 7.5 wt% to 15 wt% while keeping BC content at approximately 0.3 wt%, tangent moduli increased by 3 and 4.5 times at 0.3

and 0.6 strain. Furthermore, F-T cycling beyond three or four cycles did not affect tensile properties of the PVA-BC hydrogels.

In compression [24], the addition of 0.85 wt% BC to 10% PVA provided little improvement in stiffness compared to addition of 0.3 wt% BC, which resulted in a three-fold increase in tangent modulus at 0.45 strain compared to unfilled 10% PVA. Unlike under tension, the compressive tangent modulus of 3 FTC BC-PVA hydrogels at 0.45 strain increased by approximately 36–50% with 6 FTCs. Strain rate dependence was investigated using strain rates of 1, 10, and 100%/s. While neat 10% PVA hydrogels were only strain rate dependent after 6 FTCs, the PVA-NC hydrogels displayed strain rate dependence between 1 and 100%/s even with 1 FTC. Stress relaxation did not level off in any of the hydrogels after 1 hour at 0.45 strain, and decreased from approximately 45% of the initial stress in 10% PVA to 20–30% for hydrogels containing BC. SEM of fracture surfaces from critical point dried PVA revealed larger pores in hydrogels containing BC. It is possible that free water in larger pores was able to flow more freely from the hydrogel under constant stress, and hydrostatic pressure decreased to a larger degree over time.

The addition of even small amounts of nanofillers can result in significant changes in PVA hydrogel properties, which could be due to both the transfer of stress from the compliant hydrogel matrix to the stiffer reinforcement and to their effect on hydrogel structure. Hydrogen bonding could be disrupted, resulting in a decrease in crystallinity. Furthermore, hydrogen bonding between nanofillers and PVA could serve as additional crosslinks that increase stiffness. The water content and porous structure of F-T PVA hydrogels may also be altered with the addition of nanofillers that could impact hydrogel properties.

2.6 HYDROGEL-BASED ARTIFICIAL IVD

In addition to NP replacements, hydrogel-based TDRs have been investigated. Wang and Campbell [23] studied a series of PVA concentrations and FTCs to determine combinations that match properties of the natural NP and AF. Two combinations were found to match the NP, but no suitable replacement matched the stiffness of the AF for PVA concentrations up to 40% PVA and up to 6 FTCs. The authors suggested that in unpublished data, PVA hydrogel components of different concentrations were adherent when fabricated using a two-step method to create an IVD device.

Silva et al. [177] fabricated a lumbar IVD device by first producing an annulus of 1 FTC-35% PVA then filling it with 30% PVA solution with no F-T cycling. Both PVA solutions used a mixture of water and DMSO as the solvent. The construct was subsequently swollen in water, in which the nucleus component absorbed a large amount of water and equilibrium swelling of both components was more than 80%. Creep testing was performed in water between porous plates for 11.5 h and repeated every 2 weeks. The specimen became stiffer with each additional test and experienced dimensional change due to viscous flow in the polymer matrix. On its own, the nucleus was more permeable to water than the annulus, with water loss accounting for 13.25% versus 9.1% reduction in volume, though it was likely lower when surrounded by the annulus. The device had similar properties to the natural IVD in fluid flow and loss, and transfer of stress from nucleus to the annulus when modelled using finite element modelling.

A lumbar IVD device was made of a semi-interpenetrating network of poly(2-hydroxyethyl methacrylate) (pHEMA) and poly(methyl methacrylate) (PMMA), and reinforced in the annulus region by poly(ethylene terephthalate) (PET) fibres that were wound to simulate the alignment of collagen lamellae in the AF [178]. HAp-reinforced pHEMA/PMMA formed the endplates, likely to encourage bone ingrowth *in vivo*. The compressive stress-strain curves had a toe region up to 9% strain followed by a linear region. Strain rate dependence was similar to canine IVD in the linear region. Strain rates of 1, 5 and 10 mm/min produced moduli of 84, 102 and 120 MPa, respectively. How-

ever, unlike the natural IVD, there was no significant strain rate dependence in the toe region. Creep was lower than for the natural disc; the initial strain of 6.9% increased to 12% over 4500 s, while the creep data was fitted to a four-component viscoelastic model. Dynamic compression showed that both storage and loss moduli increased with frequency, and loss modulus was an order of magnitude lower than the storage modulus. Strain hardening was observed as the storage modulus increased with the number of loading cycles. The mechanical properties of the fibre-reinforced hydrogel device may be tuned by composition and the amount and winding angle of PET fibres, which impacted sample stiffness in PET-reinforced pHEMA/polycaprolactone discs [179].

These examples illustrate the feasibility of using hydrogels, including PVA hydrogels, in IVD prostheses. Although pure PVA hydrogels may not be able to match the modulus of the annulus, reinforcement of the hydrogel matrix may lead to the desired properties. Furthermore, by using PVA, tuning of individual properties of the annulus, nucleus and endplate components could be achieved using different formulations and number of FTCs while forming a cohesive device.

2.7 WEAR TESTING

Tribology is the study of the friction, wear and lubrication, which are important in IVD designs with articulations or motion between components to reduce friction and mitigate wear. Although a low coefficient of friction (COF), between 0.001 and 0.03, is characteristic of animal and human joints [139, 180, 181], and desirable for artificial joint replacements, wear of the materials in artificial joints generates wear particles that could elicit undesirable host response, which may lead to implant loosening [182, 183]. Thus, minimizing wear should take precedence over lowering COF. Studies of hydrogel tribology have mainly been for applications in total artificial joints, hemiarthroplasty or focal replacement of cartilage. Counter surface used in testing can be metals, ceramics, hydrogel or cartilage. Tribological properties, particularly wear, of hydrogels are examined, and crossing-paths wear testing will also be reviewed.

Compliant materials, such as hydrogels, allow for a larger contact area and lower contact stresses, which enables the formation and maintenance of fluid film lubrication during motion [184]. Increasing the conformity of contacting surfaces resulted in a smaller increase in surface roughness after wear testing between hydrogels and cartilage [185]. A lower indentation creep modulus led to better friction and wear properties between pHEMA and stainless steel [186]. Water could also be squeezed out from hydrogels under load to form a boundary layer that decreases friction [106, 187]. A PVA hydrogel, like cartilage, was able to maintain a gap supported by a fluid film when pressed against a glass plate due to its hydrophilicity [18]. In contrast, UHMWPE and glass were separated by a narrow gap and fluid pressure dropped to zero rapidly upon loading. The loss of fluid support would result in increased contact of solid surfaces, and could lead to increases in COF [185].

2.7.1 Lubricant

The fluid environment *in vivo* contains salts, proteins and other solutes. Nevertheless, tribological testing of hydrogels has been performed in air, water, salt and protein solutions, and synovial fluid. The choice of lubricant could have a significant effect on wear of hydrogels. Adhesive wear occurred in the absence of a lubricant between pHEMA hydrogel and stainless steel [188], and increased the COF between poly(acrylic acid) hydrogel (PAAc) and glass [187], and PVA hydrogel and titanium alloy [180]. While there was no difference between using water and saline as a lubricant between PVA and stainless steel, the addition of bovine serum reduced the COF by up to 50% [25, 122, 189, 190]. The interaction of proteins with sliding surfaces could have a consequence on the formation of adsorbed protein layers and their lubrication properties [191-193]. Other constituents in synovial fluid can also contribute to low friction and wear. The addition of phospholipids into HA-containing saline lubricant resulted in a decrease in COF from 0.015 to 0.01 in detergent-treated porcine shoulder joints [191]. In reciprocating tests between PVA hydrogels and CoCr, the COF averaged 0.1 in newborn calf serum, while testing in bovine synovial fluid resulted in an average COF of 0.036 [124].

Brandt investigated the effect of lubricant composition in simulator testing of total knee replacements [194]. Alpha-calf serum (ACS) was found to have a similar protein composition and profile as synovial fluid, and dilution with PBS rather than distilled water produced the equivalent osmolality. The addition of salts could also influence the protein conformation in the lubricant. To prevent microbial growth, antibiotic-antimycotic was found to be more effective than sodium azide, which was used in some tribological studies of hydrogels [124, 185, 195]. The composition of the fluid environment around the cervical intervertebral disc is not currently known [196], but a lubricant composed of ACS, PBS and antibiotic-antimycotic was used in the study of PEEK-on-PEEK for cervical disc implant applications [197].

2.7.2 Wear and Friction of Hydrogels

Adhesive wear in hydrogels is assumed to be reduced by lowering friction [198]. Friction may also cause local temperature to rise, resulting in viscous flow at the surface and increased wear [199]. While COF correlated with wear in pin-on-disc tests of PVA-HAp NC hydrogels against a titanium alloy sphere [199], no strong correlations were found between wear and friction in reciprocating tests [124, 188, 200]. This may be due to variation in sliding velocity along the wear track with reciprocating motion, in which friction peaks near the end of each cycle in reciprocating motion [188]. The wear factor in pin-on-disc testing was lower for PVA hydrogels than UHMWPE, but was up to 18 times higher in reciprocating tests because velocity became zero at end of each stroke [18]. Since hydrogels are viscoelastic, lower velocities increase the amount of time for deformation to occur, thereby increasing contact area as conformity increases [199].

Unlike solid surfaces, friction in hydrogels is related to contact area, which in turn is dependent on the amount of deformation induced by load [139, 189, 190, 199]. Since hydrogels are viscoelastic, the lack of time for deformation to occur at higher velocities reduces contact area [199], and COF decreases with increasing sliding speed [25, 180, 189, 190]. While increasing the diameter of the counter surface decreased contact

stresses and reduced deformation depth at the same load, the thickness of the lubrication film was also increased, thereby decreasing friction [25, 189]. It is possible that wear could be reduced with decreased contact stress by increasing contact area, but this would also increase the area on the hydrogel surface that is susceptible to wear damage.

Since higher water content in hydrogels is associated with decreased modulus and contact stress, and increased contact area, it would impact both the COF and wear. The COF tended to decrease with the increase in water content by decreasing polymer concentration [187, 188, 201], or addition of hydrophilic components such as alginate [202], polyacrylamide [106] and PVP [122]. However, the COF did not decrease further when water content was increased above 80% in PAAc hydrogels sliding against glass [187]. Similarly, wear decreased by raising the water content of pHEMA hydrogels from 65% to 75% [188], but increased in PVA/PVP hydrogels when water content increased from 85% to 90% [124].

The effect of a nanofiller on the COF and wear depends on filler content. The COF decreased with HAp addition of up to 4.5 wt% into PVA, beyond which the COF increased [25, 203, 204]. However, the method of HAp incorporation may be a factor. Mixing in of HAp increased both the COF and wear [199], while HAp formed in situ resulted in wear similar to or lower than that of observed for neat PVA hydrogels [203]. The COF and wear may decrease for low nanofiller additions because of improvements on hydrogel modulus, but at high filler addition or with inadequate mixing, particles may agglomerate. This increases the likelihood for agglomerates to increase surface roughness or cause third body wear.

2.7.3 Characterization of Wear

Wear in hydrogels has been characterized using a variety of methods including change in mass, depth of the wear track and wear volume. Difference in total mass of hydrogels before and after testing was used to determine wear [181, 186, 199]. However, the change in mass could be affected by fluid exudation, changes in hydration or absorp-

tion of lubricant molecules. Therefore, wear was expressed as a percentage of change in dry mass by Katta et al. [124]. Depth of wear has been determined by the displacement of the counter surface pin against hydrogel surfaces [188] and by CLSM to obtain the maximum depth of the wear track profile [200]. However, the depth of a wear track in hydrogels is likely the sum of both deformation and wear [188, 201, 204]. Soaking in PBS for two days appeared to be successful in removing reversible creep in PVA/PVP hydrogels [124]. Wear volume was calculated from decrease in mass using the same density of 1.004 g/cm^3 for PVA hydrogels with water contents ranging from 45% to 85% [205]. It was also estimated spectroscopically by adding potassium iodide indicator solution to saline lubricant containing PVA wear particles [18].

Surface roughness determination using CLSM [200] and profilometry [185, 195] was performed as a measure of surface damage. SEM was also used to qualitatively examine wear surfaces. In unfilled PVA hydrogels, abrasive wear was apparent at high contact pressures and pores were exposed [181]. With the addition of 100 nm HAp through mixing, HAp particles were pulled out and scratches could be seen in the direction of motion, but there was also evidence of fatigue wear [181, 203]. In situ formation of HAp in PVA solutions, however, resulted in predominately fatigue wear and delamination [203]. The size of hydrogel pores decreased with increased HAp [204] and silica [202] addition. Pores in PVA hydrogels containing HAp were not as easily deformed or torn, and a low number of FTCs resulted in plastic flow and adhesive wear, while there was no apparent damage with higher FTCs [204]. However, these samples were dried in air and no special care was taken to preserve hydrogel structure, which may affect surface features when examined using SEM.

Abrasive wear was found on the underside of hydrogel samples after tribological testing by Katta et al. [124]. This was caused by lateral expansion due to the high Poisson's ratio of PVA hydrogels and a lack of lubrication underneath the sample. Northwood et al. used waterproof double-side tape for sample mounting [185, 195]. Fixation could be important in isolating wear of hydrogels to the direct effect of counter surface sliding.

2.7.4 Crossing-Paths Wear

Artificial discs, and other total joint replacements, have been shown to experience multidirectional sliding *in vivo* in retrieval studies [196, 206]. Unidirectional sliding of metal or ceramic counter surfaces on UHMWPE are associated with low wear rates since strain hardening results from the alignment of polymer molecules in the direction of sliding, but also leads to softening in the perpendicular direction [207-209]. Thus, multidirectional, or crossing-paths, sliding on UHMWPE caused intermolecular rupture and increased wear when compared to unidirectional sliding, at rates of up to two or three magnitudes higher [207]. The mechanism of wear for UHMWPE in unidirectional sliding was abrasion in the direction of motion, while there was evidence of adhesion, plastic deformation and fatigue in multidirectional sliding [209]. In contrast, metal-on-metal pairs have lower wear rates in multidirectional sliding than in linear sliding. The reduction in wear is due to a polishing effect from crossing-paths motion, where abraded edges are folded back down into scratches, minimizing the likelihood of material removal [210].

Scholes and Unsworth suggested that wear testing using pin-on-plate reciprocation with rotation could be a cheaper alternative than simulator testing when screening material pairs for use in articulating joint replacement devices [210]. The effect of crossing-paths motion on sliding distance depends on the angle of rotation and contact radius between a spherical pin and a flat counter surface, which was modelled by Powell for wear of metal-on-metal contacts [211, 212]. However, simulator testing would be required for investigating wear rates in TDR devices. Flexion-extension, axial rotation, lateral bending and dynamic axial loading were combined in simulator tests according to ASTM and ISO protocols [206]. ASTM F2423-05 does not require phasing of combined motions, resulting in unidirectional curvilinear wear tracks, while phasing of the combined motions in ISO/FDIS 18192-1 (2006) resulted in oval shaped multidirectional wear tracks. Consequently, the wear rate of a lumbar UHMWPE-CoCr TDR was 20 times greater using ISO than the ASTM protocol.

Northwood and Fisher [185] performed crossing-path tests on stainless steel, cartilage and three methacrylate-based interpenetrating network hydrogels, with water contents of 14%, 19% and 37%, against bovine cartilage pins. The steady-state COF was highest for stainless steel with rotation, increasing to 0.88 from 0.7 without rotation. COF for hydrogels (approximately 0.3) and cartilage (~0.05) were not affected by the addition of rotation. Surface roughness was used to characterize the degree of wear resistance in this study, which may not be sufficient to quantify wear. In unidirectional reciprocation, the hydrogel with the highest water content had the lowest increase in surface roughness after wear testing. With multidirectional motion, the hydrogel with the lowest water content, and thus the highest modulus and strength, possessed the lowest increase in surface roughness. However, since the compositions of the hydrogels were not specified, it would be difficult to speculate the effect of rotation based solely on water content.

2.8 HIGH FREQUENCY 3D ULTRASOUND IMAGING

Ultrasound imaging (US) is a medical imaging technique that provides fast acquisition rates [213]. Parallel brightness-mode (B-mode) image planes may be stacked to form three-dimensional (3D) images for imaging of a volume [214]. Clinically, US frequencies are typically in the range of 2–15 MHz [213], but higher frequencies have been used for micro-ultrasound imaging of cardiac and tumour models in mice [215]. Frequencies of 20 to 55 MHz can provide high resolutions of 30 to 60 μm [215]. 3D US of porcine aortic valve cusps was successfully performed using a frequency of 40 MHz, which provided a B-mode image plane spacing of 32 μm [214]. However, as frequency is increased, attenuation also increases and imaging depth is sacrificed [213].

PVA hydrogels have been used as tissue mimicking phantoms for US with acoustic properties similar to human tissue [216-219]. Properties can be varied by choice of solvent (water or DMSO), water content, the number and rate of F-T cycles, and degree of hydrolysis, due to the effect of these parameters on hydrogel pore density [216, 217].

To preserve the acoustic properties of hydrogels, dehydration must be prevented during storage and imaging [216].

2.9 MOTIVATION FOR THESIS

Clinically available artificial discs for the replacement of diseased cervical IVDs, providing an alternative to fusion, are composed of materials much stiffer than the natural tissue. With the exception of the Bryan disc, they do not have the shock absorbing and fluid flow properties of a healthy IVD. F-T PVA hydrogels are highly tunable, can be produced with water content similar to IVD, and have a porous structure that allows for fluid flow under stress. The addition of nanofillers could potentially provide reinforcement and tuning of properties at low filler contents. Design criteria for PVA-based hydrogel materials for IVD applications include sufficient stiffness to withstand *in vivo* loads, dimensional stability, strain rate dependence similar to the natural IVD, resistance to wear, biocompatibility and ease of manufacture. The effects of Laponite and BC, nanofillers with low and high aspect ratios, respectively, on PVA hydrogels were studied. Since the *in vivo* environment contains salts and other solutes, compression testing to determine stress-strain, strain rate dependence, stress relaxation, creep and dynamic properties was performed in water and after aging in PBS. Furthermore, deformation volume from crossing-paths wear testing, measured from 3D US images, and SEM were used to assess wear in the hydrogels, since current TDR devices all have articulating designs. Finally, the feasibility of producing a multi-component prosthesis, comprising of different hydrogel compositions for the annulus and nucleus components, was investigated in a preliminary design to mimic the natural IVD structure.

Chapter 3

MATERIALS AND METHODS

3.1 MATERIALS

Poly(vinyl alcohol) with molecular weight of 146 000–186 000 g/mol, 99+% hydrolyzed was used as received from Sigma-Aldrich (#363065, St. Louis, MO). Laponite RD was used as obtained from Southern Clay (Gonzales, TX). Bacterial cellulose was synthesized in our laboratory and purified from shaken cultures of *Acetobacter xylinum*, and was chemically modified to obtain phosphorylated BC by others in the laboratory. Water denotes the use of distilled deionized water.

Phosphate buffered saline (PBS) was prepared in water with potassium phosphate (KH_2PO_4) (Caledon Laboratory Chemicals, Georgetown, ON), potassium chloride (KCl) (EMD Chemicals, Inc., Darmstadt, Germany), sodium chloride (NaCl) (Caledon, Georgetown, ON) and sodium phosphate dibasic heptahydrate ($\text{Na}_2\text{HPO}_4 \cdot 7\text{H}_2\text{O}$) (Sigma Aldrich, St. Louis, MO) (preparation method in Appendix A).

Alpha calf fraction serum (ACS), non-iron supplemented (Fisher Scientific # SH30212.03, HyClone Laboratory Inc., Logan, UT) and Gibco 100x antibiotic-antimycotic (Invitrogen #15240-062, Burlington, ON) were used in the lubricant for crossing-path wear testing. The antibiotic-antimycotic was delivered frozen, and was defrosted and pipetted into 5 mL portions before re-freezing in polypropylene centrifuge tubes. Sapphire ball lenses (Edmund Optics #R63-227, Barrington, NJ), 9.525 mm diameter and 0.010 μm RMS roughness, were used for the counter surface in crossing-paths wear testing. The two-part epoxy used to bond sapphire spheres to acrylic was J.B. Weld

(Sulphur Springs, TX), while PR80 3M™ Scotch-Weld™ Rubber Toughened Cyanoacrylate (3M, London, ON) was used to glue hydrogels to an aluminum substrate.

3.2 PREPARATION OF PVA AND PVA-NANOCOMPOSITE HYDROGELS

Eight PVA and PVA-nanocomposite (PVA-NC) hydrogel compositions were used in this thesis (Table 3.1); their preparation methods are described in this section. All percentages describing compositions are based on mass.

Table 3.1: PVA and PVA-NC solution compositions.

Solution composition	Nominal PVA concentration [wt%]	Nanofiller type	Nanofiller content [wt%]
10% PVA	10	–	0
15% PVA	15	–	0
20% PVA	20	–	0
0.75% Lap-10%PVA	10	Laponite	0.75
1% Lap-10%PVA	10	Laponite	1
0.48% BC-10%PVA	10	Bacterial cellulose (BC)	0.48
0.25% pBC-10%PVA	10	Phosphorylated BC	0.25
0.4% pBC-10%PVA	10	Phosphorylated BC	0.4

3.2.1 Preparation of PVA Solutions

Poly(vinyl alcohol) was used as the matrix polymer in the hydrogels. PVA powder was dissolved at 10%, 15% and 20% into water in a reaction kettle held in a 90 °C water bath for 3 hours. Mechanical stirring at 100 rpm was employed to ensure homogenization and a water-cooled condenser was used to minimize the evaporation of water [11, 13, 24]. 10% was used as the base PVA concentration for compositions containing nanofillers because 10% PVA solutions have lower viscosities resulting in less air entrapment after dissolution and solution moulding. 10% PVA hydrogels are well charac-

terized in our research group and previous studies were used as a basis for comparison [13, 14, 24].

3.2.2 Preparation of PVA-Laponite Solutions

Thermogravimetric analysis (TGA) was performed to determine the amount of water in the Laponite powder. Approximately 10 mg of Laponite was placed in the sample cell and heated from 25 °C to 500 °C at 10 °C/min.

For Laponite-containing 10% PVA hydrogels, the required amount of Laponite was first dispersed by slowly adding to the total amount of water required for the polymer solution under magnetic stirring at 500 rpm. The dispersion was stirred for 1 hour during which it went from cloudy to clear in appearance, indicating good dispersion of the nanofiller. Subsequently, it was placed in a sonicating bath for 1 hour then left at room temperature for 1 day to allow water to hydrate the clay sheets [220]. After approximately 24 hours, PVA was added to the dispersion and dissolved in the same manner as unfilled PVA solutions. Two concentrations of Laponite-containing solutions were made: 0.75% Laponite in 10% PVA and 1% Laponite in 10% PVA. However, longer dissolution times were used for these solutions, 4 hours for 0.75% Laponite solutions and 5 hours for 1% Laponite solutions, since PVA took longer to dissolve in the presence of Laponite.

Laponite-containing PVA solutions were spin-dried and examined using transmission electron microscopy (TEM) to determine the uniformity and degree of dispersion. Images were taken with an accelerating voltage of 100 kV using the Philips CM-10 TEM fitted with a Hamamatsu digital camera at the Biotron Imaging & Data Analysis Facility (London, Ontario, Canada).

3.2.3 Preparation of PVA-BC Solutions

Bacterial cellulose (BC) was obtained purified and suspended in water. Briefly, BC was harvested from shaken cultures of *Acetobacter xylinum* and autoclaved, then pro-

cessed by adding 100 mL of 0.1 mol/L NaOH and heating to 90 °C for 90 minutes [169]. After the mixture was cooled, it was washed and centrifuged, usually four to five times, until the supernatant becomes clear [221].

Phosphorylated BC (pBC) was obtained in ethanol after phosphorylation according to the procedure found in [172]. Energy-dispersive X-ray spectroscopy found that the pBC contained between 12.58 and 15.4 atomic% phosphorus (Appendix B). It was magnetically stirred with 2 L of water and filtered using a vacuum membrane filter assembly to remove as much of the solvent as possible, and repeated three times, to ensure ethanol was fully exchanged for water in the dispersion. Finally, approximately 200 mL of water was added to the filtrate for the fibres to be uniformly dispersed using a magnetic stirrer.

TEM of BC and pBC fibres was performed to examine their morphology. A 0.1 g/L suspension (dry weight) of each fibre was prepared by sonication with an ultrasonic probe set at 60 W for three minutes (Misonix XL-2000, Farmingdale, NY). A drop of the suspension from a Pasteur pipette, approximately 200 μ L, was left to settle on a Formvar carbon-coated 100 mesh copper grid (Electron Microscopy Science, Hatfield, PA) for 15 minutes and the excess was blotted off. Negative staining of the fibres was done with a 2 % w/v solution of uranyl acetate for three minutes then rinsed. Images were taken with an accelerating voltage of 80 kV using the Philips CM-10 TEM at the Biotron.

Samples of the BC and pBC dispersions were weighed then dried in a 60 °C oven to determine the fibre dry weight in suspension. The drying end-point was achieved when the mass of the dried BC or pBC did not decrease further after two subsequent measurements at an interval of 6 hours. Water was added to the dispersions to the total amount required for the polymer solution. PVA was then added and dissolved for three hours using the same method as for the other solutions. The compositions made were 0.48% BC, 0.25% pBC and 0.4% pBC, all in 10% PVA.

3.2.4 Pouring Solutions in to Moulds

Polymer solutions were left to degas overnight to remove air bubbles. The more viscous Laponite and BC containing solutions, in which air remained entrapped, were centrifuged at 5000 rpm for 15 to 30 minutes to remove air bubbles.

The polymer solutions were poured into the appropriate moulds. For compression testing, cylindrical samples were made using a 3/4" thick aluminum insert with 16 (4×4) reamed holes of 11 mm in diameter that was sealed between two sheets of natural gum rubber and two solid aluminum plates from existing moulds. Samples for crossing-paths wear testing were cut from hydrogel sheets approximately 5 mm thick. Hydrogel sheets were made using a rubber spacer of the desired sheet thickness sandwiched between two aluminum plates. The side of the hydrogels used for wear testing was moulded on a polished aluminum plate.

3.2.5 Freeze-Thaw Cycling

The polymer solution-filled moulds were placed in a refrigerating/heating circulating bath (VWR Brand, model 1187P) with 50% v/v ethylene glycol in water for freeze-thaw (F-T) cycling. They were cooled from 20 °C to -20 °C at a rate of 0.1 °C/min, held at -20 °C for 1 hour, then heated to 20 °C at 0.1 °C, for six cycles [13, 24]. Each freeze-thaw cycle (FTC) took 14 hours and 20 minutes.

Once removed from the moulds, the specimens were equilibrated in water for 24 hours before further preparation or testing. Equilibrated samples are denoted using the term “fresh.”

3.2.6 Aging in Water and Solutions

Hydrogels were placed in 1× PBS for 7 days prior to testing and also aged in distilled water for 7 days as a control. Mass and volume of the samples were determined

before and after the 7-day aging period to assess the amount of mass loss and shrinkage. Mass was measured using an analytical balance (Metler, Columbus, OH) after blotting hydrogel surfaces. ImageJ (U. S. National Institutes of Health, Bethesda, MD) was used to determine sample dimensions from images of the hydrogels, taken against a ruler for scale, in order to calculate sample volume. Samples made using the cylindrical compression sample moulds were chosen for volume determination since the diameter and thickness of hydrogels can be measured and volume was calculated using the formula,

$$V = \pi r^2 h \quad (3.1)$$

where V , r and h are the volume, radius and height of the cylindrical shaped hydrogel.

3.3 STRUCTURE STUDIES

3.3.1 Scanning Electron Microscopy

Since scanning electron microscopy (SEM) is performed under vacuum, dehydration of the hydrogels was required prior to imaging. Critical point drying using carbon dioxide (CO₂) was used to dehydrate the specimens, given that the porous structure of a hydrogel would otherwise collapse under normal drying conditions. Critical point drying, sputter coating and SEM were all performed at the Biotron.

3.3.1.1 Critical Point Drying

Hydrogel samples were placed in 100% ethanol for at least one week prior to critical point drying. The samples were dehydrated using a Samdri PVT-3B critical point dryer (Tousimis Research Corp., Rockville, MD). Drying was performed by first saturating the dryer chamber with CO₂ then holding the temperature at 31 °C and pressure at 1100 psi for one minute to obtain critical point dried samples. Fractured cross-sections of

hydrogels were obtained by immersing the dried hydrogels in liquid nitrogen before fracturing [16].

3.3.1.2 Scanning Electron Microscopy

Samples were mounted on 15 mm SEM stubs with an adhesive then were placed under vacuum (below 100 mTorr) to ensure complete removal of moisture. Since PVA is a poor electrical conductor, the samples were sputter coated with palladium-gold for 5 minutes at 8 mV to form a coating approximately 10 nm in thickness. SEM images were obtained using the Hitachi 3400-N Variable Pressure Scanning Electron Microscope at the Biotron using an accelerating voltage of 5 kV and a working distance of approximately 10 mm.

3.3.2 Differential Scanning Calorimetry

Samples were vacuum dried in the presence of a desiccant until mass of the samples stabilized prior to DSC analysis. Approximately 10 mg of each dried sample was placed in aluminum DSC pans. The scan was performed under nitrogen flow of 50 mL/min and at a heating rate of 10 °C/min from 50 °C to 250 °C [125, 128]. The area under the endothermic peak was used to determine the heat of melting in the sample. Crystallinity of the sample was calculated by,

$$X[\%] = \frac{\Delta H_{m, sample}}{\Delta H_{m, PVA}} \times 100\% \quad (3.2)$$

where X is crystallinity in %, $\Delta H_{m, sample}$ is the endothermic peak of the sample in the DSC thermogram and $\Delta H_{m, PVA}$ is ΔH_m of 100% crystalline PVA, which is 138.6 J/g [109, 125, 126]. Since PVA-NC hydrogels contained both PVA and nanofillers, the theoretical mass of the fillers was excluded and ΔH_{sample} was normalized to the mass of only PVA in the hydrogels in calculating crystallinity of PVA-NC samples. DSC of Laponite, BC and pBC showed that these nanofillers did not experience any thermal events in the temperature range tested.

3.4 MECHANICAL TESTING

Compression testing was performed with a MTS Bionix 858 Universal Testing System fitted with a 5 kg load cell. The load cell was connected to a computer through an Instron interface for control and data collection. Stainless steel platens (Figure 3.1), 30 mm in diameter, were set parallel to ensure even loading across the whole sample. For all compression testing, samples were tested in a similar manner to Millon et al. [24] in which cylindrical samples were preconditioned using 10 sinusoidal strain cycles between 0 and 0.25 strain, then left to relax for 1 hour prior to testing. Tests were done in a fluid bath held at 37 °C to prevent dehydration of samples and to maintain an aqueous testing environment near *in vivo* temperature. The composition and bath always corresponded to the solution (water or 1× PBS) in which the hydrogel samples were stored or aged.

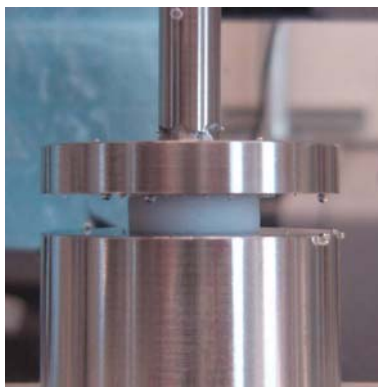


Figure 3.1: Stainless steel platens in a temperature-controlled bath used in compression testing of hydrogel cylinders.

3.4.1 Unconfined Compression

Hydrogel samples were strained to 0.45 strain at strain rates of 1%/s, 10%/s and 100%/s, with 1 hour between each strain rate to allow samples to recover. Tests were performed fresh and after aging for 7 days in 37 °C water, and after aging in 1× PBS at 37 °C. The same samples were used for the three strain rates, while different sets of samples were used for the different testing conditions.

Unconfined compression stress-strain data for individual samples were fitted to a five-parameter exponential model to generate a stress-strain curve,

$$\sigma = y_0 + ae^{b\varepsilon} + ce^{d\varepsilon} \quad (3.3)$$

where σ is the stress at strain ε , y_0 , a , b , c , d are fitting parameters. This procedure was used to fit tensile data obtained for PVA hydrogels and was discussed in detail by Millon [222]. The procedure for the treatment of compression data is outlined in Appendix C.

Tangent modulus ($E_{tangent}$) curves were obtained by differentiating Equation 3.3 with respect to ε ,

$$E_{tangent} = \sigma' = abe^{b\varepsilon} + cde^{d\varepsilon} \quad (3.4)$$

and secant modulus (E_{secant}) at strain ε , was calculated using the relationship,

$$E_{secant}(\varepsilon) = \frac{\sigma(\varepsilon)}{\varepsilon}. \quad (3.5)$$

While $E_{tangent}$ is an instantaneous modulus and describes the shape of the stress-strain curve, E_{secant} is representative of the strain of the hydrogel at a given load or stress. σ , $E_{tangent}$ and E_{secant} were evaluated for individual samples at intervals of 0.05 strain then averaged over the sample set.

3.4.2 Stress Relaxation

Stress relaxation under compression was performed on samples after 1 week of aging in $1\times$ PBS. They were strained at a rate of 10%/s to 0.25 strain then held at 0.25 strain for 1 hour. The decrease in load due to stress relaxation in each sample was tracked. Stress relaxation data for each sample was fitted to a 5-parameter exponential decay model with the equation,

$$\frac{\sigma}{\sigma_0} = \frac{\sigma_R}{\sigma_0} + ae^{-bt} + ce^{-dt} \quad (3.6)$$

where σ is the stress at time t , σ_0 is the initial stress at $t = 0$, σ_R is the residual stress for $t \rightarrow \infty$, and a , b , c and d are fitting parameters. A condition of $\sigma_R/\sigma_0=(1-a-c)$ was imposed such that $\sigma/\sigma_0=1$ at $t=0$ in the fit. The double exponential decay function is of the same form as the solution to the Maxwell-Wiechert viscoelastic model with two parallel Maxwell elements as described in Painter and Coleman [223].

3.4.3 Creep

For creep testing, a load of 0.05 MPa stress was applied and maintained on each hydrogel sample for 1 hour. The crosshead displacement was recorded and used to calculate strain over time. Samples aged in $1 \times$ PBS for 1 week were tested.

3.4.3.1 Creep Modelling

The creep data were fitted using three viscoelastic models (Figure 3.2) comprised of springs (E_i) and dashpots (η_i), representing elastic and viscous behaviour, respectively. σ_0 is the applied compressive stress.

The “three-parameter-solid” viscoelastic model, as illustrated in Figure 3.2a, was used by Burns et al. [63] and Keller et al. [64] to model the creep of intervertebral discs from humans, Kaleps et al. [65] and for rhesus monkey IVD, and Wang and Campbell [23] for PVA hydrogels. Since $\sigma_i = E_i \varepsilon_i$ for a spring and $\sigma_i = \eta_i \dot{\varepsilon}_i(t)$ for a dashpot, the solution to this model is,

$$\varepsilon(t) = \sigma_0 \left[\frac{1}{E_1} \left(1 - e^{-\frac{E_1 t}{\eta_1}} \right) + \frac{1}{E_2} \right] \quad (3.7)$$

which is the three-parameter exponential rise-to-maximum function,

$$y(t) = a(1 - e^{-bt}) + y_0 \quad (3.8)$$

such that E_1 , E_2 and η_1 can be calculated from a , b and y_0 .

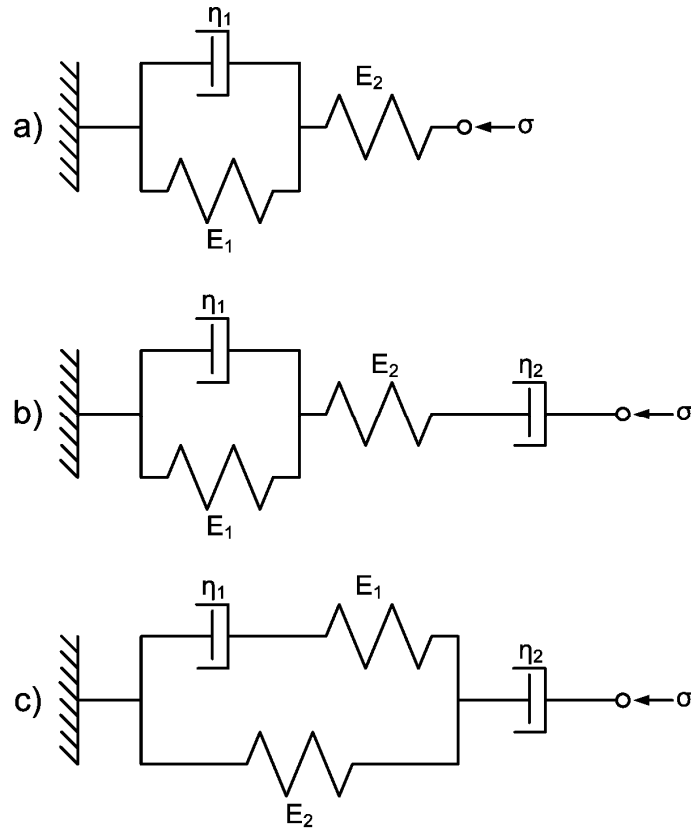


Figure 3.2: Spring (E_i) and dashpot (η_i) models for viscoelastic creep; the “three-parameter-solid” model (a), Burger’s model (b) and Bausch model (c).

Two four-parameter models, each with two springs and two dashpots, were used to attain a better fit to the creep data. The Burger’s model (Figure 3.2b), a Kelvin-Voigt element arranged in series with a Maxwell element, was used by Gloria et al. [178] to model creep curves for a composite IVD prosthesis. It has the solution,

$$\varepsilon(t) = \sigma_0 \left[\frac{1}{E_1} \left(1 - e^{-\frac{E_1 t}{\eta_1}} \right) + \frac{1}{E_2} + \frac{t}{\eta_2} \right] \quad (3.9)$$

of which the data were fitted to,

$$y = a(1 - e^{-bt}) + y_0 + ct. \quad (3.10)$$

Likewise, the solution to the model described by Bausch et al [224] (Figure 3.2c) to model cell membrane mechanics is,

$$\varepsilon(t) = \sigma_0 \left[\frac{1}{E_2} \left(1 - \frac{E_1}{E_1 + E_2} e^{-\frac{t}{\tau}} \right) + \frac{t}{\eta_2} \right], \text{ where } \tau = \eta_1 \frac{E_1 + E_2}{E_1 E_2} \quad (3.11)$$

which was fitted to,

$$y = a(1 - be^{-ct}) + dt \quad (3.12)$$

In addition to the viscoelastic models in shown in Figure 3.2, an empirical 5-parameter rise-to-maximum exponential model Equation 3.13 was also used to fit the data:

$$\varepsilon(t) = \varepsilon_0 + a(1 - e^{-bt}) + c(1 - e^{-dt}) \quad (3.13)$$

where a , b , c and d are the fitting parameters. This model allows for creep to asymptotically reach a maximum, unlike the four-parameter Burger's and Bausch models for which $\varepsilon(t) \rightarrow \infty$ as $t \rightarrow \infty$ and would be physically unfeasible for a viscoelastic solid undergoing compression.

3.4.4 Cyclic Compression Testing

Fresh and 1× PBS aged samples were compressed to 0.05 strain then held for 10 seconds prior to starting sinusoidal compression cycles between 0.05 and 0.25 strain at frequencies of 0.5, 1 and 2 Hz for 120 cycles. Stress and strain were both fitted against time to a four-parameter sinusoidal function,

$$y = y_0 + a \sin\left(\frac{2\pi t}{b} + c\right) \quad (3.14)$$

where y is the stress or strain, a is the amplitude (or half of the cyclic strain), b is the period (the inverse of frequency) and c is the shift of the waveform in radians. However, the large amount of data for all 120 cycles of testing could not yield a proper sinusoidal fit and thus only the last ten strain cycles were selected for the fit since there would be a lesser effect from relaxation of the samples. For each pair of stress and strain fits against time, $\tan \delta$ can be calculated using the formula

$$\tan \delta = \tan(c_{stress} - c_{strain}) \quad (3.15)$$

since the difference of the parameter c in the stress and strain fits from Equation 3.14 is the phase shift angle δ , in radians.

3.5 CROSSING-PATH WEAR

A crossing-path wear tester [211] was loaned to us by Prof. J. Medley (Department of Mechanical and Mechatronics Engineering, University of Waterloo) for crossing-paths wear testing of our PVA and PVA-NC hydrogels. The crossing-path wear tester was designed by Powell and Havrlant, and used to test the wear of metal-metal pairs [211]. The tester can accommodate six samples at a time. Sample holder and counter surface components were designed, with the assistance of the University Machine Services, to retrofit the machine for testing of hydrogel samples. Delrin holders fit onto the existing stainless steel base and hydrogel samples were clamped with a Delrin ring secured by six screws. A drawing of the sample holder is found in Appendix D.

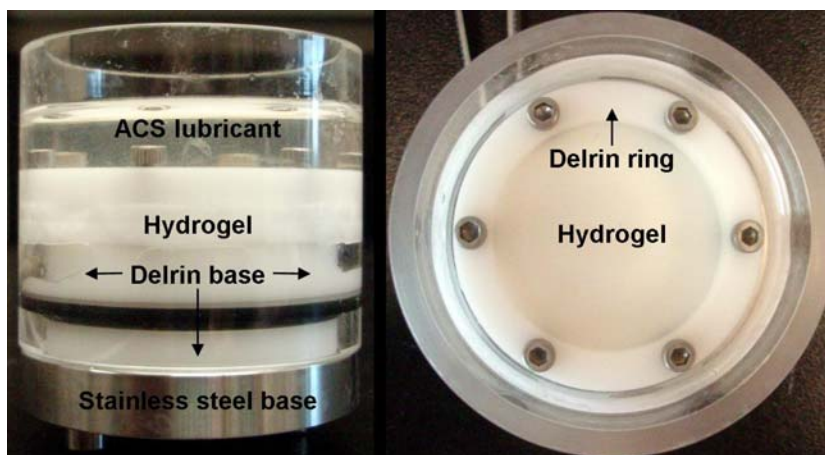


Figure 3.3: Front view (left) and top view (right) of a retrofitted wear pod set up for crossing-paths wear testing.

A sapphire sphere counter surface was chosen for its hardness and durability as the smooth counter surface, so that counter surface damage may be minimized [225]. It

was glued with epoxy to the inverted hemispherical surface machined into an acrylic post (Figure 3.4) then soaked for one week in water to leach out any unreacted epoxy components.

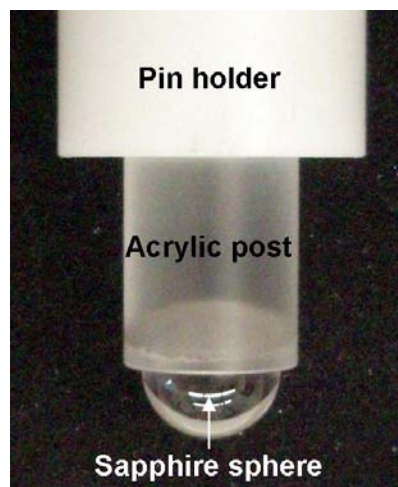


Figure 3.4: Pin for crossing-paths wear testing consisting of a sapphire sphere counter surface glued with epoxy to an acrylic post.

The lubricant was prepared according to Brandt [194, 226] and Austin [197], consisting of 25% alpha calf serum (ACS) in PBS with antibiotic-antimycotic to prevent microbial growth; the composition is listed in Table 3.2.

Table 3.2: Composition of the 25% alpha calf serum (ACS) lubricant for crossing-path wear testing.

Component	Amount (mL)
Non-iron supplemented alpha calf serum	500
1× PBS	1650
100× antibiotic-antimycotic	5

The ACS and antibiotic-antimycotic were defrosted and PBS was filtered using a 0.45 μm membrane filter before mixing. The lubricant mixture was divided into 200 mL portions and refrozen in individual polyethylene containers. Portions were thawed in a refrigerator for 48 hours before use.

Hydrogel samples were first equilibrated in PBS for at least 1 week prior to wear experiments to avoid shrinkage during testing in the ACS lubricant. Due to the high

Poisson's ratio of PVA hydrogels, the reciprocating normal load on the samples during testing caused lateral expansion of hydrogel under the load. This resulted in wear on the underside of the hydrogel sample, which was also found by Katta et al. [124]. To prevent this undesired wear damage, the bottom of each hydrogel sample was glued with rubber-toughened cyanoacrylate to a thin piece of aluminum roughened with 400 grit sandpaper (Figure 3.5). The cyanoacrylate has a 24-hour cure time according to product specifications.

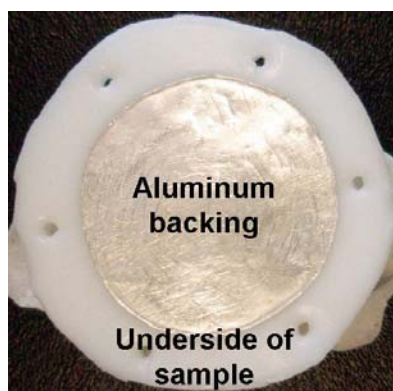


Figure 3.5: Aluminum backing glued to the underside of a hydrogel sample with rubber toughened cyanoacrylate to prevent wear on the bottom surface.

The specimens were then clamped into the wear cell and trimmed to fit into the holder. They were equilibrated in the ACS lubricant to allow the glue to cure for 2 days prior to wear testing. The lubricant was changed prior to and at three days after commencing wear testing [211]. The parameters for crossing-paths wear testing were a normal load of 5 N, stroke length of 8.5 mm, pin rotation of 28° and frequency of 1 Hz; testing for 500 000 cycles took approximately 6 days at room temperature. During testing, wear cells were wrapped with plastic wrap that was secured to the wear pin using twist ties to prevent lubricant evaporation. Samples were weighed immediately before and after wear testing and again after equilibrating for 48 hours in fresh ACS lubricant to allow hydrogels to recover any reversible creep [124].

3.5.1 Three-Dimensional Ultrasound for Characterization of Wear

High frequency three-dimensional micro-ultrasound (3D US) was used to quantify the volume of the wear track after crossing-paths wear testing. Acquisition of the 3D US images must be performed within a medium, thus the samples could be imaged in PBS, eliminating concerns about hydrogel dehydration and without detriment to sample dimensions. Hydrogels were soaked in PBS for 2 days [124] after removing from the ACS lubricant for weighing, and prior to 3D US. The aluminum backing glued on to hydrogel samples before wear testing was removed, and hydrogel samples were pinned to a rubber damper mat to prevent ultrasound waves from reflecting from the bottom of the specimen container. Images were obtained with the Vevo 770 ultrasound scanner (VisualSonics Inc., Toronto, ON) at the Robarts Research Institute using a 40 MHz transducer with a focal length of 6 mm. The procedure used to acquire images was adapted from Khan et al. [214]. The top surface of each specimen was positioned approximately 6 mm from the probe to correspond with its focal length. The ultrasound probe was translated by a linear motor over 15.05 mm, which acquired B-mode images with a square field of view (FOV) of up to 15×15 mm, at a spacing of 0.032 mm. This resulted in 3D US images formed by 473 parallel B-mode image planes.

A MATLAB program (Appendix E) was written to extract B-mode image planes as a series of 512×512 8-bit TIFF images from each raw 3D US data file. ImageJ was used to determine the area of the indent in each B-mode image. Surfaces of hydrogel samples were assumed to be flat prior to wear testing and the indent, created by the combined effects of wear and creep, was outlined using the polygon function in ImageJ and its area was measured. The volume of the indent, V , in mm^3 was then calculated by,

$$V = \sum_i \left[A_i \left(\frac{L}{512} \right)^2 s \right] \quad (3.16)$$

where A_i is the area of the groove of slice i , in pixel^2 , L is the height and width of the square FOV, in mm, and s is the spacing of the B-mode planes, in mm. The maximum depth of the groove was also measured using ImageJ.



Figure 3.6: Set-up for 3D ultrasound imaging of the hydrogel samples after crossing-paths wear testing. The linear motor translated the ultrasound probe to acquire successive B-mode image planes for 3D images.

3.5.2 Scanning Electron Microscopy

The wear surfaces and cross-sections of the hydrogels under the wear path were examined by scanning electron microscopy (SEM) after critical point drying with CO₂ as was done in Section 3.3.1. Samples were cut to fit the dimensions of the critical point dryer prior to drying. The surfaces and cross-sections of the middle and end of the wear path were compared qualitatively to those from an unworn area on the same sample.

3.6 TWO-COMPONENT HYDROGEL IVD STRUCTURE

A mould was designed to produce a two-component hydrogel structure, composed of two different hydrogel compositions representing the annulus fibrous (AF) and nucleus pulposus (NP) of the natural intervertebral disc.

3.6.1 Mould Design

The mould was constructed out of aluminum with a circular cross-section. It consisted of an outer tube of 20 mm inner diameter and a solid rod of 8 mm diameter to first produce the annulus component. Circular positioning notches on the end caps allowed for centering of the inner rod. Then each end cap, sealed with an o-ring to prevent leakage of polymer solution or the ethylene glycol coolant in the temperature-controlled bath, was secured to the outer tube with six screws. A threaded vent was drilled into one end cap to allow excess solution to flow out and prevent air pockets in the annulus component, which could be sealed with a screw. The middle rod was removed and flat end caps were used for the addition of polymer solution to create the nucleus component. The height of mould for the annulus and nucleus components was 7 mm, but its design would also allow the addition of components analogous to endplates after producing the annulus and nucleus.

3.6.2 Two-Component Hydrogel Disc

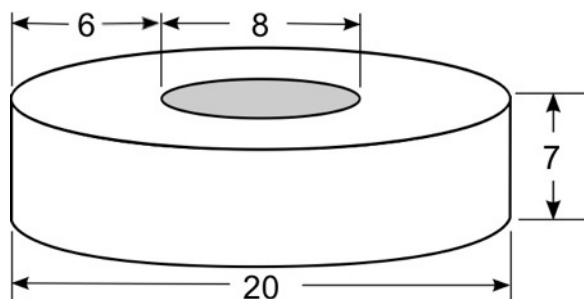


Figure 3.7: Schematic of the two-component hydrogel disc, 7 mm in thickness, consisting of an outer annulus component of 20 mm outer diameter and an inner nucleus component of 8 mm diameter. (All measurements in the diagram are in millimetres.)

Solutions with a range of PVA concentrations were used for the two-component hydrogel disc (Figure 3.7). Low concentration solutions of 1% and 3% PVA used for the nucleus component of the disc did not adhere well to the higher PVA concentration annulus component, therefore, 20% and 10% PVA were chosen for the preliminary experi-

ment. After 1 FTC on the 20% PVA annulus component, 10% PVA solution was added for the nucleus component, and the structure was subjected to six additional FTCs. The hydrogel structure was equilibrated in distilled water for one day prior to mechanical testing.

3.6.3 Compression Testing of Two-Component Hydrogel Disc

All compression testing of the two-component hydrogel was performed in water held at 37 °C. Unconfined compression at strain rates of 0.001, 0.01, 0.1, 1, 10 and 100%/s were used to compare with results from Cassidy et al. on canine IVD [55]. Since the slowest strain rates may cause irreversible deformation on the structure, the order of strain rates tested was 1, 10 and 100%/s with one hour between each test, 0.1 and 0.01%/s with 3 hours between the tests, then finally 0.001%/s. Compression was performed to 0.25 strain for each strain rate. Load was reported in addition to stress because the cross-sectional area is inhomogeneous, consisting of materials with two different compositions and properties.

Stress relaxation was performed in the same manner as done in Section 3.4.2 to 0.25 strain for one hour. Creep testing was done as in Section 3.4.3 at a load of 40 N. 40 N resulted in approximately 0.25 strain in the 20% annulus/10% nucleus PVA two-component disc and is approximately half of the axial load experienced by an IVD in the cervical region with the neck in an upright position [50].

3.7 STATISTICS

A sample size of five was used for studies in mass and volume decrease due to aging and unconfined compression (stress-strain), while $n=3$ was used for all others. One-way analysis of variance (ANOVA) and Holm-Sidak post-hoc analysis, which provides testing for all pairwise comparison and comparison versus control, were used to determine statistical differences ($p<0.05$).

Chapter 4

COMPRESSION PROPERTIES OF PVA AND PVA-NANOCOMPOSITE HYDROGELS

Intervertebral discs function to transfer and distribute load to the vertebral bodies, absorb shock, maintain disc space and allow for motion between vertebral segments. Although fusion of the vertebrae adjacent to a diseased disc is the current gold standard for surgical treatment of pain related to disc degeneration, total disc replacement (TDR) is an emerging treatment alternative. Several FDA approved devices, such as the Bryan disc, Prestige and Prodisc-C for cervical TDR, are clinically available. TDR, unlike fusion, preserves motion between the vertebral bodies, preventing adjacent level degeneration. However, with the exception of the Bryan disc, they do not allow for shock absorption like in a healthy disc, and all of the discs incorporate articulating surfaces in their designs that result in wear and could generate wear particles. In designing and selecting a material for a potential artificial disc, the properties of the natural IVD should be considered. In addition to being able to withstand the loads imposed on the disc from various activities, IVDs are viscoelastic and display strain rate dependence, as well as high degrees of stress relaxation and creep. They accomplish this through support and dissipation of load through fluid pressurization and flow in hydrated tissues, which contain a large amount of immobilized charges. These charges may create a resistance to fluid flow out of the disc when loaded and allow for fluid flow back into the disc when load is removed. Although IVDs have diurnal decreases in volume due to fluid loss, fluid is recovered during rest to regain disc height.

PVA hydrogels can be produced with large amounts of water and without the use of chemical crosslinkers for applications in medical devices. Freeze-thaw cycling of PVA solutions of varying concentrations allows for tunable and stable viscoelastic hydrogels. It may be possible to further modify PVA structure and properties with the addition of nanofillers. Two hydrophilic nanofillers were chosen – Laponite, a low aspect ratio, charged inorganic clay, and bacterial cellulose, a high aspect ratio biologically-derived fibre that was used both unmodified and phosphorylated, which added charged phosphate groups onto the fibre surface. The hydrated and viscoelastic nature of PVA hydrogels may allow for fluid flow and time-dependent properties that characterize IVD behaviour, while the addition of fillers may provide reinforcement and impart charges into the hydrogel in the case of charged nanofillers. Since these hydrogels are being investigated for use in a permanent artificial IVD device, dimensional stability and mechanical performance in a solution similar in osmolarity to fluids in the body are important in determining their suitability for the application, and to prevent unintended implant shrinkage or mechanical property changes. In this chapter, the effects of PVA concentration, nanofiller addition, and aging in water and PBS on unconfined compression and strain rate dependence were investigated. Furthermore, the effects of composition on viscoelasticity were examined using stress relaxation, creep and cyclic tests in compression.

4.1 COMPOSITION AND STRUCTURE OF HYDROGELS

The structure of PVA and PVA-nanocomposite (PVA-NC) hydrogels could be influenced by polymer concentration and the type of nanofiller added. In turn, pore structure and crystallinity may play a role in determining stiffness, viscoelasticity and fluid flow in the hydrogels. Aging and osmotic pressure could also have an effect on swelling and crystallinity. By understanding the impact of composition on structural and mechanical properties of PVA and its NC hydrogels, PVA concentration and nanofiller addition may be tailored to attain the properties required for applications in IVD replacement.

4.1.1 Laponite

A TEM image of the dispersion of 1% Laponite in a 10% PVA solution is shown in Figure 4.1. Some Laponite particles could be seen in small stacks. Although the Laponite clay discs, which are 25 nm in diameter and 1 nm in thickness, were not discretely dispersed, the agglomerated particles were still within nanometer dimensions (<100 nm), maintaining a high surface area to volume ratio characteristic of nanofillers, which may allow for a high degree of property modification with low filler content.

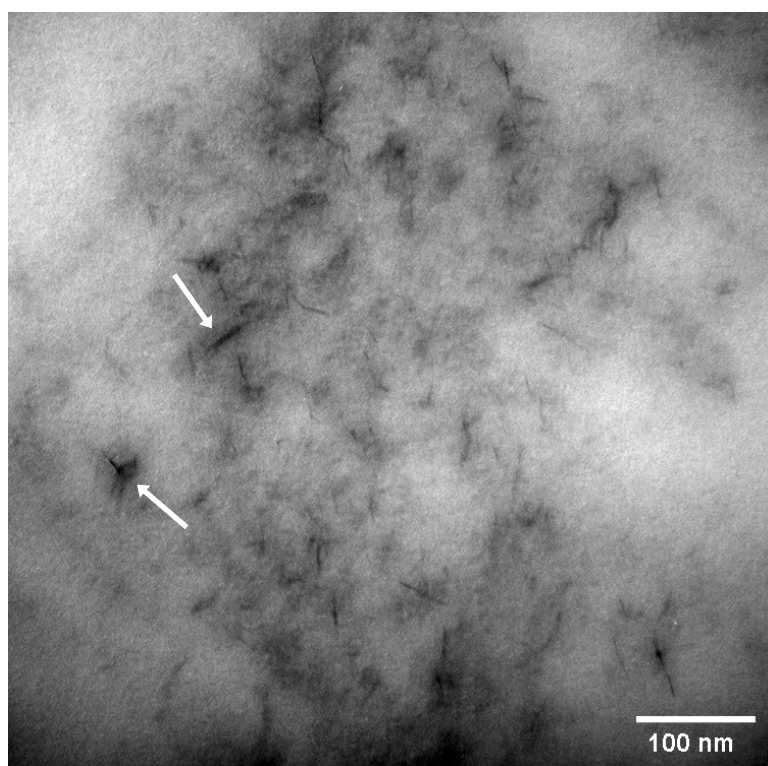


Figure 4.1: TEM of spin-coated 10% PVA solution with 1% Laponite showing dispersion of discrete discs, and agglomerated stacks (indicated by arrows).

4.1.2 Bacterial Cellulose

Phosphorylation did not appear to affect the morphology of BC when observed using TEM (Figure 4.2). Fibre diameter remained approximately the same and shortening of fibres after modification was not observed. Therefore, any effect of BC phos-

phorylation on hydrogel properties could be due to the presence of phosphate groups rather than changes in fibre morphology.

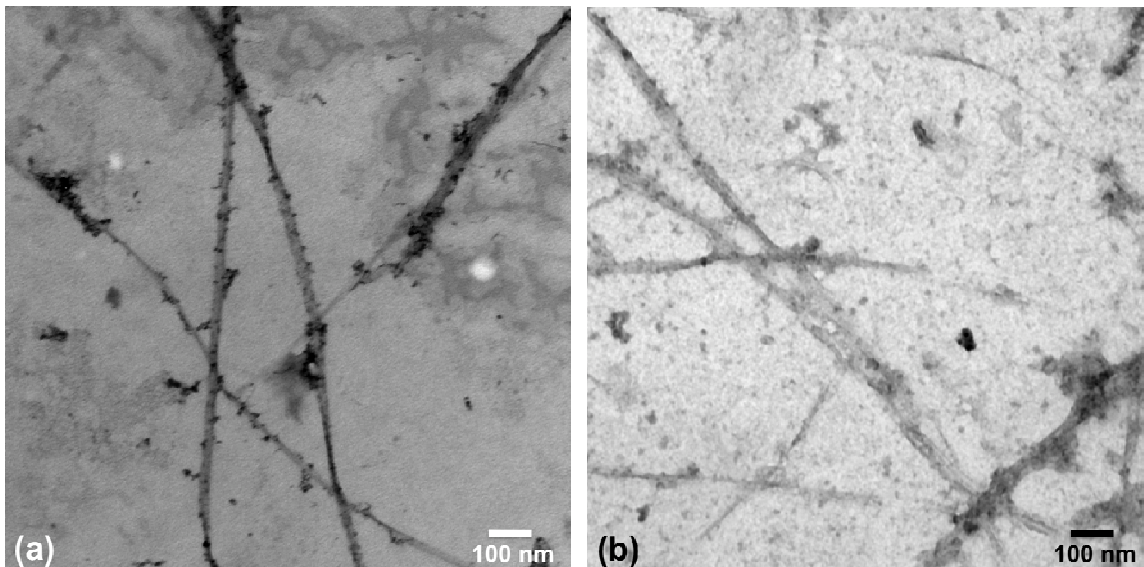


Figure 4.2: TEM of bacterial cellulose (a) and phosphorylated bacterial cellulose (b) prepared from dispersions in water.

4.1.3 Water Content of Solutions and Hydrogels

The water content of polymer solutions and hydrogels after six freeze-thaw cycles (FTC) is summarized in Table 4.1. 10% PVA solutions containing nanofillers had similar water contents to the unfilled 10% PVA solution, even though longer dissolution times were used for the Laponite-containing solutions. The amount of water in the Laponite powder was determined by TGA to be approximately 11% of the total mass. This is in agreement with the approximately 8% hydration in the Laponite crystal structure, and a moisture content of approximately 9.8% after handling and storage as reported by Cummins [158]. Water added through the addition of Laponite would be small compared to the amount of water in the polymer solution. This suggests that the hydrophilicity of Laponite may have prevented the evaporation of water during PVA dissolution.

The degree of water loss after F-T cycling decreased with increasing PVA concentration, which could be due to smaller amounts of free water in the polymer solution

Table 4.1: Water contents of unfilled PVA and 10% PVA-NC solutions and hydrogels (n=5) after 6 FTC.

Hydrogel	Water content (%)		Water loss after 6 FTC (%)
	Solution	After 6 FTC	
10% PVA	88.83	85.6 ± 0.1	3.7 ± 0.1
15% PVA	83.24	80.6 ± 0.1	3.2 ± 0.2
20% PVA	75.76	75.67 ± 0.09	0.1 ± 0.1
0.75% Lap-10% PVA	87.93	86.2 ± 0.2	1.9 ± 0.2
1% Lap-10% PVA	88.45	85.8 ± 0.3	3.0 ± 0.3
0.48% BC-10% PVA	87.81	85.61 ± 0.07	2.50 ± 0.09
0.25% pBC-10% PVA	87.93	85.92 ± 0.06	2.28 ± 0.07
0.4% pBC-10% PVA	88.76	86.9 ± 0.1	2.1 ± 0.1

[134]. Less water was expelled from the 10% PVA-NC hydrogels than the unfilled 10% PVA control after 6 FTC. The nanofillers allowed hydrogels to retain more water, most likely due to their hydrophilicity [159, 174].

4.1.4 Porous Structure of Hydrogels

SEM images of cross-sections of critical point dried hydrogels indicated that increasing the concentration of PVA in the hydrogels resulted in smaller pores and increased the amount of polymer-rich regions as shown in Figure 4.3. The decrease in pore size [103] and thickening of polymer-rich regions [116] with increasing polymer concentration were also previously observed in F-T PVA hydrogels.

In contrast, the addition of Laponite (Figure 4.4), BC and pBC (Figure 4.5) resulted in larger pores in the PVA-NC hydrogels when compared to the unfilled 10% PVA hydrogel. pBC also appeared to have increased pore size compared to BC addition.

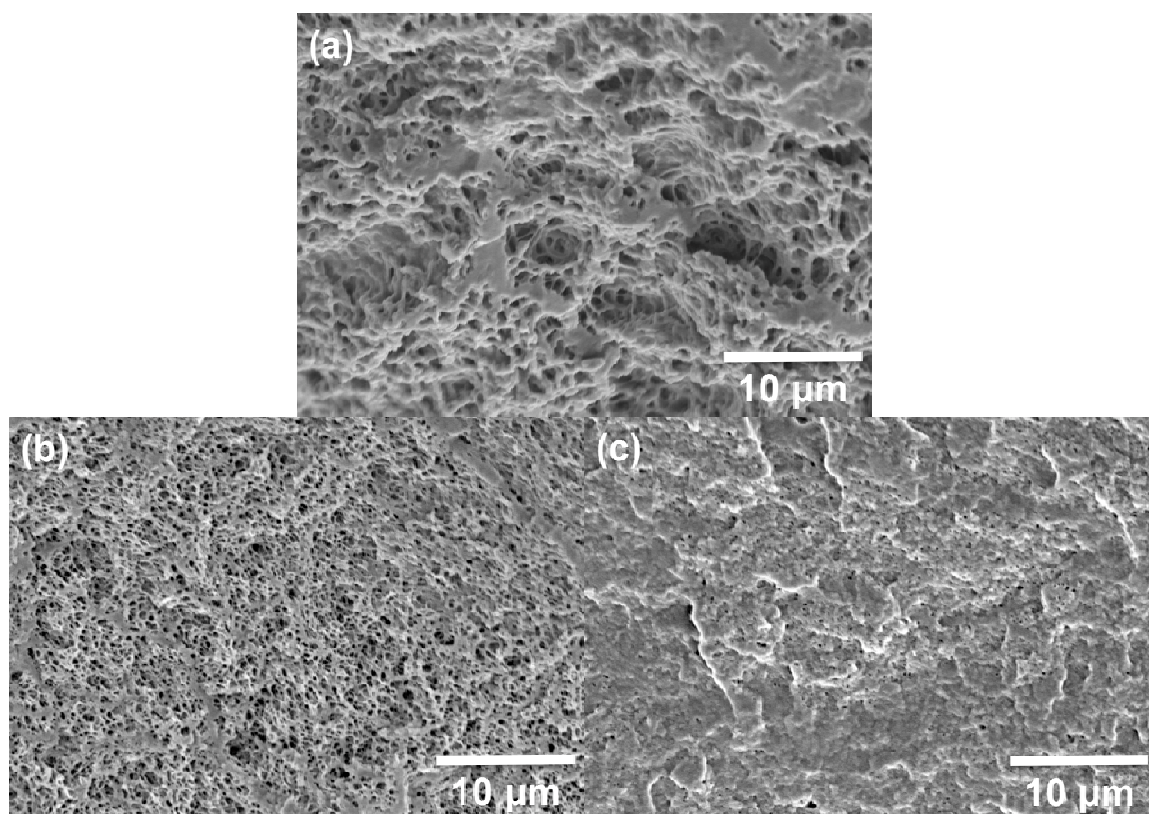


Figure 4.3: SEM of fractured cross-sections of critical point dried unfilled 10% PVA (a), 15% PVA (b), and 20% PVA hydrogels (c).

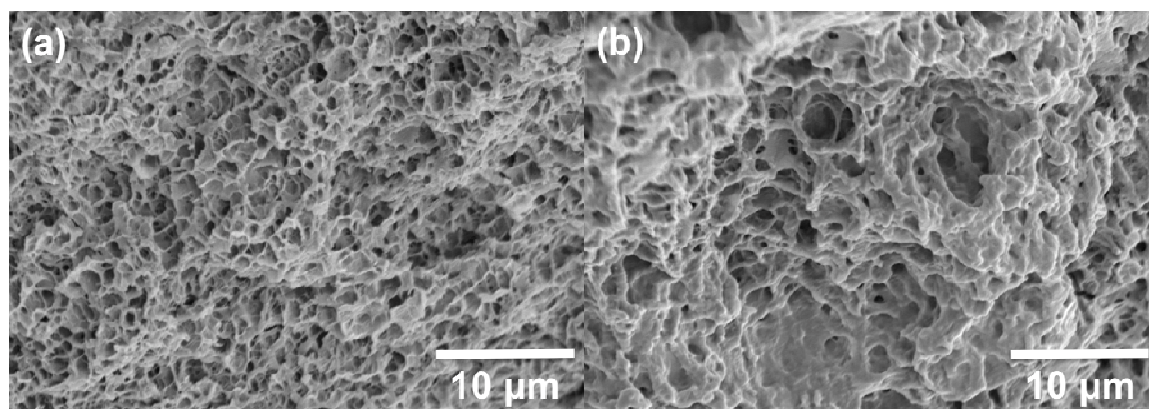


Figure 4.4: SEM of 0.75% (a) and 1% (b) Laponite-filled 10% PVA NC hydrogel fractured cross-sections.

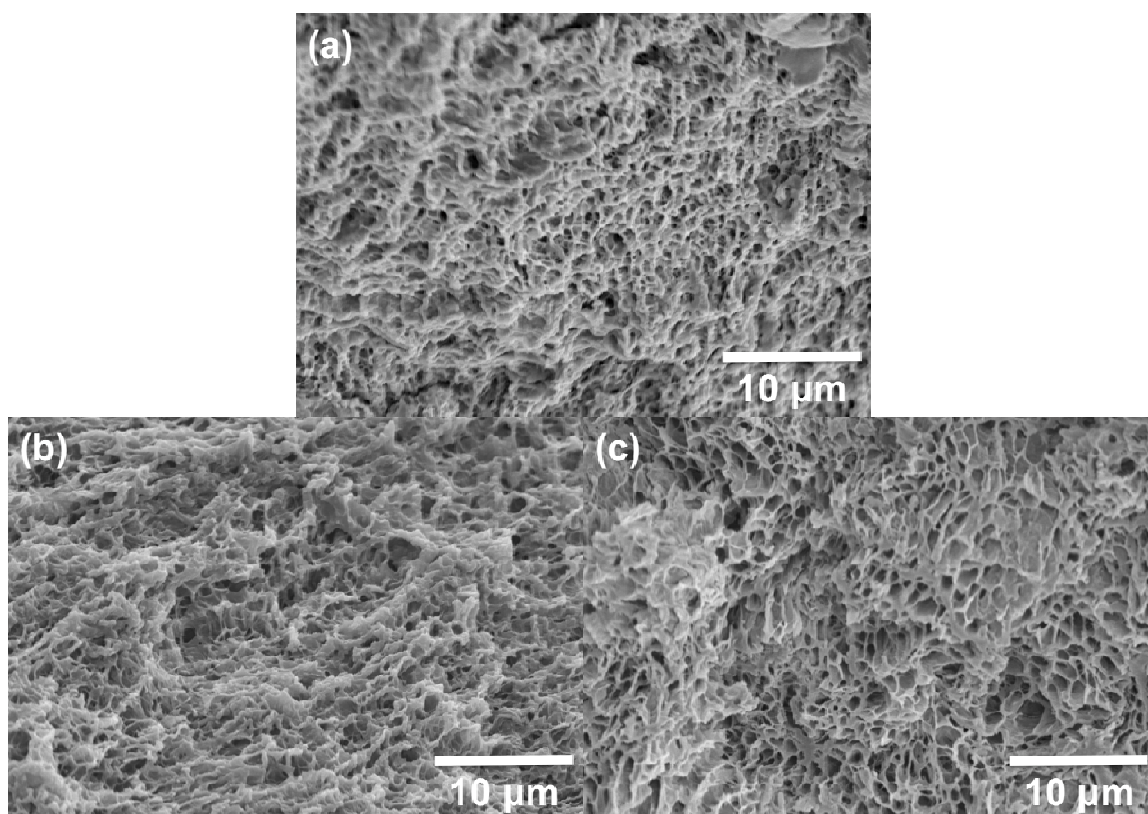


Figure 4.5: SEM of fractured cross-sections of 0.48% BC (a), 0.25% pBC (b), and 0.4% pBC (c) in 10% PVA.

4.1.5 Aging of Hydrogels in Water and PBS

Hydrogels prepared in distilled water experienced shrinkage when placed in PBS due to the osmotic effect of the presence of salt in the solution. $1\times$ PBS has an ionic strength of 0.171 mol/L and an osmolarity of 0.313 mol/L. Consequently, water would move out of a hydrogel into the solution while salts migrate into the hydrogel [116]. Hydrogels were also placed in water as a control to study the effects of aging independent from the influence of osmotic pressure.

4.1.5.1 Decrease in Mass and Volume

Mass and volume decreased in all of the hydrogels after 7 days in both water and PBS. Normalized mass and volume profiles are illustrated in the example in Figure 4.6, showing that most of the change occurred within the first 72 hours.

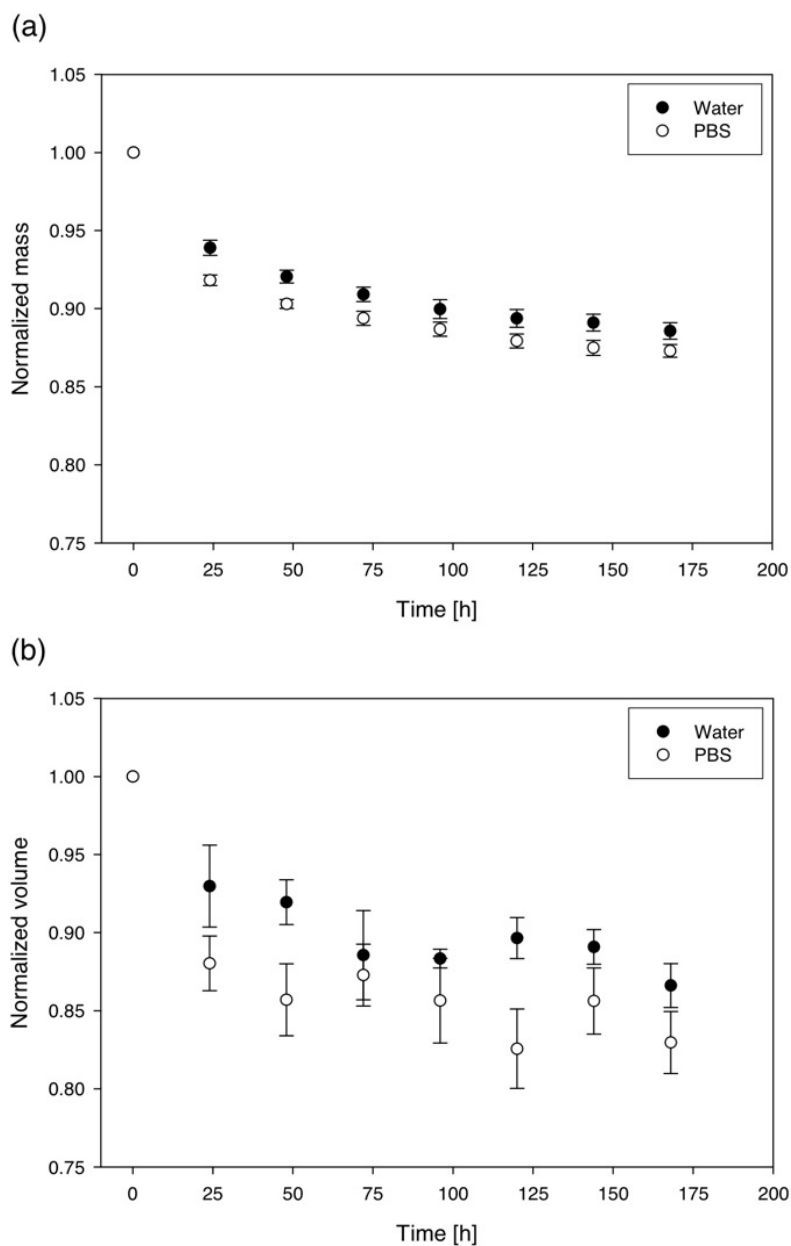


Figure 4.6: Profile of decreasing mass (a) and volume (b) of hydrogels over 7 days of aging in water and PBS (0.48% BC-10% PVA-NC hydrogels shown). Mass and volume are expressed as fractions of their initial values.

PVA hydrogel shrinkage in water [112] and deswelling in salt solutions have been found to equilibrate over time [116, 123, 144]. Hydrogel mass and volume after 7 days in water and PBS is shown in Figure 4.7.

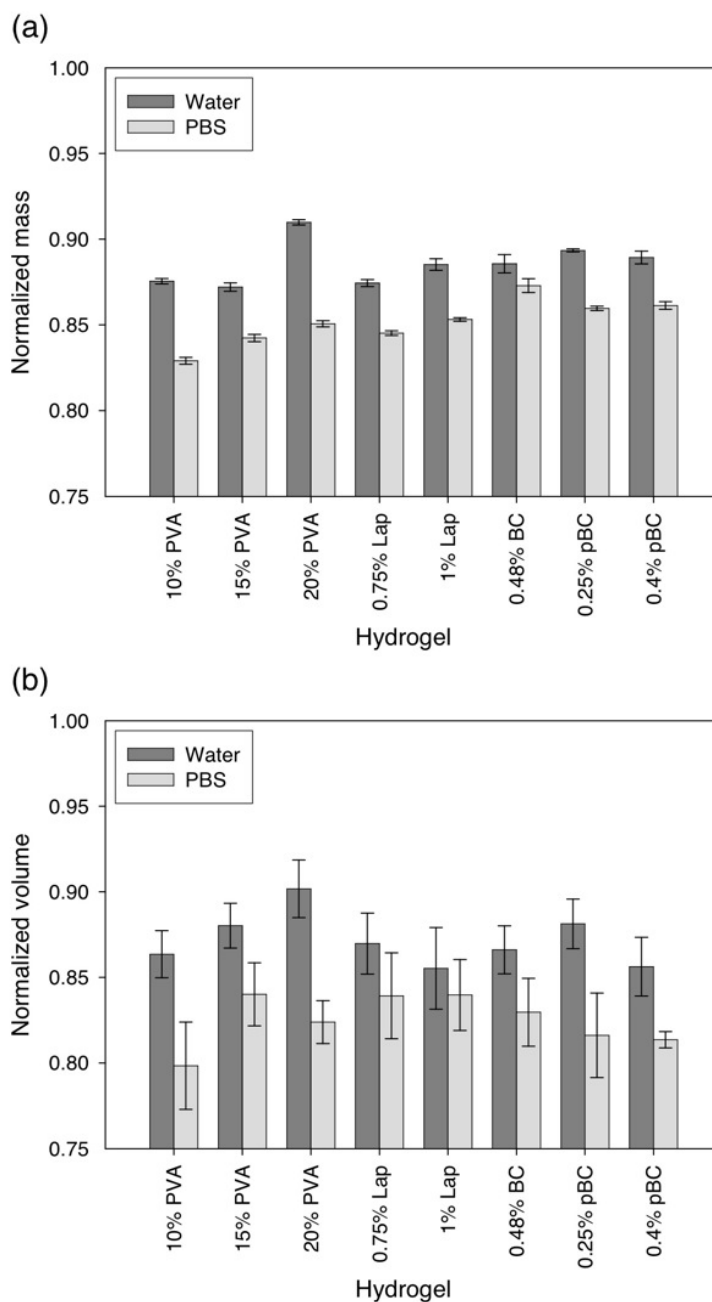


Figure 4.7: Mass (a) and volume (b) after 7 days of aging in water and PBS for unfilled PVA and 10% PVA-NC hydrogels, expressed as fractions of their initial values. All samples experienced decreases in mass and volume.

Aging hydrogels in PBS resulted in a greater decrease in hydrogel mass than aging in water for all of the hydrogels. The decrease of hydrogel volume in PBS was also higher than aging in water, with the exception of Laponite-filled 10% PVA-NC hydrogels, which were not statistically different. Increasing PVA concentration to 20% PVA resulted in the lowest mass and volume change after aging in water, while 1% Laponite addition, and all BC and pBC additions offered lower mass loss in water compared to 10% PVA. In PBS, increases in PVA concentration and the addition of nanofillers both resulted in statistically significant reduction in mass loss relative to the unfilled 10% PVA control. Only 20% PVA in water, and 15% PVA and Laponite-filled hydrogels in PBS had statistically lower decreases in volume after aging than 10% PVA. The large uncertainties associated with change in volume compared to change in mass could be due to variability in dimensional change between the hydrogel samples or the level of precision of the method of volume determination.

4.1.6 Crystallinity of Hydrogels

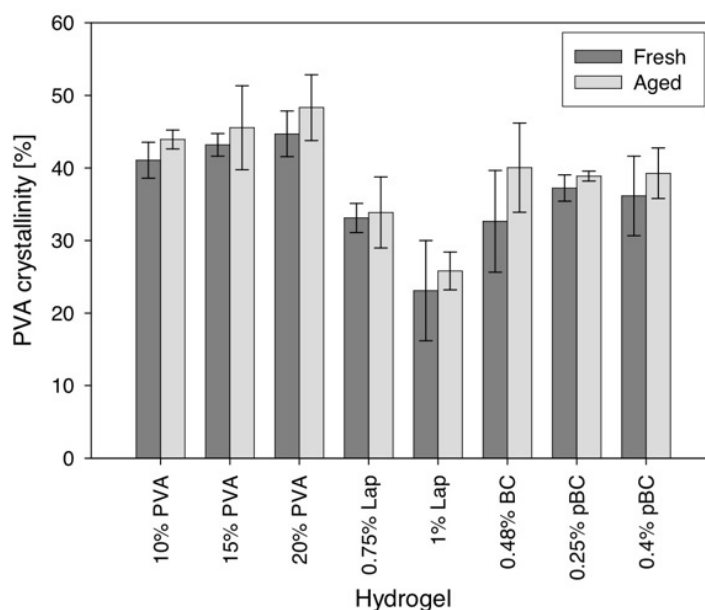


Figure 4.8: Crystallinity determined by DSC in dried PVA in unfilled PVA and 10% PVA-NC hydrogels.

The crystallinities of hydrogels before and after aging in water are shown in Figure 4.8. In the present study, there was no significant difference in crystallinity with increasing PVA concentration or with the addition of BC and pBC, but crystallinity decreased with the addition of Laponite. No significant difference was found between fresh hydrogels and hydrogels aged in water for all compositions.

4.2 UNCONFINED COMPRESSION OF HYDROGELS

IVDs contribute to the support of compressive loads in the vertebral column, along with loads from rotation, flexion-extension and lateral bending. A material used in an IVD replacement should be of sufficient stiffness to withstand loading from activities, and have similar mechanical properties to the native disc in order to prevent modifications in biomechanics that could result in adjacent level degeneration. By studying the effects of composition on the compression properties of PVA and PVA-NC hydrogels, the stiffness, shape of the stress-strain curve and degree of strain rate dependence may be tuned for IVD applications by varying parameters such as polymer concentration and nanofiller addition. Osmotic pressure in the *in vivo* environment may also impact the mechanical properties of the hydrogels, and thus should be accurately predicted to avoid unintended changes in mechanical performance.

The effects of composition and aging treatment on unconfined compression stress-strain curves, stiffness and strain rate dependence of PVA and PVA-NC hydrogels were determined. Polymer concentration, the type of nanofiller added and aging of PVA and PVA-NC hydrogels all influenced the compression properties of the hydrogels studied. While composition had an effect on hydrophilicity and structure of these hydrogels, the water content and structural properties such as porosity and crystallinity would in turn impact mechanical properties.

4.2.1 PVA Concentration

Increasing PVA concentration resulted in a significant increase in the stiffness of neat PVA hydrogels. The stress-strain curves of fresh 6 FTC 10, 15 and 20% PVA hydrogels, tested at a strain rate of 100%/s, are shown in Figure 4.9.

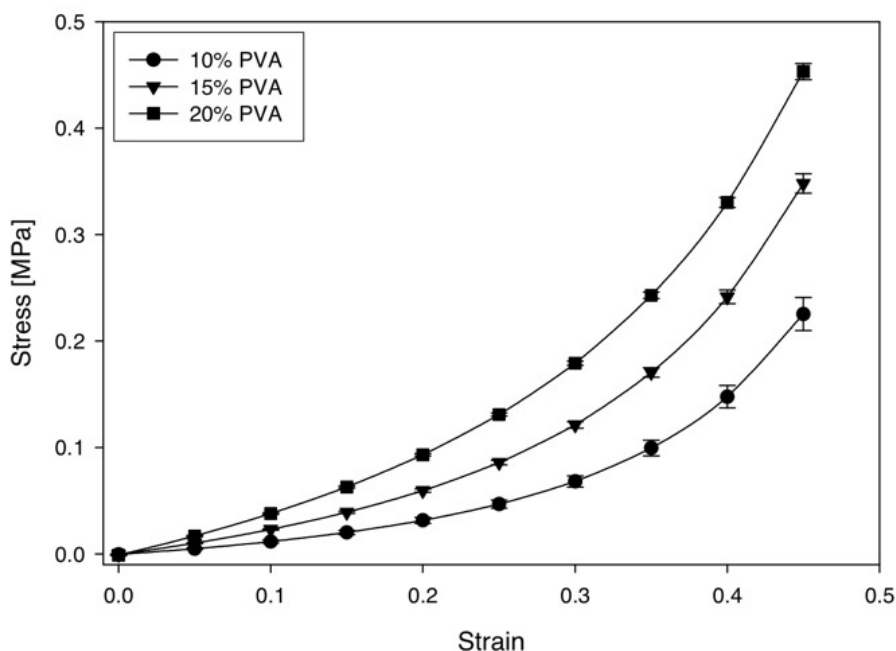


Figure 4.9: Effect of PVA concentration on stress-strain curves from unconfined compression of fresh unfilled PVA hydrogels, tested in 37 °C water at a strain rate of 100%/s.

Due to their non-linear stress-strain curves, both tangent and secant modulus were used to characterize the stiffness of the PVA and PVA-NC hydrogels. While tangent modulus ($E_{tangent}$) describes the instantaneous stiffness at a particular strain, secant modulus (E_{secant}) represents the degree of deformation in a material under a certain stress. Since the stress-strain curves of the hydrogels were non-linear and concave up in shape, $E_{tangent}$ was larger than E_{secant} (Table 4.2). $E_{tangent}$ was determined using the derivative with respect to strain of the 5-parameter exponential equation used to fit stress-strain data (Equation 3.4). Meanwhile, E_{secant} at a given strain was calculated by dividing stress by the strain (Equation 3.5). The difference between the two was more apparent at higher strains, as stress increased at a higher rate with increasing strain.

While higher PVA concentrations in unfilled hydrogels were able to increase stiffness throughout the range of strains tested, the non-linearity of the compressive stress-strain curves was also decreased. By increasing PVA concentration from 10% PVA to 15% and 20% PVA (Figure 4.9), $E_{tangent}$ increased by 69% and 137%, and E_{secant} increased by 83% and 180% at 0.25 strain, respectively. These were proportionally higher than increases in moduli at 0.45 strain as $E_{tangent}$ increased by 32% and 48%, and E_{secant} by 54% and 101%, for 15% and 20% PVA, respectively.

Table 4.2: Tangent and secant moduli of fresh PVA hydrogels at 0.25 and 0.45 strain tested at a strain rate of 100%/s.

Hydrogel	Modulus [MPa], at 0.25 strain		Modulus [MPa], at 0.45 strain	
	Tangent	Secant	Tangent	Secant
10% PVA	0.36 ± 0.02	0.19 ± 0.02	2.0 ± 0.1	0.50 ± 0.03
15% PVA	0.61 ± 0.02	0.343 ± 0.009	2.61 ± 0.08	0.77 ± 0.01
20% PVA	0.85 ± 0.01	0.523 ± 0.006	2.93 ± 0.08	1.01 ± 0.01

4.2.2 Nanofiller Addition

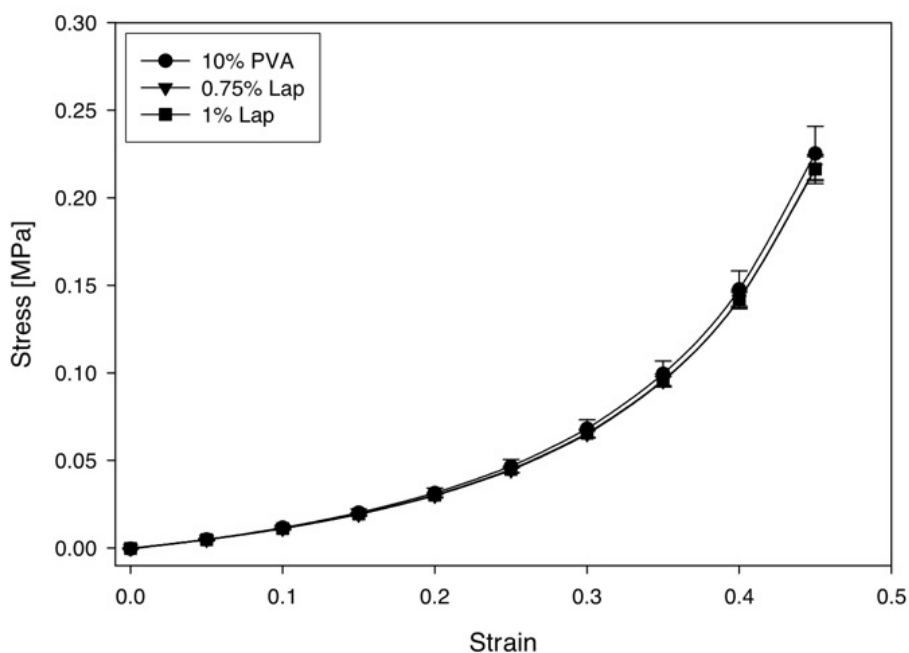


Figure 4.10: Effect of Laponite addition on the stress-strain curves of fresh 10% PVA hydrogels, tested in 37 °C water at a strain rate of 100%/s.

The stress-strain curves of Laponite-filled hydrogels did not differ from 10% PVA (Figure 4.10). Thus, both tangent and secant moduli were the same with 0.75% and 1% Laponite addition as the unfilled 10% PVA hydrogel (Table 4.3).

Table 4.3: Tangent and secant moduli of fresh Laponite-filled 10% PVA-NC hydrogels at 0.25 and 0.45 strain tested at a strain rate of 100%/s.

Hydrogel	Modulus [MPa], at 0.25 strain		Modulus [MPa], at 0.45 strain	
	Tangent	Secant	Tangent	Secant
10% PVA	0.36 ± 0.02	0.19 ± 0.02	2.0 ± 0.1	0.50 ± 0.03
0.75% Lap	0.34 ± 0.01	0.178 ± 0.005	1.90 ± 0.08	0.48 ± 0.01
1% Lap	0.34 ± 0.01	0.179 ± 0.007	1.89 ± 0.08	0.48 ± 0.01

The addition of BC and pBC into 10% PVA hydrogels increased stress above 0.25 strain when compared to the unfilled 10% PVA hydrogel (Figure 4.11), matching the stress of the 20% PVA hydrogel at 0.45 strain. Filler content and phosphorylation did not affect the stiffness of BC- and pBC-filled PVA hydrogels.

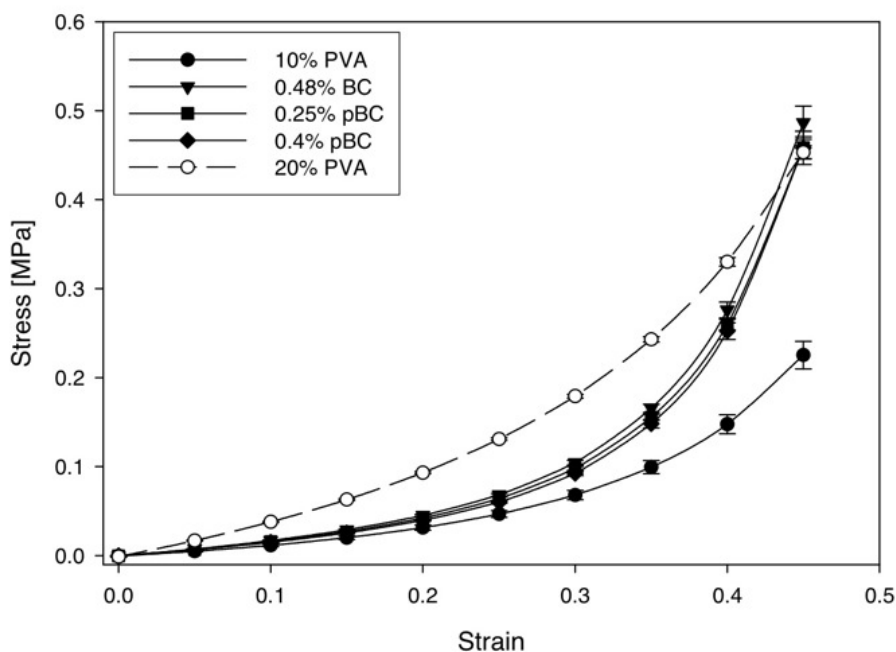


Figure 4.11: The effect of BC and pBC addition on fresh 10% PVA hydrogels, tested in 37 °C water at a strain rate of 100%/s. The stress-strain curves of 10% and 20% PVA highlights the difference in shape from those of BC- and pBC-filled hydrogels.

Secant modulus increased by 28–46% and tangent modulus by 41–59% at 0.25 strain with BC and pBC addition from those of 10% PVA, but they were approximately two and three times, respectively, higher than the control at 0.45 strain (Table 4.4). While the secant modulus of hydrogels containing BC and pBC were similar to that of 20% PVA at 0.45 strain, despite having similar water contents to 10% PVA, the tangent modulus clearly illustrates the steep increase in modulus at higher strains. The addition of BC and pBC resulted in increased non-linearity compared to unfilled and Laponite-filled PVA-NC hydrogels, displaying a low modulus region up to approximately 0.25 strain followed by a high modulus region on the stress-strain curves.

Table 4.4: Tangent and secant moduli of fresh BC and pBC-filled 10% PVA-NC hydrogels at 0.25 and 0.45 strain tested at a strain rate of 100%/s.

Hydrogel	Modulus [MPa], at 0.25 strain		Modulus [MPa], at 0.45 strain	
	Tangent	Secant	Tangent	Secant
10% PVA	0.36 ± 0.02	0.19 ± 0.01	2.0 ± 0.1	0.50 ± 0.03
0.48% BC	0.57 ± 0.01	0.273 ± 0.007	5.8 ± 0.3	1.08 ± 0.03
0.25% pBC	0.534 ± 0.008	0.256 ± 0.007	5.4 ± 0.2	1.02 ± 0.02
0.4% pBC	0.50 ± 0.01	0.240 ± 0.006	5.7 ± 0.3	1.02 ± 0.03

4.2.3 Effect of Aging in Water and PBS

Along with decreasing mass and volume, aging the PVA hydrogels in both water and PBS increased tangent and secant moduli (Figure 4.12). Figure 4.13 shows the tangent and secant moduli at 0.45 strain of 10% PVA-NC hydrogels before and after aging in water and PBS. Hydrogels containing Laponite and BC increased in both tangent or secant modulus after aging, but there was no difference between aging in water and PBS. With BC and pBC addition, aging had no effect on tangent modulus with BC and pBC addition, while only 0.48% BC and 0.25% pBC addition after aging in PBS resulted in increase in secant modulus. In contrast to the unfilled PVA hydrogels, there was no difference between aging in water or in PBS for hydrogels containing nanofillers.

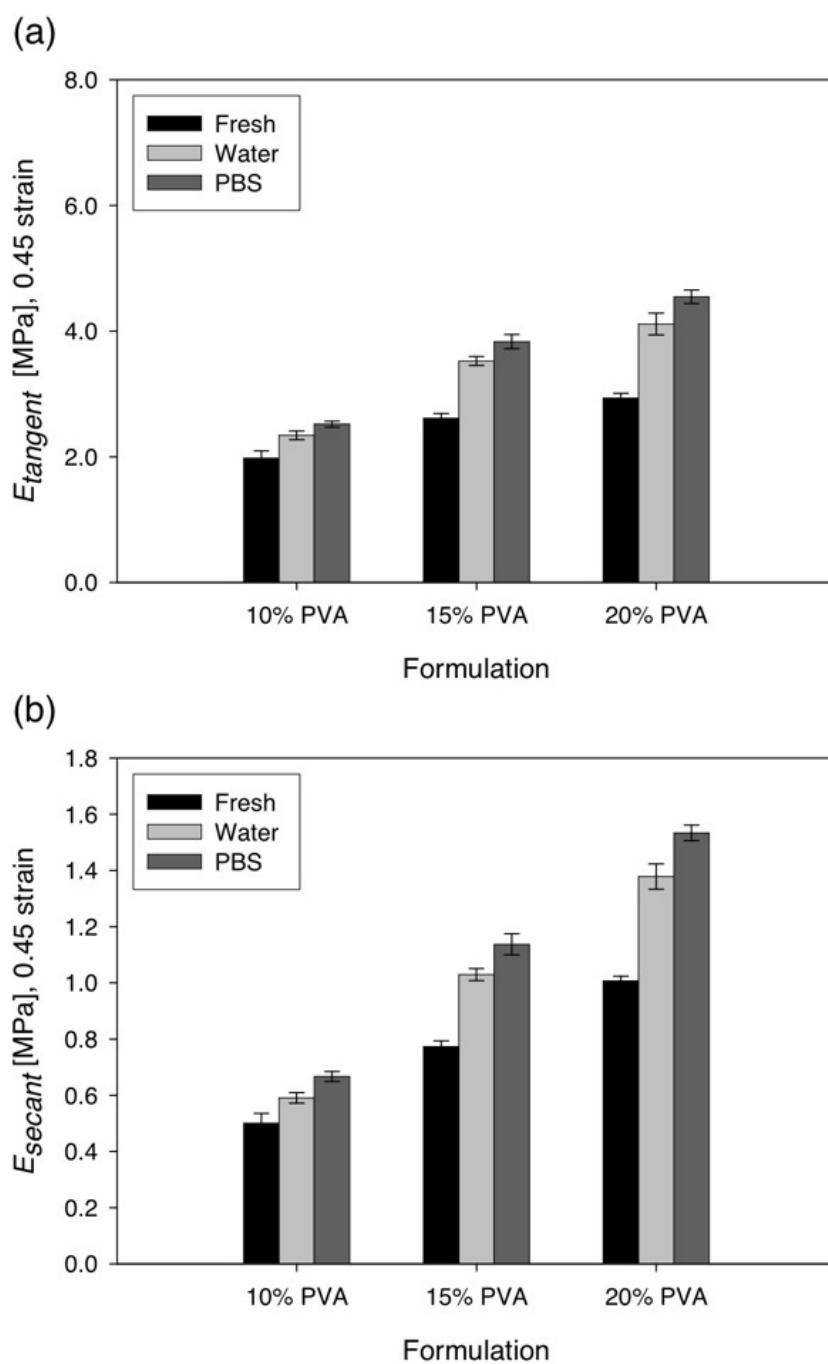


Figure 4.12: Tangent (a) and secant (b) moduli of unfilled PVA hydrogels at 0.45 strain, tested at a strain rate of 100%/s fresh, and after one week of aging in water and PBS.

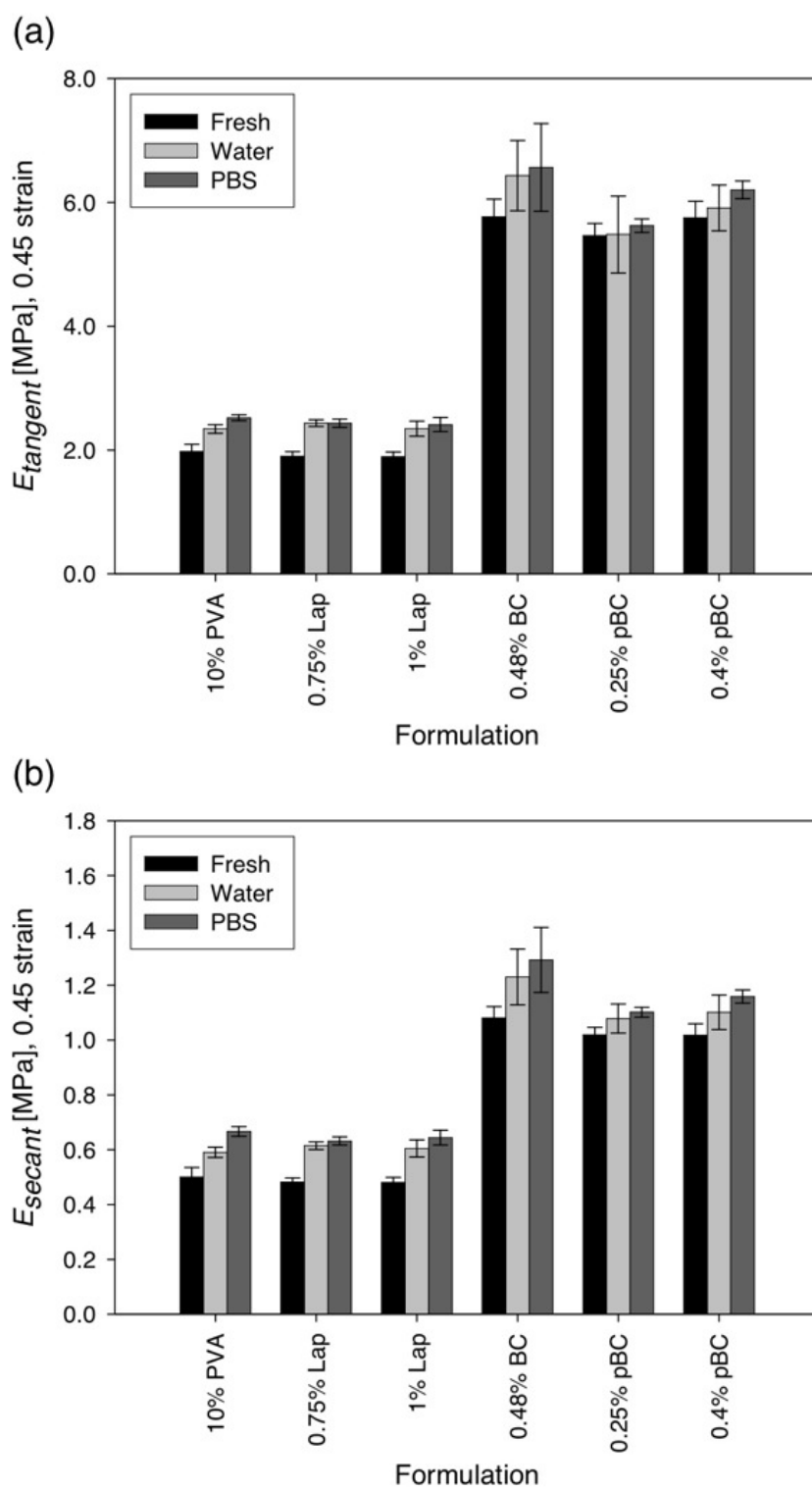


Figure 4.13: Tangent (a) and secant (b) moduli of 10% PVA-NC hydrogels at 0.45 strain, tested at a strain rate of 100%/s fresh, and after one week of aging in water and PBS.

4.2.4 Strain Rate Dependence

The stress-strain curves for strain rates of 1%/s, 10%/s and 100%/s differ to varying degrees depending on composition. The curves for the 1% Laponite-10% PVA-NC hydrogel, after one week of aging in PBS, are shown in Figure 4.14 illustrating the effect of strain rate on the stress-strain curves.

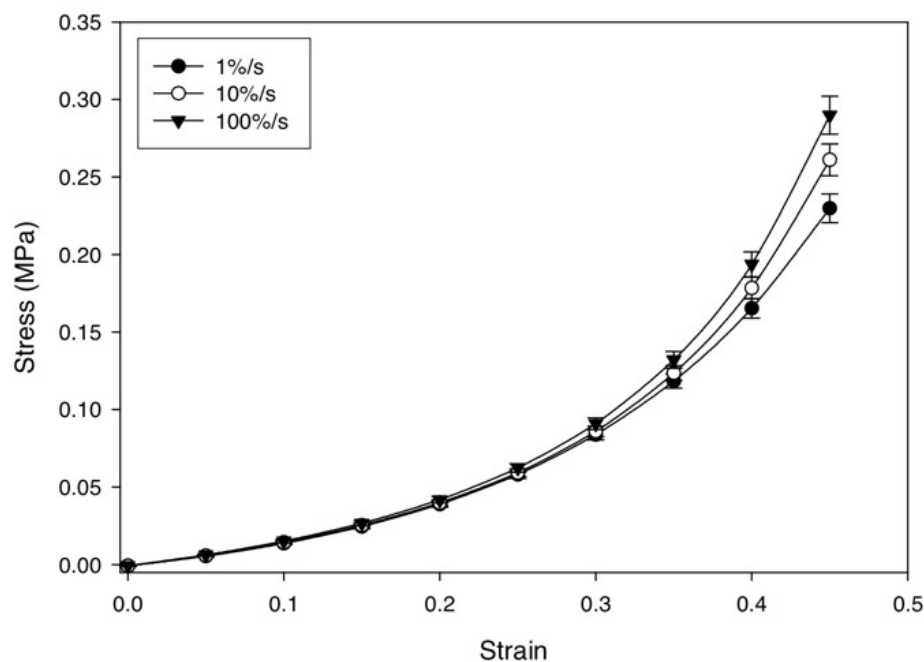


Figure 4.14: Stress-strain curves of 1% Laponite-10% PVA hydrogels, tested after one week of aging in PBS at strain rates of 1, 10 and 100%/s, demonstrating strain rate dependent behaviour.

The stress at 0.25 strain were not statistically different across the three strain rates for all of the hydrogels. As found by Millon et al. [24], statistical difference in stress at 0.45 strain for fresh 10% PVA hydrogels was only found between strain rates of 1 and 100%/s in the present study. Stress at 0.45 strain was also not statistically different between 10 and 100%/s for 20% PVA, fresh and after aging in water, and 0.48% BC in 10% PVA after aging in PBS. All other compositions and aging treatments resulted in strain rate dependence across the three strain rates tested.

By plotting stress at a specified strain against the logarithm of strain rate, a linear relationship could be found. However, in order to compare between the range of stiffness for the different compositions, the stress obtained from the three strain rates were presented as the percentage change from stress at 1%/s at the respective strain. The linear relationship between stress and logarithm of strain rate is shown graphically for the 1% Laponite-10% PVA-NC hydrogel in Figure 4.15. Slopes of the linear fits were used to quantify degree of strain rate dependence.

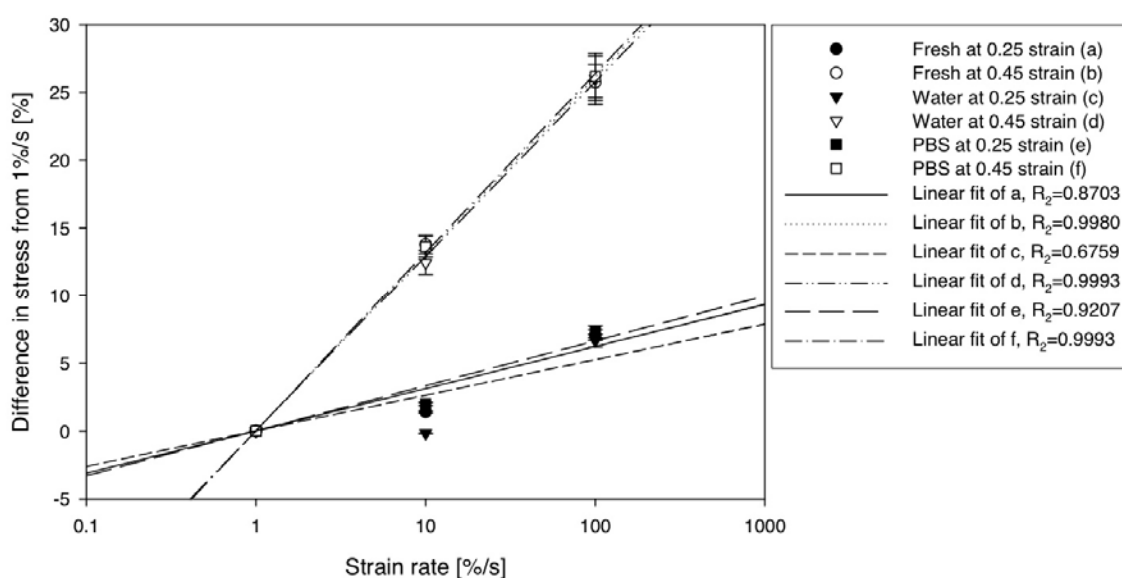


Figure 4.15: Linear relationship between change in stress from 1%/s and logarithm of strain rate. The slope was used to quantify the degree of strain rate dependence. Fits for 1% Laponite-10% PVA hydrogels, tested fresh, and after aging for 7 days in water and PBS, are shown.

Strain rate did not have a large effect on stress at low strains, but it was apparent at higher strains. In addition to a lack of statistical difference between strain rates for stress at 0.25 strain, some fits had low degrees of correlation and the largest slope of the linear fits was 3.8 %/log(%/s) for fresh 10% PVA hydrogels. Slopes for 0.45 strain (Figure 4.16), however, ranged from approximately 8.4 to 19 %/log(%/s), with R^2 values of at least 0.8 indicating there was a strong linear relationship between stress and strain rate.

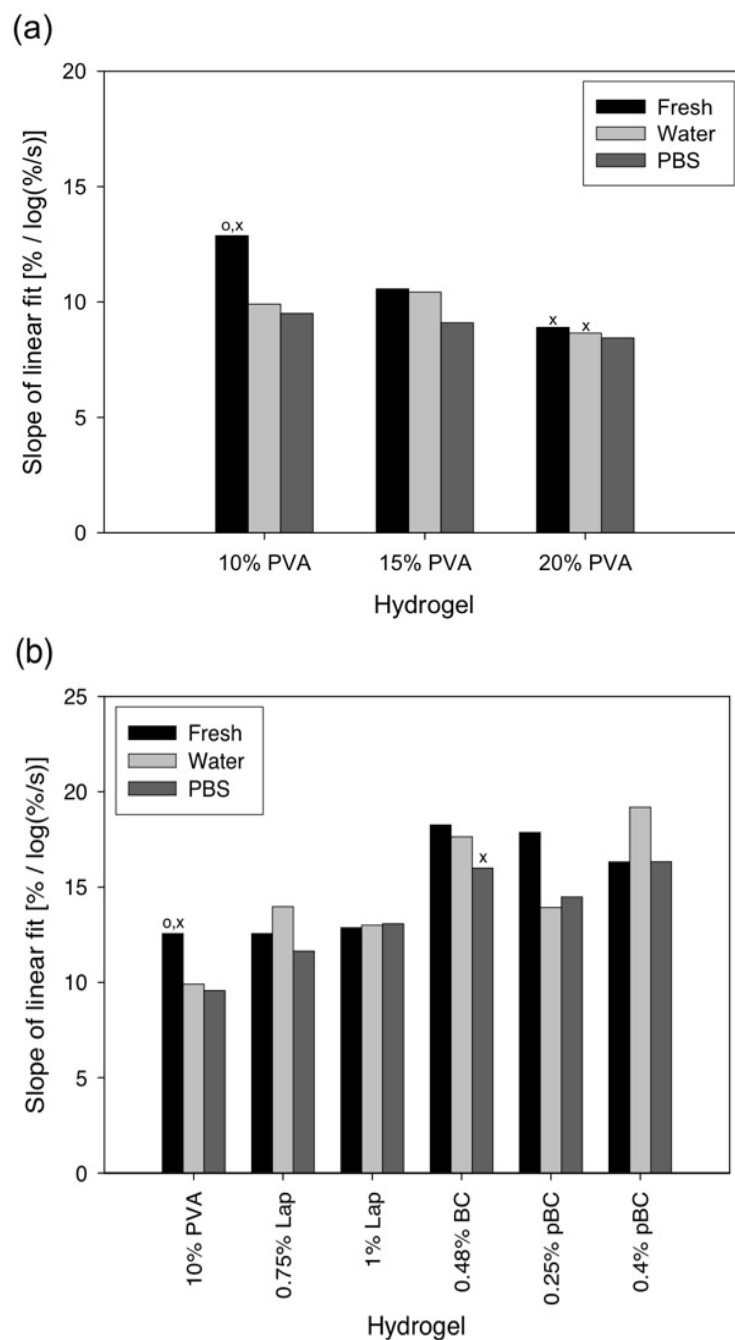


Figure 4.16: Degree of strain rate dependence at 0.45 strain for unfilled PVA (a) and 10% PVA-NC (b) hydrogels. Linear fits have R^2 of at least 0.8225. ^oNo statistical difference in stress at 0.45 strain between strain rates of 1%/s and 10%/s. ^xNo statistical difference in stress at 0.45 strain between strain rates of 10%/s and 100%/s.

Increasing PVA concentration appeared to decrease strain rate dependence in the hydrogels (Figure 4.16a). Aging did not have a clear effect on strain rate dependence.

Degree of strain rate dependence increased with the addition of nanofillers, notably with BC and pBC addition (Figure 4.16b).

4.3 STRESS RELAXATION AND CREEP

The natural IVD experiences stress relaxation and creep due to fluid flow from the disc after load application. This prevents instantaneous decrease in disc height [178], and provides energy dissipation, shock absorption and even stress distribution to the vertebrae after load is applied [227]. Stress relaxation is the decrease in stress over time by holding a specimen at constant strain, whereas creep is the deformation of a material over time under load. Both tests are used to assess viscoelasticity of polymers since viscous flow results in time-dependent response to deformation and stress [228]. However, in IVDs [55, 64] and hydrogels [137], the fluid flow under load plays a role in reducing fluid pressure and increasing compressive deformation through volume reduction. The degree of stress relaxation and creep are examined to determine the suitability of PVA and PVA-NC as a replacement material in comparison to the natural IVD.

4.3.1 Stress Relaxation

As PVA concentration increased, the degree of stress relaxation at 0.25 strain decreased (Figure 4.17). Hydrogels with higher PVA concentrations had decreased water content, which could have resulted in decreased viscous behaviour. The addition of Laponite resulted in an increased degree of stress relaxation after one hour when compared to the unfilled 10% PVA control, as shown in Figure 4.18. BC and pBC addition also resulted in increased stress relaxation (Figure 4.19) compared to 10% PVA. The amount of BC or pBC added appears to affect the degree of stress relaxation in the hydrogels – the addition of 0.48% BC had the highest degree of relaxation while 0.25% pBC had the lowest.

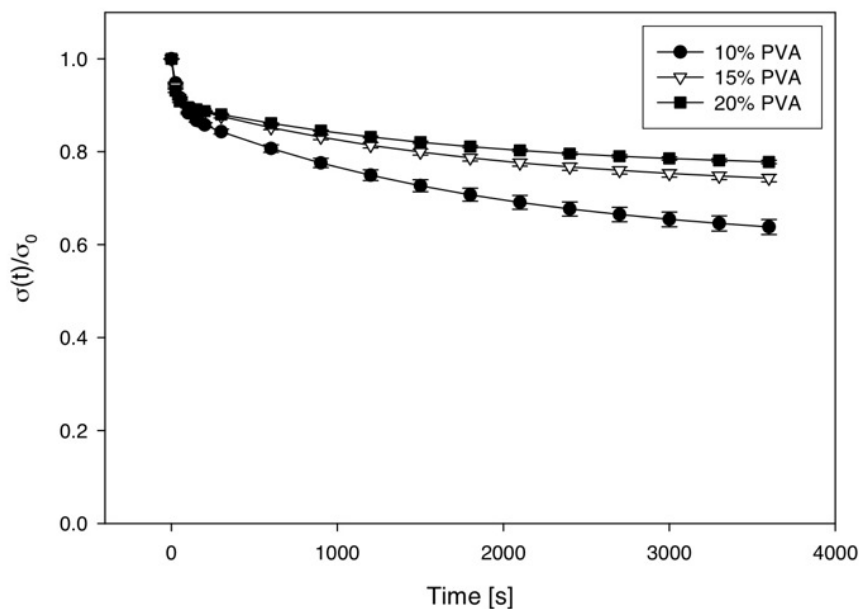


Figure 4.17: Stress relaxation at 0.25 strain of unfilled PVA hydrogels in PBS. Increased PVA concentration resulted in decreased stress relaxation.

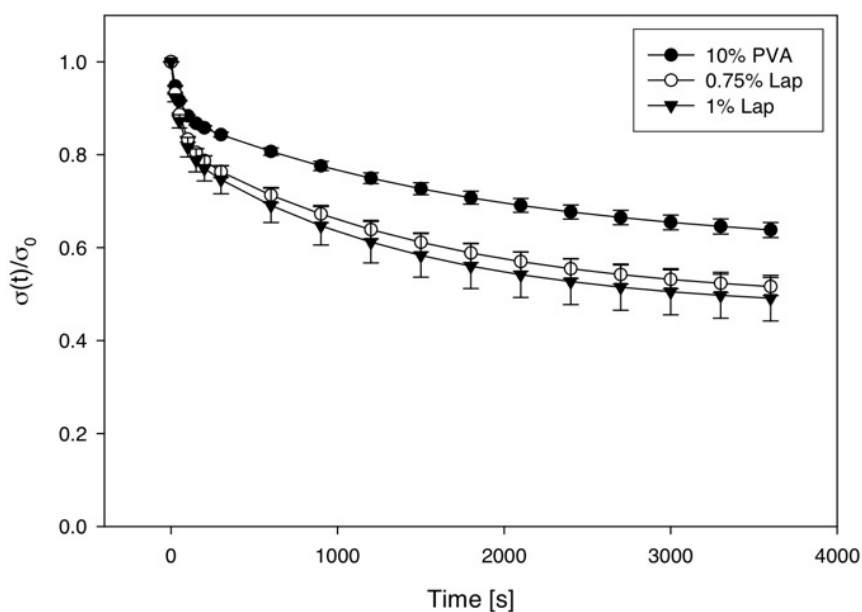


Figure 4.18: Stress relaxation at 0.25 strain of Laponite-containing 10% PVA-NC hydrogels in PBS in comparison to 10% PVA. Addition of Laponite resulted in increased stress relaxation.

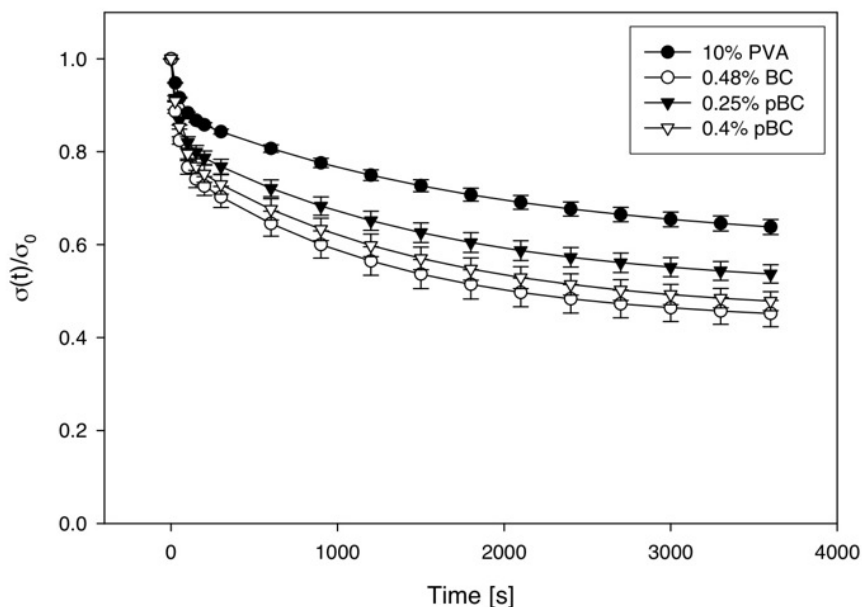


Figure 4.19: Stress relaxation at 0.25 strain of BC and pBC-containing 10% PVA-NC hydrogels in PBS compared to 10% PVA. Addition of BC and pBC resulted in increased stress relaxation.

After aging in PBS, the amount of stress relaxation decreased in unfilled PVA hydrogels and did not differ in Laponite, BC and pBC-filled hydrogels (Figure 4.20). The decrease in stress relaxation with aging was most apparent in 15% and 20% PVA hydrogels.

4.3.2 Creep

Creep data were fitted to the viscoelastic models described in Section 3.4.3.1. The four-parameter models (Equations 3.9 and 3.11) and the 5-parameter exponential rise-to-max equation (Equation 3.13) yielded similar fits. Though the difference was minimal, these models appeared to provide a better fit for the data than the three-parameter-solid model (Equation 3.7) in the initial part of the curve, close to $t=0$, but did not level off to the same degree towards the end of the test, as shown in Figure 4.21. These differences were also found by Burns when comparing between three and four-parameter viscoelastic models in fitting creep data of human IVDs [63]. For the length of

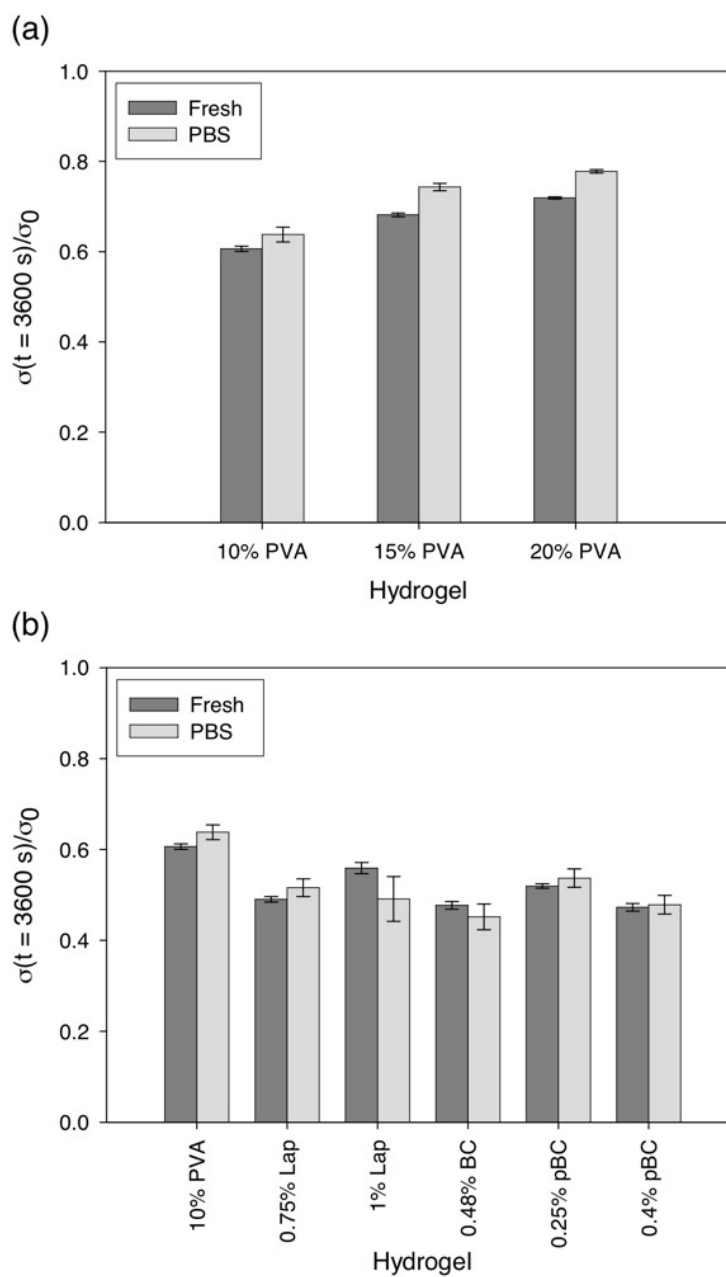


Figure 4.20: Stress remaining after one hour of stress relaxation at 0.25 strain in unfilled PVA (a) and 10% PVA-NC hydrogels (b) tested fresh in water, and after 7 days of aging in PBS.

the test, the four-parameter models fitted more closely with the shape of the data and thus were used to generate the creep curves for comparisons between PVA and PVA-NC hydrogels.

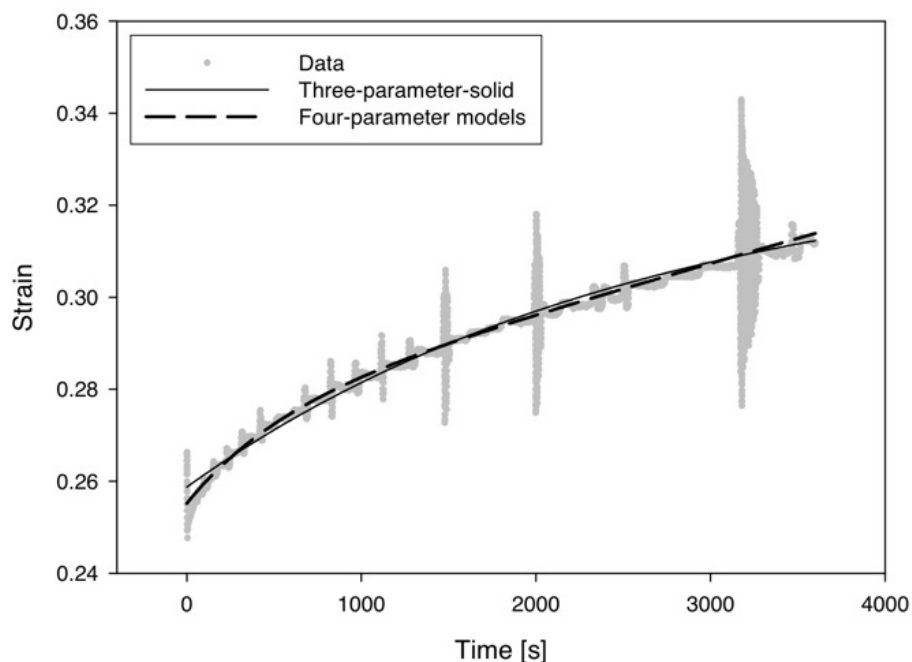


Figure 4.21: Creep data of a 10% PVA sample tested fresh in 37 °C water at a constant stress of 0.05 MPa, and fitted with the three-parameter-solid, and the four-parameter Burger’s and Bausch viscoelastic models.

Increasing PVA concentration decreased the amount of creep in the unfilled hydrogels (Figure 4.22). This is in agreement with stress relaxation results since with a lower degree of relaxation, a smaller increase in strain would be needed to maintain a constant load during creep. Furthermore, since hydrogels with higher PVA concentrations were stiffer, lower initial strains resulted from the applied stress of 0.05 MPa.

Adding nanofillers increased creep, and as such, the creep curves of the 10% PVA-NC hydrogels were less flat than the unfilled 10% PVA control. This was also expected from the stress relaxation results. Creep in the Laponite-containing 10% PVA-NC hydrogels was higher than in 10% PVA (Figure 4.23).

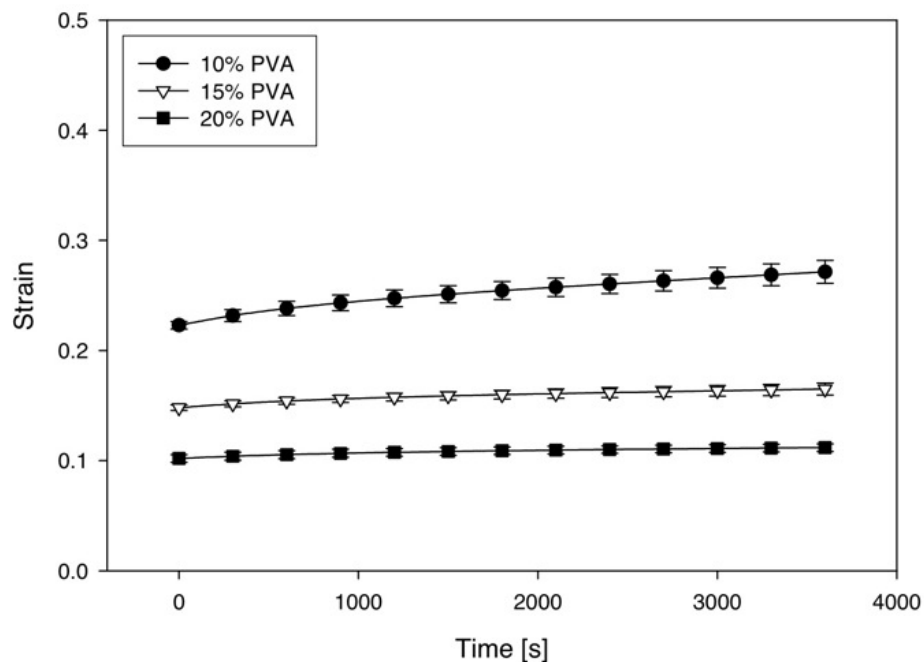


Figure 4.22: Creep curves of unfilled PVA hydrogels in 37 °C PBS at a stress of 0.05 MPa for one hour. Increased PVA concentration results in reduction of the initial strain and creep.

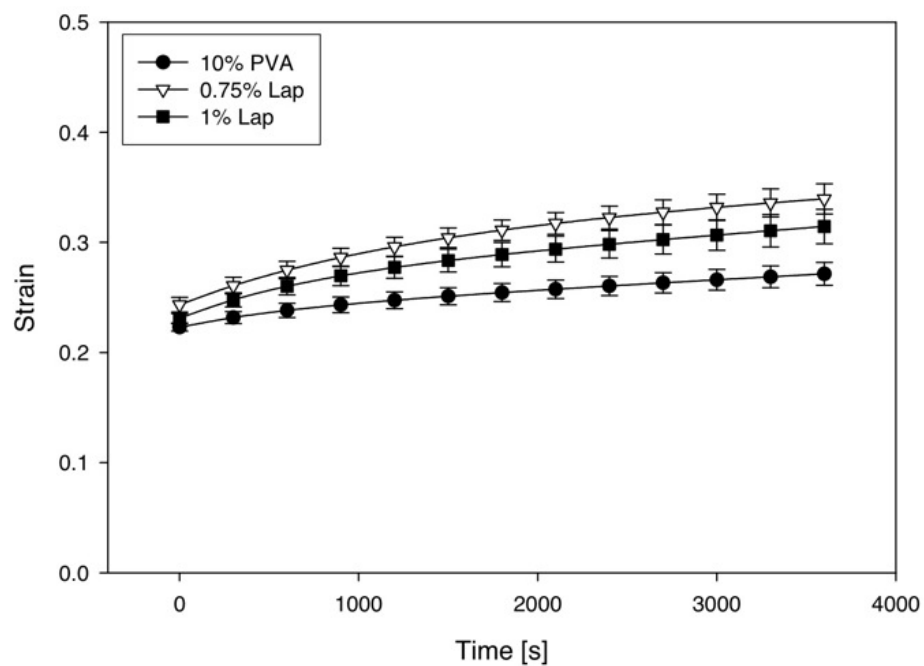


Figure 4.23: Creep of Laponite-filled hydrogels compared to 10% PVA in 37 °C PBS at a stress of 0.05 MPa for one hour. Addition of Laponite resulted in increased creep.

BC and pBC addition produced stiffer hydrogels than unfilled 10% PVA, resulting in smaller initial strains. However, it is apparent from Figure 4.24 that BC- and pBC-filled 10% PVA-NC hydrogels had higher creep strains than 10% PVA that are dependent on the amount of pBC added. Although both pBC-filled hydrogels had similar initial strains, 0.4% pBC addition resulted in a larger increase in strain that may be due to a higher water content compared to 0.25% pBC-10% PVA-NC hydrogels.

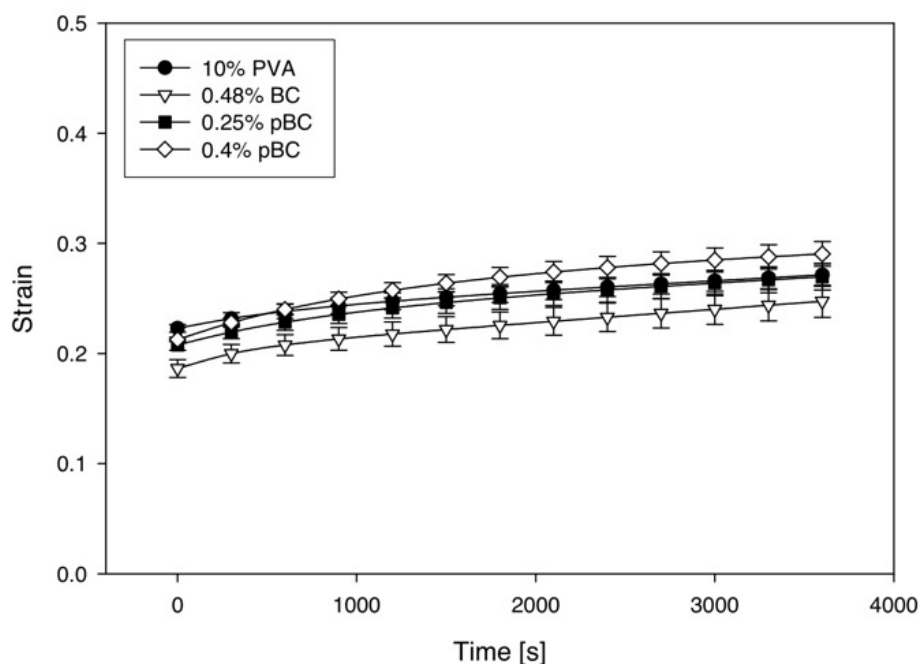


Figure 4.24: Creep of BC and pBC-filled hydrogels compared to 10% PVA in 37 °C PBS at a stress of 0.05 MPa for one hour. Addition of BC and pBC resulted in increased creep.

Figure 4.25 summarizes the increase in strain after 1 hour in of creep testing before and after aging in PBS. While creep decreased in unfilled 15% and 20% PVA hydrogels after aging in PBS, 10% PVA and PVA-NC hydrogels either had increases in creep or no change after aging.

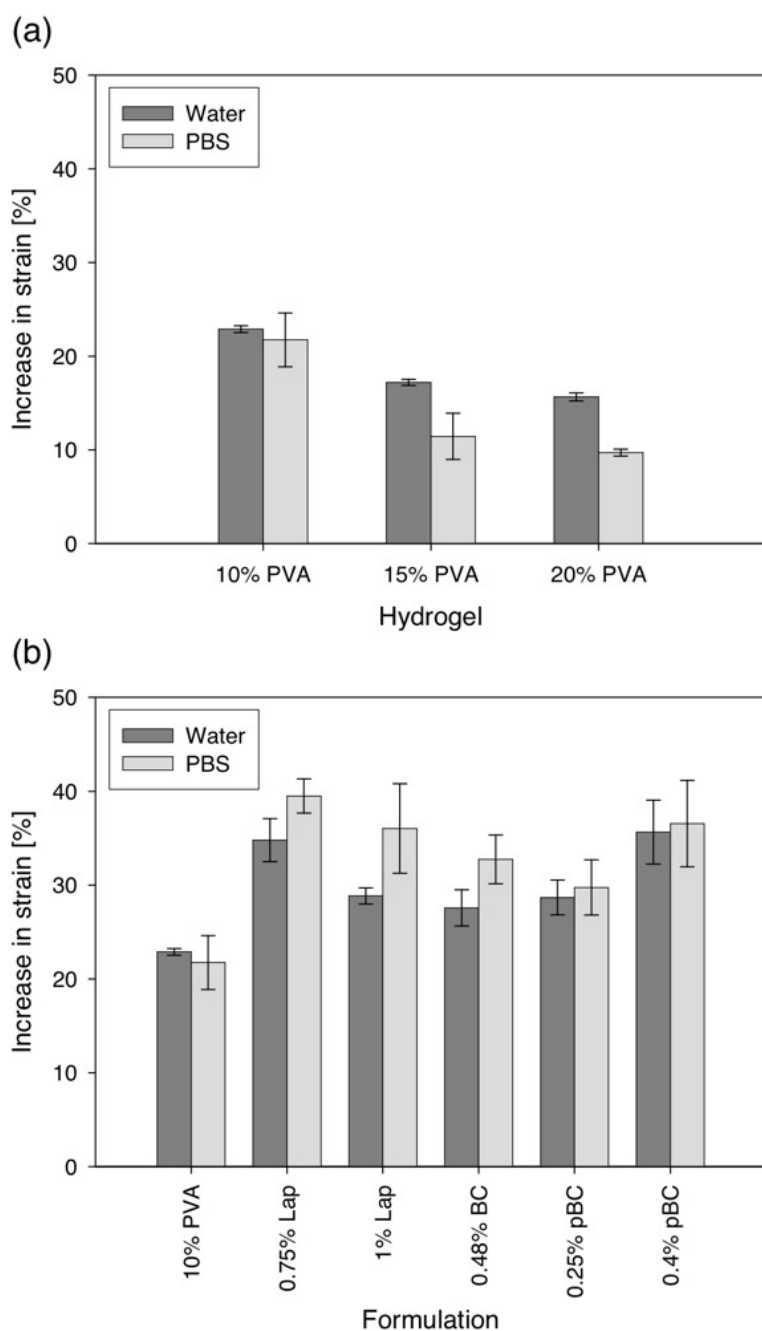


Figure 4.25: Percent increase in strain after creep testing at 0.05 MPa stress for one hour. The increase of PVA concentration (a) decreased creep, while the addition of nano-fillers into 10% PVA (b) increased the amount of creep in the hydrogels.

4.4 CYCLIC COMPRESSION TESTING

Since IVDs experience dynamic loads *in vivo*, PVA and PVA-NC hydrogels were tested with sinusoidal compressive strain cycles. Through 120 sinusoidal strain cycles at 0.5, 1 and 2 Hz, the maxima and minima in stress were found to slightly lag behind those of strain due to viscoelasticity in all of the hydrogels. This was indicative of viscous damping, which is characterized by $\tan \delta$ – a higher degree of damping corresponds to a greater phase shift, δ , between stress and strain, and a larger amount of energy dissipated.

The $\tan \delta$ values of the unfilled PVA and 10% PVA-NC hydrogels from strain frequencies of 0.5, 1 and 2 Hz after aging in PBS are shown in Figure 4.26. $\tan \delta$ was largest in the 20% PVA hydrogel tested at 2 Hz. The addition of nanofillers also increased $\tan \delta$ in the 10% PVA-NC hydrogels compared to the unfilled 10% PVA, and BC and pBC addition had greater impact than did Laponite.

4.5 DISCUSSION

4.5.1 Structure of PVA and PVA-NC Hydrogels

SEM of fractured hydrogel cross-sections in Millon et al. also showed a more open pore structure with the addition of BC in 10% PVA [24]. Increasing PVA concentration, and therefore decreasing water content, resulted in a thickening of the polymer-rich region and smaller water-filled pores. The addition of Laponite, BC and pBC to 10% PVA increased pore sizes in the PVA-NC hydrogels. The differences in structure may be due to a change in the phase separation process during F-T cycling in the presence of hydrophilic nanofillers, since they may disrupt hydrogen bonds in and between water and PVA.

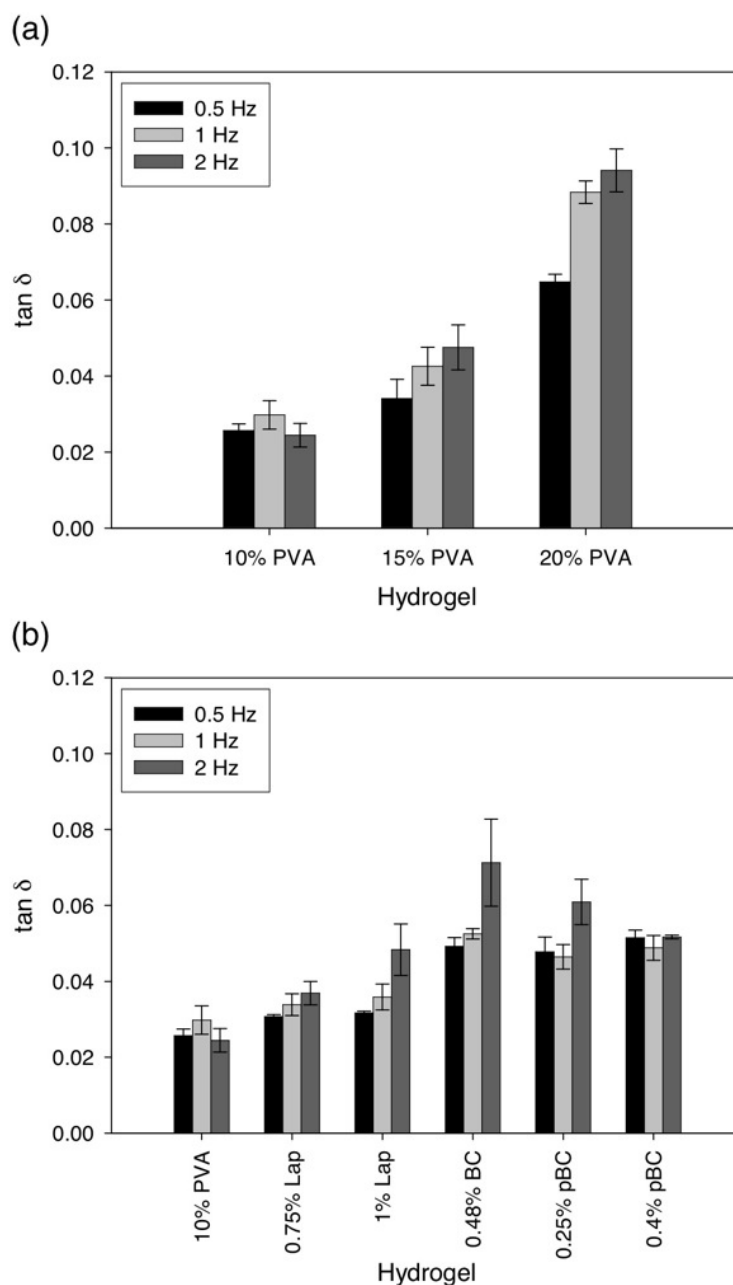


Figure 4.26: $\tan \delta$ for unfilled PVA (a) and 10% PVA-NC (b) hydrogels aged and tested in PBS. Viscous damping increased as strain frequency was increased, and with increases in polymer concentration and nanofiller addition.

The increase in polymer concentration resulted in a lower amount of water expelled during F-T cycling (Table 4.1) and increased swelling ratios after aging in water and PBS (Figure 4.7a). Hassan and Peppas reported that crystallinity increased by increasing PVA concentration from 7% to 15%, but the increases were greater between 7%

and 10% than between 10% and 15% PVA [109]. As PVA concentration increased, more polymer molecules would occupy a given volume in solution, allowing them to form crystallites more readily during F-T cycling, which could result in less molecular rearrangement during aging. However, no significant difference was observed between 10%, 15% and 20% PVA in the present study (Figure 4.8). Crystallinity in PVA hydrogels was also found to increase after aging in water [104, 115], but Hassan et al. found initial decreases in crystallinity due to dissolution of crystallites with lamellar thickness less than 185 Å, which resulted in the initial swelling of hydrogels [109, 140]. Swelling of the amorphous region may have induced organization with aging. Decrease in crystallinity at the beginning of the aging period, followed by increase in crystallinity with continued aging could have resulted in little or no change in crystallinity, as observed in the PVA and PVA-NC hydrogels.

Mass loss and shrinkage was observed in previous studies of aging in water and salt solutions of PVA hydrogels fabricated through F-T cycling. Lozinsky et al. reported shrinkage in 1 FTC-PVA hydrogel beads that equilibrated after two weeks of water flow through a bead-packed column following an initial swelling ratio of up to approximately 1.3, but there was no net change in mass because of the large initial swelling [112]. In Willcox et al., mass loss of 19 wt% PVA hydrogels aged for up to a year ranged from 8% for hydrogels produced with 1 FTC to 5% for those with 12 FTC due to weeping of water that pooled on the surface [104]. These hydrogels were sealed during aging to prevent evaporation of the exuded water. At lower PVA concentrations, polymer chains would have more mobility, and water would be displaced as ordering increases during aging, resulting in increased deswelling. Mass loss in our 6 FTC-20% PVA hydrogels after 7 days in water was approximately 9%. Hassan and Peppas found that initial swelling of the polymer structure facilitated molecular rearrangement in F-T PVA hydrogels placed in water [109]. Immersion of our 20% PVA hydrogels could have led to increased ordering and a larger degree of deswelling compared to Willcox et al.

Patachia et al. demonstrated that mass loss due to deswelling from PVA hydrogels equilibrated after approximately 25 hours in 1–3 M salt solutions, resulting in swelling

ratios of 0.5–0.95 that decreased with increasing solution concentration [144]. Using PVA concentrations similar to those of the current study, Holloway et al. obtained swelling ratios of approximately 0.75 and 0.9 for 5 FTC 10% and 20% PVA/PVP hydrogels, respectively, that equilibrated after 7–10 days in PBS [116]. While PVP has been found to lower polymer loss from PVA hydrogels [121], mass loss after aging in PBS was lower in our 10% PVA hydrogels, with a swelling ratio of 0.83 after 7 days. The use of controlled F-T cycling and an additional F-T cycle may have resulted in a more stable crystal structure, preventing deswelling during aging. Conversely, our 20% PVA hydrogels had a lower swelling ratio of 0.85 than the 0.9 found by Holloway et al. The molecular weight of the PVA used in Spiller was 89 000–98 000 g/mol [116], compared to 146 000–186 000 g/mol in our studies. There could be a larger degree of molecular rearrangement leading to deswelling in our 20% PVA hydrogels in comparison because longer chain lengths could have inhibited formation of crystalline domains during F-T cycling due to decreased mobility [109], the effect of which would be less significant with 10% PVA due to a higher water content. The presence of PVP, at 1% of the polymer content, may have also affected swelling compared to pure PVA hydrogels, contributing to the differences in swelling ratios.

More water was retained in the PVA-NC hydrogels after F-T cycling (Table 4.1) and aging in water (Figure 4.7a), which could be due to increased hydrophilicity. In water, annealed Laponite-filled PVA-NC membranes had increased swelling as temperature was increased up to 60 °C, while swelling decreased in unfilled PVA membranes, which was attributed to the hydrophilic nature of Laponite [159]. Water content was 1–2% higher in PVA-NC hydrogels containing graphene oxide than pure PVA hydrogels due to the hydrophilic nature of the fillers, which possesses carboxylic acid and hydroxyl groups [174]. However, swelling of these hydrogels with aging was not investigated. With the addition of BC into hydrophobic matrices, there were concerns of poor compatibility and moisture between BC and the polymers [166]. In a hydrophilic matrix, BC may contribute to increased material hydrophilicity and swelling.

The nanofillers could also have reduced chain rearrangement in the PVA-NC hydrogels by providing sites for adsorption of PVA molecules, decreasing polymer mobility. Adsorption of PVA molecules onto filler surfaces and disruption of hydrogen bonding would inhibit movement of the polymer chains, preventing chain folding and contributing to the decrease in crystallinity in NC hydrogels [29, 148, 159, 176]. Decreases in crystallinity in PVA-NC hydrogels with the addition of Laponite were found using DSC (Figure 4.8). Their addition may have disrupted the formation of hydrogen bonds in PVA during F-T cycling [159, 175, 176], impeding the formation of crystalline domains, and increasing the proportion of amorphous polymer and the proportion of amorphous polymer that could be swollen with water. This could explain the higher water content and decreased mass loss due to deswelling during aging with the addition of Laponite. In previous studies, graphene oxide was able to hydrogen bond with water as well as PVA, forming crosslinks in the polymer that limited swelling of the hydrogels at filler content above 0.6% [174], while oxygen and hydroxyl groups on Laponite resulted in adsorption of hydrophilic polymers onto its surface [159]. PEO chains adsorbed onto multiple clay surfaces with Laponite acting as crosslinks to form gels when induced by shaking [160]. Viscosity also increased with the addition of Laponite to PEO solutions due to adsorbed polymer and bridging of Laponite particles [162].

BC, which has a large number of alcohol groups due to its glucose subunits, should be able to hydrogen bond with PVA to allow for polymer adsorption. 0.48% BC addition into 10% PVA had the lowest decrease in mass after aging in PBS. This may suggest that surface chemistry, aspect ratio and concentration of the filler play a role in decreasing mass loss due to increased PVA adsorption and reinforcement of the hydrogel to prevent shrinkage. However, the decrease in crystallinity from the 10% PVA control, while significant in Laponite-filled PVA, was not in BC- and pBC-containing hydrogels, suggesting that the difference in filler size [154] and shape could also play a role in reducing crystallization, and that PVA could be intercalated between clay sheets [164]. Since Laponite, BC and pBC addition would have decreased chain mobility due to polymer adsorption onto nanofiller surfaces, this could have conferred stability, and may have

reduced molecular rearrangement leading to deswelling during aging in the PVA-NC hydrogels. As mechanical properties of a hydrogel depend on its polymer concentration [13, 19, 116], both the presence of the nanofillers and their effect on crystallinity and water content could have an influence on the unconfined compression properties of PVA-NC hydrogels.

4.5.2 Compression Properties

All of the PVA and PVA-NC hydrogels had concave-up, “J-shaped,” stress-strain curves in which modulus increased with strain, in a manner similar to biological tissues and unlike synthetic polymers [11, 13, 24] such as UHMWPE used in joint replacements. Silva et al. related fluid permeability in PVA hydrogels to its void ratio, which is the ratio of fluid to solid [177]. The void ratio is strain dependent as fluid is exuded with increasing strain. Stiffness would increase with strain as PVA concentration increases and permeability decreases, leading to increased fluid pressurization. Unconfined compression of the unfilled PVA hydrogels in the current study showed that stiffness increased with PVA concentration, which has also been demonstrated in previous studies [23, 116]. While modulus increased with PVA concentration, the difference between tangent and secant moduli decreased, indicating that non-linearity in the stress-strain curves decreased with decreased water content (Table 4.2). A lower increase in modulus with strain for hydrogels with higher PVA concentration could be the result of less free water [134] and lower permeability [177], which would reduce water exudation with strain.

The change in tangent and secant moduli after aging increased with increasing PVA concentration (Table 4.5). Both $E_{tangent}$ and E_{secant} increased by more than 50% in 20% PVA hydrogels aged and tested in PBS, despite having the lowest decrease in mass and volume after aging out of the hydrogels tested. Since aging tends to increase the crystallinity [104, 115] and polymer concentration [115] of PVA hydrogels, it is likely that changes in the crystalline domains and deswelling were responsible for the increase in stiffness to varying degrees depending on the hydrogel composition. However, DSC

results in the present study showed no significant increase in degree of crystallinity after aging (Figure 4.8), the increase in stiffness may be largely due to the decrease in water content in the PVA hydrogels.

Table 4.5: Change in tangent and secant modulus at 0.45 strain after one week of aging in water and PBS for unfilled PVA hydrogels tested at 100%/s.

Hydrogel	Change in E_{tangent} with aging (%)		Change in E_{secant} with aging (%)	
	Water	PBS	Water	PBS
10% PVA	18 ± 1	27 ± 2	18 ± 1	33 ± 2
15% PVA	35 ± 1	47 ± 2	33 ± 1	47 ± 2
20% PVA	40 ± 2	55 ± 2	37 ± 1	52 ± 1

The increase in stiffness for 10% PVA was on the same order as found by Lozinsky et al. after aging in water that resulted in hydrogel deswelling [112], and higher than the 20% increase in linear compressive modulus for 10% PVA/PVP hydrogels after 1 week of aging in PBS in Spiller et al. [123]. However, the modulus obtained by Spiller was from the linear region of the stress-strain curve, obtained after preloading to 0.1 strain then compressing to a total of 0.16 strain at an unspecified strain rate. Furthermore, PVP was added to stabilize F-T PVA hydrogels and lower polymer dissolution [121], which may have also prevented greater increases in modulus with aging.

There were no apparent changes in the stress-strain curves with the addition of Laponite (Figure 4.10). Water contents of Laponite-filled PVA-NC hydrogels were similar to 10% PVA, but crystallinity was 22% and 41% lower with additions of 0.75% and 1% Laponite, respectively. Stiffness in PVA hydrogels increases as crystallinity increases with F-T cycling [13, 24, 103, 105, 114, 116]. However, the addition of Laponite resulted in decreases in crystallinity that did not lead to changes in the unconfined compression stress-strain curve compared to the 10% PVA hydrogel. While there was a decrease in the proportion of crystalline domains that form the physical crosslinks, adsorption of PVA molecules on Laponite may have acted as additional crosslinks [160], and provided reinforcement by the formation of a stiffer amorphous phase, in which polymer chain movement was confined and impeded by adsorption to Laponite filler surfaces [159, 164]. The opposing effects of decreased crystallinity and reduction of molecular

movement with the addition of Laponite did not have a net impact on unconfined compression of 10% PVA hydrogels, but would affect time-dependent viscoelastic properties relevant to applications in IVD replacement.

BC and pBC addition increased non-linearity in which modulus rapidly increased above 0.25 strain (Figure 4.11). The large surface area of the high aspect ratio BC and pBC would also allow for a strong interface, contributing to its reinforcing efficiency [13, 24]. Since PVA and BC both possess alcohol groups, hydrogen bonding would be possible at the interface between the filler and hydrogel matrix. While the filler-matrix interface may have been affected by phosphorylation, electrostatic repulsion of negatively charged phosphate groups could have led to more discretely dispersed nanofibres. Since some of the alcohol groups were substituted, hydrogen bonding between PVA and pBC could be decreased. The charged groups could also have a greater affinity for water, and bind water more tightly, preventing fluid flow from the hydrogel structure during unconfined compression.

The stress-strain curves of BC- and pBC-filled 10% PVA-NC hydrogels were all similar despite the varying amounts of BC and pBC added. Since the phosphate group substitution along the BC backbone is heavier than the original $-OH$ group, there would be fewer nanofibres for a given mass of pBC than BC. However, Millon et al. also did not find a large difference between additions of 0.3% and 0.85% BC in 10% PVA in unconfined compression [24], and so the current results were not unexpected. In a study of electrospun PVA nanofibres reinforced with carbon nanotubes (CNT), modulus was not dependent on CNT loading but increased as CNT aspect ratio was increased, agreeing with theoretical models that improvements in reinforcement efficiency mostly depended on filler aspect ratio [229]. This could explain the increase in hydrogel stiffness in the current study and in Millon et al. with BC and pBC addition, in which stiffness was largely independent of the amount that was added. Since phosphorylation did not appear to change the dimensions of BC fibres or the stress-strain curves of the hydrogels, aspect ratio could be a factor in PVA hydrogel reinforcement.

Hydrogels containing Laponite had similar increases in tangent and secant moduli at 0.45 strain after aging in both water and PBS, with larger increases in moduli than 10% PVA after aging in water, and similar increases in moduli to 10% PVA after aging in PBS (Table 4.6). Since the decrease in water content after aging in water was similar for unfilled 10% PVA, and 0.75% and 1% Laponite-filled 10% PVA-NC hydrogels, which were $1.690 \pm 0.003\%$, $1.888 \pm 0.004\%$ and $1.488 \pm 0.006\%$, respectively, the addition of Laponite may have resulted in structural changes such as adsorption of PVA to the filler surface that resulted in a larger increase in modulus after aging in water. Aging in PBS, however, did not affect hydrogels containing Laponite to the same degree as the unfilled 10% PVA hydrogel, decreasing in water content by $3.81 \pm 0.01\%$ and $3.68 \pm 0.01\%$ with 0.75% and 1% Laponite addition, respectively, rather than $4.277 \pm 0.008\%$ for 10% PVA. This may be due to charges that had been introduced into the Laponite-filled PVA-NC hydrogels through the clay nanofiller, making them less susceptible to deswelling due to osmotic pressure. BC- and pBC-containing hydrogels had the lowest increase in moduli with aging. Since the main contribution of stiffness in these hydrogels at 0.45 strain may be nanofibre reinforcement, the effect of aging, osmotic pressure and decrease in water content would not have the same effect on BC- and pBC-filled hydrogels as in the other hydrogels.

Table 4.6: Change in tangent and secant modulus at 0.45 strain after one week of aging in water and PBS for 10% PVA-NC hydrogels tested at 100%/s (– indicates no statistical change).

Hydrogel	Change in $E_{tangent}$ with aging (%)		Change in E_{secant} with aging (%)	
	Water	PBS	Water	PBS
10% PVA	18 ± 1	27 ± 2	18 ± 1	33 ± 2
0.75% Lap	28 ± 1	28 ± 1	28 ± 1	31 ± 1
1% Lap	24 ± 2	27 ± 2	26 ± 2	34 ± 2
0.48% BC	11 ± 1	14 ± 2	14 ± 1	20 ± 2
0.25% pBC	–	–	–	8.1 ± 0.3
0.4% pBC	–	7.9 ± 0.4	8.2 ± 0.6	13.8 ± 0.6

Change in mass with aging did not have a clear relationship with the resulting change in stiffness. PVA-NC hydrogels had smaller decreases in mass and volume than 10% PVA, but aging had a larger effect on the modulus of Laponite-filled hydrogels than

10% PVA, and BC- and pBC-filled had little to no change in stiffness. However, stress at 0.45 strain varied linearly with water content as shown in Figure 4.27. As such, the increase in stiffness with aging may largely be due to the decrease in water content.

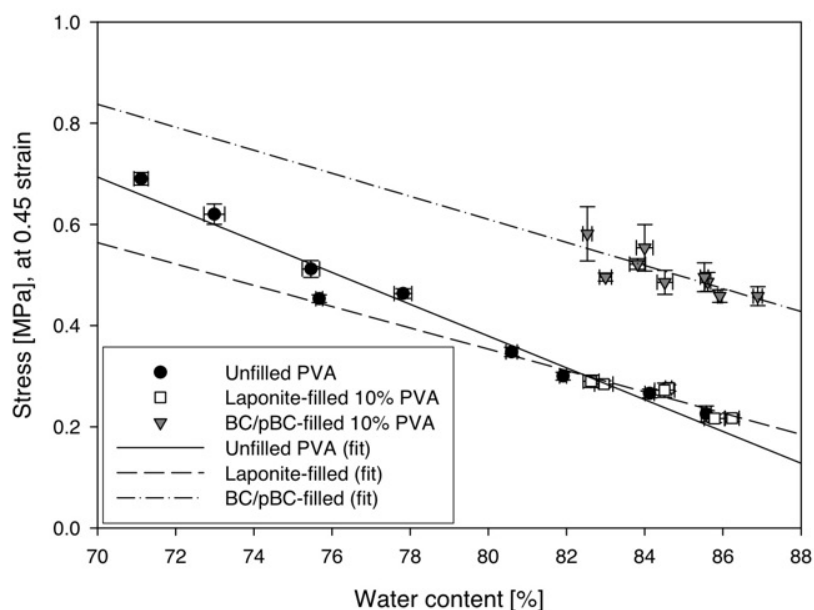


Figure 4.27: Linear relationship of stress to water content in unfilled PVA and 10% PVA-NC hydrogels, fresh and after aging in water and PBS (strain: 0.45, strain rate: 100%/s). Hydrogels filled with the high aspect ratio BC and pBC were stiffer than unfilled and Laponite-filled hydrogels relative to its water content.

The unfilled PVA hydrogels had a larger dependence on water content than the 10% PVA-NC hydrogels. The slope of the linear fits of stress vs. water content for the unfilled PVA hydrogels, and Laponite-filled and BC-/pBC-filled 10% PVA-NC hydrogels were -0.0314 , -0.0211 and -0.0228 MPa/% water, respectively. However, the dependence on water content for the unfilled 10% PVA hydrogels only was -0.0200 MPa/% water, indicating that greater increases in stiffness could be achieved with higher initial PVA concentrations. Figure 4.27 also shows that Laponite-filled hydrogels had stiffness similar to neat PVA hydrogels and did not show any net improvement with Laponite addition, while BC and pBC-filled hydrogels were stiffer even with similar water contents to 10% PVA due to higher aspect ratio of the filler. Although addition of nanofillers to PVA hydrogels of higher concentrations were not investigated in this study, Mil-

lon et al. was able to increase tensile tangent modulus by 3 and 4.5 times at 0.3 and 0.6 strain, respectively, by raising PVA concentration from 7.5% to 15% while keeping BC content constant at 0.3% [13]. Reduction of water content with the increase in PVA concentration in the presence of BC or pBC could present an opportunity to increase stiffness to what would be required for a cervical IVD device.

4.5.3 Strain Rate Dependence

Stress correlated linearly with the logarithm of strain rate in the PVA and PVA-NC hydrogels (Figure 4.15). The slope of this linear fit was used to quantify strain rate dependence (Figure 4.16). The linear relationship between compressive yield stress and logarithm of strain rate had been previously found in amorphous thermoplastic polymers [230-232]. The relationship was predicted by the classic Eyring model [233], which could be simplified to a linear function between stress and log strain rate. At the yield point, molecular movement is believed to be due to an activated process and is purely viscous. Wendlandt et al. also found that the linear relationship can exist at strains above the yield point [230]. Since hydrogels are viscoelastic in nature, the logarithmic relationship between stress and strain rate may have arisen from the viscous nature of the material. Another possible contribution is the movement of water through the porous structure of hydrogels during compression. Whether the relationship between stress and logarithm of strain rate is due to a physical process or of an empirical nature, the slope of this fit could be used to quantify strain rate dependence for the purposes of comparison. Strain rate dependence of the PVA and PVA-NC hydrogels was not apparent at low strains, and so stress at 0.45 strain was used for comparison between hydrogel compositions.

Viscous flow would contribute to strain rate dependence in the PVA and PVA-NC hydrogels, resulting in the logarithmic dependence on strain rate. At slow strain rates, there would be sufficient time for viscous flow to proceed with increasing strain, but at high strain rates, viscous flow is slow compared to the rate of deformation, and a higher stress would be required to compress the hydrogel to the same strain. In hydrogels with

higher PVA concentrations, viscous flow may be decreased, resulting in decreased strain rate dependence. Increase in strain rate dependence with the addition of Laponite may be due to increased viscous flow. In aqueous solutions of Laponite and PEO that form reversible gels with shaking, PEO molecules adsorbed onto clay surfaces were deformed and desorbed as shear is introduced into the system, exposing the surface for further polymer adsorption to bridge Laponite particles [161]. In response to strain, PVA molecules adsorbed onto nanofiller surfaces in Laponite-filled PVA-NC hydrogels may also be deformed and desorbed, resulting in increased molecular movement. This, along with decreased crystallinity in the Laponite-filled hydrogels, would lead to increased viscous flow compared to unfilled PVA hydrogels. Meanwhile, the presence of nanofillers may also increase resistance to viscous flow since Laponite, BC and pBC may impede chain motion.

Since fluid flow with strain depends on the permeability of the hydrogel [137, 177], the rate at which load is applied could affect the response of the hydrogel. At low strain rates, fluid flow would have sufficient time to proceed, and load would mainly be born by the solid matrix. At high rates of loading, fluid flow could be slow compared to strain rate, and the hydrogels would experience fluid pressurization and internal stress. These events increase the energy required for deformation, and strain rate dependence arises. At higher PVA concentrations, there is an increased proportion of bound water in the hydrogels that cannot be exuded with compressive deformation regardless of strain rate. Reducing the amount of fluid that can be exuded may play a role in reducing strain rate dependence with increasing PVA concentration. With the addition of Laponite, BC and pBC, an increase in hydrophilicity may have decreased rate of fluid flow, increasing fluid pressure upon high rates of loading.

4.5.4 Stress Relaxation and Creep

The PVA and PVA-NC hydrogels tested did not relax completely after one hour of stress relaxation (Figures 4.17–4.19), which was also observed in previous studies.

Millon et al. reported that after one hour at 0.45 strain, relaxation was not complete in 10% PVA hydrogels and PVA-BC hydrogels, which relaxed to 45% and 20–30% of the initial stress, respectively [24]. Relaxation continued to increase after 24 hours in 25% PVA hydrogels studied by Stammen et al., which relaxed to 45% of the initial stress at 0.2 strain [19]. Since stress relaxation tests in the current study were performed at 0.25 strain for one hour, the degrees of stress relaxation were lower than those found in the other two studies, with the PVA and PVA-NC hydrogels retaining between 45% (0.4% pBC-10% PVA) and 78% (20% PVA) of the initial stress (Figure 4.20).

During stress relaxation, fluid would flow out of the structure until hydrostatic pressure is equilibrated under constant strain. In creep, sustained application of load would lead to fluid flow from the hydrogel to relieve fluid pressurization. While increases in PVA concentration in the hydrogels would reduce fluid permeability [137, 177], the amount of water available to be exuded under load would also decrease [134], resulting in decreased stress relaxation and creep. Other studies have also found that creep decreased as water content decreased in PVA hydrogels [19, 137].

The addition of Laponite resulted in increased stress relaxation and creep possibly due to increased viscous flow and initial fluid pressurization. Decreased crystallinity in Laponite-filled hydrogels would have resulted in increased swelling of the amorphous regions and a higher propensity for polymer molecules to deform under stress [223]. Desorption of polymer from filler surfaces during loading could also increase chain mobility. Thus, there would be increased dissipation in stress and hydrogel deformation through viscous flow and increased movement of polymer molecules. Laponite-filled hydrogels had approximately the same water content as 10% PVA and therefore could have similar fluid permeability based on the ratio of fluid to solid volume [137, 177], but fluid permeability could also depend on the pore structure. However, the addition of Laponite may have allowed water to bind more tightly due to increased hydrophilicity, reducing exudation of fluid during the initial deformation and increasing fluid pressurization in the hydrogel. 0.75% Laponite-10% PVA hydrogels had a slightly higher water

content than the other two hydrogels, which could have resulted in a greater amount of creep.

In contrast to Laponite-filled hydrogels, crystallinity with BC and pBC addition was similar to the unfilled 10% PVA hydrogel. Increased hydrophilicity of BC- and pBC-filled hydrogels would also increase fluid pressurization upon loading and subsequent reduction of fluid support that increased with filler content. Millon et al. also saw an increase in stress relaxation with higher BC content, which was attributed an increase in viscoelasticity through the addition of BC [24].

Aging in PBS decreased the amount of stress relaxation (Figure 4.20a) and creep (Figure 4.25a) in neat PVA hydrogels. The effect of water content on stress relaxation is a possible explanation for this observation for these hydrogels. Since PVA hydrogels increased in polymer concentration and stiffness with aging, they would undergo less stress relaxation and creep in the same manner as increasing PVA concentration. Meanwhile, stress relaxation did not differ after aging in PBS in hydrogels containing Laponite, BC and pBC (Figure 4.20b). Although PVA-NC hydrogels became stiffer in unconfined compression due to the decrease in water content with aging, higher proportions of amorphous PVA in the case of Laponite, desorption of PVA molecules from filler surfaces, and increase in hydrophilicity would still have contributed to creep due to viscous and fluid flow when compared to unfilled hydrogels (Figure 4.25b). The presence of free ions in PBS could have disrupted hydrogen bonding between PVA and BC after aging that resulted in the increase in creep in the BC-filled hydrogel. Creep in pBC-filled hydrogels, however, was not affected by aging in PBS as it also had a minimal effect on modulus. If either aging or the presence of ions negatively affect the interface between PVA molecules and certain nanofillers, then pBC could be the preferred choice as a nanofiller for long-term use since it appears to be least affected by aging.

A limitation of performing creep tests in the MTS Bionix 858 UTS was the response of the actuator. The controller was set to load-control mode since a constant load was specified for creep tests, but feedback from the load cell was required as crosshead

position was varied in order to maintain the load. At times, the actual load on the hydrogels deviated by as much as 373 gf (3.65 N) from the specified load as crosshead position overcompensated for creep and overshot the target load. This resulted in data that was noisy, as observed in Figure 4.21.

4.5.5 Cyclic Compression Testing

As polymer concentration increased, the density of the polymer network and viscosity increased as well. A decrease in water content would increase internal friction in the polymer, thereby increasing $\tan \delta$. Gong stated in [139] that $\tan \delta$ is approximately 0.01 for PVA hydrogels, although this value may be from dynamic testing in shear, and frequency and PVA concentration were not specified. The presence of large amounts of water in PVA hydrogels decreased internal friction, resulting in low $\tan \delta$ values that would increase with an increase in polymer concentration. Increases in $\tan \delta$ with frequency in the hydrogels could be due to the resistance to polymer chain motion in the hydrogel, resulting in viscous damping where energy is dissipated. Since 10% PVA had a high water content, it would have the lowest internal friction where increases in strain frequency did not affect $\tan \delta$ (Figure 4.26a). Yang et al. [234] found that the loss modulus of PVA hydrogels dominated at high frequencies, and since $\tan \delta$ is the ratio of loss modulus to storage modulus, $\tan \delta$ would therefore increase with increased frequency. The increase in loss modulus was attributed to the effects of viscous movement of polymer molecules in the hydrogel that become more significant at high frequencies. Resistance to viscous flow would be more pronounced in hydrogels of higher PVA concentrations since more polymer molecules would occupy a given volume.

The increase in $\tan \delta$ with the addition of Laponite, BC and pBC could be due to increased viscous flow of PVA chains in the hydrogels (Figure 4.26b), as discussed in the above section on stress relaxation and creep. Resistance to viscous flow was further increased with the addition of BC and pBC since $\tan \delta$ increased to a greater extent. This would result in higher viscous loss than with Laponite, possibly due to adsorption and

hydrogen bonding of PVA to the nanofiller surface, and hindrance of chain movement by the stiffer nanofibre. This further supports the hypothesis that BC addition increases viscous response in PVA hydrogels by Millon [13, 24].

While this test provided an insight into the dynamic compressive behaviour of PVA and PVA-NC hydrogels, long-term testing should be performed in the future to determine whether there are permanent deformation and fatigue effects after a high number of loading cycles. Joshi et al. [58] performed compressive cyclic loading on a 15% PVA/PVP hydrogel nucleus pulposus replacement to 0.15 strain at 5 Hz, up to 10 million cycles to assess fatigue. While tangent modulus from unconfined compression decreased by 24% at 0.15 strain after 10 million cycles of fatigue cycling, it was not affected at higher strains. Permanent deformation of the hydrogels, which should be minimized in an IVD device to prevent loss of disc height, resulted in a 17% decrease in height, along with a 5% increase in diameter, but no change in polymer concentration was found.

4.5.6 Comparison to the Natural IVD and Application to IVD Device Design

In the IVD, the nucleus pulposus (NP) provides swelling potential and becomes pressurized to support load, as the annulus fibrosus (AF) confines and resists tensile loads placed upon it by the NP [135]. Meanwhile, the endplates regulate fluid flow to and from primarily the NP and the vertebral bodies [40, 41]. It is the regulation of fluid flow that allows the IVD to experience strain rate dependence, and high degrees of stress relaxation and creep [55]. At high rates of loading, fluid pressurization is increased and the disc bulges so that water content does not decrease as quickly, possibly explaining the decrease in $\tan \delta$ with high loading frequencies [62]. In addition to collagen, which confers structural support [135], fixed charges on the large amounts of proteoglycans in the IVD provide the osmotic potential for fluid to flow back into the disc once load is removed to recover disc height and prevent permanent deformation [37].

The stress-strain curves of the natural IVD are highly non-linear, displaying an initial low modulus toe region and a high modulus region beyond 0.05–0.1 strain [55, 57]. A toe region in this range of strains was not observed in the PVA and PVA-NC hydrogels. However, with the addition of BC and pBC into 10% PVA hydrogels, the transition from low to high modulus region occurs at approximately 0.25 strain (Figure 4.11).

The tangent and secant moduli of the PVA and PVA-NC hydrogels at 0.45 strain were 1.2–5.8 MPa and 0.38–1.0 MPa, respectively, and much lower than the linear modulus of IVDs, which were approximately 11–34 MPa [56]. While the PVA and 10% PVA-NC hydrogels tested were not of sufficient stiffness as a cervical IVD replacement, the relative effects of composition, particularly with nanofiller addition, on strain rate dependence could still be examined. As such, even though the healthy human IVD experiences up to approximately 0.15 strain physiologically [58], the modulus at 0.45 strain was used for comparison between strain rates in this study since strain rate dependence was more apparent at higher strains.

Strain rate dependence in compression has been observed in IVDs studied by Cassidy et al. [55]. The maximum stress from the stress-strain curves of IVDs, which were left attached to the vertebral bone and tested at strain rates of 1.67×10^{-5} to 1.67 s^{-1} , was shown to vary linearly against the logarithm of strain rate in that study. Using the same procedure as for the PVA and PVA-NC hydrogels, we determined the slope of this linear relationship to be 17.5 %/log(%/s) ($R^2 = 0.9562$) for the canine IVDs. While strain rate dependence in the canine IVDs was apparent at strains above the toe region, little to no strain rate dependence was observed in PVA and PVA-NC hydrogels at low strains. However, the degree of strain rate dependence for the canine IVDs was similar to 0.48% BC- and 0.4% pBC-10% PVA-NC hydrogels at 0.45 strain, which ranged from 16.0 to 19.2 %/log(%/s) (Figure 4.16b).

Cassidy et al. [55] found that after stress relaxation, water content decreased in canine IVDs preferentially from regions of high water content in and around the nucleus, with fluid moving through the endplates and into the vertebral bodies. Rate dependence

in IVDs was also believed to be due to the transport of water. Since load bearing due to hydrostatic pressure occurs in IVDs, decreased volume loss with compressive strain at high strain rates would increase fluid pressure inside the disc [61, 235]. At slow strain rates, in which volume loss due to fluid flow is greater, bulging of the annulus to accommodate the nucleus with increased compressive strain would be less pronounced, resulting in lower circumferential strains on the collagen lamellae in the AF. The lamellae have a low modulus toe region up to 0.1 strain [55, 57], in which there was no strain rate dependence as reorientation of the lamellae and uncrimping of collagen occurs, followed by a high modulus region, in which the stretched fibres are loaded in tension [68]. Lower circumferential strains on the AF with lower strain rates would then result in lower stresses in the IVD as it is compressed. The viscoelasticity of the natural tissue matrix is also implicated in strain rate dependence of the IVD [55, 61]. However, the natural IVD is multi-component and anisotropic, and in contrast, the PVA and PVA-NC hydrogels in the current study were isotropic materials. The mechanism of strain rate dependence in the PVA and PVA-NC hydrogels could also be due to the flow of fluid from the hydrogels during compression. Increased hydrophilicity in PVA-NC hydrogels leading to increased pressurization upon loading could contribute to increased strain rate dependence, as could increased viscoelasticity due to increases in the amount of and resistance to viscous flow.

Compared to the natural IVD, in which stress relaxed to less than 10% of the initial stress just after 30 minutes at 0.05 and 0.15 strain [55], the degree of stress relaxation in PVA-based hydrogels was much lower at 0.25 strain. The greatest amount of stress relaxation was found in the 0.48% BC-10% PVA hydrogel, in which stress decreased to approximately 52% and 50% of the initial stress after 30 minutes and 60 minutes, respectively. Non-porous platens were used in stress relaxation testing of hydrogels in the current study as well as in Millon et al. [24] and Stammen et al. [19], which found similar degrees of stress relaxation. This would have prevented fluid flow from the top and bottom of the hydrogels. In contrast, the IVDs were tested while still attached to the verte-

bral bodies, which would allow fluid flow through the endplates into the vertebrae, resulting in greater rates of stress relaxation due to increased fluid flow.

Human IVDs have been found to increase in strain by 20–108% after 30 minutes of creep [23, 64]. Strain did not reach equilibrium deformation after 30 minutes under the estimated body weight at the lumbar disc level [64] or 15 hours at 177.92 N [63]. Creep in the PVA and PVA-NC hydrogels in this study was low compared to human IVDs. Unfilled PVA increased in strain by 10–25% after 1 hour, and by 30–40% with nanofiller addition (Figure 4.20). However, we used a low creep stress in this study, equal to approximately 25–33% of the stress used in the IVD tests, since the hydrogels were more compliant than the natural IVD, and the initial strains in the IVDs were approximately half of those in the 10% PVA and PVA-NC hydrogels. Although creep in IVDs is an important mechanism for energy dissipation following loading, a low degree of creep in the hydrogels would be desirable from the viewpoint of engineering design. The decrease in IVD height due to fluid is recovered each day during rest [42]. In polymeric systems however, viscous flow of amorphous regions could lead to unrecoverable deformations that would have implications for the performance of the device *in vivo*, since the disc space could decrease in height and would eventually require intervention. Viscous movement of PVA molecules in PVA and PVA-NC hydrogels may cause permanent deformation to occur. However, the hydrophilicity of the PVA-NC hydrogels may also encourage swelling and fluid flow back into the structure upon removal of load to aid in restoring height during rest. Future investigations of viscoelastic properties should include testing of the hydrogels between porous platens since endplate permeability also has an impact on both creep and creep recovery of IVDs [235]. Porous platens would allow for unimpeded fluid flow back into the hydrogels for determining the rate of creep recovery. Furthermore, unconfined compression testing between porous platens may have implications on stress-strain curves, and decrease modulus and strain rate dependence.

Previous studies of human lumbar IVD [63, 64] and PVA hydrogels [23] have reported the elastic and viscous component parameters from the three-parameter-solid

model fits (Equation 3.7). E_1 , E_2 and η_1 from PVA and PVA-NC hydrogels tested after aging in PBS are tabulated in Table 4.7 along with the range of values from human IVDs and 3%–40% PVA hydrogels found in literature.

Table 4.7: Parameters of elastic and viscous components from fitting of the three-parameter-solid model to creep data from unfilled PVA and 10% PVA NC hydrogels after aging in PBS, and of human lumbar IVD and PVA hydrogels from literature.

Material	E_1 (MPa)	E_2 (MPa)	η_1 (MPa·s)
10% PVA	0.77 ± 0.09	0.221 ± 0.005	2400 ± 300
15% PVA	2.8 ± 0.8	0.336 ± 0.006	5100 ± 700
20% PVA	4.6 ± 0.3	0.49 ± 0.02	8600 ± 800
0.75% Lap-10% PVA	0.45 ± 0.05	0.204 ± 0.007	910 ± 30
1% Lap-10% PVA	0.54 ± 0.08	0.213 ± 0.005	1130 ± 10
0.48% BC-10% PVA	0.65 ± 0.09	0.26 ± 0.01	2000 ± 200
0.25% pBC-10% PVA	0.70 ± 0.06	0.238 ± 0.005	1500 ± 200
0.4% pBC-10% PVA	0.6 ± 0.1	0.233 ± 0.005	1100 ± 200
Human lumbar IVD [63]	4.162 – 207.3	2.935 – 49.93	16340 – 2098000
Human lumbar IVD [64]	4.204 – 10.48	1.057 – 2.245	–
3–40% PVA hydrogels [23]	0.0800 – 63.22	0.0119 – 1.112	–

The elastic parameters of the three-parameter-solid model, E_1 and E_2 , varied with the modulus of the material, as indicated by their increase in 15% and 20% PVA hydrogels compared to 10% PVA hydrogels. Increases in the viscous parameter, η_1 , in higher PVA concentration hydrogels were due to decreases in time-dependent creep deformation. E_2 was higher with the addition of BC and pBC than 10% PVA due to lower initial strains. It is interesting to note that η_1 decreased compared to 10% PVA in hydrogels containing Laponite and pBC, which carry charges, but not with BC addition. The addition of unmodified BC did not have a significant effect on the viscous component of the model compared to 10% PVA according to the value of η_1 . Hydrogen bonding between BC and PVA could have resulted in a better interface between the nanofiller and the polymer, and hydrogen bonding within PVA was not disrupted. This suggests that while the addition of BC increased the modulus of PVA hydrogels, creep could be significantly increased by the addition of charges to the hydrogels through fillers. The parameters for 10% PVA and PVA-NC hydrogels were one order of magnitude lower than the minimum values in Burns et al. [63], and although E_1 in 20% PVA approached

those of human IVDs, E_2 and η_1 were still much lower than the natural disc. Wang and Campbell indicated that 40% PVA hydrogels had E_2 values in the range of those found in Keller et al. [64], but η_1 values were not given for these hydrogels. Higher concentration PVA hydrogels may provide the stiffness required to match the initial strains of the natural IVD. It may also be possible to use nanofillers of different characteristics, such as aspect ratio and fixed charges, in tuning creep properties to match those of natural IVDs.

Increasing PVA concentration to 20% PVA (Figure 4.26a) was able to increase the value of $\tan \delta$ to the range found by Costi et al. from dynamic compression of human IVDs (0.10–0.16) [61]. The addition of nanofillers was also able to increase $\tan \delta$ to varying degrees (Figure 4.26b). However, while $\tan \delta$ either remained constant or increased with increasing frequency in PVA and PVA-NC hydrogels, it decreased by 36% with increasing frequency between 0.001 and 1 Hz in IVDs. Costi et al. pointed to the effects of fluid pressurization and flow on $\tan \delta$ when loaded in compression [61]. While the $\tan \delta$ increase in the PVA and PVA-NC hydrogels could be in part due to viscous flow, which plays a role in energy dissipation in the hydrogels, decrease in $\tan \delta$ at higher frequencies in IVDs is likely due to decreased fluid flow and increased fluid pressurization. Bulging of the IVD would compensate for compressive deformation as volume is preserved [236], and fluid pressurization would result in increased elastic behaviour in the IVD.

4.5.7 Proposed PVA Hydrogel IVD Design

In order to attain the modulus required to function as a cervical IVD replacement, higher PVA concentrations must be used in the hydrogel, which would decrease non-linearity in the stress-strain curve and result in low degrees of stress relaxation. This may not be desirable in a potential IVD replacement if it eliminates the low modulus toe region, the function of which may be to provide compliance for shock absorption as load is applied, while the high modulus region provides support of load and prevents excess deformation. A decrease in stress relaxation may result high residual stresses in the mate-

rial as sustained loads are applied. However, although stress relaxation and creep of the hydrogels were lower than the natural IVD, lower degrees of creep may be advantageous in preventing large deformations. Nanofiller addition could be an effective method of modifying PVA hydrogel properties without drastically decreasing water content of hydrogels, and only a small amount is required to modify properties. Laponite, BC and pBC addition would increase stress relaxation in PVA-NC hydrogels, and BC and its derivatives in particular may be able to increase modulus at high strains while preserving a low modulus at low strains.

The shrinkage and extrusion of a PVA hydrogel NP replacement was demonstrated following implantation into baboons [146]. 20% PVA hydrogels had the highest resistance to decrease in mass and volume after aging in PBS (Figure 4.7), which could mitigate the possibility of shrinkage and migration after device implantation in a solute-rich fluid environment *in vivo*. Since PVA and PVA-NC hydrogels increase in modulus with aging, this could be exploited to obtain a stiffer hydrogel if the increase in modulus with aging could be well characterized and reproduced. By fabricating hydrogels in water then storing them in an osmotic solution, handling of a higher concentration polymer solution with increased viscosity could be avoided. Also, using a solution with similar osmolarity [123] to store a hydrogel device may mitigate the effects of aging following implantation. Conversely, with the addition of BC and pBC, aging in PBS resulted in a lower change in modulus, stress relaxation and creep than unfilled PVA hydrogels, which may be beneficial as hydrogel properties would be more predictable.

PVA hydrogels possess a high Poisson's ratio [58, 124] of approximately 0.45–0.5 [138, 237, 238]. During unconfined compression, there would be circumferential tensile forces on the structure due to lateral expansion. Since BC is a fibrous reinforcement, it may resist lateral expansion at high strains. The hydrated porous structure could also be subjected to tension due to hydrostatic pressure upon compression, which is similar to the behaviour of cartilage tissue and collagen under stress before reaching equilibrium [239]. The AF in the natural IVD, which consists of aligned collagen lamellae, also resists circumferential tensile loads from pressurization of the NP during compression [6,

82]. BC and pBC, therefore, could be used to impart the desired stress-strain behaviour to PVA hydrogels by mimicking the function of collagen fibres in natural tissues, including those in IVDs. While nanofibres were isotropically dispersed in the BC and pBC PVA-NC hydrogels tested, circumferential alignment of these fibres may offer a method to limit lateral expansion and improve compressive modulus in an IVD device. This was done with poly(ethylene terephthalate) fibres in previous studies by Ambrosio and workers, in which a toe region below 0.1 strain was observed on the stress-strain curves of pHEMA-based hydrogel IVD devices [178, 179]. Since BC and pBC-filled PVA hydrogels possess a toe region of up to approximately 0.25 strain, alignment of BC nanofibres in PVA-NC hydrogels may also be a potential method to limit toe region strain to the range found in the natural IVD.

Further studies into the composition and structure of these hydrogels to achieve the similar degrees of strain rate dependence as the natural IVD at low strains should be pursued. The role of rate dependence in the natural IVD is likely to limit deformation with high loading rates, preventing damage to the surrounding tissue by maintaining disc height. Increased fluid pressure inside the disc would also assist in distributing and transferring the load to the vertebral bodies. The effect of strain rate on fluid flow in the hydrogels could be investigated by comparing the degree of lateral expansion during unconfined compression and decrease in water content over a range of strain rates. If fluid flow could be modulated at different strain rates, it would influence fluid pressurization and lateral expansion. A higher degree of strain rate dependence would therefore be possible through a mechanism similar to the natural IVD. In designing a PVA hydrogel-based disc design, the structure and function of components in the native IVD could be mimicked. Creating a multi-component structure to limit fluid flow at the peripheries of a hydrogel device and to resist lateral expansion is a possible strategy to increase fluid pressurization, thereby increasing stiffness, and strain rate dependence at lower strains. Since fluid permeability in PVA hydrogels, as modelled by Silva [177] and Liu [137], is related to the ratio of fluid to solid in the hydrogels, fluid flow could be limited by using higher

PVA concentration hydrogels for the annulus and endplate components than the nucleus component of a hydrogel device to increase fluid pressurization.

The Bryan disc design is based on the structure of the IVD. It consists of a hyperelastic polyurethane (PU) core forming biconvex articulating surfaces between titanium alloy endplates, and saline is injected into the device during implantation to lubricate the wear surfaces [77, 90, 93, 94]. The core is surrounded and sealed by a stiffer PU sheath that contains the saline lubricant and wear particles, as well as prevent tissue ingrowth. Kurtz stated that the sheath is permeable to water [90], but there are no other references attesting to the permeability of the sheath. However, it is unclear whether fluid flow through the sheath would contribute to pressurization and energy dissipation in the Bryan disc. The stiffness of the PU core is also unclear. Studies modelling the biomechanics of the Bryan disc after implantation have used moduli of 25 MPa [240] and 70 MPa [241] for the core. A modulus of 25 MPa would be comparable to the stiffness of the cervical IVD, but both values are much lower than the moduli of UHMWPE, used in Prodisc-C, and metal alloys in the Prestige disc. However, the relatively low modulus of the PU core resulted in a displacement of 5–10 times greater than Prodisc-C and Prestige under load [240], which placed higher forces on the facet joints at the implanted level [241]. Increased range of motion of the Bryan disc would also increase strain on the facets and surrounding tissues, but the potential for heterotopic ossification and fusion of the artificial disc is decreased [240, 242]. Compared to Prodisc-C and Prestige, which use keels and rails for fixation, the convex endplates of the Bryan disc distribute stress more evenly while the PU core absorbs more energy [240]. This lowers the risk of subsidence of the implant into the vertebral bodies, but the potential still exists. The use of a hydrogel material that has similar mechanical properties to the native IVD and supports fluid flow in an IVD device should allow for recovery of natural motion at the affected level and decrease the risk of complications in TDR.

4.6 CONCLUDING REMARKS

PVA hydrogels produced through F-T cycling were chosen for investigation as a material for intervertebral disc replacement. They were fabricated without a chemical crosslinker and have concave up stress-strain curves similar to the natural IVD. Increasing PVA concentration increased stiffness, and decreased strain rate dependence, stress relaxation and creep. The addition of Laponite, BC and pBC nanofillers to 10% PVA resulted in increased hydrophilicity and pore sizes of the hydrogels. Laponite addition in 10% PVA-NC hydrogels decreased crystallinity but did not decrease stiffness, while BC and pBC addition increased hydrogel stiffness above 0.25 strain. Furthermore, the 10% PVA-NC hydrogels experienced increased strain rate dependence, stress relaxation and creep compared with the unfilled 10% PVA hydrogel. Meanwhile, aging the PVA and PVA-NC hydrogels in water and PBS decreased their mass and volume, and increased stiffness.

While the PVA and PVA-NC hydrogels examined in this study were not of sufficient stiffness for application in the cervical IVD, modulus improvements could be achieved through the increase of PVA concentration and addition of nanofillers. The optimization of a PVA-based hydrogel device with similar stiffness, viscoelastic behaviour, fluid flow and height recovery as the natural IVD could involve a combination of parameters including PVA concentration, nanofiller characteristics and concentration, and the fabrication of a multi-component structure to introduce location specific properties.

Chapter 5

CROSSING-PATHS WEAR OF PVA AND PVA-NANOCOMPOSITE HYDROGELS

Cervical TDR devices like the Prestige, Prodisc-C and Bryan discs integrate articulating surfaces into their designs, necessitating investigation of their tribological properties. Crossing-paths wear testing was performed to determine the suitability of PVA and PVA-NC hydrogels in articulating TDR designs since they are subjected to multidirectional sliding *in vivo*. The volume of the wear track after crossing-paths wear, which combined rotation with linear reciprocating motion, was determined using high frequency three-dimensional ultrasound (3D US) imaging. The wear surfaces and cross-sections of the hydrogels under the wear track were also examined using SEM to investigate the type of wear damage incurred.

5.1 CROSSING-PATHS WEAR TESTING

While unidirectional sliding of UHMWPE against metals or ceramics results in low rates of wear due to alignment of polymer molecules and orientation hardening, multidirectional wear in the polymer increases significantly due to intermolecular rupture of UHMWPE [207-209]. Crossing-paths wear testing is appropriate in TDRs because they experience multidirectional wear *in vivo* [196, 206]. Linear reciprocation with rotation between potential sliding pairs was presented as a cost-effective method for screening of materials using crossing-paths testing prior to simulator studies [210]. To compare between hydrogel compositions, crossing-paths wear testing was performed for 500 000

cycles against a spherical sapphire counter surface pin, applied with a normal load of 5 N. The crossing-paths wear tester had a linear stroke length of 8.5 mm with 28° pin rotation at 1 Hz (Figure 5.1). These parameters were based on the combined *in vivo* motion of 20° flexion-extension and 14° axial rotation at C5-C6, which was doubled to maximize the tested area of the sample and ensure the feasibility of the mechanical design in the tester [212]. Volume and depth of the wear track after crossing-path wear testing were determined using high frequency 3D US images after a period of recovery of two days each in ACS lubricant and PBS. The hydrogel surface and cross-sections under the wear track were examined using SEM following critical point drying.

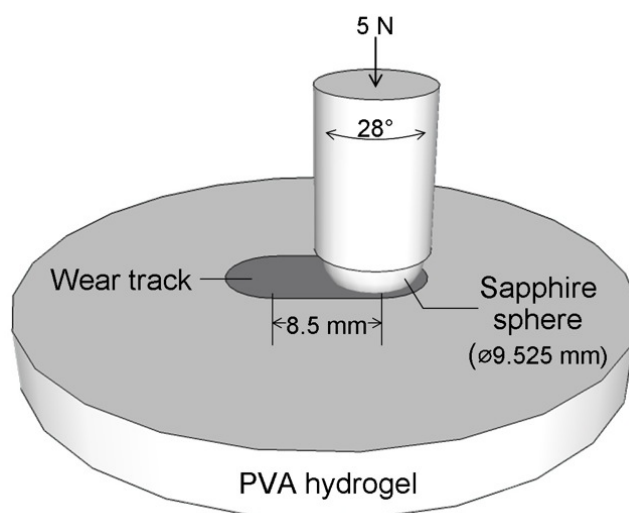


Figure 5.1: Schematic of crossing-paths wear testing on PVA and PVA-NC hydrogel surfaces. The 9.525 mm diameter spherical sapphire counter surface pin was translated linearly over a length of 8.5 mm and rotated over 28° for each stroke under a normal load of 5 N. Each sample was tested at a frequency of 1 Hz for 500 000 cycles.

5.2 VOLUME AND DEPTH OF WEAR TRACK

Brightness-mode (B-mode) US image planes were acquired in slices perpendicular to the surface of the hydrogel while the US probe was translated along the length of the wear track to obtain the 3D US image. The 40 MHz US transducer had a resolution of approximately 30 μm at the 15 mm \times 15 mm field of view used to cover the width of the

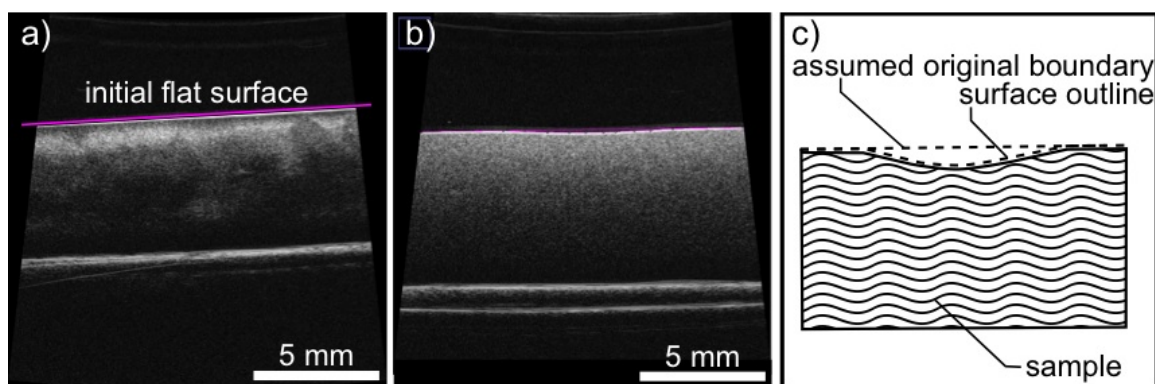


Figure 5.2: B-mode plane from 3D US showing the flat surface of 10% PVA hydrogel before testing (a), outlining of the indent on the top surface of the hydrogel to determine area using the polygon function in ImageJ (b), and a schematic of indent outlining (c).

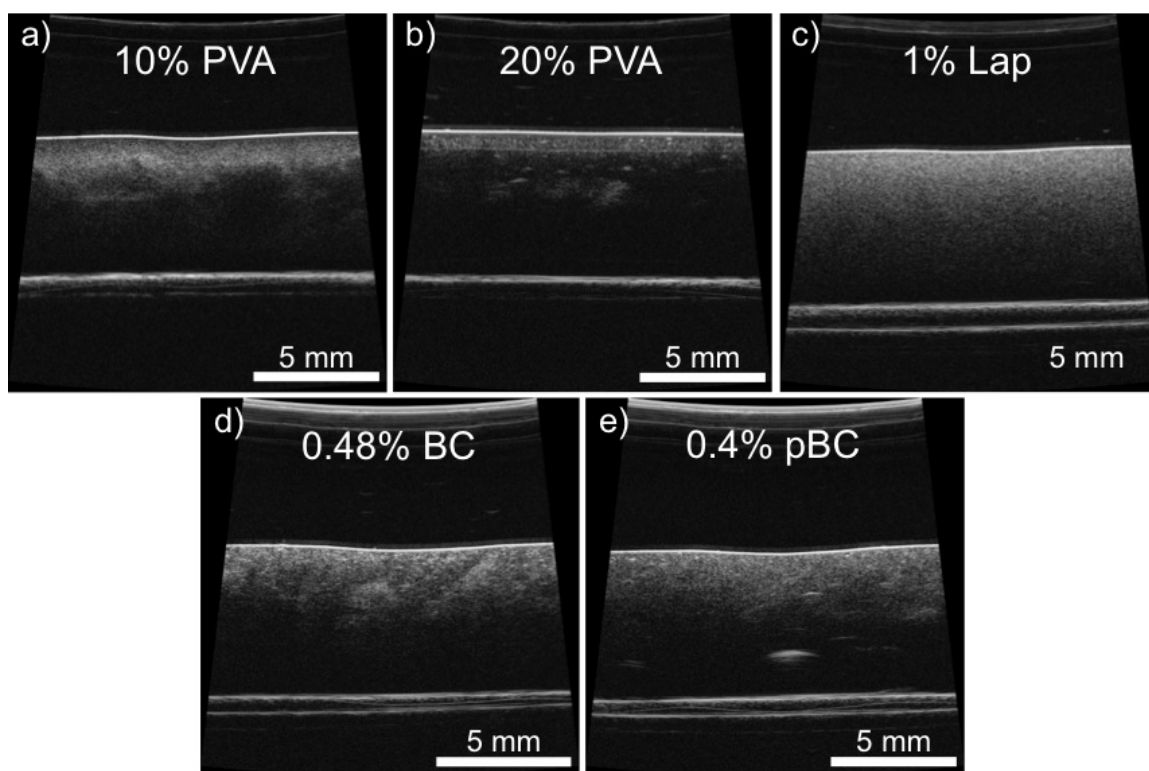


Figure 5.3: B-mode images from 3D US of hydrogels showing the cross-sections of wear tracks in 10% PVA (a), 20% PVA (b), and nanocomposites of 10% PVA with 1% Laponite (c), 0.48% BC (d) and 0.4% pBC (e).

wear tracks, and sample surfaces were placed near the 6 mm focal length to ensure optimal imaging so that image acquisition did not involve contact with the hydrogel. Volume of the wear track was determined from the sum of the areas of the indent in B-mode planes, assuming the initial surface was flat (Figure 5.2). The indents imaged in B-mode

planes after crossing-paths wear testing of selected hydrogels are shown in Figure 5.3. The depth of the indent was smaller in 20% PVA than in unfilled 10% PVA and 10% PVA-NC hydrogels.

Consequently, 10% PVA and PVA-NC hydrogels had greater wear track volumes than unfilled hydrogels of higher PVA concentrations (Figure 5.4). Wear volume from crossing-paths wear was likely a combination of the loss of material and permanent creep deformation. The maximum depth, found near the middle of the wear tracks, was also determined (Figure 5.5), which followed a similar trend as volume loss in the samples. Our results indicated that the addition of nanofillers did not significantly affect the volume or depth of the wear track in 10% PVA-based hydrogels after crossing-paths wear testing, whereas the increase in PVA concentration resulted in significant decreases in wear volume and maximum wear depth.

5.3 WEAR TRACK SURFACES AND SUBSTRUCTURE

Examination of surface damage could be used to determine the mechanism and consequence of wear on the hydrogels. This would be useful for evaluating the suitability of using the material in an IVD device with articulating surfaces that result in wear. Furthermore, since the reciprocating wear tests produced cyclic loading on the hydrogels, the structure under the wear track could be altered by fatigue loading. The cross-sections under the wear track were exposed by freeze-fracturing critical point dried hydrogels.

After crossing-paths wear testing, the samples had an indented wear track (Figure 5.6) that was observed visually to have a duller surface than the unworn region, indicating surface damage. Immediately after wear testing, the ends of the wear track were deeper than the middle portion (Figure 5.6b), but this was not apparent after 2 days of creep recovery. The middle and end portions were examined to determine if there were any differences in the surface and underlying structure with respect to location of the

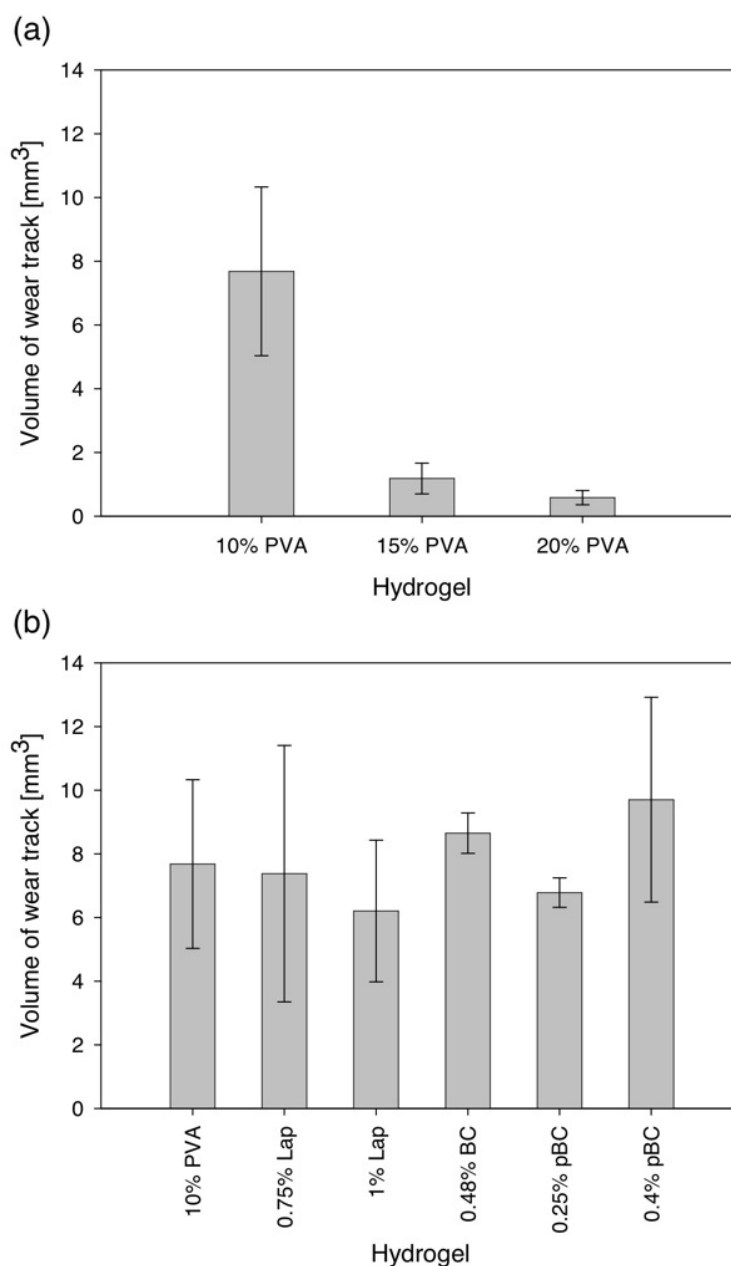


Figure 5.4: Volume of the indent created after crossing-paths wear testing on unfilled PVA hydrogels (a) and 10% PVA-NC hydrogels (b), measured using ImageJ on 3D US image planes. Wear testing was performed under a normal load of 5 N with a linear reciprocating stroke length of 8.5 mm and 28° pin rotation at 1 Hz for 500 000 cycles. The spherical sapphire counter surface was 9.525 mm in diameter.

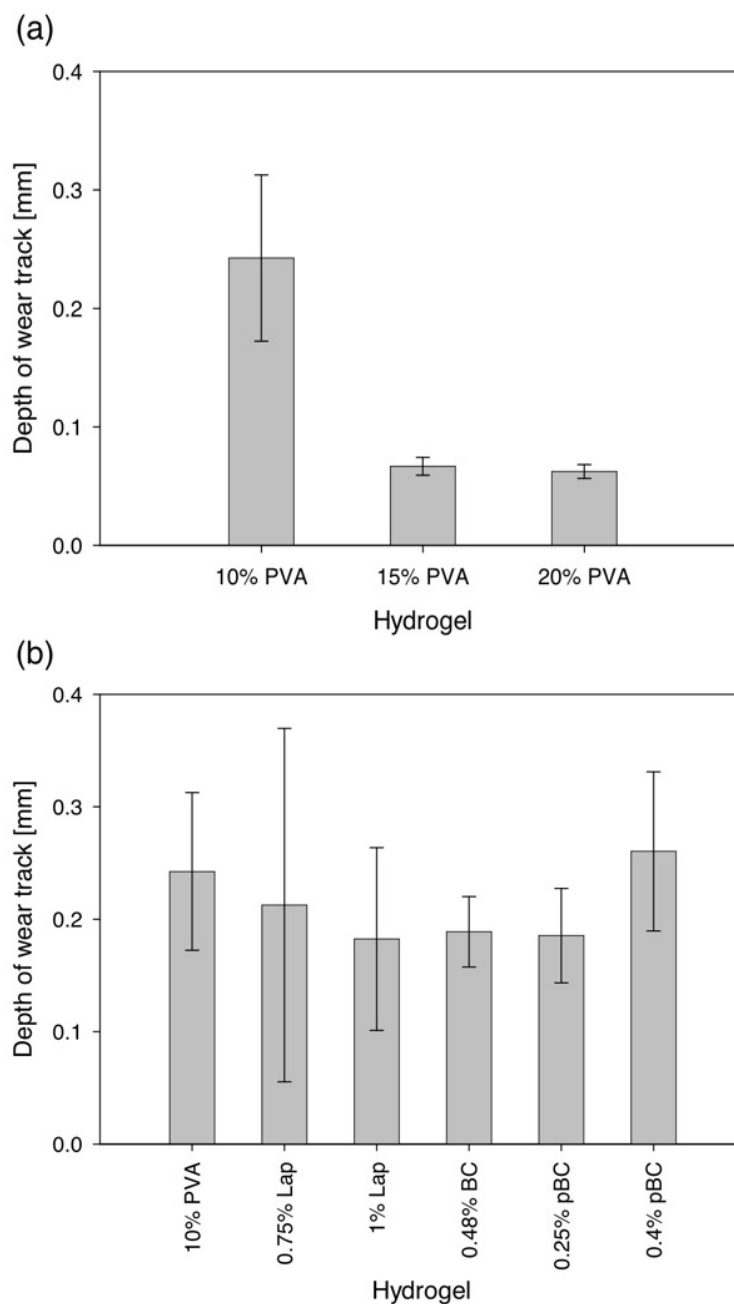


Figure 5.5: Maximum depth of wear tracks after crossing-paths wear testing on unfilled PVA hydrogels (a) and 10% PVA-NC hydrogels (b), measured from 3D US image planes using ImageJ. Wear testing was performed under a normal load of 5 N with a linear reciprocating stroke length of 8.5 mm and 28° pin rotation at 1 Hz for 500 000 cycles. The spherical sapphire counter surface was 9.525 mm in diameter.

wear track. After wear testing, the wear track was slightly yellowed from testing in the presence of the ACS lubricant.

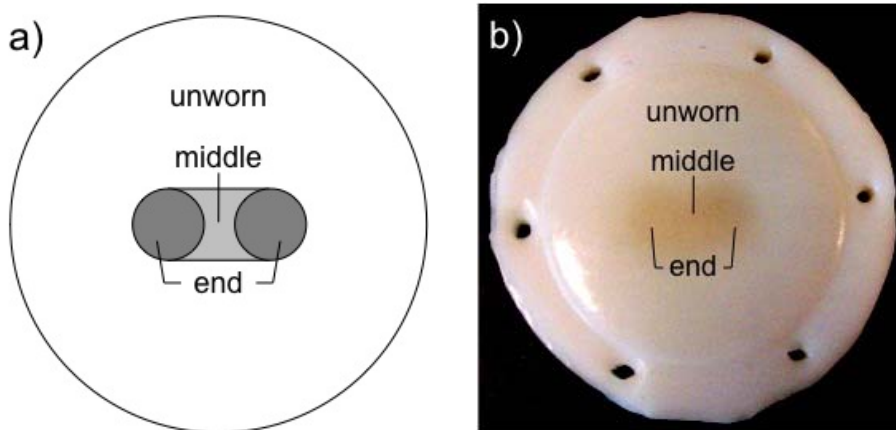


Figure 5.6: Schematic showing the unworn portion of the hydrogel, and middle and ends of the wear track (a), and a photograph of a hydrogel sample immediately after wear testing (b). The wear track was slightly yellow in colour from the ACS lubricant and the ends of the wear track were more indented than in the middle.

5.3.1 Surface of Unworn Areas

The unworn areas of the hydrogel surfaces (Figure 5.7) appeared flat and smooth, though there was some evidence of imperfections that appeared as pores on the surfaces. SEM images showed that addition of nanofillers affected the surface morphology of PVA hydrogels. While the addition of 0.25% pBC resulted in a surface that resembled unfilled PVA hydrogels, fewer pores were visible on the surfaces with Laponite, BC and 0.4% pBC. Since these surfaces were from unworn sections of the hydrogel samples used in crossing-paths wear testing, debris from hydrogel wear was deposited on some of the surfaces.

5.3.2 Wear Track Surfaces

In SEMs of the wear track surfaces, porous structure of the hydrogels became visible with wear (Figure 5.8 and Figure 5.9). There were scratches along the wear track

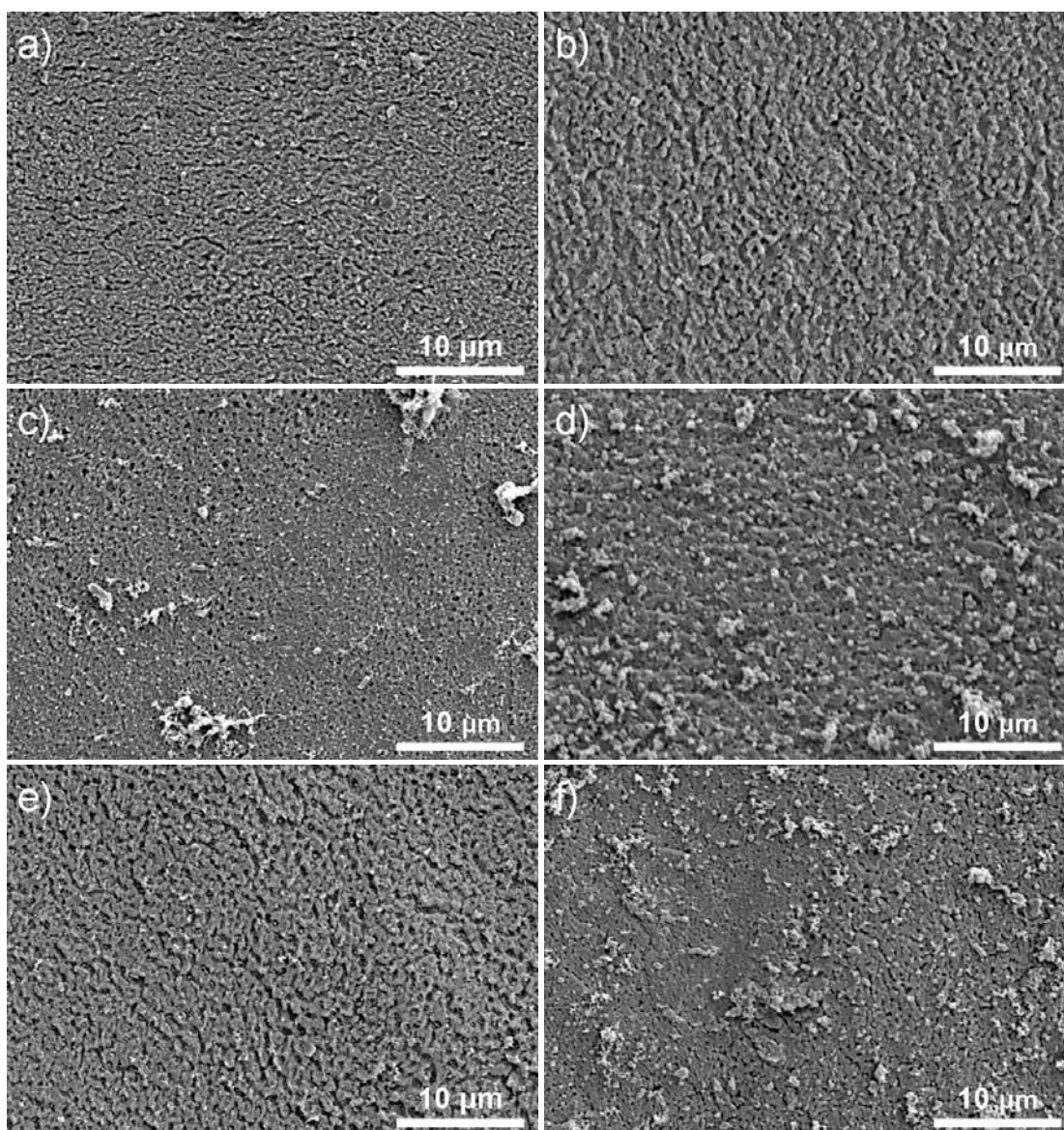


Figure 5.7: SEM of critical point dried unworn sections of hydrogel samples after cross-path wear testing: 10% PVA (a), 20% PVA (b), and 10% PVA-NC filled with 1% Laponite (c), 0.48% BC (d), 0.25% pBC (e) and 0.4% pBC (f). Debris on the hydrogel surfaces was likely material worn away from wear testing.

in the direction of reciprocating motion indicating abrasive wear. Some worn surfaces also appeared to have plastic flow and adhesive wear. The wear scars were aligned along the direction of reciprocating motion, and the effect of rotation did not appear to be significant.

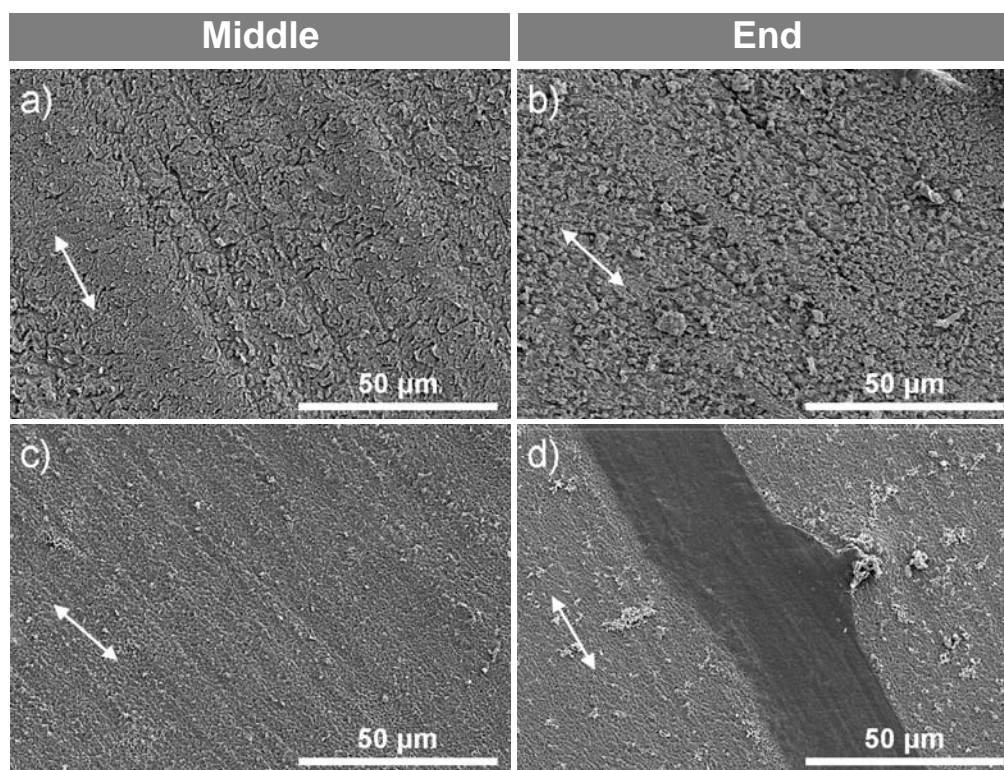


Figure 5.8: SEM of the middle (left column) and end (right column) portions of the wear track surfaces of critical point dried the 10% PVA hydrogel (a, b) and 20% PVA hydrogel (c, d). Arrows indicate the direction of linear reciprocation.

5.3.2.1 PVA Hydrogels

Scratches on the worn 10% PVA surface were accompanied by permanent compressive deformation adjacent to the abrasions. In addition, cracks were formed in the middle portion of the wear track surface (Figure 5.8a) that may have been due to fatigue wear. There was increased surface damage at the ends of the wear track (Figure 5.8b), where the porous structure appeared elongated and some material had broken off, which could be a combination of adhesive and fatigue wear.

The surface of the 20% PVA wear track appeared flattened as a result of adhesive wear and plastic deformation (Figure 5.8c,d). Scratches in the direction of motion were also present, indicating abrasive wear. The thick dark scar shown at the end of the wear track (Figure 5.8d) could have been the result of third-body wear, either from wear debris or a foreign particle, rather than from counter surface asperities. Compared to the un-

worn surfaces (Figure 5.7a, b), 20% PVA appeared smoother after crossing-paths wear testing, while 10% PVA appeared less smooth.

15% PVA (not shown) had a combination of the plastic deformation found in 20% PVA and abrasions. The scratches did not have adjacent deformations like those in 10% PVA, possibly due to higher creep. In general, increased hydrogel concentration resulted in less surface damage when observed qualitatively under SEM, in addition to decreased wear volume and depth.

5.3.2.2 PVA-NC Hydrogels

There was no evidence of the surface cracking in the 10% PVA NC hydrogels that was found on the unfilled 10% PVA hydrogel surface. Selected SEM images from the worn surfaces of the PVA-NC hydrogels are shown in Figure 5.9. The addition of Laponite resulted in a smoother unworn surface (Figure 5.7c), but their larger pore size was apparent on the surface of the wear track. Abrasive wear in the form of scratches were found on these hydrogels, and were more severe at ends (Figure 5.9b) of the wear track than in the middle (Figure 5.9a). Indentation around scratches that was found on 10% PVA was also on the 0.75% Laponite-10% PVA surface (not shown), but was not apparent on 1% Laponite-10% PVA. Adhesive wear was also more evident at the ends of the wear track.

The addition of 0.48% BC to 10% PVA resulted in a rough surface with large, raised patches in the middle portion of the wear track (Figure 5.9c). Those could be areas where BC fibres were located, conferring a higher modulus and higher wear resistance. The end of the wear track had a patchy appearance (Figure 5.9d) that could have been due to unevenness of the surface, and there appeared to be fibres pulled out from the surface. Scratches and cracks were not obvious on the surface, so the mechanism of wear was likely adhesive wear. With 0.25% pBC, abrasive wear was obvious (Figure 5.9e, f), but the wear track was smooth compared to 10% PVA and the other PVA-NC hydrogels.

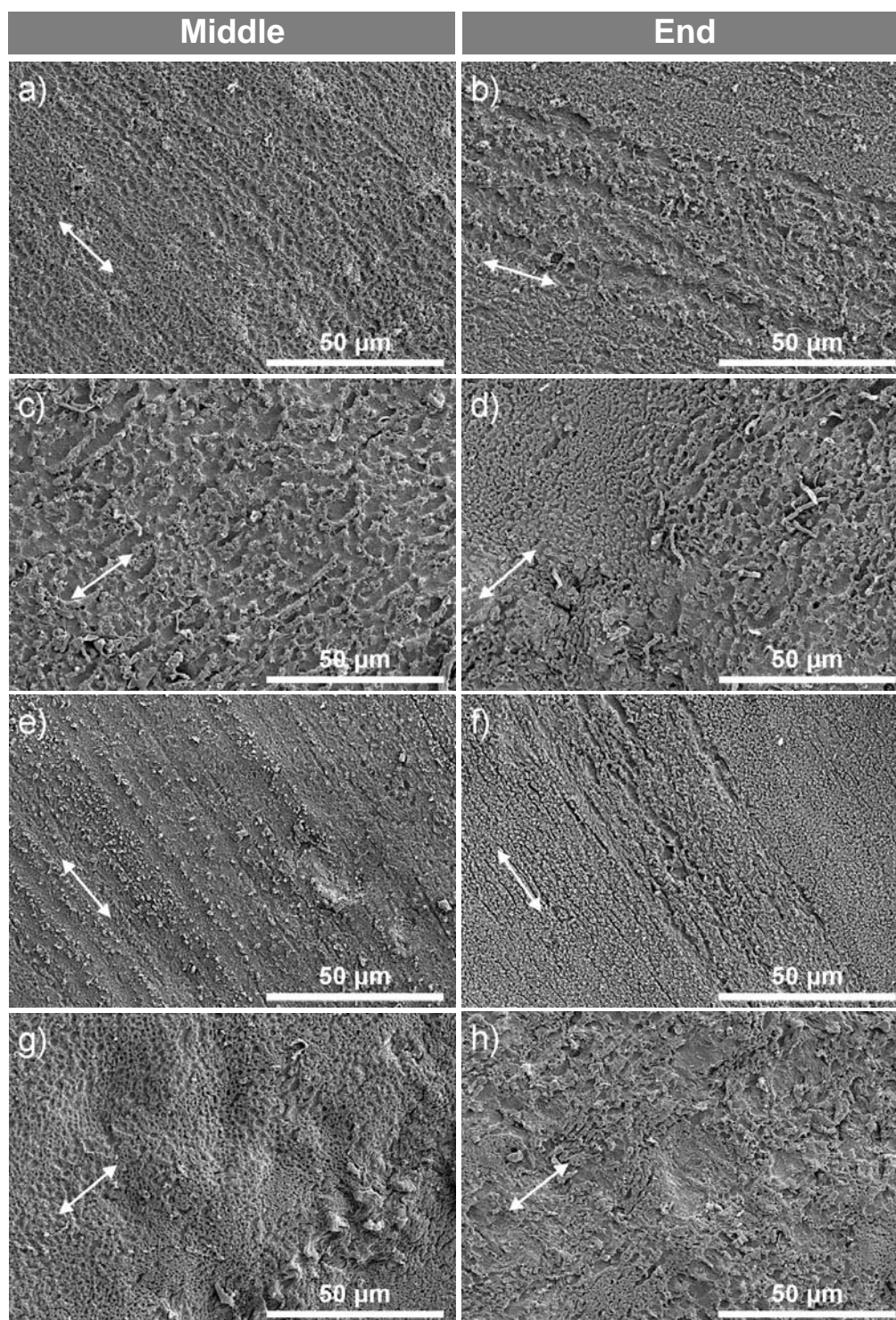


Figure 5.9: SEM of the middle (left column) and end (right column) portions of the wear track surfaces of critical point dried 10% PVA-NC hydrogels filled with 1% Laponite (a, b), 0.48% BC (c, d), 0.25% pBC (e, f) and 0.4% pBC (g, h). Arrows indicate the direction of linear reciprocation.

Some small fibres could be seen in and around voids on the surface of 10% PVA-0.25% pBC, and while some raised clumps were found on the hydrogel surface (Figure 5.9e). By increasing pBC concentration to 0.4% pBC, abrasive wear was decreased. However, an uneven surface was easily observed and could have affected wear during crossing-paths wear testing. Clumping of pBC could have led to areas where the linear wear pattern was disturbed and fibres were partially pulled out from the surface (Figure 5.9g). The ends of the wear track (Figure 5.9h) suffered more damage than the middle portion where there was increased abrasion, adhesive wear and plastic deformation. Randomly dispersed pBC fibres not aligned in the direction of linear reciprocating motion were also apparent. Similar to increasing PVA concentration, addition of nanofillers appeared to decrease the depth of the scratches on the surface.

5.3.3 Subsurface Structure

The underlying porous structure was examined using SEM after freeze fracturing of the critical point dried hydrogels. This was done to determine if creep and fatigue after crossing-paths wear testing had caused any change in the hydrogel structure. Changes in structure could alter mechanical properties and durability of the material that affect the performance of the hydrogel in a device over time.

Figure 5.10 shows SEM images of the porous hydrogel structure under the wear track. Compared to the structure prior to wear testing (Figures 4.3–4.5), the porous structure under the wear tracks had compressed pores and areas of low porosity, possibly due to collapsed pores, or had no noticeable changes, depending on hydrogel composition. Material surrounding the pores that remained did not appear torn or fractured. 10% PVA (Figure 5.10a) and 15% PVA (not shown) both had some areas of flattened pores and high solid polymer density. 10% PVA-0.75% Laponite (not shown) also exhibited some solid areas. Meanwhile, the porous structure of 20% PVA (Figure 5.10b), and 10% PVA containing 1% Laponite (Figure 5.10c) and 0.48% BC (Figure 5.10d) were similar to the

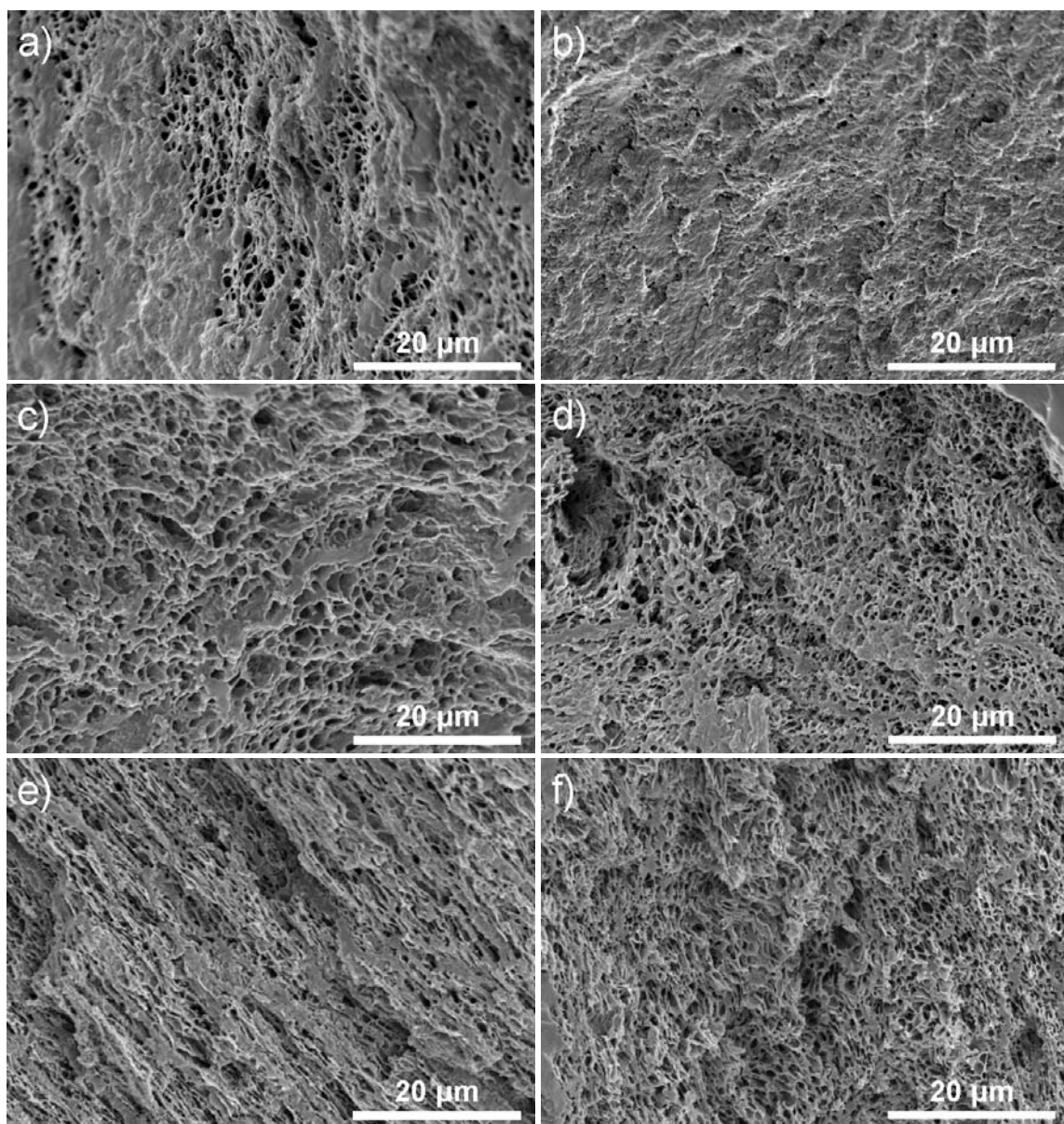


Figure 5.10: SEM images of liquid nitrogen freeze-fractured, critical point dried hydrogel cross-sections under the wear track of unfilled 10% PVA (a) and 20% PVA (b), and 10% PVA-NC containing 1% Laponite (c), 0.48% BC (d), 0.25% pBC (e) and 0.4% pBC (f). Pores under the wear tracks were collapsed and deformed in 10% PVA and 10% PVA-0.25% pBC.

unworn structure (Figure 4.3c, Figure 4.4b and Figure 4.5a, respectively). Hydrogels containing pBC had pores that appeared deformed throughout the wear track for 10% PVA-0.25% pBC (Figure 5.10e). Although the cross-section of the middle portion of the wear track of 10% PVA-0.4% pBC (Figure 5.10f) was similar to the unworn cross-

section (Figure 4.5c), the pores under the ends of the wear track were deformed, resembling the porous structure under the 10% PVA-0.25% pBC wear track (Figure 5.10e). In hydrogels with deformed pores, the direction of pore deformation did not appear to have a preferred orientation and varied through the hydrogel structure.

5.4 DISCUSSION

In previous studies that have quantified wear of hydrogels using wear depth, the effects of material loss and creep deformation were not distinguished from one another [188, 201, 204]. In hydrogels of higher polymer concentrations, smaller wear volumes and depths could be due to lower degrees of creep deformation. With higher moduli, these hydrogels may not be as susceptible to damage. Lower strains in stiffer hydrogels could also lead to decreased contact area, decreasing the surface area that would be susceptible to wear damage. However, there is no simple method to separate the effects of material loss due to generation of wear debris from those of creep deformation in wear volume in hydrogels, and further studies to decouple the two would be required.

Reversible creep was allowed to recover over a period of two days in PVA/PVP hydrogels prior to characterizing wear after tribological studies by Katta et al. [124]. In an attempt to determine wear through mass loss after crossing-paths wear testing, the PVA and PVA-NC hydrogels were placed in fresh ACS lubricant for two days of recovery. However, mass loss of the hydrogels determined before, during and after crossing-paths wear testing was inconsistent across the samples. This could have been due to fluid loss under the load from clamping of the hydrogel in the sample holder. Therefore, mass loss from the hydrogels was an ineffective method of characterizing wear in this experimental setup. The hydrogels were equilibrated for an additional two days in PBS to remove lubricant components prior to 3D US imaging in PBS since the composition of the fluid medium can affect speed of sound and thus distance measurements [243]. Since any reversible creep should be recovered after two days according to Katta et al., the amount of recovery for the additional two days would be negligible.

Decreases in volume (Figure 5.4a) and depth (Figure 5.5a) of the wear track with the increase in PVA concentration are likely dependent on deformation from loading, since hydrogel stiffness increased with PVA concentration as found in Chapter 4. Freeman et al. also found an increase in wear depth with increased water content in reciprocating tests of pHEMA hydrogels against stainless steel [188]. The relationship between wear volume and modulus of PVA and PVA-NC hydrogels from the present study is shown in Figure 5.11. While the applied load of 5 N would have resulted in different strains in the various hydrogels depending on their stiffness, the secant modulus at 0.25 strain was chosen as a value for comparison since strains would be close to or below 0.25 strain at 5 N, and the stress-strain curves of the hydrogels were relatively linear in this range.

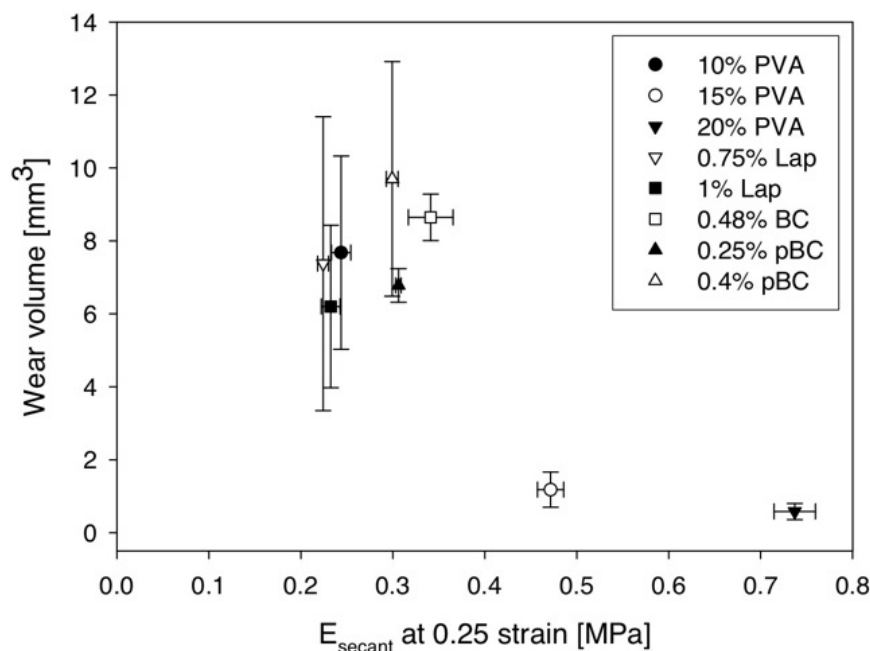


Figure 5.11: Wear volume versus secant modulus (1%/s strain rate) for unfilled PVA hydrogels and 10% PVA-NC hydrogels in PBS. Wear volume decreased with increased PVA concentration as 10% PVA-based hydrogels had significantly greater wear volumes compared to 15% and 20% PVA hydrogels.

Wear volume after crossing-paths wear appeared to be dependent on PVA concentration rather than modulus. Since the volume of the wear track is a combination of

permanent deformation due to creep and material loss from crossing-paths wear, the stiffer 15% and 20% PVA hydrogels experienced less creep and were likely more resistant to wear than the 10% PVA-based hydrogels. However, the amount of wear may depend on both contact area and contact stress, which are functions of hydrogel stiffness. While stiffer hydrogels experience less deformation, and therefore would have a smaller contact area with the counter surface, the contact stress would also be higher. A higher contact stress could reduce the thickness of the lubrication layer, bringing the surfaces to closer proximity and increasing the likelihood of wear to occur in the area of contact [25, 184, 189]. Furthermore, even though the strain after creep testing increased in the 10% PVA-based hydrogels with nanofiller addition, they had similar values for the wear track depth and volume to those of the unfilled 10% PVA. This may be due to recovery of reversible deformation after removal of the load by the hydrogels, particularly ones containing Laponite and pBC. The presence of charges in these hydrogels may have provided osmotic potential for fluid to flow back into the structure, and allowed volume recovery after load-induced fluid exudation. This is similar to the mechanism by which negatively charged proteoglycans in the structure aid in the recovery of disc height after load removal in natural IVDs [37].

There were large variations in the volume (Figure 5.4) and depth (Figure 5.5) of the wear track between PVA and PVA-NC hydrogel samples of the same composition. This was likely due to variability in sample flatness, of which some irregularity in surface geometry was observed in the image planes adjacent to the wear track (Figure 5.12). The area and height measurements, however, were performed with the assumption that samples were completely flat prior to testing. This was more apparent in the 10% PVA-based hydrogels than in 15% and 20% PVA hydrogels as sample flatness improved with increases in PVA concentration. Therefore, it would be beneficial to ensure all hydrogel samples were flat prior to testing. Imaging the sample prior to testing in order to determine initial volume for comparison to sample volume after testing may also be a possible method of overcoming measurement variations. Reducing measurement error would help

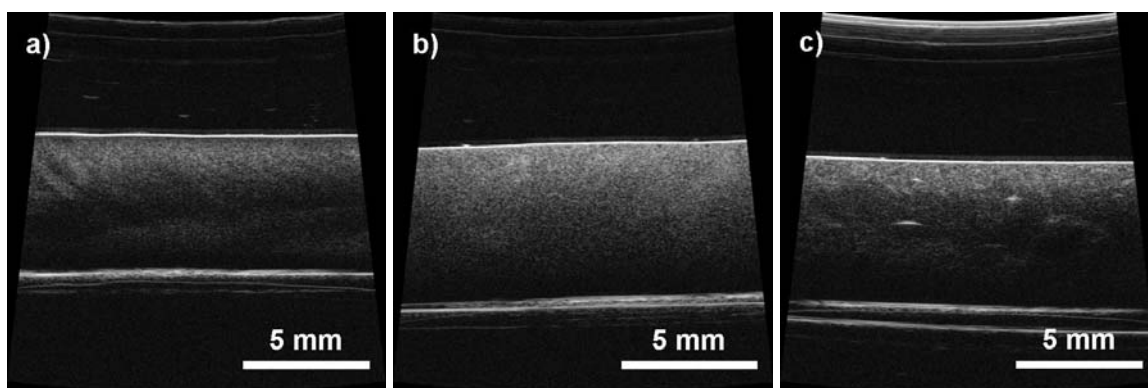


Figure 5.12: Examples of deviations from flatness at the surface of hydrogels in B-mode 3D US planes away from the wear track: 10% PVA showing a slightly irregular surface (a), 0.75% Laponite in 10% PVA with convexity at the surface (b), and 0.4% pBC in 10% PVA with concavity at the surface (c).

determine if wear track volume and depth are consistent across samples, and elucidate the effects of nanofiller addition on the formation of the wear track.

Despite the variation in wear volume and depth measured in this study, high frequency 3D US was a fast and effective tool for imaging small deformations in PVA hydrogels after crossing-paths wear testing. Since the US probe does not contact the hydrogel surface, deformation due to load during imaging is thus avoided. The same 3D US system was used as a non-destructive method to measure the thickness of tissue layers in aortic valve cusps [214]. PVA hydrogels have been used as tissue-mimicking phantoms in US imaging [216-219], and as such, the technique was well suited for imaging the wear samples in this study. Furthermore, since it was the edge between the hydrogel and PBS that was segmented and used in determining the area of the wear track indent in each B-mode plane, the measurement is independent of the speed of sound through hydrogels of different compositions [216, 217]. Speed propagation error and the effect of attenuation with high frequency US through the thickness of the hydrogels could therefore be avoided [243]. This technique could be used as long as there is a difference in impedance between the fluid and the material being imaged to result in the reflection of sound.

Table 5.1 summarizes the measurement of wear depth and volume in hydrogels from literature and the current study.

Table 5.1: Comparison of hydrogel wear depth and volume measurements from the literature and current study.

Study	Hydrogel material	Counter surface	Test type	Load/contact pressure	Stroke length	Length of test	Wear measurement method	Wear
Current study	Unfilled 10–25% PVA; Laponite, BC and pBC-filled 10% PVA	Sapphire ball (D=9.525 mm, $R_a=0.010 \mu\text{m}$)	Crossing-paths (linear reciprocation with rotation)	5 N	8.5 mm with 28° rotation	5×10^5 cycles	High frequency 3D US of wear track after 2 days of recovery in ACS lubricant followed by 2 days in PBS	Depth [mm]: 0.06–0.26 Volume [mm ³]: 0.58–9.7 Wear factor [mm ³ /Nm]: 2.73–45.6 $\times 10^{-3}$
Oka 2000 [18]	PVA (DMSO, annealed) pin (D=4 mm)	Alumina disc	Pin-on-plate	3 MPa	Unknown	Not known	Spectroscopy of PVA wear debris in lubricant	Wear factor [mm ³ /Nm]: 10×10^{-7} (40% PVA) 4×10^{-9} (55%, 75% PVA)
Freeman 2000 [188]	65–75% pHEMA	Stainless steel ball (D=6 mm)	Reciprocating	6, 20 N	Unknown	30 min	Pin displacement	Depth [mm]: 0.02–1.32 (average 0.1–0.87)
Suciu 2004 [244]	15–23% PVA; annealed 45, 50% PVA	Stainless steel plate ($R_a=0.02 \mu\text{m}$)	Walking simulator	Mean axial load 490 N	Unknown	10^5 cycles	Gravimetric, after 24 h of recovery in water for every hour of testing	Wear factor [mm ³ /Nm]: 10^{-5} – 10^{-3}
Yasuda 2005 [200]	Polyacrylamide and cellulose based double network hydrogels (85–90% water)	Alumina ball (D=20 mm, $R_a=0.006 \mu\text{m}$)	Reciprocating	4.7 N (0.1 MPa)	25 mm	10^6 cycles	CLSM of wear track profile after 24 h recovery in distilled water	Depth [μm]: 3.20–9.5 Surface roughness (R_a) [μm]: 0.008–0.34
Zhang 2009 [204]	3.5, 7 FTC-15% PVA + 1, 3% HAp (<20 nm)	Bovine knee cartilage (D=7.4 mm)	Reciprocating	0.58 MPa	10 mm	1 h	Unknown	Depth [mm]: 0.01–0.12
Northwood 2007 [185, 195]	63–86% methacrylate-based IPN hydrogels ($R_a=150 \text{ nm}$)	Bovine cartilage pins (D=9 mm)	Reciprocating; crossing-paths (linear reciprocation with rotation)	30 N (0.5 MPa)	10 mm; 10 mm with $\pm 10^\circ$ rotation	8 h (28800 cycles)	Profilometer to measure surface roughness	Increase in R_a [μm]: Reciprocating 0–0.2 increase ($R_a = 0.35$ – 0.8) Crossing-paths 0.1–0.25 increase (R_a unknown)

While depth was used in characterizing wear of hydrogels in the literature, it is representative of only one dimension of wear. Wear volume would be more useful since it takes into account the three-dimensional form of the wear track. Wear factor could also be easily calculated for comparisons to other studies that use different loads and test lengths. By using high frequency 3D US as a wear measurement technique for hydrogels, both wear depth and volume values could be generated from the images.

Oka et al. used UV-Vis spectrophotometry to determine PVA hydrogel wear from the saline lubricant containing wear particles after staining with potassium iodide indicator [18]. The wear factors determined using spectrophotometry would be considerably less than using the 3D US technique, as only wear particle volume and not deformation, was taken into account. This study also used a hydrogel pin and a ceramic plate in the pin-on-plate wear test, so that the hydrogel pin was in constant contact against the ceramic plate, in contrast to the periodic contact of a point along the wear track of a hydrogel disc with a rigid pin. Since ACS lubricant was used in the current study, spectroscopic determination of wear may require consideration of the presence of proteins. This method may be adapted to determine the relative effects of creep and wear on formation of the wear track in the hydrogels, which remains to be discerned, in order to appropriately determine wear rate and wear factor in PVA hydrogels when comparing to other materials used in TDR and other joint replacement devices. In an attempt to isolate material loss from deformation, Katta et al. [124] measured wear of PVA/PVP hydrogels by drying the samples before and after testing. The hydrogels were vacuum dried after fabrication to determine initial mass, rehydrated for testing, then dehydrated again to determine the final mass. Thus, wear determined from this study was of the dry polymer mass. However, the wear particles presented for host response *in vivo* environment would be from the hydrated hydrogel, and should be correlated to the dry wear mass if this method were to be used for wear determination in hydrogels. Although not likely to impact the measurement of mass loss due to wear, the authors did not specify whether the hydrogels were able to fully rehydrate after initial dessication prior to wear testing, since this step may alter hydrogel properties from its as-made state.

Displacement of the counter surface pin during reciprocating wear testing of pHEMA hydrogels was used to characterize wear depth by Freeman et al. [188]. However, in addition to permanent deformation and material loss, the depth may be overstated due to compression of the hydrogels by the axially loaded pin. Indeed, the average pin displacement of approximately 0.25 mm under a 6 N axial load in pHEMA hydrogels was higher than the wear depths in unfilled PVA and PVA-NC hydrogels from the current study, even though water content was much lower at 25–35%. However, since the test duration was only 30 minutes, hydrogels were not allowed to recover after testing, and no information was provided on stiffness of the pHEMA hydrogels, it would be difficult to compare the degree of wear as a result of wear testing in the two studies.

Wear volume was determined from mass loss by using a PVA hydrogel density of $1.004 \times 10^{-3} \text{ g/mm}^3$ in Suciu et al. [244], in which the authors stated that hydrogel density was found to be independent of hydrogel water content and degree of polymerization. Wear of hydrogels was characterized by mass loss in studies by Bavaresco et al. [186] and Wu et al. [181, 199]. However, similar to wear determination by wear depth and volume, determination of wear through mass loss in hydrogels could also be problematic. The difference in mass before and after testing could be due to a combination of wear, exudation of fluid due to load, and adsorption and absorption of lubricant components such as salts and proteins. The contribution from each process would be difficult to separate. The hydrogels in Suciu et al. were allowed to recover for 24 hours for every hour of testing to minimize load-induced fluid loss that could have led to reduction of mass loss and deformation compared to continuous testing. Wear factors calculated from the volumes of the wear tracks for 10% PVA and PVA-NC hydrogels were approximately $3\text{--}4.5 \times 10^{-4} \text{ mm}^3/\text{Nm}$, and approximately $3\text{--}5 \times 10^{-5} \text{ mm}^3/\text{Nm}$ for 15% and 20% PVA. Comparable to the results of the current study, Suciu et al. found that wear factors were on the order of $10^{-5}\text{--}10^{-4} \text{ mm}^3/\text{Nm}$ in F-T 23% PVA hydrogels with a PVA molecular weight of 198 000 g/mol after $10^5\text{--}10^6$ anterior-posterior displacement cycles against stainless steel [205]. In comparison, wear factors found by mass loss after crossing-paths wear testing

of UHMWPE pins against stainless steel were in the range of 10^{-7} to 10^{-6} mm³/Nm [208, 245].

Yasuda et al. used confocal laser scanning microscopy as a non-contacting method of measuring wear depth in polyacrylamide and cellulose based double network hydrogels. A line scan of the wear scar profile was obtained at a cross-section near the centre of the wear scar, which was used to determine depth of wear and surface roughness [30]. However, this only characterized a small portion of the wear scar. We attempted to characterize the wear track volume after crossing-paths wear testing using CLSM under both phase contrast and fluorescence. A fluorescent label, 5-DTAF, was tagged to the worn hydrogel sample after equilibrating in 0.15 M sodium bicarbonate solution [31-33]. However, the solution caused hydrogel shrinkage due to osmotic pressure, similar to aging in PBS. Image stitching and stacking was required in order to cover both the lateral dimensions and the depth of wear. Since the lowest magnification objective for the microscope was 5 \times , at least one hour was needed to acquire multiple image stacks in the area of interest. Thus, there were concerns of the hydrogel drying during data acquisition since they cannot be immersed during imaging with CLSM. This issue was avoided with 3D US since imaging must be performed with the hydrogels in solution. The depths measured using CLSM by Yasuda et al. were one order of magnitude lower than those in the PVA and PVA-NC hydrogels, despite having similar water contents. The double network hydrogels have either higher wear resistance, or greater rates and degrees of creep recovery than the PVA and PVA-NC hydrogels.

Our measurements of wear depths in the PVA and PVA-NC hydrogels were slightly higher than the wear depths of 0.01–0.12 mm found by Zhang et al. in HAp-filled 15% PVA against bovine cartilage at a contact stress of 0.58 MPa after one hour [204]. By increasing the number of FTCs and the amount of HAp in the hydrogels, modulus increased while wear depth, which included both material loss and viscoelastic deformation, decreased. Cartilage is a more compliant surface compared to the sapphire counter surface used in the current study, which may have reduced deformation in the hydrogels. Similarly, after only one hour of testing, there was less time for creep to take place.

However, the initial contact stresses on the PVA and PVA-NC hydrogels were lower, estimated using Hertzian theory [25, 197, 238] to be between 0.09 MPa for unfilled and Laponite-filled 10% PVA, and 0.18 MPa for 20% PVA. Zhang et al. did not appear to have allowed viscoelastic deformation to recover prior to measuring wear depth, so the measured depth likely included reversible deformation.

Northwood and workers characterized the degree of wear resistance using surface roughness in methacrylate-based hydrogels [185, 195]. In unidirectional reciprocating tests, the hydrogel with the highest water content had the lowest increase in surface roughness [195]. In contrast, the hydrogel with the lowest water content possessed the lowest increase in surface roughness after crossing-paths wear testing [185]. In the present study on PVA and PVA-NC hydrogels, wear volume and depth were lowest in 20% PVA, which had the lowest water content of the hydrogels tested. However, neither the volume nor depth of the wear track was reported by Northwood and Fisher [185], which was the only study on multidirectional wear testing of hydrogels in the literature. While surface roughness could be used to characterize the wear track surface, it is not sufficient to quantify the degree of wear. In addition, surface profilometry was used to measure surface roughness, which makes use of a contacting stylus to map the surface. The authors reported that the method produced repeatable measurements and no detectable surface damage, and was fast enough to prevent sample dehydration [195]. However, this may not be an appropriate method for a compliant hydrogel since the stylus may compress or tear the hydrogel during surface scanning. As a non-contacting and non-destructive imaging method that is performed in fluid, there is no risk of sample damage or dehydration with 3D US, regardless of material composition and strength. As such, 3D US could also be used to measure wear volume and depth at various points during testing to determine wear rate with respect to number of wear cycles, as well as rate of recovery with respect to time.

Wear rates in simulator tested TDRs were lower than in PVA hydrogels despite higher applied loads in simulator testing. The volumetric wear rate of the stainless steel in Prestige ST, after simulator testing of 10 million cycles (Mc) of flexion-extension at

150 N and 5 Mc of combined lateral bending and axial rotation at 50 N, was 0.18 mm³/Mc [91]. In Prodisc-C, the wear rate of UHMWPE was 0.88 mg/Mc, however, the load was not specified [86]. The wear of polyurethane (PU) in the Bryan disc depended on the testing protocol. After 10 Mc of combined flexion-extension and axial rotation at 130 N, the volumetric wear rate was found to be 0.96 mm³/Mc [93], but it was 0.57 mm³/Mc after 10 Mc of flexion-extension was followed by 10 Mc of axial rotation at 150 N [91]. Since flexion-extension and axial rotation were performed separately in the latter study, the wear patterns would be largely unidirectional. This could be the reason for higher wear rates when the two motions were combined in the former study. Meanwhile, the Bryan disc was predicted to have a decrease in height of 0.023 mm after 1 Mc at 150 N of non-combined motion in a simulator [91], but it was not clear if this would be due to wear only, or to what degree creep would contribute to deformation of the PU core. In contrast, 20% PVA had the lowest wear depth of 0.062 ± 0.006 mm in the current study, despite a much lower applied load and number of wear cycles than used in the testing of the Bryan disc. Further increases in polymer concentration could be one of the options in lowering the degree of deformation to preserve disc height, which would be desirable for the application of PVA hydrogels in IVD replacement.

Wear factor tended to decrease with increasing PVA concentration and molecular weight [18, 205], which are parameters that could be used to minimize wear. While the current results also indicated that low wear volume and depth could be achieved with a high PVA concentration hydrogel, the implications of nanofiller addition are unclear. Since nanofillers could be used to impart mechanical properties desirable in an IVD device such as modulus enhancement, strain rate dependence and creep recovery, their impact on wear should be further investigated. In future studies, improvements to the use of 3D US in wear measurements and development of a reliable method of measuring material loss would enable the determination of how PVA concentration and nanofiller addition could minimize both deformation and generation of wear debris in the hydrogels, which are desirable in an articulating TDR design.

In the SEM images in Figure 5.7, variation of the unworn areas of hydrogel surfaces with composition could be due to interaction of the polymer solution with the aluminum substrate. Others have found that the substrate on which a hydrogel is formed influenced the structure at the hydrogel surface. Hydrophobic substrates resulted in lower crosslinking densities and dangling linear chains that have less shear resistance, which resulted in lower frictional stress [139] and reduced wear factor up to 50 000 simulator walking cycles [244]. Increased hydrophilicity of polymer solutions containing nanofillers could have caused increased crosslinking against the hydrophilic oxide passivation layer on the aluminum substrate, resulting in smoother surfaces to reduce wear resistance.

In Figure 5.8 and Figure 5.9, the ends of reciprocating wear track surfaces had higher degrees of damage. During direction changes, lower speeds of the counter surface increase the time for polymer chain adsorptions [139] and deformation of the hydrogel to occur [199]. Gong and Osada also hypothesized that friction due to adhesion predominates at slower speeds [139, 246]. Increased adhesion and decreased separation between the surfaces may have resulted in increased adhesive and abrasive wear damage. In contrast, as maximum speed during reciprocating motion occurs the middle of the wear track, an increase in lubricant layer thickness would increase separation between the surfaces and reduce surface damage.

The surface of 10% PVA appeared to have fatigue cracking and wear (Figure 5.8a, b). Oka et al. had also found fatigue wear to be the main mode of wear in reciprocating wear tests of PVA hydrogels under “severe” conditions, but the parameters of the test were not specified [247]. In contrast, the wear mechanisms of hydrogels of higher PVA concentrations and those containing nanofillers were mainly abrasive or adhesive wear. The higher modulus of 20% PVA would have produced lower conformity and higher contact stresses with the counter surface, which may have decreased the lubrication film thickness [25, 189]. This would bring the two surfaces into closer proximity for contact with asperities [139], resulting in the abrasions shown in Figure 5.8c. Higher contact pressures also resulted in increased abrasive wear in unfilled PVA hydrogels

tested against stainless steel in Wu et al. [181]. In addition, increased solid content and material modulus, and decreased porosity all likely contributed to increased wear resistance at higher polymer concentrations. Hydrogels with smaller pore sizes had smoother wear surfaces, possibly due to a lower surface roughness after the underlying porous structures were exposed [202]. Large pores in PVA-NC hydrogels exposed by wear likely contributed to surface damage because of increased surface roughness, and wear would have been perpetuated by the relatively low modulus of the material. Zhang et al. found that as pore size decreased with addition of nano-HAp, pores were not as easily damaged [204], although it would be unclear if this were due to smaller pores or increased material strength.

In BC and pBC-filled hydrogels (Figure 5.9c–h), addition of nanofibrous fillers may have influenced wear. Surface features, likely from the distribution and random alignment of the nanofibres, were observed on the worn hydrogel surfaces, especially with higher filler content. The material surrounding the nanofibres appeared to be deformed around the fillers, where the fibres may have strengthened the polymer and prevented plastic deformation and wear. Pull-out was more prominent in BC-filled hydrogels compared to those with pBC, possibly due to electrostatic repulsion leading to more discretely dispersed pBC fibres. Any filler pull-out in Laponite-filled hydrogels would not be observed at the magnification used to image wear surfaces due to their small size. In studies of pin-on-plate unidirectional wear in PVA-HAp hydrogels against stainless steel by Wu and workers, the addition of HAp through mixing resulted in scratches in the direction of motion, as well as evidence of particle pull-out, which was not apparent in hydrogels containing *in situ*-formed HAp [181, 203]. Mixed HAp were approximately 500 nm in length and 70 nm in width, while the largest dimension of *in situ* HAp was less than 50 nm. The HAp particles would be much stiffer and of a lower aspect ratio than BC and pBC nanofibres, which could have resulted in detachment from the PVA hydrogel matrix rather than deformation as seen in the BC- and pBC-filled hydrogels. In addition to surface damage from filler pull-out, detachment of stiffer nanofillers could lead to third-body wear.

Although hydrogel samples were soaked in PBS solution after testing, additional rinsing should be done in future studies to remove wear debris observed on unworn surface sections of the hydrogels. Figure 5.7 shows that wear debris generated from PVA and PVA-NC hydrogels could adsorb onto the surface. This could in turn affect wear by acting as third-body wear particles, or by modifying contact and adhesion of the counter surface with the hydrogel surface.

In wear testing of UHMWPE against a Si_3N_4 ceramic ball [209], SEM of the polymer surface showed that the main mechanism in linear reciprocating wear was abrasion in the direction of motion. However, in crossing-paths configurations, there was evidence of adhesive wear from fibrous piling, shredding and cavities. Ripples caused by plastic deformation, cracking and pitting due to fatigue also contributed to increased loss of material in crossing-paths wear of UHMWPE. In unidirectional sliding, polymer chains of UHMWPE align in the direction of sliding, but during crossing-paths motion, wear increases due to intermolecular rupture in the direction perpendicular to chain alignment [207-209]. Pin-on-plate unidirectional sliding between UHMWPE pins and stainless steel also revealed abrasive and adhesive wear mechanism, in addition to plastic deformation [248]. In simulator testing of active® L [206], a lumbar TDR with UHMWPE articulating against CoCrMo endplates, the mechanisms of wear were abrasive and adhesive wear, plastic deformation and creep. There was no evidence of pitting, delamination, crack formation or fatigue wear after 17 million cycles.

PVA hydrogels had similar types of wear after crossing-paths wear testing as UHMWPE – abrasive and adhesive wear, plastic deformation and fatigue. However, unlike the hydrophobic solid polymeric material of UHMWPE, the PVA and PVA-NC hydrogels tested consist of large proportions of water within porous polymer networks. Thus, the evolution of wear of these surfaces against a counter surface would differ. Oka et al. found that PVA hydrogels were able to maintain fluid film pressure and separation against glass, in contrast to UHMWPE which saw fluid pressure drop rapidly after loading and resulted in a narrow fluid gap [18]. This may have reduced contact with counter surface asperities in the hydrogels, and as such, the effect of rotation was not apparent in

SEM images of the surfaces. Depending on load, sliding velocity and lubrication, UHMWPE may experience a rise in surface temperature during sliding that could negatively affect mechanical properties, creep and wear of the polymer [249, 250]. Since PVA hydrogels are composed of large amounts of water that could absorb heat, it may be possible to mitigate surface temperature elevations, and heat-induced wear would be avoided. However, all of the hydrogels suffered from wear damage that exposed the porous structure on the surface. Since these hydrogels have relatively low stiffness and strength, which would increase the likelihood and amount of wear, further investigation into the amount and type of wear from PVA hydrogels in an articulating TDR design is required when considering the generation of wear debris *in vivo*, as well as the longevity of the implant with respect to wear, creep and fatigue.

In SEMs of hydrogel cross-sections (Figure 5.10), at least some of the porous structure was maintained under the wear track, possibly due to pressurization of fluid inside the pores. No breakage of the material surround pores was found, and damage to the porous structure was probably limited to permanent deformation of pores. Since 20% PVA had a small wear track volume, its structure was maintained as expected. Pores in the PVA-NC hydrogels were not as easily deformed. In the case of Laponite and pBC-reinforced hydrogels, pores were deformed, but most did not collapse. The addition of charges through nanofillers to PVA hydrogels may aid in preserving the porous structure and recovery of deformation as a result of osmotic pressure. This should warrant further study to design a hydrogel that could provide strain rate dependence and shock absorption in response to load, as well as rapid recovery upon the removal of load. However, without mechanical testing of the hydrogels after wear testing, any effects of fatigue loading from reciprocating wear on moduli and strength could not be determined. Joshi et al. [58] performed compressive fatigue loading to 15% strain on PVA/PVP hydrogels (16% polymer) up to one million cycles. Unconfined compression testing after fatigue loading showed that while stress-strain curves were flattened up to 15% strain, fatigue loading did not affect the curves at higher strains and there were no significant differences in moduli. The authors concluded that the hydrogel structure did not change during fatigue loading.

However, there have not been any investigations to date on changes in hydrogel structure after wear testing or fatigue loading to our knowledge.

The loss of porosity in a hydrogel structure may affect stiffness, fluid flow and viscoelastic properties. A decrease in porosity could decrease permeability of a hydrogel to fluid flow, akin to increasing polymer concentration in hydrogels [137, 177]. As shown in Chapter 4, increasing PVA concentration in unfilled PVA hydrogels resulted in decreased non-linearity of the stress-strain curve and lower dependence of modulus on strain. Since structural changes after 0.5 Mc of reciprocating crossing-paths wear appeared to involve a densification and no breakage or tearing of the PVA-based hydrogel porous structure, the mechanical properties of the bulk hydrogel may not have deteriorated. However, the number of wear cycles used in this study was small, and therefore, fatigue of the hydrogels should be characterized when testing is extended to higher number of cycles to represent the *in vivo* lifetime of the implant.

5.5 CONCLUDING REMARKS

There is an acute lack of multidirectional wear studies on hydrogel materials in the literature, which is relevant to the development of hydrogels for IVD replacements, as well as for applications in cartilage and joint replacements. Crossing-paths wear testing incorporating linear reciprocation and pin rotation was performed on PVA and PVA-NC hydrogels to investigate their potential use in articulating TDR designs and the effect of composition on wear. High frequency 3D US, a non-destructive technique, was applied to determine wear track volume and depth of the hydrogels while immersed in fluid. Since 3D US imaging does not involve contact with the compliant hydrogels, deformation due to load during contact is eliminated during wear measurement. This method could be applied to quantify wear in hydrogels and other viscoelastic materials that are difficult measure using conventional techniques.

Wear volume and depth were successfully decreased with increases in PVA concentration, but did not change with the addition of nanofillers. Increases in PVA concentration and the addition of nanofillers appeared to eliminate fatigue damage on the hydrogel surfaces as well. Wear damage was more severe at the ends of the wear track than in the middle portion. After crossing-paths wear, increases in PVA concentration and the addition nanofillers prevented deformation and collapse of the porous structure under the wear tracks. Further studies to separate wear volume from creep deformation is required to determine resistance to wear and establish if PVA-based hydrogels are suitable in TDR designs that incorporate articulation.

Chapter 6

DESIGN OF A MULTI-COMPONENT PVA HYDROGEL-BASED CERVICAL IVD PROSTHESIS

A multi-component PVA hydrogel-based IVD device was proposed in Chapter 4 to improve stiffness, strain rate dependence and control fluid flow in order to achieve compressive properties of the natural cervical IVD. A PVA hydrogel prototype composed of different polymer concentrations for the annulus and nucleus was fabricated using a modular process, allowing for unique hydrogel compositions for each component in the cervical IVD prototype. The endplates, though not pursued in this study, may be later added to the construct. PVA concentrations of 20% and 10% were chosen for the annulus and nucleus, respectively, for the two-component hydrogel produced via freeze-thaw cycling. Unconfined compression, strain rate dependence, stress relaxation and creep of the prototype were investigated in the two-component hydrogel construct, and compared to the compression properties of single component PVA hydrogels studied in Chapter 4.

6.1 IVD PROTOTYPE COMPOSITION

The PVA hydrogel-based IVD device proposed in Chapter 4 suggested that the nucleus component should have a high degree of swelling, while the annulus should have a lower permeability to limit fluid flow, similar to the analogous components in the natural IVD. The annulus should also possess a high stiffness to resist tensile loads due to

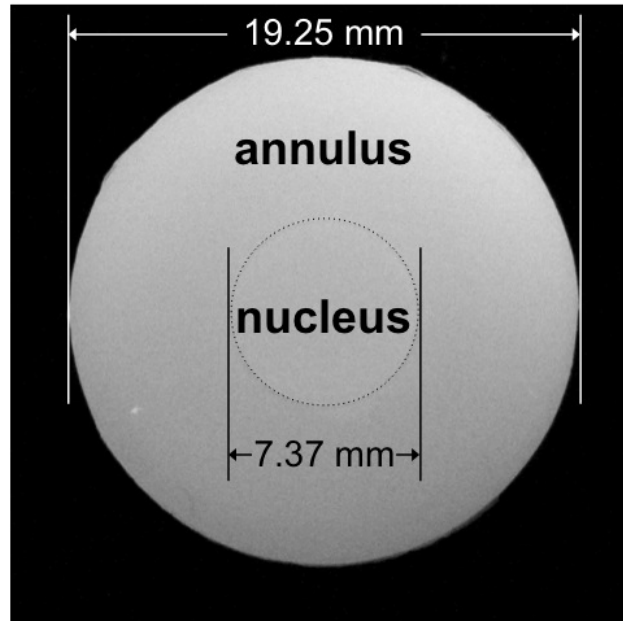


Figure 6.1: Photograph of the two-component PVA hydrogel prototype with concentric 20% PVA annulus and 10% PVA nucleus components. The dotted circle delineates the interface between the two components.

pressurization of the nucleus. As such, the nucleus component could be composed of a lower PVA concentration hydrogel than the annulus.

A combination of a 20% PVA annulus and a 10% PVA nucleus was chosen for the prototype to correspond with the unfilled PVA hydrogels discussed in Chapter 4. At 0.25 strain, 20% and 10% PVA hydrogels had tangent moduli of 0.85 ± 0.01 MPa and 0.36 ± 0.02 MPa, and secant moduli of 0.523 ± 0.006 MPa and 0.19 ± 0.02 MPa, respectively. The 20% PVA solution for the annulus component was gelled with one FTC before adding the 10% PVA solution for the nucleus, and the two components had a strong interface after six additional FTCs. The mould for the hydrogel IVD prototype has an annulus diameter of 20 mm, a nucleus diameter of 8 mm, and a height of 7 mm. These dimensions were chosen based on cervical IVD width and depth of 16.0–23.5 mm and 12.0–18.0 mm, respectively [38], a NP volume of 15% of the total disc [251, 252], and a disc height of 4.5–7 mm [37, 38]. A circular, rather than elliptical [36], cross-section was chosen for the prototype since it was a simpler geometry for both mould fabrication and measurement of cross-sectional area for mechanical testing. The circular profile was also

successfully implemented in the Bryan disc. Since PVA hydrogels tended to shrink after F-T cycling, the average diameter of the annulus and nucleus in the hydrogel construct became 19.25 ± 0.05 mm and 7.4 ± 0.2 mm, respectively, for the three samples fabricated, as shown in Figure 6.1.

6.2 UNCONFINED COMPRESSION

The 20%/10% PVA hydrogel construct was tested at six strain rates from 0.001%/s to 100%/s (Figure 6.2), corresponding approximately with the strain rates used in Cassidy et al. to test canine IVDs [55]. Load was reported in addition to stress because of the inhomogeneous cross-section. The concave up J-shape was retained in the stress-strain curves for the prototype, which also displayed a small toe region up to 0.02 strain as shown in the curves for one of the prototype samples in Figure 6.2a. While the 5-parameter exponential growth model used to fit stress-strain curves of single component hydrogels generally provided a good fit for the two-component hydrogel, it was not able to fit the toe region of the two-component hydrogel (Figure 6.2b).

The average fitted load and stress-strain curves for three trials of the 20%/10% PVA hydrogel prototype are shown in Figure 6.3. They were found to be repeatable and the standard deviations in load for each of the six strain rates were small.

6.2.1 Strain Rate Dependence

The degree of strain rate dependence of the two-component hydrogel was characterized by determining significant difference between load at 0.25 strain at the tested strain rates, and the slope of the linear fit between load and logarithm of strain rate. There were no statistical differences in load at 0.25 strain between 0.001, 0.01 and 0.1%/s, and between 1, 10 and 100%/s, similar to 10% PVA (Table 6.1). In contrast,

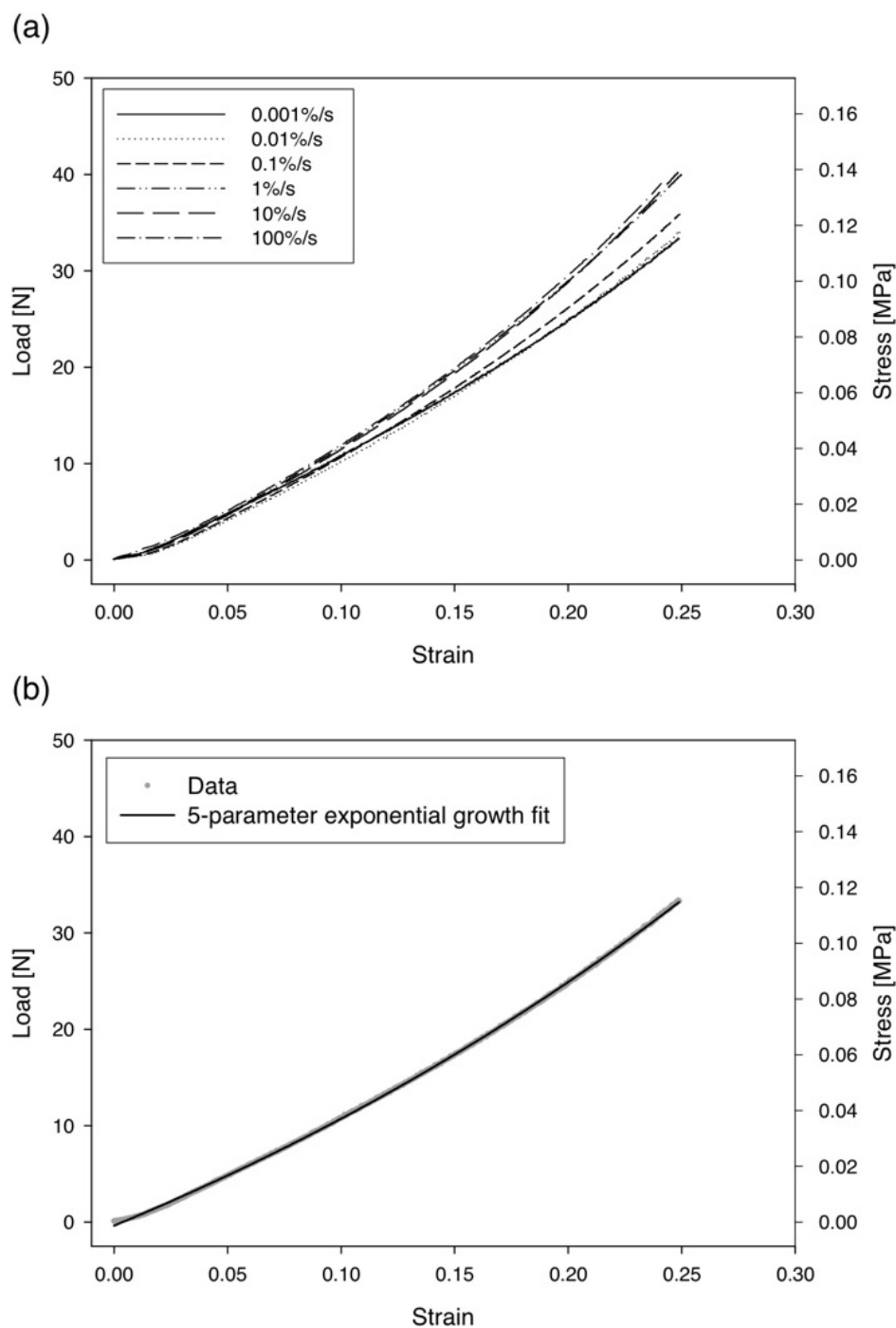


Figure 6.2: Data from unconfined compression of the 20%/10% PVA two-component hydrogel (Sample 1) at strain rates between 0.001%/s and 100%/s (a), and the data from 0.001%/s fitted with the 5-parameter exponential growth model (b). The model was not able to fit the toe region between 0 to 0.02 strain.

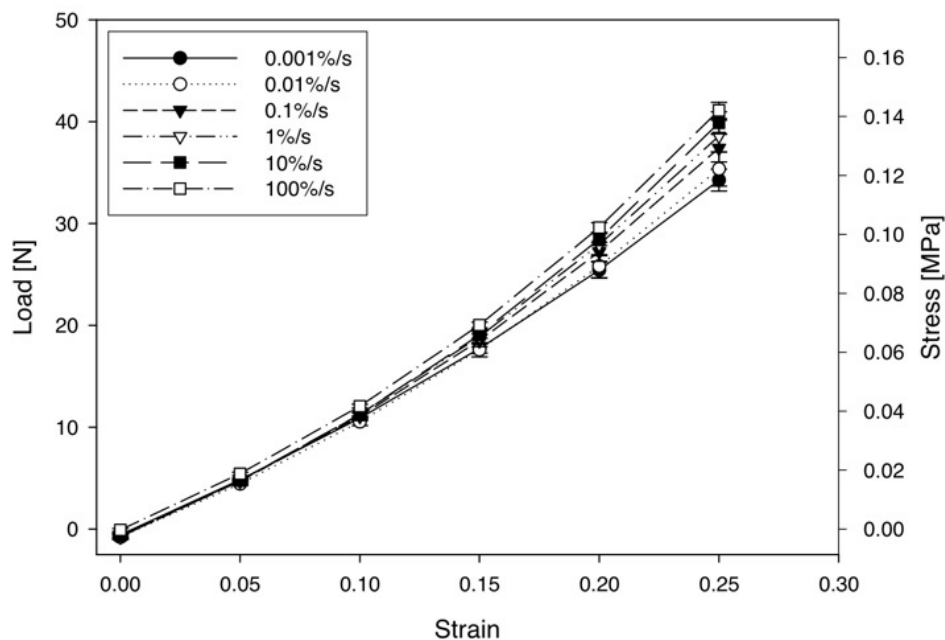


Figure 6.3: Average loading curves from unconfined compression of the 20%/10% PVA two-component hydrogel, tested at strain rates from 0.001%/s to 100%/s.

load at 0.25 strain using a strain rate of 1%/s was statistically different from 10 and 100%/s in 20% PVA. However, there was a larger spread in the data for the hydrogel prototype than for 20% PVA, and a sample size of three was used, rather than five in the single component hydrogels.

Table 6.1: Statistical differences in load at 0.25 strain found between strain rates for the two-component and single component PVA hydrogels ($p < 0.05$).

Specimen	Significant difference in load at 0.25 strain between strain rate [%/s] pairs
20%/10% PVA prototype	0.001/1, 0.001/10, 0.001/100, 0.01/10, 0.01/100, 0.1/100
10% PVA	None
15% PVA	1/100, 10/100
20% PVA	1/10, 1/100

A linear relationship between change in load and the logarithm of strain rate was also found for the two-component hydrogel, as shown in Figure 6.4. Since load is proportional to stress by the cross-sectional area of the sample, fitting to either load or stress would yield the same slope.

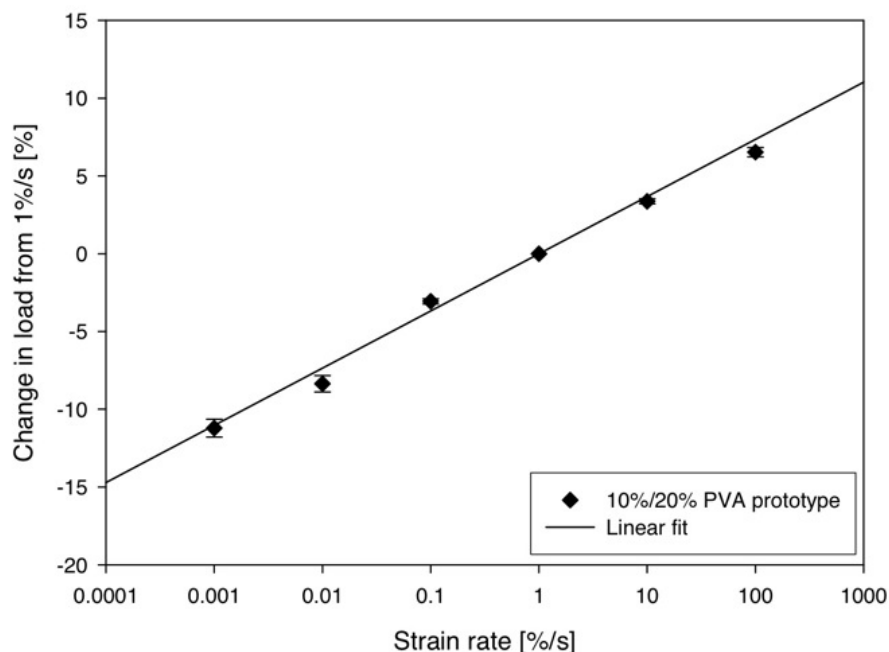


Figure 6.4: Linear relationship between change in load at 0.25 strain from 1%/s and logarithm of strain rate for the 20%/10% PVA two-component hydrogel prototype.

The slopes of the linear fits at 0.25 strain for the prototype, 10%, 15% and 20% PVA hydrogels, and canine IVD are tabulated in Table 6.2. The slope of the two-component hydrogel was between those of 10% and 20% PVA, but was closer to that of 10% PVA than 20% PVA. However, strain rate dependence, evaluated at 0.25 strain, remains lower than the canine IVDs tested by Cassidy et al. [55].

Table 6.2: Slopes from linear fits of percent change in load from 1%/s at 0.25 strain to logarithm of strain rate of two-component and single component PVA hydrogels, and canine IVD. (R^2 values of the fits are shown in parentheses.)

Specimen	Slope at 0.25 strain
20%/10% PVA prototype	3.677 (0.9905)
10% PVA	3.835 (0.9680)
15% PVA	2.971 (0.9777)
20% PVA	2.441 (0.8581)
Canine IVD [55]	17.5 (0.9562)

6.3 STRESS RELAXATION AND CREEP

Stress relaxation of the two-component hydrogel prototype at 0.25 strain was less than that of 10% and 20% PVA hydrogels, even though it was expected to fall between the two single component hydrogels (Figure 6.5). The hydrogel construct appeared to be approaching a higher equilibrium stress, and thus a smaller degree of relaxation. While canine IVDs relaxed to less than 10% of the initial stress after 30 minutes [55], the hydrogel prototype retained more than 80% of its initial stress after 1 hour.

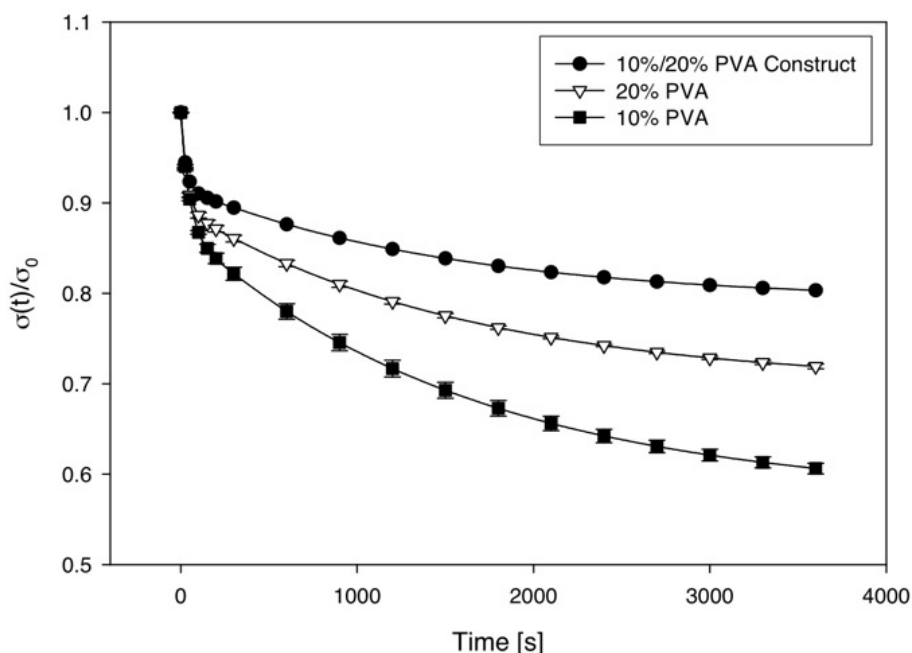


Figure 6.5: Stress relaxation at 0.25 strain of the 20%/10% PVA two-component hydrogel prototype after 1 h was decreased compared to 10% and 20% PVA.

In creep, strain increased rapidly at the beginning of the test in the two-component hydrogel (Figure 6.6). None of the models used to fit the creep data from single component hydrogels were able to fit this feature in the initial part of the creep curve (Figure 6.6a). While the four parameter viscoelastic models (Equations 3.9 and 3.11) and double exponential rise-to-max (Equation 3.13) model all provided better fits than the three-parameter-solid model (Equation 3.7), the double exponential model yielded the closest fit for strain near $t=0$.

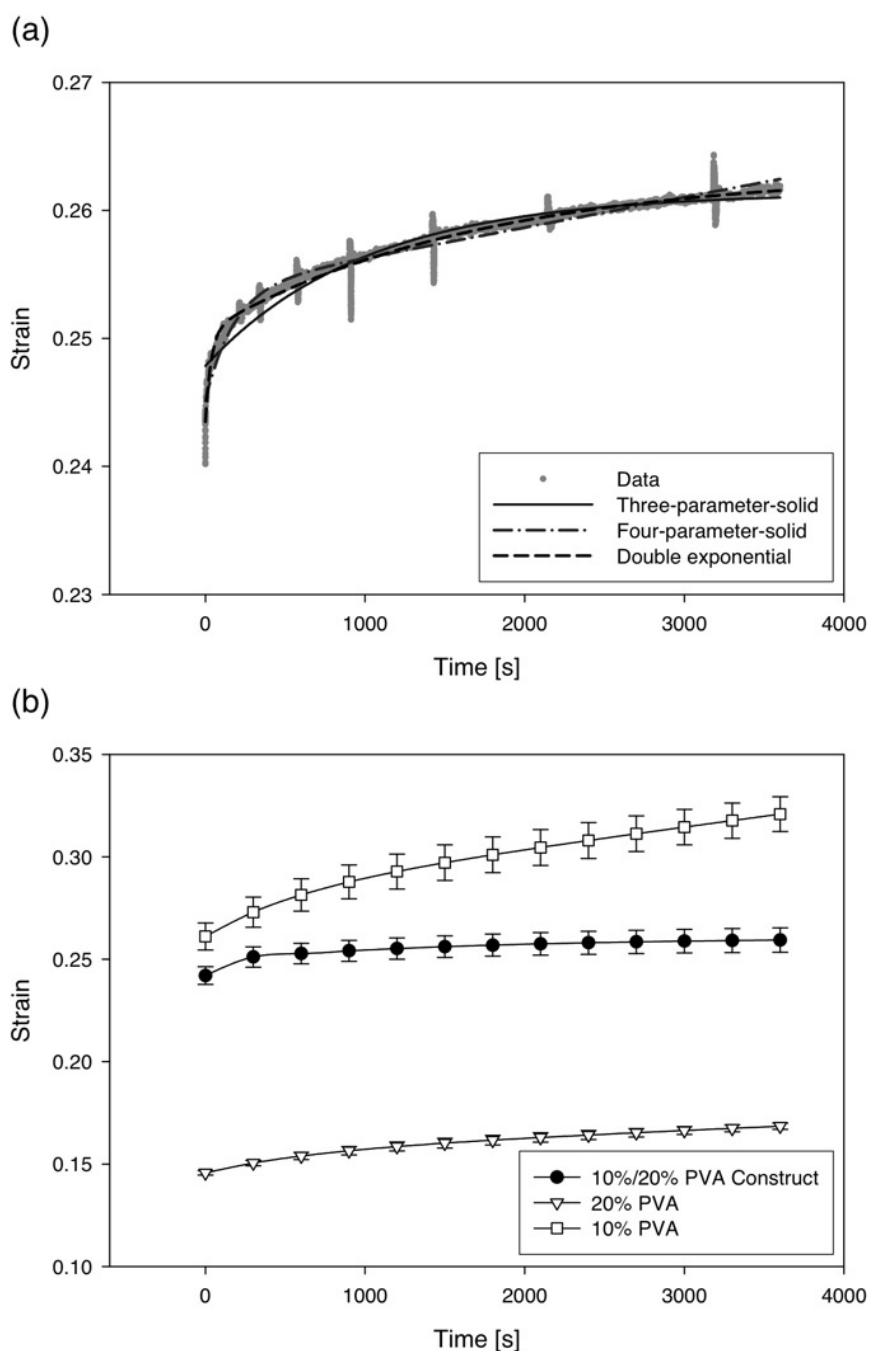


Figure 6.6: The four-parameter viscoelastic models and the double exponential model provided better fits than the three-parameter-solid viscoelastic model for Sample 1 of the 20%/10% PVA two-component hydrogel prototype (a). The average creep curves for the two-component hydrogel prototype under an axial load of 40 N, and for 20% and 10% PVA under an applied stress of 0.05 MPa (b).

Compared to 10% and 20% PVA, the creep curve of the hydrogel prototype was flatter and had a sharper increase in strain near $t=0$ (Figure 6.6b). The average increase in strain was $8.9 \pm 0.5\%$ after one hour of creep for the hydrogel prototype, whereas it was $22.9 \pm 0.4\%$ and $15.6 \pm 0.4\%$ for 10% and 20% PVA, respectively. The decrease in creep was in spite of a higher applied stress in the two-component hydrogel, approximately 0.14 MPa, versus 0.05 MPa for 10% and 20% PVA.

6.4 DISCUSSION

6.4.1 Prototype Design and Performance

In choosing PVA hydrogel concentrations for the nucleus, it was important for the nucleus component to have a high degree of swelling, as well as the ability to form a strong interface with the annulus component in the final hydrogel construct. Results from Wang and Campbell suggested that a 3 FTC-3% PVA hydrogel would be a suitable match in stiffness for the nucleus pulposus [23], which also has a high degree of hydration. However, in our attempts to prepare a two-component hydrogel structure, 3% PVA easily separated from a higher PVA concentration annulus component after F-T cycling. Since PVA hydrogels of very low polymer concentrations would consist mostly of water, the number of hydrogen bonds that could be formed at the interface between PVA molecules in opposing components would be low. Also, they would experience a higher degree of shrinkage during F-T cycling. Hence, 3% PVA was not able to form a strong interface with the annulus. Furthermore, unconfined compression of PVA hydrogels in Wang was performed between solid platens at a constant strain rate [23], while the values of NP modulus, between 2 and 8 kPa, they used for comparison were obtained from equilibrium unconfined compression between porous platens, in which stress relaxation was allowed to occur between strain increments [73]. Equilibrium modulus would thus be lower and would not be appropriate for direct comparison. Meanwhile, Stokes et al. calculated the isotropic solid modulus of NP to be much higher at 140 kPa [72]. A stiffer

hydrogel would therefore be required for the nucleus component than suggested by Wang. Since no match in stiffness for the annulus fibrosus could be found for PVA concentrations up to 40% PVA [23], using a stiffer hydrogel than the natural NP for the nucleus would increase the proportion of load supported by this component, and the challenge of producing a stiffer annulus component may be circumvented.

In our experiments, the PVA solutions were kept at approximately 60 °C prior to moulding to decrease viscosity for ease of handling. While a small degree of melting at the surface of the 20% PVA hydrogel annulus during the addition of the nucleus polymer solution could be beneficial for the formation of a strong interface, it could affect the thickness of the interface. The interface, in turn, would impact the mechanical properties of the hydrogel construct. The effect of temperature of the nucleus polymer solution on the interface and hydrogel properties should be investigated, and solution temperature should be fixed to ensure consistency between specimens.

At 0.25 strain, the load on the two-component hydrogel was 30–40 N, increasing with strain rate (Figure 6.3). By using PVA dissolved in mixture of water and DMSO, Silva et al. [177] fabricated a lumbar IVD device approximately 30 mm in diameter by first producing a ring of 1 FTC-35% PVA then filling it with a 30% PVA solution, with no subsequent F-T cycling. After swelling in water, the nucleus component absorbed a large amount of water and both components had an equilibrium swelling of more than 80%, while the amount of free water available for exudation was above 60%. During unconfined compression between porous nylon endplates at a strain rate of 100%/min, the PVA lumbar IVD supported a load of approximately 200 N, equivalent to a stress of 0.3 MPa, at 0.25 strain. In the current study of the 20%/10% PVA two-component hydrogel, unconfined compression at the closest strain rate of 1%/s between solid platens yielded a stress of approximately 0.13 MPa at 0.25 strain. Since cervical IVDs in humans can be loaded in compression to at least 155 N [50], and natural IVDs are compressed only to approximately 0.15 strain physiologically [58], this prototype did not achieve the stiffness required for cervical IVD applications. However, we were able to demonstrate the plausibility of producing a multi-component PVA hydrogel device by using water as the

solvent and F-T cycling, negating the need to remove an organic solvent after hydrogel formation as done in Silva.

A toe region of up to 0.02 strain was demonstrated in the two-component hydrogel that was not present in the single component unfilled PVA hydrogels from Chapter 4 (Figure 6.2). The toe region in natural IVDs range from 0.05 to 0.1 strain [55, 57], and the PET-reinforced PMMA-pHEMA artificial IVD device fabricated by Gloria et al. had toe strain of 0.09 strain [178]. The toe region in the natural IVD is the result of collagen uncrimping [55] and reorientation of the lamellae with strain as tensile stress is imposed on the AF [68]. In the pHEMA-based IVD, the toe region could be due to slack in the PET fibres [253], as well as the initial winding angle of the filaments, allowing reorientation similar to collagen in the AF during loading. Although the origin of the small toe region in the PVA hydrogel construct is unclear since it did not contain aligned reinforcing fibres, it could be due to the presence of the 10% PVA nucleus within the 20% PVA annulus. Future modelling studies should be performed to investigate the effect of confinement of the inner nucleus component on fluid pressurization and increase in modulus after the initial toe region in a multi-component structure.

The value of using a multi-component hydrogel over single component hydrogels was assessed by comparing the stress-strain behaviour of the two-component hydrogel with single component 10% and 20% PVA hydrogels. Since during axial compression, the annulus and nucleus components undergo the same strain in the hydrogel, unconfined compression curves based on the cross-sectional area and composition of the two-component prototype at strain rates of 1, 10 and 100%/s were predicted using the Voigt composite model. The total load on the construct, according to the model, would be the sum of the loads supported by the individual components, which are the product of stress, σ , and cross-sectional area, A , of each component, as shown in Equation 6.1.

$$F = \sigma_{annulus} A_{annulus} + \sigma_{nucleus} A_{nucleus} \quad (6.1)$$

Since stress as a function of strain was non-linear in the hydrogels, the 5-parameter exponential functions used to fit stress-strain data of 10% and 20% PVA were used for $\sigma_{nucleus}$ and $\sigma_{annulus}$, respectively. The loads predicted using this model and for a single component 20% PVA hydrogel of the same diameter as the hydrogel prototype were both lower than the experimental data for strain rates of 1, 10 and 100%/s (Figure 6.7).

The differences between the actual and predicted loading curves could be due to differences in lateral expansion of the hydrogels. Confinement of the 10% PVA nucleus by the 20% PVA annulus could have limited lateral expansion and increased stiffness in the nucleus component. Since the 10% PVA nucleus was not able to expand laterally to the same degree as the single component 10% PVA hydrogel in response to uniaxial compression, a larger force would have been required for the same degree of deformation. The contribution of load support from the nucleus would therefore be higher than calculated in Equation 6.1.

Fluid flow may also be a factor in the loading behaviour of the hydrogel prototype. Since 20% PVA would have a lower permeability to fluid than 10% PVA [137, 177], the rate of flow from the nucleus could be limited by the presence of the higher PVA concentration annulus. This would lead to increased support of load through fluid pressurization in the nucleus during unconfined compression beyond what was predicted by the Voigt model. It was interesting to find that for the corresponding strain rate, the hydrogel prototype was stiffer than what was predicted for 20% PVA despite containing the inclusion of the lower PVA concentration nucleus. The additional load carried through fluid pressurization in the nucleus could have contributed to increased stiffness. Finite element modelling by Silva et al. of their two-component PVA hydrogel disc produced also accounted for fluid permeability and flow, and the prediction was in good agreement with their experimental results [177]. It was also possible that the loading curves of single component 20% PVA in Figure 6.7b could be under-predicted due to

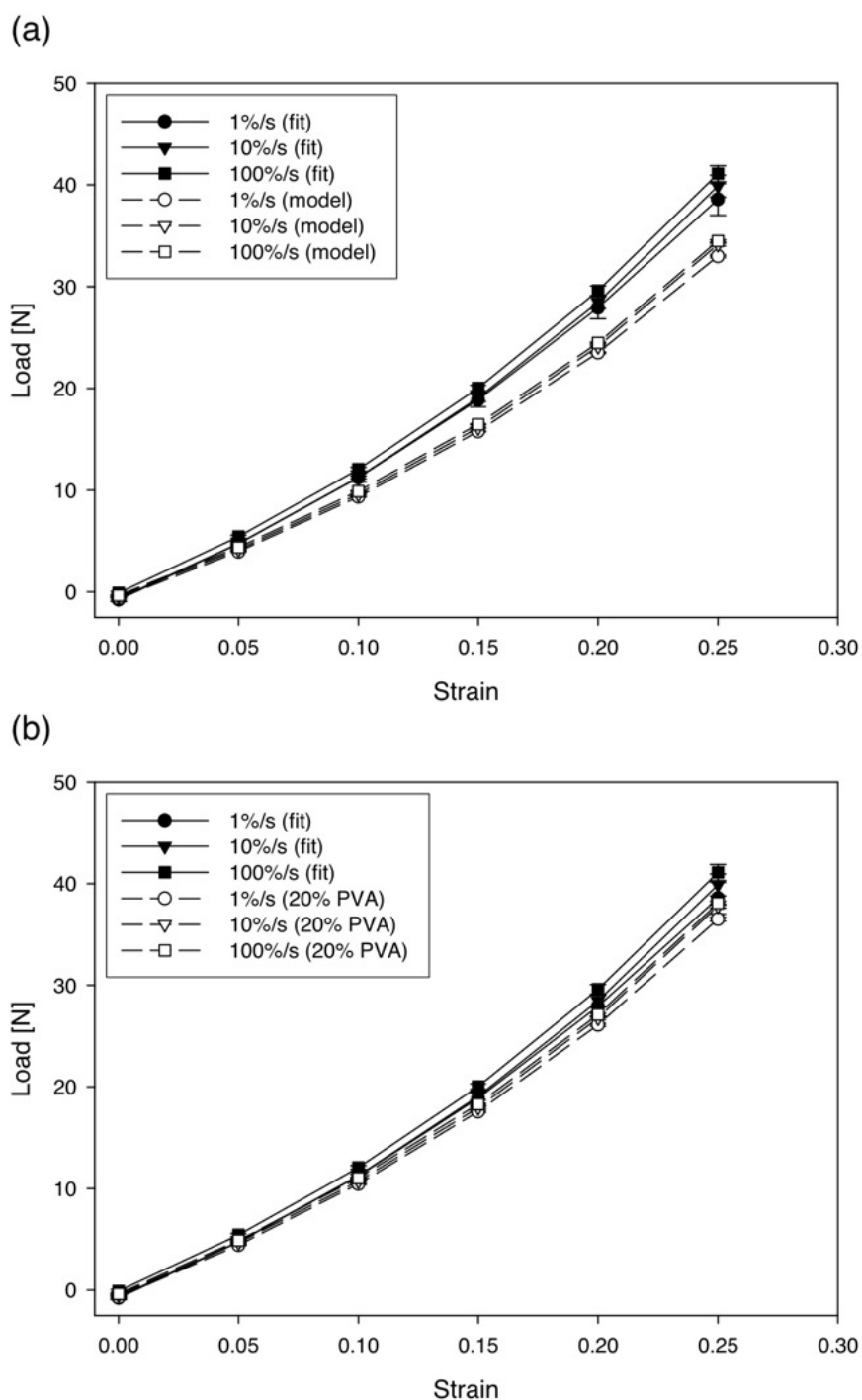


Figure 6.7: Experimental load-strain curves of the 20%/10% PVA two-component hydrogel prototype compared to predictions from the Voigt model (a), and 20% PVA of the same cross-sectional area as the two-component prototype (b). The two-component hydrogel was capable of supporting higher loads than predicted in both instances.

fluid flow effects. Since unconfined compression of single component hydrogels was performed on specimens of smaller cross-sectional area than the two-component structure, the surface area-to-volume ratio would be lower in the prototype, and could allow proportionally less water to flow out of the hydrogel at a given time. Testing of the single component 20% PVA with the same external dimensions as the two-component hydrogel could help determine whether fluid flow and modulus of the hydrogels are dependent on cross-sectional area, or if modification of fluid flow by using a higher concentration PVA hydrogel for the annulus had a beneficial effect on modulus. This information would be used to justify the value of designing a more complex hydrogel IVD replacement with components of different compositions over the use of a single component hydrogel.

Fluid flow may also be a factor in the loading behaviour of the hydrogel prototype. Since 20% PVA would have a lower permeability to fluid than 10% PVA [137, 177], the rate of flow from the nucleus could be limited by the presence of the higher PVA concentration annulus. This would lead to increased support of load through fluid pressurization in the nucleus during unconfined compression beyond what was predicted by the Voigt model. It was interesting to find that for the corresponding strain rate, the hydrogel prototype was stiffer than what was predicted for 20% PVA despite containing the inclusion of the lower PVA concentration nucleus. The additional load carried through fluid pressurization in the nucleus could have contributed to increased stiffness. Finite element modelling by Silva et al. of their two-component PVA hydrogel disc produced also accounted for fluid permeability and flow, and the prediction was in good agreement with their experimental results [177]. It was also possible that the loading curves of single component 20% PVA in Figure 6.7b could be under-predicted due to fluid flow effects. Since unconfined compression of single component hydrogels was performed on specimens of smaller cross-sectional area than the two-component structure, the surface area-to-volume ratio would be lower in the prototype, and could allow proportionally less water to flow out of the hydrogel at a given time. Testing of the single component 20% PVA with the same external dimensions as the two-component hy-

drogel could help determine whether fluid flow and modulus of the hydrogels are dependent on cross-sectional area, or if modification of fluid flow by using a higher concentration PVA hydrogel for the annulus had a beneficial effect on modulus. This information would be used to justify the value of designing a more complex hydrogel IVD replacement with components of different compositions over the use of a single component hydrogel.

Since using a higher PVA concentration annulus could limit the rate of fluid flow from the nucleus with compressive strain, increasing fluid pressurization at high strain rates could also contribute to strain rate dependence in addition to providing additional support of load in the hydrogel construct. However, the contribution of fluid flow from the nucleus may be small since the nucleus volume was only 15% of the two-component hydrogel and the thickness of the annulus was large. The fluid would also have to traverse some distance through the annulus in order to flow out of the hydrogel since testing was performed between solid platens. At very slow strain rates such as 0.001%/s, fluid movement would not be limited by permeability, and Silva et al. used a similar rate of compressive displacement in PVA hydrogels to determine stiffness of the solid matrix [177]. The load at 0.25 strain was 20% higher when the hydrogel was tested at a strain rate of 100%/s compared to 0.001%/s. While the increased load could have been carried through fluid pressurization, it was possible that viscous flow of the polymer could contribute to strain rate dependence and additional load support due to internal stresses in the polymer during rapid loading. However, strain rate dependence in the natural IVD is likely the result of fluid flow [55], which is regulated through the endplates since very little fluid flows through the AF except at low strain rates [40, 62]. Since testing of the hydrogels was performed between solid platens, the use of porous platens in future studies may provide a better insight into the role of fluid flow in strain rate dependence. Future development of a PVA-based hydrogel disc could also focus on an endplate material that is capable of modulating the rate of fluid flow as a function strain rate.

The linear dependence of stress to logarithm of strain rate (Figure 6.4) could be due to viscous molecular movement in PVA hydrogels, as discussed in Chapter 4. In the

two-component hydrogel, the same mechanisms of mechanical behaviour would be present as in the individual components. If their contributions to strain rate dependence were additive in the combined hydrogel, then the linear relationship between stress and logarithm of strain rate would hold. Since the 10% PVA nucleus component only comprised 15% of the hydrogel construct, it would be expected that the slope of the linear relationship would be closer to that of 20% PVA. However, the degree of strain rate dependence of the two-component hydrogel tested was closer to 10% PVA (Table 6.2), suggesting that other factors such as fluid flow affect strain rate dependence. The inclusion of a nucleus lower in PVA concentration than the annulus component may be able to increase strain rate dependence while increasing stiffness in the two-component hydrogel, which could be a strategy to simultaneously increase these two properties to the levels found in the natural cervical IVD in future designs. This was not possible when polymer concentration was increased to increase stiffness in the single component unfilled PVA hydrogels since strain rate dependence decreased as a result.

The decrease in stress relaxation (Figure 6.5) and creep (Figure 6.6b) in the hydrogel prototype compared to the individual components may have been caused by decreases in the rate and amount of fluid flow. While fluid flow could have occurred more slowly due to a decrease in the surface area-to-volume ratio in the larger hydrogel construct than the single component hydrogels, stress relaxation and creep strain should equilibrate to similar values over time. On the contrary, the degree of stress relaxation and creep was lower than both of the individual components. Silva et al. [177] speculated that a decrease in permeability at the annulus-nucleus interface of a two-component PVA hydrogel disc might have resulted in an overall decrease in fluid loss during creep. If flow is restricted at the interface between the two components, and above and below the hydrogel at the solid platens, fluid pressurization would have been maintained during stress relaxation and creep, which would allow the hydrogel construct to retain its volume and height with sustained loading. Modelling of fluid flow patterns in Silva et al. also indicated that while a large portion of the flow occurred through the porous nylon end-plates, fluid did move from the nucleus into the annulus in the hydrogel disc [177]. They

also postulated that since fluid permeability of the annulus in the natural IVD is almost negligible, stress transfer to the solid matrix would be delayed, and thus hydrostatic pressure could function to protect the collagen lamellae from damage. Viscous flow in the 10% PVA nucleus may have been reduced due to confinement by the annulus component when compared to the single component 10% PVA hydrogel since the nucleus is capable of sustaining a higher stress at the same strain. This would also lead to decreased viscoelastic response, lowering the degree of stress relaxation and creep.

In contrast to the decrease in creep in the two-component hydrogel compared to single component 10% and 20% PVA hydrogels, an increase in creep was observed in the PVA hydrogel disc manufactured by Silva et al. [177]. Under a load of 100 N, the individual hydrogels comprising the 35% PVA annulus and 30% PVA nucleus increased in strain by approximately 17% and 20%, respectively, while the combined disc increased in strain by approximately 22% after 1 hour at 200 N. However, creep experiments were performed between porous nylon plates that would have allowed for fluid flow. Gloria et al. fabricated a pHEMA-PMMA disc, reinforced with PET fibre reinforcement in the annulus region and hydroxyapatite in endplates [178]. It had a low initial strain of 0.069 that increased to 0.12 strain after 4500 s of creep at a stress of 2 MPa. Similar to the two-component PVA hydrogel in the current study, the pHEMA disc also experienced a rapid increase in strain after initial loading, and had a flatter creep curve than did natural IVDs. Low initial and creep strains were attributed to solid platens that did not allow flow from the hydrogels. While the discontinuity in hydrogel concentration could have decreased fluid flow in the two-component PVA hydrogels from the current study and those studied by Silva et al., the composition of the hydrogel was homogeneous throughout the pHEMA disc. However, the presence of the reinforcing PET fibres and HAp fillers could also have decreased fluid flow in those regions since there would be a lower proportion of hydrogel through which fluid can move. The PVA hydrogel prototype in the present study had a lower amount of creep than the other hydrogel-based IVD designs, as well as non-degenerated human lumbar IVDs, which increase in strain by 20% after 30 minutes of creep at loads corresponding to body weight at the disc level [64]. The two-

component PVA hydrogel structure tested in this study also conferred greater creep resistance than its individual components, which may be beneficial for long-term stability as an IVD replacement.

As discussed in Chapter 4, creep recovery and fatigue loading should be also be determined to ensure preservation of disc height and mechanical properties over time. Moreover, the performance of the hydrogel prototype between porous platens has yet to be determined to examine fluid flow and pressurization effects. As modelled by Silva, fluid in a two-component hydrogel flowed preferentially from the lower PVA concentration nucleus through the porous nylon endplates during creep [177]. Allowing fluid flow above and below the hydrogel would be more representative of the conditions between the vertebrae, and likely decrease the apparent stiffness, and increase stress relaxation and creep strain compared to compression between solid platens.

6.4.2 Parameters for Optimization of Properties

While the two-component PVA hydrogel structure showed the presence of a toe region, and increased stiffness and creep resistance compared to its single component PVA components, these properties, along with strain rate dependence, must be optimized for applications in the cervical IVD. Parameters that could be varied include construct geometry, PVA concentration, the addition of nanofillers, and introduction of anisotropy.

Since the toe region appeared as the result of the two-component structure, it may be possible to alter toe strain by varying nucleus volume relative to the annulus as the degree of nucleus confinement and pressurization by the stiffer annulus could be impacted. By increasing the nucleus volume, it may be possible to extend the toe region if increased compressive strain is required for the same degree of pressurization in the nucleus and resistance of tensile stress by the annulus. However, increasing the volume of the nucleus would increase the proportion of low modulus hydrogel in the construct, and could result in a decrease in overall stiffness. Nonetheless, the ratio of nucleus to annulus volume should be investigated as a means of optimizing the toe region, while increases in

hydrogel stiffness could be achieved by increasing hydrogel concentrations in both components, and with the addition of reinforcing fillers. It may also be possible that a greater degree of strain rate dependence could result from increasing nucleus volume, decreasing annulus thickness, and increasing the difference in PVA concentration between the components by modifying the amount and rate of fluid flow from the hydrogel disc.

A multi-component PVA hydrogel IVD device could be designed with PVA-NC hydrogel components to increase strain rate dependence. Although strain rate dependence of PVA-NC hydrogels in Chapter 4 was not apparent at 0.25 strain, they were more strain rate dependent than unfilled PVA hydrogels at 0.45 strain and have the potential to increase strain rate dependence in a multi-component hydrogel. Strain rate dependence also decreased in unfilled 10% PVA after aging in PBS, but did not change in Laponite-filled-10% PVA hydrogels. Therefore, addition of Laponite could preserve strain rate dependence of hydrogels the *in vivo* environment, possibly through the addition of charges from Laponite within the PVA-NC hydrogel. Moreover, the addition of BC and pBC resulted in a similar degree of rate dependence as canine IVD in Cassidy et al. [55]. While PVA concentration must be increased to improve the stiffness of the hydrogels, it would simultaneously decrease strain rate dependence as evidenced by increasing polymer concentration from 10% to 20% PVA. The addition of Laponite, and the orientation of BC or modified BC could be employed in a multi-component hydrogel disc design to attain the level of strain rate dependence that exists in natural IVDs within physiological strains. Charged nanofillers such as Laponite or pBC could also be added as fixed charges in the hydrogel, particularly in the nucleus, to create an osmotic potential for water to flow back into the disc upon load removal. The presence of fixed negative charges from proteoglycans in the natural IVD allows the tissue to re-swell after fluid is exuded during loading and regain disc height upon load removal [37].

Both device stiffness and toe region could be improved with the addition of fibrous reinforcement, particularly in the annulus region. A nanofibrous filler such as bacterial cellulose could be used as reinforcement and aligned in the circumferential or radial direction to resist tensile loads and bulging from nucleus pressurization. If the nanofibres

can be aligned circumferentially prior to incorporation into a PVA solution for the annulus, then stiffness in the circumferential direction could be anisotropically increased in the annulus component, functioning like collagen in the natural AF. The addition of randomly aligned BC or pBC into PVA hydrogels changed the shape of the stress-strain curves, increasing modulus significantly at high strains while maintaining a low modulus up to approximately 0.25 strain. By winding the nanofibres in angled lamellae similar to PET fibres in the pHEMA-based disc fabricated by Gloria et al. [178], it may be possible to have a toe region in a multi-component PVA hydrogel disc up to the 0.1 strain range found in the pHEMA disc and the native cervical IVD.

While the addition of nanofillers could be a strategy to increase modulus and the toe region of the hydrogel disc, it could also affect stress relaxation and creep response. In the single component hydrogels, Laponite, BC and pBC addition increased stress relaxation and creep, and their use in a multi-component PVA hydrogel may bring viscoelastic characteristics closer to those of natural IVDs. On the other hand, 20%/10% PVA two-component hydrogel had increased creep resistance compared to its individual components. Since resistance to creep would be desirable for long-term loading in the cervical spine, the increased creep with the addition of nanofillers could perhaps be minimized by the formation of a multi-component hydrogel disc.

In addition to alignment of nanofibrous fillers in the annulus region, stretching of the annulus component prior to the addition of the nucleus during F-T cycling could also confer anisotropic properties, allowing increased resistance to circumferential tension. Increased tensile stiffness was demonstrated in the direction of stretching by Millon et al. [14, 105], in which PVA hydrogel sheets were stretched after 1 FTC prior to additional F-T cycling. Structural studies indicated that the polymer-rich regions in these anisotropic hydrogels were elongated in the direction of stretching. Compression of the two-component construct during F-T cycling could also induce anisotropy and increased stiffness in compression for the hydrogel disc, as well as in tension around the periphery of the hydrogel due to lateral expansion during unconfined compression. Alignment of nanofibrous fillers, and pre-straining of the hydrogels during F-T cycling to create an ani-

sotropic structure could also possibly allow strain rate dependence to be apparent at lower strains.

Endplates that are permeable to fluids and can regulate flow would be appended to both ends of the disc. To increase stiffness, pre-compression of the disc could be done during freeze-thaw cycling, in a process similar to stretching to create anisotropic PVA hydrogel sheets [105]. This would compress pores and increase stiffness of the annulus region due to lateral expansion of the hydrogel upon compression. It may also be possible to decrease toe strain with this method due to pre-straining.

In a cervical IVD device, properties such as sufficient stiffness, presence of a toe region, strain rate dependence, creep resistance and creep recovery similar to the natural IVD are desired. Volume and PVA concentration of the components, nanofiller addition and alignment, inclusion of fixed charges, and straining of the hydrogel during F-T cycling for anisotropy could be used to achieve the desired mechanical properties in a multi-component PVA hydrogel. However, varying these parameters to achieve a particular property would also alter other properties. This interdependence would be due to the influence of design parameters on fluid flow and polymer viscoelasticity mechanisms in the mechanical response of PVA hydrogels. Therefore, testing of all relevant hydrogel properties would be important during optimization of parameters in future designs.

6.4.3 Implementation of a Hydrogel-Based IVD Device

Looking towards the implementation of a PVA hydrogel IVD device, the endplates must be designed for fixation to the adjacent vertebral bodies either mechanically or through tissue ingrowth. Since wear in PVA hydrogels may not be desirable due to hydrogel surface damage and generation of wear debris over time, designs that result in motion between the hydrogel material and a component used for implant fixation could be avoided. Metals such as cobalt chromium and titanium alloys are typically used in orthopedic and spinal implants, and participate in mechanical and/or bony fixation of an

implant. However, it could be a challenge to integrate the hydrogel with a metal component in the implant without relative motion between the two components.

Our mould design accommodates the addition of endplates to the two-component hydrogel structure. PVA-based endplates could be fabricated separately from the annulus-nucleus construct then adhered to the construct using a PVA solution and F-T cycling. Depending on endplate design, platens used in compression testing of a PVA hydrogel-based IVD could be solid or porous. Solid platens should be used for a solid endplate design, while porous platens should be used if the hydrogel is to be attached through porous endplates or directly to the vertebral bodies. Allowing fluid flow from the ends of the hydrogel disc would decrease pressurization, and likely decrease stiffness, affect strain rate dependence, and increase stress relaxation and creep. *In vitro* testing, including mechanical testing, of a multi-component PVA hydrogel IVD replacement should reflect the implementation and *in vivo* environment of the device in its application in the cervical IVD.

Freeze-thaw PVA hydrogels have also been studied extensively as controlled drug delivery devices, including applications in treatment of respiratory, skin and cardiovascular diseases [10, 26, 118, 254-262]. Therapeutic agents, such as antibiotics to prevent infection, anti-inflammatory agents to mitigate heterotopic ossification [98], or growth factors to encourage bone or cartilage growth, may be incorporated into a PVA hydrogel device to achieve sustained localized release. The mechanism and rate of release depends on factors including, but not limited to, the concentration and solubility of the drug, hydrogel concentration, number of FTCs, and the structure of the hydrogel device. For example, a reservoir-type system could achieve zero-order release, the rate of which does not change with time. Kennedy demonstrated this in a bilayer 10% PVA hydrogel structure composed of a 3 FTC membrane and 1 FTC reservoir [262]. A multi-component PVA hydrogel-based IVD would be well suited as a reservoir-type drug delivery system since the drug could be loaded into the lower polymer concentration nucleus, while the higher concentration annulus would control the rate of release. In a matrix-type system, where the drug is distributed uniformly in the hydrogel, the rate of release decreases with

time. This would be useful if therapeutic activity is required for a period of time immediately after implantation. Depending on the desired timing and location of release, therapeutic agents may be placed selectively within the different components of the PVA hydrogel IVD to tailor the release profile, location, and bioactivity.

6.5 CONCLUDING REMARKS

A two-component PVA hydrogel structure was successfully produced by F-T cycling, consisting of annulus and nucleus components of two different PVA concentrations, 20% and 10% PVA, respectively. Unconfined compression to 0.25 strain at strain rates between 0.001%/s and 100%/s were performed. In contrast to the single component 10% and 20% hydrogels, a small toe region of 0.02 strain was observed in the J-shaped stress-strain curves. The two-component hydrogel was expected to have stiffness and viscoelastic response between those of 10% and 20% PVA. However, it was stiffer than the model prediction based on the cross-sectional area of the components and the stress-strain curves of 10% and 20% PVA hydrogels, as well as the single component 20% PVA hydrogel, despite the presence of the more compliant 10% PVA nucleus. The degree of strain rate dependence was between those of single component 10% and 20% PVA hydrogels, but was closer to the more strain rate dependent 10% PVA, even though the 20% PVA annulus comprised 85% of the construct. Meanwhile, the hydrogel prototype experienced less stress relaxation and had higher creep resistance compared to both the 10% and 20% PVA hydrogels.

This two-component PVA hydrogel prototype demonstrated that a hydrogel structure with multiple components could be produced. However, it was not of sufficient stiffness to be used as a cervical IVD replacement with its current composition. Stiffness, strain rate dependence, stress relaxation and creep must be optimized for applications in the cervical spine. PVA hydrogels possess a great deal of versatility towards producing a functional multi-component cervical IVD prosthesis. Parameters that could be varied to modify PVA hydrogel properties include polymer concentration, the ratio of annulus to

nucleus volume, nanofiller placement and alignment, and straining of the hydrogel during F-T cycling to induce anisotropy. The addition of endplates could also affect compression properties by modulating fluid flow. Creep recovery and resistance to fatigue should also be evaluated for its suitability in the cervical spine. Further considerations in the design of a PVA-based hydrogel TDR could include drug delivery and fixation of the device to adjacent vertebral bodies.

Chapter 7

CONCLUSIONS AND FUTURE WORK

7.1 CONCLUSIONS

This thesis focused on the effects of composition on compression and wear properties of PVA and PVA-NC hydrogels for potential application in cervical IVD replacements. PVA hydrogels, physically crosslinked through freeze-thaw cycling, were selected based on their similarities in water content and mechanical properties to natural tissues, and have been previously investigated as biomaterials for cardiovascular and orthopedic applications. Furthermore, nanofillers were added to PVA hydrogels since it is possible to significantly modify properties of a material with low nanofiller content. Since tissue components in the natural IVD include negatively charged proteoglycans and reinforcing collagen fibres, nanofillers possessing negative charges or that were nanofibrous were chosen. Hydrophilic nanofillers were used in this thesis to obtain a strong interface between the nanofillers and the hydrophilic PVA matrix: Laponite, a low aspect ratio synthetic clay with negatively charged surfaces; BC, a high aspect ratio nanofibre produced through *Acetobacter xylinum* fermentation; and phosphorylated-BC, BC that was surface modified to add negative charges. The effects of PVA concentration, and nanofiller content, aspect ratio and charge on PVA hydrogels were investigated.

In Chapter 4, stiffness and viscoelasticity of PVA and PVA-NC hydrogels in unconfined compression were examined as a function of composition. While the stiffness of the hydrogels tested were not sufficient for use in the cervical IVD, increases in PVA concentration and addition of high aspect ratio fillers such as BC could be used to increase the modulus of the material. Since time-dependent response in the natural IVD is

important in shock absorption and the distribution of load, the addition of nanofillers was able to increase strain rate dependence, stress relaxation and creep in the hydrogels, all of which decreased with increased PVA concentration. There was also increased creep and decreased viscous damping with the addition of negative charges to BC. The increase in hydrophilicity, adsorption of PVA molecules to nanofiller surfaces, and modification of polymer chain motion with the addition of nanofillers could have contributed to the stiffness and time-dependent viscoelastic properties in the PVA-NC hydrogels. While mass loss and shrinkage due to deswelling in the unfilled hydrogels decreased with the increase in PVA concentration, which would reduce the loss of disc height and incidence of implant extrusion, PVA-NC hydrogels were more resistant to changes in modulus due to osmotic pressure, which could lead to more predictable properties in the *in vivo* fluid environment.

In Chapter 5, crossing-paths wear in the PVA and PVA-NC hydrogels was investigated since TDRs with articulating surfaces experience multidirectional sliding. Minimizing the generation of wear debris and permanent deformation is important in materials used in TDR. A method using high frequency 3D US was developed to determine wear volume and depth in hydrogels, which has the advantages of being non-contacting and allowing for imaging in fluid to prevent dehydration of hydrogel samples. Wear volume and depth decreased with increases in PVA concentration but the addition of nanofillers resulted in no significant change. However, the addition of nanofillers eliminated fatigue damage on the wear track surfaces, as did increases in PVA concentration. PVA concentration increase and nanofillers addition also prevented deformation and collapse of the porous structure under the wear tracks.

In Chapter 6, the compressive properties of a hydrogel structure with annulus and nucleus components of different PVA concentrations were examined. This two-component structure resembles the structure of the natural IVD. It had a small toe region in the stress-strain curve, increased stiffness, and decreased stress relaxation and creep compared to its components. Strain rate dependence of the two-component material, however, was closer to that of the lower concentration PVA hydrogel component, which

had a higher degree of strain rate dependence. Therefore, in contrast to increasing PVA concentration in the single component hydrogels, the multi-component structure could be used to increase stiffness and limit loss of disc height due to creep, while preserving strain rate dependence for use in the cervical IVD.

7.2 FUTURE WORK

This work has demonstrated that PVA concentration and nanofiller addition are parameters that could be varied to obtain the stiffness, viscoelasticity, wear and *in vivo* behaviour. However, the precise mechanism by which nanofillers alter the structure and mechanical properties of PVA hydrogels has yet to be determined. Additional methods to determine the effects of nanofiller addition on hydrogel crystallinity include FTIR [10, 125, 263], XRD [117, 128, 129, 263] and NMR [129]. Neutron scattering could also be employed to determine the length scales of features such as crystallites, crystallite separation and pores in hydrogels, as well as characterize anisotropy [105, 130, 264].

Strategies to improve upon stiffness and strain rate dependence should focus on the addition of BC or its derivatives to hydrogels with PVA concentrations of at least 20%. Stress-strain curves of IVDs are characterized by a low modulus toe region up to approximately 0.1 strain followed by a stiffer linear region with increasing strain. Since the addition of BC and pBC changed the shape of the 10% PVA stress-strain curve, resulting in a low modulus region followed by a high modulus region, their use show promise in replicating the compressive stress-strain behaviour of the natural IVD. Compression of BC-filled PVA-NC hydrogels during F-T cycling may induce anisotropy, decrease toe strain and increase strain rate dependence at low strains. Since the structure of the native IVD is multi-component and anisotropic, optimization of a multi-component PVA hydrogel disc could involve adjusting the nucleus volume, polymer concentration, and addition and alignment of nanofillers, particularly BC and modified-BC. A hydrogel-based device created by aligning BC in a stiffer annulus region surrounding a higher water content nucleus region could result in increased stiffness and strain rate de-

pendence. The goals would be to increase stiffness, strain rate dependence and toe strain to ranges appropriate for use as a cervical IVD replacement. However, since increases in PVA concentration and addition of nanofillers would result in increased viscosity, a reliable method of filling moulds with viscous polymer solutions, while preventing air entrapment, should be developed. Also, alignment of nanofibres may present a challenge in fabricating a device. Manufacturing techniques such as injection moulding and fibre spinning could be considered in order to investigate filler alignment in PVA-NC hydrogels for application in an IVD replacement device.

Future investigation into the compression properties of PVA and PVA-NC hydrogels, and multi-component designs should include compression, creep and creep recovery, and dynamic loading between porous platens. Since fluid flow through the endplates into vertebral bodies is important in compression of IVDs, it may affect the behaviour of the hydrogels during compression. Studies could also be performed to quantify the rate of fluid flow, since increased hydrophilicity with nanofiller addition may affect hydrogel performance. Creep recovery is important in determining if deformation would be recovered after load is removed to preserve disc height. Furthermore, fatigue testing should be performed to determine the effects of long-term loading on the hydrogel material. While only compression testing of the PVA and PVA-NC hydrogels was performed in this study, IVDs experience additional loads. Costi et al. investigated dynamic loading of intervertebral discs in anteroposterior shear, lateral shear, compression, lateral bending and axial rotation [61], which should be undertaken with the hydrogels intended for use in IVD replacements.

Further development into the 3D US wear measurement technique used could help improve measurement precision, and determine if the addition of nanofillers could increase deformation and wear resistance in PVA-NC hydrogels. Delineation of wear from creep deformation would also be required to establish if PVA-based hydrogels are suitable in TDR designs that incorporate articulation. Future investigation into the tribology of PVA and PVA-NC hydrogels could focus on the effects of polymer concentration and addition of fixed ionic charges on friction, the amount, size and shape of wear particles generated,

and the consequence of fatigue from wear testing on hydrogel structure and properties relevant to TDRs. In the future, reproduction of the shape of the wear scar from 3D US images could be useful in visualizing wear of an articulating hydrogel-based TDR device in simulator studies.

BIBLIOGRAPHY

- [1] Strine TW, Hootman JM. US national prevalence and correlates of low back and neck pain among adults. *Arthritis & Rheumatism-Arthritis Care & Research*. 2007;57:656-65.
- [2] Cote P, van der Velde G, Cassidy JD, Carroll LJ, Hogg-Johnson S, Holm LW, et al. The burden and determinants of neck pain in workers - Results of the bone and joint decade 2000-2010 task force on neck pain and its associated disorders. *Spine*. 2008;33:S60-S74.
- [3] Cote P, Kristman V, Vidmar M, Van Eerd D, Hogg-Johnson S, Beaton D, et al. The prevalence and incidence of work absenteeism involving neck pain - A cohort of Ontario lost-time claimants. *Spine*. 2008;33:S192-S8.
- [4] Hoy D, March L, Brooks P, Woolf A, Blyth F, Vos T, et al. Measuring the global burden of low back pain. *Best Practice & Research in Clinical Rheumatology*. 2010;24:155-65.
- [5] Kovacs FM, Abraira V, Zamora J, del Real MTG, Llobera J, Fernandez C, et al. Correlation between pain, disability, and quality of life in patients with common low back pain. *Spine*. 2004;29:206-10.
- [6] Adams MA, Roughley PJ. What is intervertebral disc degeneration, and what causes it? *Spine*. 2006;31:2151-61.
- [7] Smith LJ, Nerurkar NL, Choi KS, Harfe BD, Elliott DM. Degeneration and regeneration of the intervertebral disc: lessons from development. *Disease Models & Mechanisms*. 2011;4:31-41.
- [8] Causa F, Manto L, Borzacchiello A, De Santis R, Netti PA, Ambrosio L, et al. Spatial and structural dependence of mechanical properties of porcine intervertebral disc. *Journal of Materials Science-Materials in Medicine*. 2002;13:1277-80.
- [9] Denoziere G, Ku DN. Biomechanical comparison between fusion of two vertebrae and implantation of an artificial intervertebral disc. *Journal of Biomechanics*. 2006;39:766-75.
- [10] Hassan CM, Peppas NA. Structure and applications of poly(vinyl alcohol) hydrogels produced by conventional crosslinking or by freezing/thawing methods. *Biopolymers/Pva Hydrogels/Anionic Polymerisation Nanocomposites*. Berlin: Springer-Verlag Berlin; 2000. p. 37-65.

-
- [11] Wan WK, Campbell G, Zhang ZF, Hui AJ, Boughner DR. Optimizing the tensile properties of polyvinyl alcohol hydrogel for the construction of a bioprosthetic heart valve stent. *Journal of Biomedical Materials Research*. 2002;63:854-61.
- [12] Pazos V, Mongrain R, Tardif JC. Polyvinyl alcohol cryogel: Optimizing the parameters of cryogenic treatment using hyperelastic models. *Journal of the Mechanical Behavior of Biomedical Materials*. 2009;2:542-9.
- [13] Millon LE, Wan WK. The polyvinyl alcohol-bacterial cellulose system as a new nanocomposite for biomedical applications. *Journal of Biomedical Materials Research Part B-Applied Biomaterials*. 2006;79B:245-53.
- [14] Millon LE, Mohammadi H, Wan WK. Anisotropic polyvinyl alcohol hydrogel for cardiovascular applications. *Journal of Biomedical Materials Research Part B-Applied Biomaterials*. 2006;79B:305-11.
- [15] Mathews DT, Birney YA, Cahill PA, McGuinness GB. Mechanical and morphological characteristics of poly(vinyl alcohol)/chitosan hydrogels. *Journal of Applied Polymer Science*. 2008;109:1129-37.
- [16] Padavan DT, Hamilton AM, Millon LE, Boughner DR, Wan WK. Synthesis, characterization and in vitro cell compatibility study of a poly(amic acid) graft/cross-linked poly(vinyl alcohol) hydrogel. *Acta Biomaterialia*. 2011;7:258-67.
- [17] Noguchi T, Yamamuro T, Oka M, Kumar P, Kotoura Y, Hyon SH, et al. Poly(vinyl alcohol) hydrogel as an artificial articular-cartilage - evaluation of biocompatibility. *Journal of Applied Biomaterials*. 1991;2:101-7.
- [18] Oka M, Ushio K, Kumar P, Ikeuchi K, Hyon SH, Nakamura T, et al. Development of artificial articular cartilage. *Proceedings of the Institution of Mechanical Engineers Part H-Journal of Engineering in Medicine*. 2000;214:59-68.
- [19] Stammen JA, Williams S, Ku DN, Guldberg RE. Mechanical properties of a novel PVA hydrogel in shear and unconfined compression. *Biomaterials*. 2001;22:799-806.
- [20] Covert RJ, Ott RD, Ku DN. Friction characteristics of a potential articular cartilage biomaterial. *Wear*. 2003;255:1064-8.
- [21] Kobayashi M, Chang YS, Oka M. A two year in vivo study of polyvinyl alcohol-hydrogel (PVA-H) artificial meniscus. *Biomaterials*. 2005;26:3243-8.
- [22] Maher SA, Doty SB, Torzilli PA, Thornton S, Lowman AM, Thomas JD, et al. Nondegradable hydrogels for the treatment of focal cartilage defects. *Journal of Biomedical Materials Research Part A*. 2007;83A:145-55.

-
- [23] Wang BH, Campbell G. Formulations of Polyvinyl Alcohol Cryogel That Mimic the Biomechanical Properties of Soft Tissues in the Natural Lumbar Intervertebral Disc. *Spine*. 2009;34:2745-53.
- [24] Millon LE, Oates CJ, Wan WK. Compression Properties of Polyvinyl Alcohol - Bacterial Cellulose Nanocomposite. *Journal of Biomedical Materials Research Part B- Applied Biomaterials*. 2009;90B:922-9.
- [25] Pan YS, Xiong DS. Friction properties of nano-hydroxyapatite reinforced poly(vinyl alcohol) gel composites as an articular cartilage. *Wear*. 2009;266:699-703.
- [26] Hassan CM, Stewart JE, Peppas NA. Diffusional characteristics of freeze/thawed poly(vinyl alcohol) hydrogels: Applications to protein controlled release from multilaminate devices. *European Journal of Pharmaceutics and Biopharmaceutics*. 2000;49:161-5.
- [27] Nugent MJD, Hanley A, Tomkins PT, Higginbotham CL. Investigation of a novel freeze-thaw process for the production of drug delivery hydrogels. *Journal of Materials Science-Materials in Medicine*. 2005;16:1149-58.
- [28] Pan YS, Xiong DS, Chen XL. Mechanical properties of nanohydroxyapatite reinforced poly(vinyl alcohol) gel composites as biomaterial. *Journal of Materials Science*. 2007;42:5129-34.
- [29] Pan YS, Xiong DS, Gao F. Viscoelastic behavior of nano-hydroxyapatite reinforced poly(vinyl alcohol) gel biocomposites as an articular cartilage. *Journal of Materials Science-Materials in Medicine*. 2008;19:1963-9.
- [30] Jordan J, Jacob KI, Tannenbaum R, Sharaf MA, Jasiuk I. Experimental trends in polymer nanocomposites - a review. *Materials Science and Engineering a-Structural Materials Properties Microstructure and Processing*. 2005;393:1-11.
- [31] Hogg-Johnson S, van der Velde G, Carroll LJ, Holm LW, Cassidy JD, Guzman J, et al. The burden and determinants of neck pain in the general population - Results of the bone and joint decade 2000-2010 task force on neck pain and its associated disorders. *Spine*. 2008;33:S39-S51.
- [32] Gray H. *Anatomy of the Human Body*. Philadelphia: Lea & Febiger; 1918. p. Bartleby.com, 2000. www.bartleby.com/107/. [Accessed: 11 November 8].
- [33] Carette S, Fehlings MG. Cervical radiculopathy. *New England Journal of Medicine*. 2005;353:392-9.

-
- [34] Bao QB, McCullen GM, Higham PA, Dumbleton JH, Yuan HA. The artificial disc: Theory, design and materials. *Biomaterials*. 1996;17:1157-67.
- [35] Guerin HAL, Elliott. Structure and Properties of Soft Tissues in the Spine. In: Kurtz SM, Edidin AA, editors. *Spine Technology Handbook*. Amsterdam ; Boston: Elsevier Academic Press; 2006. p. 35-62.
- [36] Pooni JS, Hukins DWL, Harris PF, Hilton RC, Davies KE. Comparison of the structure of human intervertebral disks in the cervical, thoracic and lumbar regions of the spine. *Surgical and Radiologic Anatomy*. 1986;8:175-82.
- [37] Arlet V, Antoniou J. Macro- and Microscopic Anatomy of the Disk and End Plate. In: Dewald RL, editor. *Spinal Deformities: The Comprehensive Text*. New York: Thieme; 2003. p. 78-89.
- [38] Panjabi MM, Summers DJ, Pelker RR, Videman T, Friedlaender GE, Southwick WO. Three-Dimensional Load-Displacement Curves Due to Forces on the Cervical Spine. *Journal of Orthopaedic Research*. 1986;4:152-61.
- [39] Roberts S, Menage J, Urban JPG. Biochemical and structural-properties of the cartilage endplate and its relation to the intervertebral-disk. *Spine*. 1989;14:166-74.
- [40] Ayotte DC, Ito K, Tepic S. Direction-dependent resistance to flow in the endplate of the intervertebral disc: an ex vivo study. *Journal of Orthopaedic Research*. 2001;19:1073-7.
- [41] Urban JPG, Smith S, Fairbank JCT. Nutrition of the intervertebral disc. *Spine*. 2004;29:2700-9.
- [42] Botsford DJ, Esses SI, Ogilvieharris DJ. In Vivo Diurnal Variation in Intervertebral Disc Volume and Morphology *Spine*. 1994;19:935-40.
- [43] Moore RJ. The vertebral endplate: disc degeneration, disc regeneration. *European Spine Journal*. 2006;15:S333-S7.
- [44] Setton LA, Zhu W, Weidenbaum M, Ratcliffe A, Mow VC. Compressive properties of the cartilaginous end-plate of the baboon lumbar spine. *Journal of Orthopaedic Research*. 1993;11:228-39.
- [45] Edwards CA, O'Brien WD. Modified assay for determination of hydroxyproline in a tissue hydrolyzate. *Clinica Chimica Acta*. 1980;104:161-7.
- [46] Adams MA, Dolan P. Spine biomechanics. *Journal of Biomechanics*. 2005;38:1972-83.

-
- [47] Mirza SK, Deyo RA. Systematic review of randomized trials comparing lumbar fusion surgery to nonoperative care for treatment of chronic back pain. *Spine*. 2007;32:816-23.
- [48] Stokes IAF, Iatridis JC. Mechanical conditions that accelerate intervertebral disc degeneration: Overload versus immobilization. *Spine*. 2004;29:2724-32.
- [49] Korecki CL, MacLean JJ, Iatridis JC. Dynamic compression effects on intervertebral disc mechanics and biology. *Spine*. 2008;33:1403-9.
- [50] Cripton PA, Kroeker SG, Saari A. Musculature Actuation and Biomechanics of the Spine. In: Kurtz SM, Edidin AA, editors. *Spine Technology Handbook*. Amsterdam ; Boston: Elsevier Academic Press; 2006. p. 99-143.
- [51] Keller TS, Holm SH, Hansson TH, Spengler DM. The dependence of intervertebral-disk mechanical-properties on physiological conditions. *Spine*. 1990;15:751-61.
- [52] White AA, Panjabi MM. *Clinical Biomechanics of the Spine*. New York: Lippincott; 1990.
- [53] Hattori S, Oda H, Kawai S. Cervical Intra-Discal Pressure in Movements and Traction of the Cervical Spine. *Zeitschrift Fur Orthopadie Und Ihre Grenzgebiete*. 1981;119:568-9.
- [54] Nachemson AL. Disk Pressure Measurements. *Spine*. 1981;6:93-7.
- [55] Cassidy JJ, Hiltner A, Baer E. The response of the hierarchical structure of the intervertebral-disk to uniaxial compression. *Journal of Materials Science-Materials in Medicine*. 1990;1:69-80.
- [56] Moroney SP, Schultz AB, Miller JAA, Andersson GBJ. Load displacement properties of lower cervical-spine motion segments. *Journal of Biomechanics*. 1988;21:769-79.
- [57] Race A, Broom ND, Robertson P. Effect of loading rate and hydration on the mechanical properties of the disc. *Spine*. 2000;25:662-9.
- [58] Joshi A, Fussell G, Thomas J, Hsuan A, Lowman A, Karduna A, et al. Functional compressive mechanics of a PVA/PVP nucleus pulposus replacement. *Biomaterials*. 2006;27:176-84.
- [59] Morel W, Quinn TM. Cartilage injury by ramp compression near the gel diffusion rate. *Journal of Orthopaedic Research*. 2004;22:145-51.

-
- [60] Oloyede A, Gudimetla P, Crawford R, Hills BA. Biomechanical responses of normal and delipidized articular cartilage subjected to varying rates of loading. *Connective Tissue Research*. 2004;45:86-93.
- [61] Costi JJ, Stokes IA, Gardner-Morse MG, Iatridis JC. Frequency-dependent behavior of the intervertebral disc in response to each of six degree of freedom dynamic loading - Solid phase and fluid phase contributions. *Spine*. 2008;33:1731-8.
- [62] Iatridis JC, Furukawa M, Stokes IAF, Gardner-Morse MG, Laible JP. Spatially Resolved Streaming Potentials of Human Intervertebral Disk Motion Segments Under Dynamic Axial Compression. *Journal of Biomechanical Engineering-Transactions of the Asme*. 2009;131:6.
- [63] Burns ML, Kaleps I, Kazarian LE. Analysis of compressive creep-behavior of the vertebral unit subjected to a uniform axial loading using exact parametric solution equations of Kelvin-solid models – Part I. Human intervertebral joints. *Journal of Biomechanics*. 1984;17:113-&.
- [64] Keller TS, Spengler DM, Hansson TH. Mechanical-behavior of the human lumbar spine. I. Creep analysis during static compressive loading. *Journal of Orthopaedic Research*. 1987;5:467-78.
- [65] Kaleps I, Kazarian LE, Burns ML. Analysis of compressive creep-behavior of the vertebral unit subjected to a uniform axial loading using exact parametric solution equations of Kelvin-solid models – Part II. Rhesus-monkey intervertebral joints. *Journal of Biomechanics*. 1984;17:131-6.
- [66] Iatridis JC, MacLean JJ, O'Brien M, Stokes IAF. Measurements of proteoglycan and water content distribution in human lumbar intervertebral discs. *Spine*. 2007;32:1493-7.
- [67] Elliott DM, Setton LA. Anisotropic and inhomogeneous tensile behavior of the human annulus fibrosus: Experimental measurement and material model predictions. *Journal of Biomechanical Engineering-Transactions of the Asme*. 2001;123:256-63.
- [68] Guerin HAL, Elliott DM. Degeneration affects the fiber reorientation of human annulus fibrosus under tensile load. *Journal of Biomechanics*. 2006;39:1410-8.
- [69] Iatridis JC, Setton LA, Foster RJ, Rawlins BA, Weidenbaum M, Mow V. Degeneration affects the anisotropic and nonlinear behaviors of human annulus fibrosus in compression. *Journal of Biomechanics*. 1998;31:535-44.
- [70] Iatridis JC, Setton LA, Weidenbaum M, Mow VC. Alterations in the mechanical behavior of the human lumbar nucleus pulposus with degeneration and aging. *Journal of Orthopaedic Research*. 1997;15:318-22.

-
- [71] Perie D, Korda D, Iatridis JC. Confined compression experiments on bovine nucleus pulposus and annulus fibrosus: sensitivity of the experiment in the determination of compressive modulus and hydraulic permeability. *Journal of Biomechanics*. 2005;38:2164-71.
- [72] Stokes IAF, Laible JP, Gardner-Morse MG, Costi JJ, Iatridis JC. Refinement of Elastic, Poroelastic, and Osmotic Tissue Properties of Intervertebral Disks to Analyze Behavior in Compression. *Annals of Biomedical Engineering*. 2011;39:122-31.
- [73] Cloyd JM, Malhotra NR, Weng L, Chen W, Mauck RL, Elliott DM. Material properties in unconfined compression of human nucleus pulposus, injectable hyaluronic acid-based hydrogels and tissue engineering scaffolds. *European Spine Journal*. 2007;16:1892-8.
- [74] Johannessen W, Elliott DM. Effects of degeneration on the biphasic material properties of human nucleus pulposus in confined compression. *Spine*. 2005;30:E724-E9.
- [75] Grant JP, Oxland TR, Dvorak MF. Mapping the structural properties of the lumbosacral vertebral endplates. *Spine*. 2001;26:889-96.
- [76] Bhadra AK, Raman AS, Casey ATH, Crawford RJ. Single-level cervical radiculopathy: clinical outcome and cost-effectiveness of four techniques of anterior cervical discectomy and fusion and disc arthroplasty. *European Spine Journal*. 2009;18:232-7.
- [77] Anderson PA, Rouleau JP. Intervertebral disc arthroplasty. *Spine*. 2004;29:2779-86.
- [78] King JT, Abbed KM, Gould GC, Benzel EC, Ghogawala Z. Cervical spine reoperation rates and hospital resource utilization after initial surgery for degenerative cervical spine disease in 12 338 patients in Washington state. *Neurosurgery*. 2009;65:1011-22.
- [79] Di Martino A, Vaccaro AR, Lee JY, Denaro V, Lim MR. Nucleus pulposus replacement - Basic science and indications for clinical use. *Spine*. 2005;30:S16-S22.
- [80] Leckie S, Kang J. Recent advances in nucleus pulposus replacement technology. *Current Orthopaedic Practice*. 2009;20.
- [81] Brown T, Bao QB, Kilpela T, Songer M. An In Vitro Biotribological Assessment of NUBAC, a Polyetheretherketone-on-Polyetheretherketone Articulating Nucleus Replacement Device Methodology and Results From a Series of Wear Tests Using Different Motion Profiles, Test Frequencies, and Environmental Conditions. *Spine*. 2010;35:E774-E81.

-
- [82] Nerurkar NL, Elliott DM, Mauck RL. Mechanical design criteria for intervertebral disc tissue engineering. *Journal of Biomechanics*. 2010;43:1017-30.
- [83] Hsieh AH, Twomey JD. Cellular mechanobiology of the intervertebral disc: New directions and approaches. *Journal of Biomechanics*. 2010;43:137-45.
- [84] Masuda K, Oegema TR, An HS. Growth factors and treatment of intervertebral disc degeneration. *Spine*. 2004;29:2757-69.
- [85] Whatley BR, Kuo J, Shuai C, Damon BJ, Wen XJ. Fabrication of a biomimetic elastic intervertebral disk scaffold using additive manufacturing. *Biofabrication*. 2011;3.
- [86] Bartels R, Donk RD, Pavlov P, van Limbeek J. Comparison of biomechanical properties of cervical artificial disc prosthesis: A review. *Clinical Neurology and Neurosurgery*. 2008;110:963-7.
- [87] Steinmetz MP, Patel R, Traynelis V, Resnick DK, Anderson PA. Cervical disc arthroplasty compared with fusion in a workers' compensation population. *Neurosurgery*. 2008;63:741-7.
- [88] Sasso RC, Smucker JD, Hacker RJ, Heller JG. Clinical outcomes of BRYAN cervical disc arthroplasty: A prospective, randomized, controlled, multicenter trial with 24-month follow-up. *Journal of Spinal Disorders & Techniques*. 2007;20:481-91.
- [89] Galbusera F, Bellini CM, Brayda-Bruno M, Fornari M. Biomechanical studies on cervical total disc arthroplasty: A literature review. *Clinical Biomechanics*. 2008;23:1095-104.
- [90] Kurtz SM. Total disc arthroplasty. In: Kurtz SM, Edidin AA, editors. *Spine technology handbook*. Amsterdam ; Boston: Elsevier Academic Press; 2006. p. 303-70.
- [91] Anderson PA, Rouleau JP, Toth JM, Riew KD. A comparison of simulator-tested and -retrieved cervical disc prostheses. *Journal of Neurosurgery-Spine*. 2004;1:202-10.
- [92] Ingham E, Fisher J. The role of macrophages in osteolysis of total joint replacement. *Biomaterials*. 2005;26:1271-86.
- [93] Anderson PA, Rouleau JP, Bryan VE, Carlson CS. Wear analysis of the Bryan Cervical Disc prosthesis. *Spine*. 2003;28:S186-S94.
- [94] McCullen GM, Yuan HA. Artificial disc: current developments in artificial disc replacement. *Current Opinion in Orthopaedics*. 2003;14:138-43.

-
- [95] Quan GMY, Vital JM, Hansen S, Pointillart V. Eight-Year Clinical and Radiological Follow-Up of the Bryan Cervical Disc Arthroplasty. *Spine*. 2011;36:639-46.
- [96] McAfee PC, Cunningham BW, Devine J, Williams E, Yu-Yahiro J. Classification of heterotopic ossification (HO) in artificial disk replacement. *Journal of Spinal Disorders & Techniques*. 2003;16:384-9.
- [97] Baird EO, Kang QK. Prophylaxis of heterotopic ossification - an updated review. *Journal of orthopaedic surgery and research*. 2009;4:12.
- [98] Pracyk JB, Traynelis VC. Treatment of the painful motion segment - Cervical arthroplasty. *Spine*. 2005;30:S23-S32.
- [99] Mehren C, Suchomel P, Grochulla F, Barsa P, Sourkova P, Hradil J, et al. Heterotopic ossification in total cervical artificial disc replacement. *Spine*. 2006;31:2802-6.
- [100] Sekhon LHS, Sears W, Duggal N. Cervical arthroplasty after previous surgery: results of treating 24 discs in 15 patients. *Journal of Neurosurgery-Spine*. 2005;3:335-41.
- [101] Leung C, Casey AT, Goffin A, Kehr P, Liebig K, Lind B, et al. Clinical significance of heterotopic ossification in cervical disc replacement: A prospective multicenter clinical trial. *Neurosurgery*. 2005;57:759-62.
- [102] Hanley EN, Herkowitz HN, Kirkpatrick JS, Wang JC, Chen MN, Kang JD. AOA Symposium Debating the Value of Spine Surgery. *Journal of Bone and Joint Surgery-American Volume*. 2010;92A:1293-304.
- [103] Yokoyama F, Masada I, Shimamura K, Ikawa T, Monobe K. Morphology and structure of highly elastic poly(vinyl alcohol) hydrogel prepared by repeated freezing-and-melting. *Colloid and Polymer Science*. 1986;264:595-601.
- [104] Willcox PJ, Howie DW, Schmidt-Rohr K, Hoagland DA, Gido SP, Pudjijanto S, et al. Microstructure of poly(vinyl alcohol) hydrogels produced by freeze/thaw cycling. *Journal of Polymer Science Part B-Polymer Physics*. 1999;37:3438-54.
- [105] Millon LE, Nieh MP, Hutter JL, Wan WK. SANS characterization of an anisotropic poly(vinyl alcohol) hydrogel with vascular applications. *Macromolecules*. 2007;40:3655-62.
- [106] Bodugoz-Senturk H, Choi J, Oral E, Kung JH, Macias CE, Braithwaite G, et al. The effect of polyethylene glycol on the stability of pores in polyvinyl alcohol hydrogels during annealing. *Biomaterials*. 2008;29:141-9.

-
- [107] Bodugoz-Senturk H, Oral E, Choi J, Macias C, Muratoglu OK. Molecular weight effect on theta-gel formation in poly(vinyl alcohol)-poly(ethylene glycol) mixtures. *Journal of Applied Polymer Science*. 2012;125:2890-5.
- [108] Choi J, Bodugoz-Senturk H, Kung HJ, Malhi AS, Muratoglu OK. Effects of solvent dehydration on creep resistance of poly(vinyl alcohol) hydrogel. *Biomaterials*. 2007;28:772-80.
- [109] Hassan CM, Peppas NA. Structure and morphology of freeze/thawed PVA hydrogels. *Macromolecules*. 2000;33:2472-9.
- [110] Lozinsky VI, Damshkaln LG, Shaskol'skii BL, Babushkina TA, Kurochkin IN, Kurochkin, II. Study of cryostructuring of polymer systems: 27. Physicochemical properties of poly(vinyl alcohol) cryogels and specific features of their macroporous morphology. *Colloid Journal*. 2007;69:747-64.
- [111] Hatakeyama T, Yamauchi A, Hatakeyama H. Effect of thermal hysteresis on structural change of water restrained in poly(vinyl alcohol) pseudo-gel. *European Polymer Journal*. 1987;23:361-5.
- [112] Lozinsky VI, Zubov AL, Savina IN, Plieva FM. Study of cryostructuring of polymer systems. XIV. Poly(vinyl alcohol) cryogels: Apparent yield of the freeze-thaw-induced gelation of concentrated aqueous solutions of the polymer. *Journal of Applied Polymer Science*. 2000;77:1822-31.
- [113] Lozinsky VI, Damshkaln LG. Study of cryostructuring of polymer systems. XVII. Poly(vinyl alcohol) cryogels: Dynamics of the cryotropic gel formation. *Journal of Applied Polymer Science*. 2000;77:2017-23.
- [114] Stauffer SR, Peppas NA. Poly(vinyl alcohol) hydrogels prepared by freezing-thawing cyclic processing. *Polymer*. 1992;33:3932-6.
- [115] Ricciardi R, D'Errico G, Auriemma F, Ducouret G, Tedeschi AM, De Rosa C, et al. Short time dynamics of solvent molecules and supramolecular organization of poly (vinyl alcohol) hydrogels obtained by freeze/thaw techniques. *Macromolecules*. 2005;38:6629-39.
- [116] Holloway JL, Spiller KL, Lowman AM, Palmese GR. Analysis of the in vitro swelling behavior of poly(vinyl alcohol) hydrogels in osmotic pressure solution for soft tissue replacement. *Acta Biomaterialia*. 2011;7:2477-82.
- [117] Ricciardi R, Auriemma F, De Rosa C, Laupretre F. X-ray diffraction analysis of poly(vinyl alcohol) hydrogels, obtained by freezing and thawing techniques. *Macromolecules*. 2004;37:1921-7.

-
- [118] Shaheen SM, Yamaura K. Preparation of theophylline hydrogels of atactic poly(vinyl alcohol)/NaCl/H₂O system for drug delivery system. *Journal of Controlled Release*. 2002;81:367-77.
- [119] Patachia S, Florea C, Friedrich C, Thomann Y. Tailoring of poly(vinyl alcohol) cryogels properties by salts addition. *Express Polymer Letters*. 2009;3:320-31.
- [120] Savina IN, Hanora A, Plieva FM, Galaev IY, Mattiasson B, Lozinsky VI. Cryostructuration of polymer systems. XXIV. Poly(vinyl alcohol) cryogels filled with particles of a strong anion exchanger: Properties of the composite materials and potential applications. *Journal of Applied Polymer Science*. 2005;95:529-38.
- [121] Thomas J, Lowman A, Marcolongo M. Novel associated hydrogels for nucleus pulposus replacement. *Journal of Biomedical Materials Research Part A*. 2003;67A:1329-37.
- [122] Ma RY, Xiong DS, Miao F, Zhang JF, Peng Y. Novel PVP/PVA hydrogels for articular cartilage replacement. *Materials Science & Engineering C-Materials for Biological Applications*. 2009;29:1979-83.
- [123] Spiller KL, Laurencin SJ, Lowman AM. Characterization of the Behavior of Porous Hydrogels in Model Osmotically-Conditioned Articular Cartilage Systems. *Journal of Biomedical Materials Research Part B-Applied Biomaterials*. 2009;90B:752-9.
- [124] Katta JK, Marcolongo M, Lowman A, Mansmann KA. Friction and wear behavior of poly(vinyl alcohol)/poly(vinyl pyrrolidone) hydrogels for articular cartilage replacement. *Journal of Biomedical Materials Research Part A*. 2007;83A:471-9.
- [125] Mallapragada SK, Peppas NA. Dissolution mechanism of semicrystalline poly(vinyl alcohol) in water. *Journal of Polymer Science Part B-Polymer Physics*. 1996;34:1339-46.
- [126] Peppas N, Merrill E. Differential scanning calorimetry of crystallized PVA hydrogels. *Journal of Applied Polymer Science*. 1976;20:1457-65.
- [127] Hatakeyema T, Uno J, Yamada C, Kishi A, Hatakeyama H. Gel-sol transition of poly(vinyl alcohol) hydrogels formed by freezing and thawing. *Thermochimica Acta*. 2005;431:144-8.
- [128] Paranhos CM, Soares BG, Machado JC, Windmoller D, Pessan LA. Microstructure and free volume evaluation of poly(vinyl alcohol) nanocomposite hydrogels. *European Polymer Journal*. 2007;43:4882-90.

-
- [129] Ricciardi R, Auriemma F, Gaillet C, De Rosa C, Laupretre F. Investigation of the crystallinity of freeze/thaw poly(vinyl alcohol) hydrogels by different techniques. *Macromolecules*. 2004;37:9510-6.
- [130] Ricciardi R, Mangiapia G, Lo Celso F, Paduano L, Triolo R, Auriemma F, et al. Structural organization of poly(vinyl alcohol) hydrogels obtained by freezing and thawing techniques: A SANS study. *Chemistry of Materials*. 2005;17:1183-9.
- [131] Fergg F, Keil F, Quader H. Investigations of the microscopic structure of poly(vinyl alcohol) hydrogels by confocal laser scanning microscopy. *Colloid and Polymer Science*. 2001;279:61-7.
- [132] Hyon SH, Cha WI, Ikada Y. Preparation of transparent poly(vinyl alcohol) hydrogel. *Polymer Bulletin*. 1989;22:119-22.
- [133] Trieu HH, Qutubuddin S. Polyvinyl alcohol hydrogels I. Microscopic structure by freeze-etching and critical point drying techniques. *Colloid and Polymer Science*. 1994;272:301-9.
- [134] Nakaoki T, Yamashita H. Bound states of water in poly(vinyl alcohol) hydrogel prepared by repeated freezing and melting method. *Journal of Molecular Structure*. 2008;875:282-7.
- [135] Whatley BR, Wen XJ. Intervertebral disc (IVD): Structure, degeneration, repair and regeneration. *Materials Science & Engineering C-Materials for Biological Applications*. 2012;32:61-77.
- [136] Kobayashi M. A study of Polyvinyl Alcohol-Hydrogel (PVA-H) artificial meniscus in vivo. *Bio-Medical Materials and Engineering*. 2004;14:505-15.
- [137] Liu KF, Ovaert TC. Poro-viscoelastic constitutive modeling of unconfined creep of hydrogels using finite element analysis with integrated optimization method. *Journal of the Mechanical Behavior of Biomedical Materials*. 2011;4:440-50.
- [138] Mamada K, Fridrici V, Kosukegawa H, Kapsa P, Ohta M. Friction Properties of Poly(vinyl alcohol) Hydrogel: Effects of Degree of Polymerization and Saponification Value. *Tribology Letters*. 2011;42:241-51.
- [139] Gong JP. Friction and lubrication of hydrogels - its richness and complexity. *Soft Matter*. 2006;2:544-52.
- [140] Hassan CM, Ward JH, Peppas NA. Modeling of crystal dissolution of poly(vinyl alcohol) gels produced by freezing/thawing processes. *Polymer*. 2000;41:6729-39.

-
- [141] Gordon MJ. Controlling the mechanical properties of PVA hydrogels for biomedical applications [MESc]. London, Ont.: The University of Western Ontario; 1999.
- [142] Briscoe B, Luckham P, Zhu S. The effects of hydrogen bonding upon the viscosity of aqueous poly(vinyl alcohol) solutions. *Polymer*. 2000;41:3851-60.
- [143] Feng LG, Jia YX, Chen XL, Li X, An LJ. A multiphasic model for the volume change of polyelectrolyte hydrogels. *Journal of Chemical Physics*. 2010;133:8.
- [144] Patachia S, Valente AJM, Baciuc C. Effect of non-associated electrolyte solutions on the behaviour of poly(vinyl alcohol)-based hydrogels. *European Polymer Journal*. 2007;43:460-7.
- [145] Cascone MG, Laus M, Ricci D, Delguerra RS. Evaluation of poly(vinyl alcohol) hydrogels as a component of hybrid artificial tissues. *Journal of Materials Science-Materials in Medicine*. 1995;6:71-5.
- [146] Allen MJ, Schoonmaker JE, Bauer TW, Williams PF, Higham PA, Yuan HA. Preclinical evaluation of a poly (vinyl alcohol) hydrogel implant as a replacement for the nucleus pulposus. *Spine*. 2004;29:515-23.
- [147] Oka M, Chang YS, Nakamura T, Ushio K, Togochida J, Gu HO. Synthetic osteochondral replacement of the femoral articular surface. *Journal of Bone and Joint Surgery-British Volume*. 1997;79B:1003-7.
- [148] Schadler LS. Polymer-based and polymer-filled nanocomposites. In: Ajayan PM, Schadler LS, Braun PV, editors. *Nanocomposite Science and Technology*. Weinheim: Wiley-VCH; 2003. p. pp. 77-153.
- [149] Manias E. Nanocomposites - Stiffer by design. *Nature Materials*. 2007;6:9-11.
- [150] Zeng QH, Yu AB, Lu GQ. Multiscale modeling and simulation of polymer nanocomposites. *Progress in Polymer Science*. 2008;33:191-269.
- [151] Schadler LS, Kumar SK, Benicewicz BC, Lewis SL, Harton SE. Designed interfaces in polymer nanocomposites: A fundamental viewpoint. *Mrs Bulletin*. 2007;32:335-40.
- [152] Ogata N, Kawakage S, Ogihara T. Poly(vinyl alcohol)-clay and poly(ethylene oxide)-clay blends prepared using water as solvent. *Journal of Applied Polymer Science*. 1997;66:573-81.

-
- [153] Yu YH, Lin CY, Yeh JM, Lin WH. Preparation and properties of poly(vinyl alcohol)-clay nanocomposite materials. *Polymer*. 2003;44:3553-60.
- [154] Lee J, Lee KJ, Jang J. Effect of silica nanofillers on isothermal crystallization of poly(vinyl alcohol): In-situ ATR-FTIR study. *Polymer Testing*. 2008;27:360-7.
- [155] Bonn D, Kellay H, Tanaka H, Wegdam G, Meunier J. Laponite: What is the difference between a gel and a glass? *Langmuir*. 1999:7534-6.
- [156] Martin C, Pignon F, Piau JM, Magnin A, Lindner P, Cabane B. Dissociation of thixotropic clay gels. *Physical Review E*. 2002;66.
- [157] Mourchid A, Delville A, Lambard J, Lecolier E, Levitz P. Phase-diagram of colloidal dispersions of anisotropic charged-particles - equilibrium properties, structure, and rheology of Laponite suspensions. *Langmuir*. 1995:1942-50.
- [158] Cummins HZ. Liquid, glass, gel: The phases of colloidal Laponite. *Journal of Non-Crystalline Solids*. 2007;353:3891-905.
- [159] Nair SH, Pawar KC, Jog JP, Badiger MV. Swelling and mechanical behavior of modified poly(vinyl alcohol)/laponite nanocomposite membranes. *Journal of Applied Polymer Science*. 2007;103:2896-903.
- [160] Schexnailder P, Schmidt G. Nanocomposite polymer hydrogels. *Colloid and Polymer Science*. 2009;287:1-11.
- [161] Zebrowski J, Prasad V, Zhang W, Walker LM, Weitz DA. Shake-gels: shear-induced gelation of laponite-PEO mixtures. *Colloids and Surfaces a-Physicochemical and Engineering Aspects*. 2003;213:189-97.
- [162] Daga VK, Wagner NJ. Linear viscoelastic master curves of neat and laponite-filled poly(ethylene oxide)-water solutions. *Rheologica Acta*. 2006;45:813-24.
- [163] Mongondry P, Nicolai T, Tassin JF. Influence of pyrophosphate or polyethylene oxide on the aggregation and gelation of aqueous laponite dispersions. *Journal of Colloid and Interface Science*. 2004;275:191-6.
- [164] Korley LTJ, Liff SM, Kumar N, McKinley GH, Hammond PT. Preferential association of segment blocks in polyurethane nanocomposites. *Macromolecules*. 2006;39:7030-6.
- [165] Liff SM, Kumar N, McKinley GH. High-performance elastomeric nanocomposites via solvent-exchange processing. *Nature Materials*. 2007;6:76-83.

-
- [166] Klemm D, Kramer F, Moritz S, Lindstrom T, Ankerfors M, Gray D, et al. Nanocelluloses: A New Family of Nature-Based Materials. *Angewandte Chemie-International Edition*. 2011;50:5438-66.
- [167] Eichhorn SJ, Dufresne A, Aranguren M, Marcovich NE, Capadona JR, Rowan SJ, et al. Review: current international research into cellulose nanofibres and nanocomposites. *Journal of Materials Science*. 2010;45:1-33.
- [168] Klemm D, Schumann D, Kramer F, Hessler N, Hornung M, Schmauder HP, et al. Nanocelluloses as innovative polymers in research and application. *Polysaccharides II*. 2006;205:49-96.
- [169] Guhadós G, Wan WK, Hutter JL. Measurement of the elastic modulus of single bacterial cellulose fibers using atomic force microscopy. *Langmuir*. 2005;21:6642-6.
- [170] Favier V, Dendievel R, Canova G, Cavaille JY, Gilormini P. Simulation and modeling of three-dimensional percolating structures: Case of a latex matrix reinforced by a network of cellulose fibers. *Acta Materialia*. 1997;45:1557-65.
- [171] Bodin A, Gustafsson L, Gatenholm P. Surface-engineered bacterial cellulose as template for crystallization of calcium phosphate. *Journal of Biomaterials Science-Polymer Edition*. 2006;17:435-47.
- [172] Wan YZ, Huang Y, Yuan CD, Raman S, Zhu Y, Jiang HJ, et al. Biomimetic synthesis of hydroxyapatite/bacterial cellulose nanocomposites for biomedical applications. *Materials Science & Engineering C-Biomimetic and Supramolecular Systems*. 2007;27:855-64.
- [173] Gordon MJ. Controlling the mechanical properties of PVA hydrogels for biomedical applications [M E Sc]. London, Ont.: The University of Western Ontario; 1999.
- [174] Zhang L, Wang ZP, Xu C, Li Y, Gao JP, Wang W, et al. High strength graphene oxide/polyvinyl alcohol composite hydrogels. *Journal of Materials Chemistry*. 2011;21:10399-406.
- [175] Xu FL, Li YB, Wang XJ, Wei J, Yang AP. Preparation and characterization of nano-hydroxyapatite/poly(vinyl alcohol) hydrogel biocomposite. *Journal of Materials Science*. 2004;39:5669-72.
- [176] Wang JH, Gao C, Zhang YS, Wan YZ. Preparation and in vitro characterization of BC/PVA hydrogel composite for its potential use as artificial cornea biomaterial. *Materials Science & Engineering C-Materials for Biological Applications*. 2010;30:214-8.

-
- [177] Silva P, Crozier S, Veidt M, Pearcy MJ. An experimental and finite element poroelastic creep response analysis of an intervertebral hydrogel disc model in axial compression. *Journal of Materials Science-Materials in Medicine*. 2005;16:663-9.
- [178] Gloria A, Causa F, De Santis R, Netti PA, Ambrosio L. Dynamic-mechanical properties of a novel composite intervertebral disc prosthesis. *Journal of Materials Science-Materials in Medicine*. 2007;18:2159-65.
- [179] Ambrosio L, Netti PA, Iannace S, Huang SJ, Nicolais L. Composite hydrogels for intervertebral disc prostheses. *Journal of Materials Science-Materials in Medicine*. 1996;7:251-4.
- [180] Pan YS, Xiong DS, Ma RY. A study on the friction properties of poly(vinyl alcohol) hydrogel as articular cartilage against titanium alloy. *Wear*. 2007;262:1021-5.
- [181] Wu G, Zhang WG, Wang CT. Tribological properties of polyvinyl alcohol hydrogel reinforced with nanometer hydroxy apatite. *Journal of Wuhan University of Technology-Materials Science Edition*. 2008;23:46-9.
- [182] Hall RM, Unsworth A. Friction in hip prostheses. *Biomaterials*. 1997;18:1017-26.
- [183] Jacobs JJ, Hallab NJ, Urban RM, Wimmer MA. Wear particles. *Journal of Bone and Joint Surgery-American Volume*. 2006;88A:99-102.
- [184] Wu G, Su B, Zhang W, Wang C. In vitro behaviors of hydroxyapatite reinforced polyvinyl alcohol hydrogel composite. *Materials Chemistry and Physics*. 2008;107:364-9.
- [185] Northwood E, Fisher J. A multi-directional in vitro investigation into friction, damage and wear of innovative chondroplasty materials against articular cartilage. *Clinical Biomechanics*. 2007;22:834-42.
- [186] Bavaresco VP, Zavaglia CAC, Reis MC, Gomes JR. Study on the tribological properties of pHEMA hydrogels for use in artificial articular cartilage. *Wear*. 2008;265:269-77.
- [187] Liu XJ, Nanao H, Li TS, Mori S. A study on the friction properties of PAAc hydrogel under low loads in air and water. *Wear*. 2004;257:665-70.
- [188] Freeman ME, Furey MJ, Love BJ, Hampton JM. Friction, wear, and lubrication of hydrogels as synthetic articular cartilage. *Wear*. 2000;241:129-35.

-
- [189] Pan YS, Xiong DS, Chen XL. Friction behavior of poly(vinyl alcohol) gel against stainless steel ball in different lubricant media. *Journal of Tribology-Transactions of the Asme*. 2008;130.
- [190] Ma RY, Xiong DS, Miao F, Zhang JF, Peng Y. Friction properties of novel PVP/PVA blend hydrogels as artificial cartilage. *Journal of Biomedical Materials Research Part A*. 2010;93A:1016-9.
- [191] Murakami T, Higaki H, Sawae Y, Ohtsuki N, Moriyama S, Nakanishi Y. Adaptive multimode lubrication in natural synovial joints and artificial joints. *Proceedings of the Institution of Mechanical Engineers Part H-Journal of Engineering in Medicine*. 1998;212:23-35.
- [192] Nakashima K, Sawae Y, Murakami T. Study on wear reduction mechanisms of artificial cartilage by synergistic protein boundary film formation. *Jsm International Journal Series C-Mechanical Systems Machine Elements and Manufacturing*. 2005;48:555-61.
- [193] Nakashima K, Sawae Y, Murakami T. Influence of protein conformation on frictional properties of poly (vinyl alcohol) hydrogel for artificial cartilage. *Tribology Letters*. 2007;26:145-51.
- [194] Brandt J-M. *Wear and boundary lubrication in modular total knee replacements*. Waterloo, Ont.: University of Waterloo; 2009.
- [195] Northwood E, Fisher J, Kowalski R. Investigation of the friction and surface degradation of innovative chondroplasty materials against articular cartilage. *Proceedings of the Institution of Mechanical Engineers Part H-Journal of Engineering in Medicine*. 2007;221:263-79.
- [196] Pare PE, Chan FW, Powell ML. Wear characterization of the A-MAV (TM) anterior motion replacement using a spine wear simulator. *Wear*. 2007;263:1055-9.
- [197] Austin H. *Wear of PEEK all-polymer articulations for cervical spinal disc arthroplasty*. Waterloo, Ont.: University of Waterloo; 2008.
- [198] Suciu AN, Iwatsubo T, Matsuda M. Theoretical investigation of an artificial joint with micro-pocket-covered component and biphasic cartilage on the opposite articulating surface. *Journal of Biomechanical Engineering-Transactions of the Asme*. 2003;125:425-33.
- [199] Wu G, Wang C, Zhang W. The factors of speeds and loads on the tribological properties of PVA-H/HA composites. *Journal of Applied Polymer Science*. 2007;106:3908-14.

-
- [200] Yasuda K, Gong JP, Katsuyama Y, Nakayama A, Tanabe Y, Kondo E, et al. Biomechanical properties of high-toughness double network hydrogels. *Biomaterials*. 2005;26:4468-75.
- [201] Thomas BH, Fryman JC, Liu KF, Mason J. Hydrophilic-hydrophobic hydrogels for cartilage replacement. *Journal of the Mechanical Behavior of Biomedical Materials*. 2009;2:588-95.
- [202] Lin HR, Ling MH, Lin YJ. High Strength and Low Friction of a PAA-Alginate-Silica Hydrogel as Potential Material for Artificial Soft Tissues. *Journal of Biomaterials Science-Polymer Edition*. 2009;20:637-52.
- [203] Wu G, Zhao CH, Wang CT, Zhang WG. The Effect of Preparation Methods on Tribological Properties of PVA-H/HA Composites. *Iranian Polymer Journal*. 2008;17:811-9.
- [204] Zhang DK, Shen YQ, Ge SR. Research on the friction and wear mechanism of Poly(vinyl alcohol)/hydroxylapatite composite hydrogel. *Science in China Series E-Technological Sciences*. 2009;52:2474-80.
- [205] Suciu AN, Iwatsubo T, Matsuda M, Nishino T. Wear characteristics of a novel bearing system for artificial knee joint - (Micro-pocket-covered femoral component and tibial poro-elastic-hydrated cartilage). *Jsm International Journal Series C-Mechanical Systems Machine Elements and Manufacturing*. 2004;47:209-17.
- [206] Grupp TM, Yue JJ, Garcia R, Basson J, Schwiesau J, Fritz B, et al. Biotribological evaluation of artificial disc arthroplasty devices: influence of loading and kinematic patterns during in vitro wear simulation. *European Spine Journal*. 2009;18:98-108.
- [207] Wang A. A unified theory of wear for ultra-high molecular weight polyethylene in multi-directional sliding. *Wear*. 2001;248:38-47.
- [208] Galvin A, Kang L, Tipper J, Stone M, Ingham E, Jin ZM, et al. Wear of crosslinked polyethylene under different tribological conditions. *Journal of Materials Science-Materials in Medicine*. 2006;17:235-43.
- [209] Ge SR, Wang SB, Gitis N, Vinogradov M, Xiao J. Wear behavior and wear debris distribution of UHMWPE against Si₃N₄ ball in bi-directional sliding. *Wear*. 2008;264:571-8.
- [210] Scholes SC, Unsworth A. Pin-on-plate studies on the effect of rotation on the wear of metal-on-metal samples. *Journal of Materials Science-Materials in Medicine*. 2001;12:299-303.

-
- [211] Powell ML. An investigation into wear of materials for metal-on-metal cervical disc implants. Waterloo, Ont.: University of Waterloo; 2005.
- [212] Powell ML, Medley JB, Varano R. Metal-metal cervical disc implants: A material investigation using pin-on-plate tests. In: D. Dowson MPGDaAAL, editor. Tribology and Interface Engineering Series: Elsevier; 2005. p. 845-52.
- [213] Hangiandreou NJ. AAPM/RSNA physics tutorial for residents: Topics in US - B-mode US: Basic concepts and new technology. *Radiographics*. 2003;23:1019-33.
- [214] Khan Z, Boughner DR, Lacefield JC. Reconsidering the layer thickness distribution in aortic valve cusps using high-frequency ultrasound. 2007 4th IEEE International Symposium on Biomedical Imaging : Macro to Nano, Vols 1-3. New York: Ieee; 2007. p. 868-71.
- [215] Beckmann N, Kneuer R, Gremlich HU, Karmouty-Quintana H, Ble FX, Muller M. In Vivo mouse imaging and spectroscopy in drug discovery. *Nmr in Biomedicine*. 2007;20:154-85.
- [216] Kharine A, Manohar S, Seeton R, Kolkman RGM, Bolt RA, Steenbergen W, et al. Poly(vinyl alcohol) gels for use as tissue phantoms in photoacoustic mammography. *Physics in Medicine and Biology*. 2003;48:357-70.
- [217] Devi CU, Vasu RM, Sood AK. Design, fabrication, and characterization of a tissue-equivalent phantom for optical elastography. *Journal of Biomedical Optics*. 2005;10:10.
- [218] Zell K, Sperl JI, Vogel MW, Niessner R, Haisch C. Acoustical properties of selected tissue phantom materials for ultrasound imaging. *Physics in Medicine and Biology*. 2007;52:N475-N84.
- [219] Xia WF, Piras D, Heijblom M, Steenbergen W, van Leeuwen TG, Manohar S. Poly(vinyl alcohol) gels as photoacoustic breast phantoms revisited. *Journal of Biomedical Optics*. 2011;16:10.
- [220] Baghdadi H, Sardinha H, Bhatia S. Rheology and gelation kinetics in laponite dispersions containing poly(ethylene oxide). *Journal of Polymer Science Part B-Polymer Physics*. 2005:233-40.
- [221] Joseph G, Rowe G, Margaritis A, Wan W. Effects of polyacrylamide-co-acrylic acid on cellulose production by *Acetobacter xylinum*. *Journal of Chemical Technology and Biotechnology*. 2003:964-70.

-
- [222] Millon LE. Isotropic and anisotropic polyvinyl alcohol based hydrogels for biomedical applications [PhD]. London, Ontario: The University of Western Ontario; 2006.
- [223] Painter PC, Coleman MM. Fundamentals of Polymer Science: An Introductory Text. 2nd ed. Lancaster, Pa.: Technomic Pub. Co.; 1997.
- [224] Bausch AR, Ziemann F, Boulbitch AA, Jacobson K, Sackmann E. Local measurements of viscoelastic parameters of adherent cell surfaces by magnetic bead microrheometry. *Biophysical Journal*. 1998;75:2038-49.
- [225] Medley JB, Pilliar RM, Wong EW, Strong AB. Hydrophilic polyurethane elastomers, for hemiarthroplasty: a preliminary in vitro wear study. *ARCHIVE: Engineering in Medicine 1971-1988 (vols 1-17)*. 1980;9:59-65.
- [226] Brandt J-M, Charron KD, Zhao L, Medley JB, MacDonald SJ. Lubricant for wear testing of joint replacements and associated materials. US patent application 12/069,280. 2008.
- [227] Kulkarni AG, Diwan AD. Prosthetic Lumbar disc replacement for degenerative disc disease. *Neurology India*. 2005;53:499-505.
- [228] Vizesi F, Jones C, Lotz N, Gianoutsos M, Walsh WR. Stress relaxation and creep: Viscoelastic properties of common suture materials used for flexor tendon repair. *Journal of Hand Surgery-American Volume*. 2008;33A:241-6.
- [229] Wong KKH, Zinke-Allmang M, Hutter JL, Hrapovic S, Luong JHT, Wan W. The effect of carbon nanotube aspect ratio and loading on the elastic modulus of electrospun poly(vinyl alcohol)-carbon nanotube hybrid fibers. *Carbon*. 2009;47:2571-8.
- [230] Wendlandt M, Tervoort TA, Suter UW. Non-linear, rate-dependent strain-hardening behavior of polymer glasses. *Polymer*. 2005;46:11786-97.
- [231] Mulliken AD, Boyce MC. Mechanics of the rate-dependent elastic-plastic deformation of glassy polymers from low to high strain rates. *International Journal of Solids and Structures*. 2006;43:1331-56.
- [232] Tsui NT, Yang Y, Mulliken AD, Torun L, Boyce MC, Swager TM, et al. Enhancement to the rate-dependent mechanical behavior of polycarbonate by incorporation of triptycenes. *Polymer*. 2008;49:4703-12.
- [233] Eyring H. Viscosity, Plasticity, and Diffusion as Examples of Absolute Reaction Rates. *The Journal of Chemical Physics*. 1936;4:283-91.

-
- [234] Yang N, Wong KKH, de Bruyn JR, Hutter JL. Frequency-dependent viscoelasticity measurement by atomic force microscopy. *Measurement Science & Technology*. 2009;20:9.
- [235] MacLean JJ, Owen JP, Iatridis JC. Role of endplates in contributing to compression behaviors of motion segments and intervertebral discs. *Journal of Biomechanics*. 2007;40:55-63.
- [236] Cassidy JJ, Silverstein MS, Hiltner A, Baer E. A Water Transport Model for The Creep Response of the Intervertebral-Disk. *Journal of Materials Science-Materials in Medicine*. 1990;1:81-9.
- [237] Lozinsky VI, Zubov AL, Titova EF. Swelling behavior of poly(vinyl alcohol) cryogels employed as matrices for cell immobilization. *Enzyme and Microbial Technology*. 1996;18:561-9.
- [238] Mamada K, Kosukegawa H, Fridrici V, Kapsa P, Ohta M. Friction properties of PVA-H/steel ball contact under water lubrication conditions. *Tribology International*. 2011;44:757-63.
- [239] Li LP, Buschmann MD, Shirazi-Adl A. Strain-rate dependent stiffness of articular cartilage in unconfined compression. *Journal of Biomechanical Engineering-Transactions of the Asme*. 2003;125:161-8.
- [240] Lin CY, Kang H, Rouleau JP, Hollister SJ, La Marca F. Stress Analysis of the Interface Between Cervical Vertebrae End Plates and the Bryan, Prestige LP, and ProDisc-C Cervical Disc Prostheses An In Vivo Image-Based Finite Element Study. *Spine*. 2009;34:1554-60.
- [241] Galbusera F, Bellini CM, Raimondi MT, Fornari M, Assietti R. Cervical spine biomechanics following implantation of a disc prosthesis. *Medical Engineering & Physics*. 2008;30:1127-33.
- [242] Lazaro BCR, Yucesoy K, Yuksel KZ, Kowalczyk I, Rabin D, Fink M, et al. Effect of arthroplasty design on cervical spine kinematics: analysis of the Bryan Disc, ProDisc-C, and Synergy Disc. *Neurosurgical Focus*. 2010;28:8.
- [243] Lieu D. Ultrasound Physics and Instrumentation for Pathologists. *Archives of Pathology & Laboratory Medicine*. 2010;134:1541-56.
- [244] Suci AN, Iwatsubo T, Matsuda M, Nishino T. A study upon durability of the artificial knee joint with PVA hydrogel cartilage. *Jsme International Journal Series C-Mechanical Systems Machine Elements and Manufacturing*. 2004;47:199-208.

-
- [245] Vassiliou K, Unsworth A. Is the wear factor in total joint replacements dependent on the nominal contact stress in ultra-high molecular weight polyethylene contacts? *Proceedings of the Institution of Mechanical Engineers Part H-Journal of Engineering in Medicine*. 2004;218:101-7.
- [246] Gong J, Osada Y. Gel friction: A model based on surface repulsion and adsorption. *Journal of Chemical Physics*. 1998;109:8062-8.
- [247] Oka M, Noguchi T, Kumar P, Ikeuchi K, Yamamuro T, Hyon SH, et al. Development of an artificial articular cartilage. *Clinical Materials*. 1990;6:361-81.
- [248] Davim JP, Marques N. Evaluation of tribological behaviour of polymeric materials for hip prostheses application. *Tribology Letters*. 2001;11:91-4.
- [249] Imado K, Miura A, Nagatoshi M, Kido Y, Miyagawa H, Higaki H. A study of contact temperature due to frictional heating of UHMWPE. *Tribology Letters*. 2004;16:265-73.
- [250] Galetz MC, Uth T, Wimmer MA, Adam P, Glatzel U. Determination of the temperature rise within UHMWPE tibial components during tribological loading. *Acta Biomaterialia*. 2010;6:552-62.
- [251] Bull JWD. A Review Of Cerebral Angiography. *Proceedings of the Royal Society of Medicine-London*. 1949;42:880-90.
- [252] Lestini WF, Wiesel SW. The Pathogenesis Of Cervical Spondylosis. *Clinical Orthopaedics and Related Research*. 1989;239:69-93.
- [253] Holloway JL, Lowman AM, Palmese GR. Mechanical evaluation of poly(vinyl alcohol)-based fibrous composites as biomaterials for meniscal tissue replacement. *Acta Biomaterialia*. 2010;6:4716-24.
- [254] Li JK, Wang N, Wu XS. Poly(vinyl alcohol) nanoparticles prepared by freezing-thawing process for protein/peptide drug delivery. *Journal of Controlled Release*. 1998;56:117-26.
- [255] Mandal TK, Bostanian LA. Effect of peptide loading and surfactant concentration on the characteristics of physically crosslinked hydrogel. *Pharmaceutical Development and Technology*. 2000;5:555-60.
- [256] Shaheen SM, Ukai K, Dai LX, Yamaura K. Properties of hydrogels of atactic poly(vinyl alcohol)/NaCl/H₂O system and their application to drug release. *Polymer International*. 2002;51:1390-7.

-
- [257] Lyoo WS, Shin DS, Han SS, Noh SK, Kim JA, Choi HG, et al. Release behaviour of bovine serum albumin in syndiotactic poly(vinyl alcohol) hydrogel, prepared by freezing-thawing. *Polymers & Polymer Composites*. 2006;14:39-46.
- [258] Abdel-Mottaleb MMA, Mortada ND, El-Shamy AA, Awad GAS. Physically Cross-Linked Polyvinyl Alcohol for the Topical Delivery of Fluconazole. *Drug Development and Industrial Pharmacy*. 2009;35:311-20.
- [259] Yang L. Poly(vinyl alcohol) hydrogel-based controlled release system for wound treatment [PhD]. London, Ont.: The University of Western Ontario; 2008.
- [260] Vicosa AL, Gomes ACO, Soares BG, Paranhos CM. Effect of sepiolite on the physical properties and swelling behavior of rifampicin-loaded nanocomposite hydrogels. *Express Polymer Letters*. 2009;3:518-24.
- [261] Kenawy ER, El-Newehy MH, Al-Deyab SS. Controlled release of atenolol from freeze/thawed poly(vinyl alcohol) hydrogel. *Journal of Saudi Chemical Society*. 2010;14:237-40.
- [262] Kennedy KL. Controlled delivery of Serp-1 protein from poly(vinyl alcohol) hydrogel. London, Ontario: The University of Western Ontario; 2010.
- [263] Wong KKH, Zinke-Allmang M, Wan WK. Effect of annealing on aqueous stability and elastic modulus of electrospun poly(vinyl alcohol) fibers. *Journal of Materials Science*. 2010;45:2456-65.
- [264] Aurienua F, De Rosa C, Ricciardi R, Lo Celso F, Triolo R, Pipich V. Time-resolving analysis of cryotropic gelation of water/poly(vinyl alcohol) solutions via small-angle neutron scattering. *Journal of Physical Chemistry B*. 2008;112:816-23.

Appendix A

PBS PREPARATION

Materials

Chemical Name	Mass (g)
Potassium phosphate (KH ₂ PO ₄)	2.4
Potassium chloride (KCl)	2.0
Sodium chloride (NaCl)	80.0
Sodium phosphate dibasic heptahydrate (Na ₂ HPO ₄ ·7H ₂ O)	26.8

Methods

The chemicals above were added to water to make 1 L of stock 10× PBS solution. The 10× PBS was diluted to the desired concentration as required before use.

Calculations

Ionic Strength of 1× PBS

$$I_c = \frac{1}{2} \sum_i c_i z_i^2$$

where I_c is ionic strength in mol/L, i is the ion in solution, c_i is the molarity of ion i in mol/L, and z_i is the charge of ion i .

Chemical	Mass for 1×PBS [g]	Molar mass [g/mol]	Molarity [mol/L]	Ions	Ion molarity (c_i) [mol/L]	Ion charge (z_i)	$c_i z_i^2$ [mol/L]
KH ₂ PO ₄	0.24	136.09	0.0018	K ⁺	0.0018	1	0.0018
				H ₂ PO ₄ ⁻	0.0018	1	0.0018
KCl	0.20	74.55	0.0027	K ⁺	0.0027	1	0.0027
				Cl ⁻	0.0027	1	0.0027
NaCl	8.00	58.44	0.137	Na ⁺	0.137	1	0.137
				Cl ⁻	0.137	1	0.137
Na ₂ HPO ₄ ·7H ₂ O	2.68	268.07	0.0100	Na ⁺ ×2	0.0200	1	0.0200
O				HPO ₄ ²⁻	0.0100	2	0.0400

Therefore, the ionic strength of 1× PBS is 0.171 mol/L.

Osmolarity of 1× PBS

$$osmol = \sum_i \varphi_i n_i c_i$$

where *osmol* is osmolarity in mol/L, φ_i is the osmotic coefficient, *i* is the molecule in solution, n_i is the number of dissociated particles in molecule *i*, and c_i is the molarity of molecule *i* in mol/L.

Chemical	Mass for 1×PBS [g]	Molar mass [g/mol]	Molarity (c) [mol/L]	n_i	$n_i c_i$ [mol/L]
KH ₂ PO ₄	0.24	136.09	0.0018	2	0.0035
KCl	0.20	74.55	0.0027	2	0.0054
NaCl	8.00	58.44	0.137	2	0.274
Na ₂ HPO ₄ ·7H ₂ O	2.68	268.07	0.0100	3	0.0300

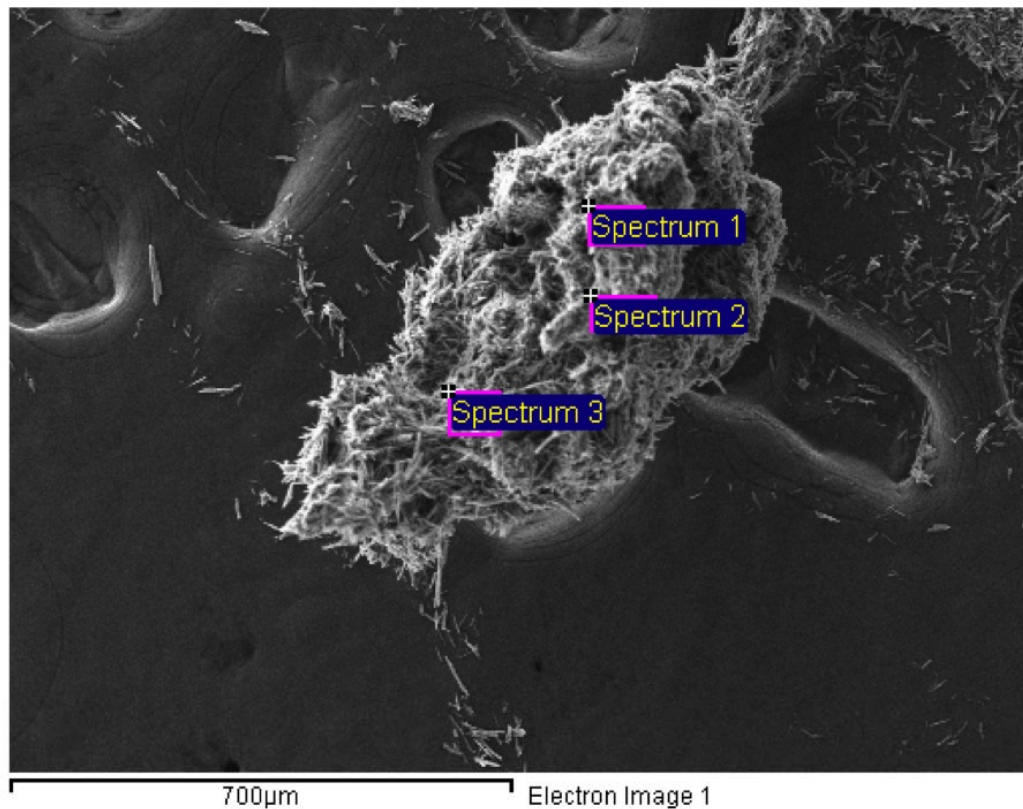
Assuming an ideal solution, where $\varphi_i=1$, the osmolarity of 1× PBS is 0.313 mol/L.

Appendix B

**ENERGY-DISPERSIVE X-RAY
SPECTROSCOPY OF PHOSPHORYLATED-
BACTERIAL CELLULOSE**

Project 1

8/2/2012 11:57:06 AM



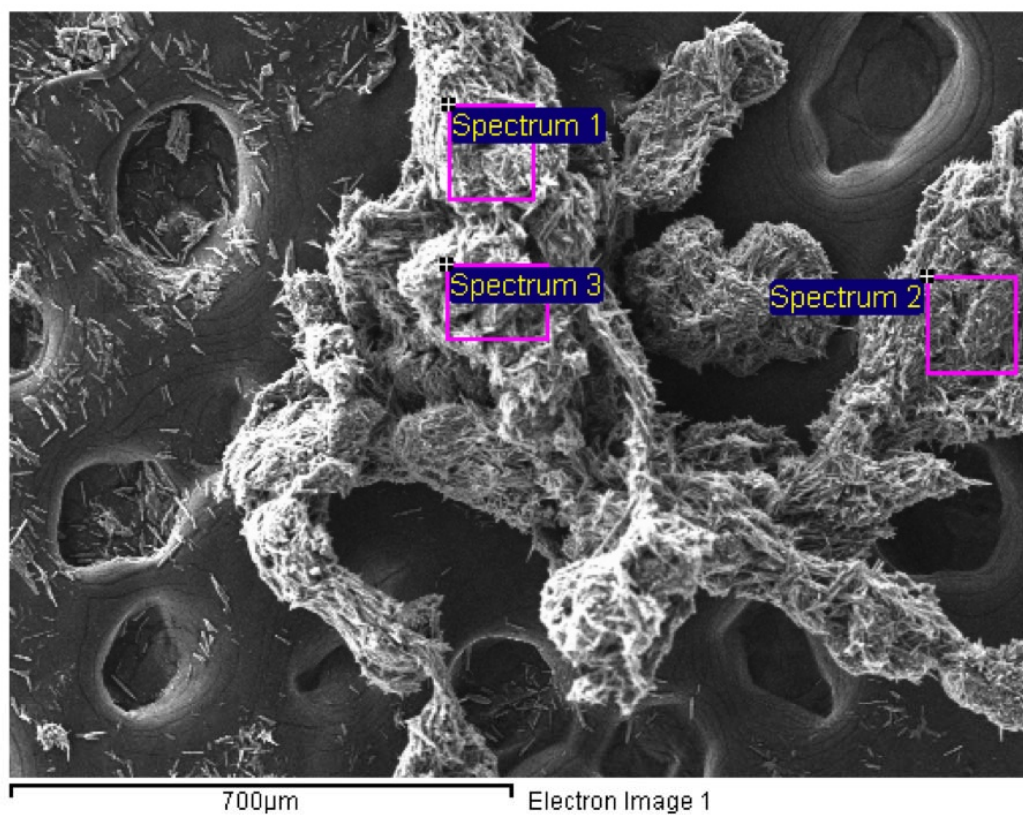
Processing option : All elements analysed (Normalised)

Spectrum	In stats.	C	N	O	P
Spectrum 1	Yes	21.68	11.41	53.96	12.95
Spectrum 2	Yes	28.06	11.34	46.68	13.92
Spectrum 3	Yes	23.81	12.21	53.12	10.86
Mean		24.52	11.65	51.25	12.58
Std. deviation		3.25	0.48	3.99	1.57
Max.		28.06	12.21	53.96	13.92
Min.		21.68	11.34	46.68	10.86

All results in atomic%

Project 1

8/2/2012 11:57:28 AM



Processing option : All elements analysed (Normalised)

Spectrum	In stats.	C	N	O	P
Spectrum 1	Yes	18.49	10.92	55.78	14.82
Spectrum 2	Yes	20.28	12.44	51.51	15.77
Spectrum 3	Yes	15.93	11.47	56.78	15.82
Mean		18.23	11.61	54.69	15.47
Std. deviation		2.19	0.77	2.80	0.57
Max.		20.28	12.44	56.78	15.82
Min.		15.93	10.92	51.51	14.82

All results in atomic%

Appendix C

**PROCEDURE FOR FITTING OF
UNCONFINED COMPRESSION DATA**

The Instron WaveMaker software generated a file containing the positions of the crosshead, in mm, and loads measured by the load cell, in units of gram-force (gf), for the duration of each unconfined compression test. For each set of position-load data, displacement of the crosshead from its initial position at zero strain was calculated by

$$\Delta z = z - z_0 \quad (\text{C.1})$$

where Δz is the displacement of the crosshead from zero strain in mm, z is the instantaneous position of the crosshead in mm, and z_0 is the position of the crosshead at zero strain in mm.

Strain is the engineering strain, calculated by the change in height divided by the initial height of the sample,

$$\varepsilon = \frac{\Delta z}{l_0}$$

where ε is strain, which is dimensionless, and l_0 is the initial height of the sample measured prior to testing.

Load was converted from units of gf to newtons (N), with 1 gf equal to 9.81×10^{-3} N. Stress was then calculated using the formula for engineering stress

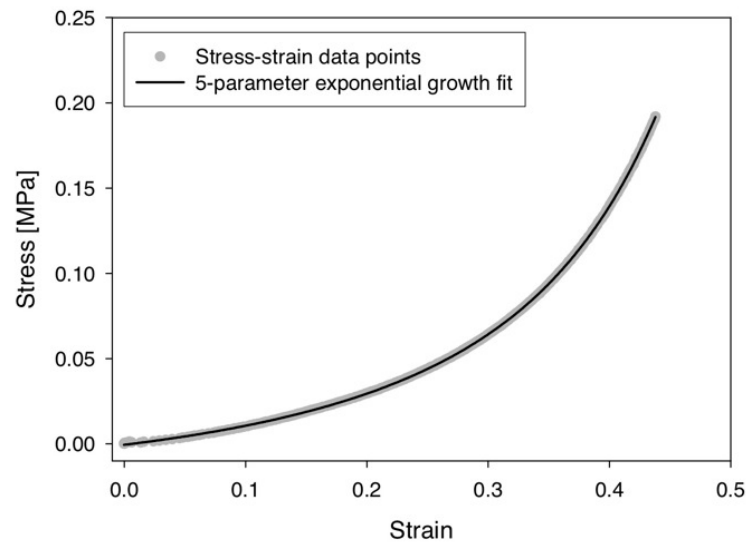
$$\sigma = \frac{F}{A_0}$$

where σ is stress in MPa, F is the load in N, and A_0 is the initial area of the sample, calculated from the measured diameter of the sample prior to testing.

Stress was plotted against strain for the data set, then fitted to the 5-parameter exponential growth equation

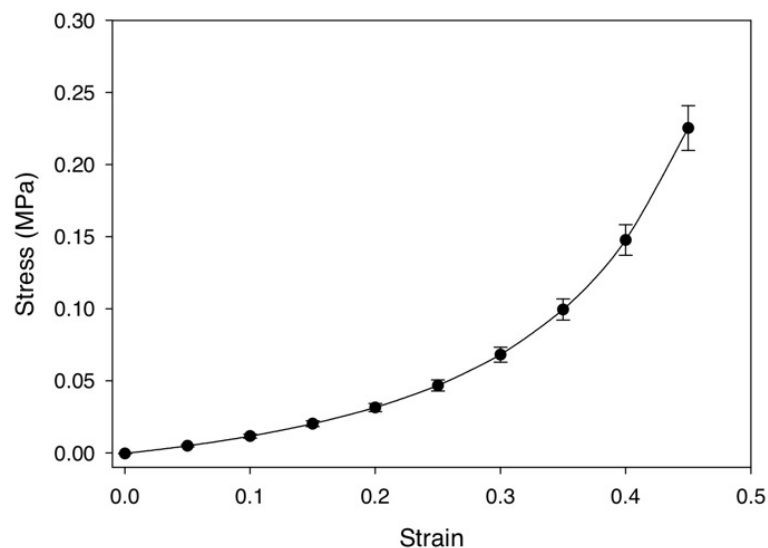
$$\sigma = y_0 + ae^{b\varepsilon} + ce^{d\varepsilon}$$

where σ is the stress at strain ε , y_0 , a , b , c , d are fitting parameters, as shown in the following figure for a 10% PVA hydrogel sample, tested fresh in 37 °C water at a strain rate of 100%/s.



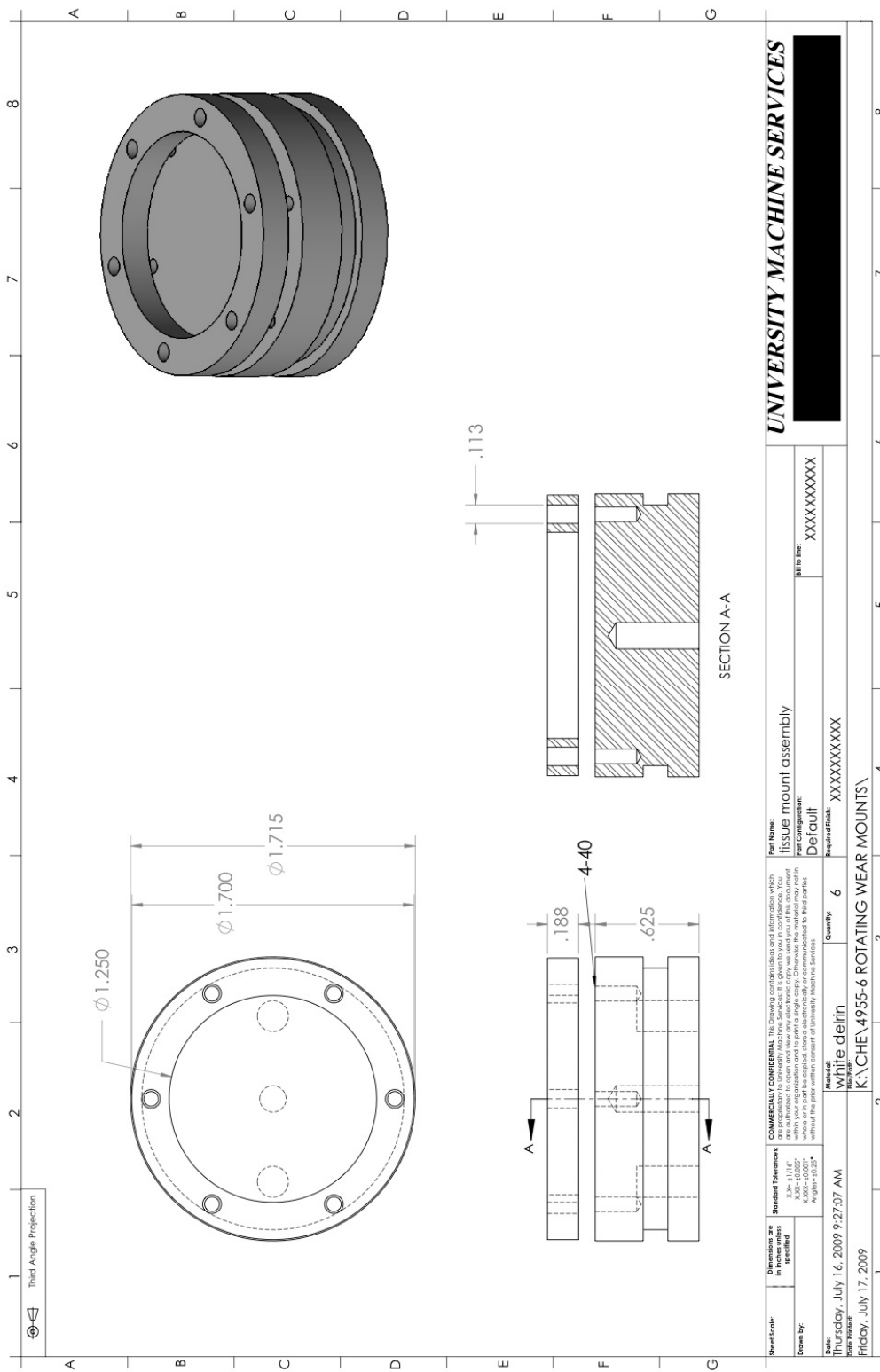
The R^2 values of these fits were at least 0.9987, with a power of 1.0000 at $\alpha=0.05$, for all the unconfined compression tests performed in this thesis.

The 5-parameter exponential growth fit was used to evaluate stress at intervals of 0.05 strain for strains from 0 to 0.45, then the averages and standard deviations of stress for each 0.05 strain interval were determined. The average stress at every 0.05 strain from 0 to 0.45 strain was plotted against strain for each set, using a line and scatter plot, and the error bars were the standard deviations for each point. This is shown below for 10% PVA, tested fresh in 37 °C water at a strain rate of 100%/s.



Appendix D

**SAMPLE HOLDERS FOR CROSSING-PATHS
WEAR TESTER**



Appendix E

**MATLAB PROGRAM FOR EXTRACTION
OF ULTRASOUND IMAGES**

Saving B-Mode Images Planes in a 3D Ultrasound File (.rdb) as a Series of TIFF Image Files

Adapted from code written by Z. Khan

```
%rdb_to_tiff.m
clear
filename='filename.rdb';
fid=fopen(filename,'r');
frames=427;

pathname = strrep(filename, '.rdb', '\');
mkdir(pathname);

for pos=1:frames
    fseek(fid,pos*512*512,'bof'); %find position of each 512x512 frame
    im = fread(fid, [512,512], 'uint8');
    im = uint8(im);
    im = im';
    imname=[strrep(filename, '.rdb', '') '_' num2str(pos) '.tif'];
    imwrite(im, [pathname imname], 'TIFF')
end
```

Appendix F

COPYRIGHT PERMISSIONS

Figure 2.1b

Formal permission not required for reproduction in thesis/dissertation.

Figure 2.4

Rightslink Printable License

22/08/12 4:00 PM

**WOLTERS KLUWER HEALTH LICENSE
TERMS AND CONDITIONS**

Aug 22, 2012

This is a License Agreement between Elaine Wong ("You") and Wolters Kluwer Health ("Wolters Kluwer Health") provided by Copyright Clearance Center ("CCC"). The license consists of your order details, the terms and conditions provided by Wolters Kluwer Health, and the payment terms and conditions.

All payments must be made in full to CCC. For payment instructions, please see information listed at the bottom of this form.

License Number	2974380087043
License date	Aug 22, 2012
Licensed content publisher	Wolters Kluwer Health
Licensed content publication	Spine
Licensed content title	Effect of Loading Rate and Hydration on the Mechanical Properties of the Disc
Licensed content author	Amos Race, Neil Broom, and Peter Robertson
Licensed content date	Jan 1, 2000
Volume Number	25
Issue Number	6
Type of Use	Dissertation/Thesis
Requestor type	Individual
Title of your thesis / dissertation	Poly(vinyl alcohol) Nanocomposite Hydrogels For Intervertebral Disc Prostheses
Expected completion date	Aug 2012
Estimated size(pages)	280
Billing Type	Invoice
Billing address	Biomedical Engineering Graduate Program The University of Western Ontario ████████████████████ ████████
Customer reference info	
Total	0.00 USD
Terms and Conditions	

Terms and Conditions

1. A credit line will be prominently placed and include: for books - the author(s), title of book, editor, copyright holder, year of publication; For journals - the author(s), title of article, title of journal, volume number, issue number and inclusive pages.
2. The requestor warrants that the material shall not be used in any manner which may be considered derogatory to the title, content, or authors of the material, or to Wolters Kluwer.
3. Permission is granted for a one time use only within 12 months from the date of this invoice. Rights herein do not apply to future reproductions, editions, revisions, or other derivative works. Once the 12-month term has expired, permission to renew must be submitted in writing.
4. Permission granted is non-exclusive, and is valid throughout the world in the English language and the languages specified in your original request.
5. Wolters Kluwer cannot supply the requestor with the original artwork or a "clean copy."
6. The requestor agrees to secure written permission from the author (for book material only).
7. Permission is valid if the borrowed material is original to a Wolters Kluwer imprint (Lippincott-Raven Publishers, Williams & Wilkins, Lea & Febiger, Harwal, Igaku-Shoin, Rapid Science, Little Brown & Company, Harper & Row Medical, American Journal of Nursing Co, and Urban & Schwarzenberg - English Language).
8. If you opt not to use the material requested above, please notify Rightslink within 90 days of the original invoice date.
9. Please note that articles in the ahead-of-print stage of publication can be cited and the content may be re-used by including the date of access and the unique DOI number. Any final changes in manuscripts will be made at the time of print publication and will be reflected in the final electronic version of the issue.
Disclaimer: Articles appearing in the Published Ahead-of-Print section have been peer-reviewed and accepted for publication in the relevant journal and posted online before print publication. Articles appearing as publish ahead-of-print may contain statements, opinions, and information that have errors in facts, figures, or interpretation. Accordingly, Lippincott Williams & Wilkins, the editors and authors and their respective employees are not responsible or liable for the use of any such inaccurate or misleading data, opinion or information contained in the articles in this section.
10. Other Terms and Conditions:

v1.3

If you would like to pay for this license now, please remit this license along with your payment made payable to "COPYRIGHT CLEARANCE CENTER" otherwise you will be invoiced within 48 hours of the license date. Payment should be in the form of a check or money order referencing your account number and this invoice number RLNK500843594.

Once you receive your invoice for this order, you may pay your invoice by credit card. Please follow instructions provided at that time.

Make Payment To:

██
██

Rightslink Printable License

22/08/12 4:00 PM

[REDACTED]
[REDACTED]

For suggestions or comments regarding this order, contact RightsLink Customer

Support: [REDACTED] or [REDACTED]
[REDACTED]

Gratis licenses (referencing \$0 in the Total field) are free. Please retain this printable license for your reference. No payment is required.

Figure 2.5

Rightslink Printable License

03/07/12 1:22 AM

**WOLTERS KLUWER HEALTH LICENSE
TERMS AND CONDITIONS**

Jul 03, 2012

This is a License Agreement between Elaine Wong ("You") and Wolters Kluwer Health ("Wolters Kluwer Health") provided by Copyright Clearance Center ("CCC"). The license consists of your order details, the terms and conditions provided by Wolters Kluwer Health, and the payment terms and conditions.

All payments must be made in full to CCC. For payment instructions, please see information listed at the bottom of this form.

License Number	2941170787650
License date	Jul 03, 2012
Licensed content publisher	Wolters Kluwer Health
Licensed content publication	Spine
Licensed content title	Intervertebral Disc Arthroplasty
Licensed content author	Paul Anderson and Jeffrey Rouleau
Licensed content date	Jan 1, 2004
Volume Number	29
Issue Number	23
Type of Use	Dissertation/Thesis
Requestor type	Individual
Title of your thesis / dissertation	Poly(vinyl alcohol) Nanocomposite Hydrogels For Intervertebral Disc Prostheses
Expected completion date	Aug 2012
Estimated size(pages)	280
Billing Type	Invoice
Billing address	Biomedical Engineering Graduate Program The University of Western Ontario ████████████████████ ██████
Customer reference info	
Total	0.00 USD
Terms and Conditions	

Terms and Conditions

1. A credit line will be prominently placed and include: for books - the author(s), title of book, editor, copyright holder, year of publication; For journals - the author(s), title of article, title of journal, volume number, issue number and inclusive pages.
2. The requestor warrants that the material shall not be used in any manner which may be considered derogatory to the title, content, or authors of the material, or to Wolters Kluwer.
3. Permission is granted for a one time use only within 12 months from the date of this invoice. Rights herein do not apply to future reproductions, editions, revisions, or other derivative works. Once the 12-month term has expired, permission to renew must be submitted in writing.
4. Permission granted is non-exclusive, and is valid throughout the world in the English language and the languages specified in your original request.
5. Wolters Kluwer cannot supply the requestor with the original artwork or a "clean copy."
6. The requestor agrees to secure written permission from the author (for book material only).
7. Permission is valid if the borrowed material is original to a Wolters Kluwer imprint (Lippincott-Raven Publishers, Williams & Wilkins, Lea & Febiger, Harwal, Igaku-Shoin, Rapid Science, Little Brown & Company, Harper & Row Medical, American Journal of Nursing Co, and Urban & Schwarzenberg - English Language).
8. If you opt not to use the material requested above, please notify Rightslink within 90 days of the original invoice date.
9. Please note that articles in the ahead-of-print stage of publication can be cited and the content may be re-used by including the date of access and the unique DOI number. Any final changes in manuscripts will be made at the time of print publication and will be reflected in the final electronic version of the issue.
Disclaimer: Articles appearing in the Published Ahead-of-Print section have been peer-reviewed and accepted for publication in the relevant journal and posted online before print publication. Articles appearing as publish ahead-of-print may contain statements, opinions, and information that have errors in facts, figures, or interpretation. Accordingly, Lippincott Williams & Wilkins, the editors and authors and their respective employees are not responsible or liable for the use of any such inaccurate or misleading data, opinion or information contained in the articles in this section.
10. Other Terms and Conditions:

v1.3

If you would like to pay for this license now, please remit this license along with your payment made payable to "COPYRIGHT CLEARANCE CENTER" otherwise you will be invoiced within 48 hours of the license date. Payment should be in the form of a check or money order referencing your account number and this invoice number RLNK500810846.

Once you receive your invoice for this order, you may pay your invoice by credit card. Please follow instructions provided at that time.

**Make Payment To:
Copyright Clearance Center**

Rightslink Printable License

03/07/12 1:22 AM

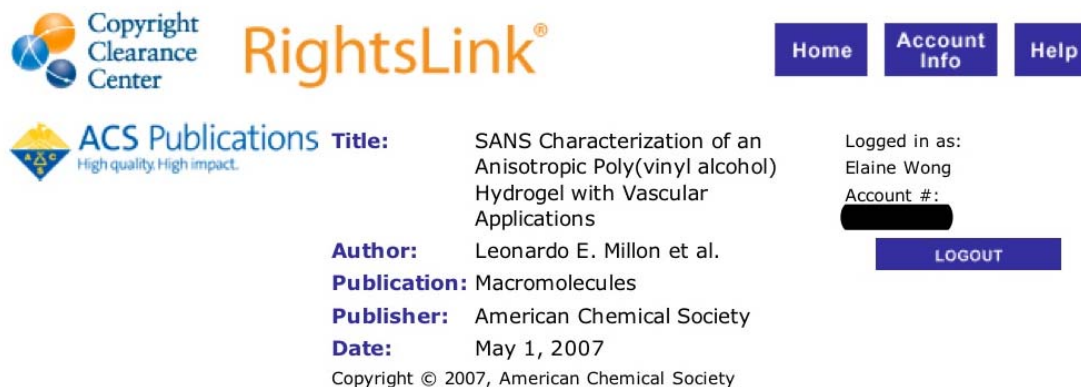
[REDACTED]
[REDACTED]

For suggestions or comments regarding this order, contact RightsLink Customer

Support: [REDACTED] or [REDACTED]
[REDACTED].

Gratis licenses (referencing \$0 in the Total field) are free. Please retain this printable license for your reference. No payment is required.

Figure 2.6



The screenshot shows the Copyright Clearance Center RightsLink interface. At the top left is the Copyright Clearance Center logo. To its right is the RightsLink logo. Further right are three navigation buttons: Home, Account Info, and Help. Below the Copyright Clearance Center logo is the ACS Publications logo with the tagline "High quality High impact." The main content area displays the following information:

Title: SANS Characterization of an Anisotropic Poly(vinyl alcohol) Hydrogel with Vascular Applications

Author: Leonardo E. Millon et al.

Publication: Macromolecules

Publisher: American Chemical Society

Date: May 1, 2007

Copyright © 2007, American Chemical Society

On the right side, it shows the user is logged in as Elaine Wong with account number [REDACTED]. There is a LOGOUT button below this information.

PERMISSION/LICENSE IS GRANTED FOR YOUR ORDER AT NO CHARGE

This type of permission/license, instead of the standard Terms & Conditions, is sent to you because no fee is being charged for your order. Please note the following:

- Permission is granted for your request in both print and electronic formats.
- If figures and/or tables were requested, they may be adapted or used in part.
- Please print this page for your records and send a copy of it to your publisher/graduate school.
- Appropriate credit for the requested material should be given as follows: "Reprinted (adapted) with permission from (COMPLETE REFERENCE CITATION). Copyright (YEAR) American Chemical Society." Insert appropriate information in place of the capitalized words.
- One-time permission is granted only for the use specified in your request. No additional uses are granted (such as derivative works or other editions). For any other uses, please submit a new request.

[BACK](#)[CLOSE WINDOW](#)

CURRICULUM VITAE

ELAINE Y. L. WONG

EDUCATION

- 2012 **Doctor of Philosophy (PhD) in Biomedical Engineering**
The University of Western Ontario, London, Ontario
*Poly(vinyl alcohol) Nanocomposite Hydrogels for Intervertebral Disc
Prostheses*
Supervisor: Dr. Wankei Wan
- 2003 **Bachelor of Applied Science (BASc) in Engineering Science**
University of Toronto, Toronto, Ontario
Biomedical Option, Professional Experience Year Program

AWARDS

- 2005 – 2008 Western Graduate Research Scholarship (WGRS) (\$6600 per year)
- 2003 – 2005 Special University Scholarship

RELATED WORK EXPERIENCE

- 2005 – 2010 **Graduate Teaching Assistant in Biomaterials Engineering**
Biomedical Engineering Graduate Program
The University of Western Ontario
Supervisors: Dr. A. Rizkalla and Dr. W.K. Wan
-

- 2003 – 2004 **Graduate Teaching Assistant in Industrial Organic Chemistry**
Department of Chemical and Biochemical Engineering
The University of Western Ontario
Supervisor: Dr. Paul Charpentier
- 2001 – 2002 **Research Assistant**
Corporate Research and Development
ShawCor Ltd.
Supervisor: Dr. Dennis Wong

CONFERENCE PRESENTATIONS

- Wong, E.Y.L.**, Brown, R., Ma, R., Xiong, D.S., Wan, W.K. (2009) Poly(vinyl alcohol) hydrogels and its nanocomposites for applications in artificial intervertebral disc and cartilage replacement. Poster Presentation. 28th Annual Meeting of the Canadian Biomaterials Society, Kingston, Ontario.
- Wong, E.Y.L.**, Brown, R., Wan, W.K. (2009) Poly(vinyl) alcohol nanocomposite hydrogels for medical applications in compression. Poster Presentation. 27th Annual Meeting of the Canadian Biomaterials Society, Quebec City, Quebec.
- Wong, E.Y.L.**, Wan, W.K. (2009) Poly(vinyl alcohol) hydrogels for biomedical applications in compression. Western Research Forum, London, Ontario.
- Wong E.Y.L.**, Wan, W.K. (2007) Mechanical properties of poly(vinyl alcohol)-Laponite nanocomposite hydrogels. Poster Presentation. 26th Annual Meeting of the Canadian Biomaterials Society, London, Ontario.

Wong, E.Y.L., Kennedy, K.L., and Wan, W.K. (2006) Mechanical Properties of Optically Transparent Poly(Vinyl Alcohol) by the Freeze-Thaw Method. Poster Presentation. 25th Annual Meeting of the Canadian Biomaterials Society, Calgary, Alberta.